A CFD AND EXPERIMENTAL INVESTIGATION OF UNDER-VENTILATED COMPARTMENT FIRES

Dissertation for the Degree of Doctor of Philosophy

Georges Guigay

SCHOOL OF ENGINEERING AND NATURAL SCIENCES
UNIVERSITY OF ICELAND

A CFD AND EXPERIMENTAL INVESTIGATION OF UNDER-VENTILATED COMPARTMENT FIRES

Georges Guigay

Dissertation for the Degree of Doctor of Philosophy

Doctoral Committee

Prof. Jónas Elíasson

Dr. Björn Karlsson

Prof. Jennifer Wen

Prof. Jean-Michel Most

Opponents

Prof. Patrick Van Hees
Lund University

Dr. Halldór Pálsson
University of Iceland

Department of Civil and Environmental Engineering

School of Engineering and Natural Sciences

University of Iceland

Reykjavik, September 2008

A CFD and experimental investigation of under-ventilated compartment fires

Dissertation for the Degree of Doctor of Philosophy

Department of Civil and Environmental Engineering

School of Engineering and Natural Sciences
University of Iceland

Hjardarhaga 2-6

107 Reykjavik, Iceland

Telephone + 354 525 4000

Printed by Gutenberg

Reykjavik, Iceland 2008

ISBN 978-9979-9812-4-4

À mon père, Jean-Pierre Guigay

PREFACE

This dissertation has been prepared as a requirement for a Ph.D. degree in Engineering at the University of Iceland. The doctoral study has been carried out at the Department of Civil and Environmental Engineering at the University of Iceland. The experiments were carried out at the Laboratoire de Combustion et de Détonique, CNRS – ENSMA, Poitiers, France.

The doctoral study was funded by the EU Research Training Network FIRENET and the University of Iceland.

Reykjavík, Iceland, September 2008.

Georges Guigay.

ABSTRACT

This thesis work is dedicated to the study of under-ventilated compartment fires, focusing especially on its most complex and hazardous related phenomenon: a deflagration or rapid combustion called backdraft. In order to predict and mitigate the risk of a backdraft, it is essential to have a good understanding of the gas dynamics which can lead to the ignition and the propagation of the flame, resulting in backdraft.

This thesis work is divided into two parts. The first part introduces the theme of under-ventilated fires and backdraft, describes the means and techniques used during this thesis work, presents and discusses the main results and gives final conclusion and recommendations for further work. The second part contains the research papers written during this thesis work, published in reviewed scientific journals or presented in international conferences.

Computational Fluid Dynamics (CFD) models are shown to be very useful in fire safety engineering, for example to help design modern and safer buildings. In this thesis work, CFD calculations are carried out to estimate the effectiveness of common fire-fighting tactics on backdraft mitigation. Considerable experimental work was carried out as a part of the thesis work and CFD techniques were used to simulate vent flows and other flow patterns in under-ventilated fires. However, the modeling of the incomplete combustion and the extinction of strongly under-ventilated fires is still a challenge for the combustion community.

The occurrence and intensity of a backdraft are directly related to the mixing level and therefore to the properties of the gravity wave. In this thesis work, the combination of analytical, numerical and experimental methodologies gives a good description of the hydrodynamic process prior to backdraft ignition.

ÚTDRÁTTUR

Rannsóknarefnið er eldsvoði í súrefnislitlu rými með sérstakri áherslu á hættuna af fyrirbrigðinu reyksprengingu (backdraft). Til fræðilegrar meðhöndlunar á þessu fyrirbrigði er notuð straumfræði og rannsakað hvernig meta skal og vinna gegn hættunni af sprengingum sem geta orðið þegar kviknar í eldfimu reykgasi.

Ritgerðin skiptist í tvo hluta. Sá fyrri er greining á fyrirbrigðinu, lýsing á þeirri aðferðafræði sem notuð er við rannsóknina og helstu niðursöðum hennar ásamt þeim atriðum sem þurfa frekari rannsóknar við í framtíðinni. Síðari hlutinn fjallar um ritgerðir sem birtar hafa verið í ritrýndum vísindaritum eða á alþjóðlegum ráðstefnum.

Sýnt er fram á að tölvuvædd straumfræðilíkön eru mjög hentug í brunavarnarverkfræði, einkum til að tryggja öryggi í nýjum byggingum á hönnunarstigi. Í ritgerðinni eru tölvuvædd straumfræðilíkön notuð til að meta varnarmátt eldvarnaraðferða sem notaðar eru til að vinna gegn reyksprengingum. Hluti af rannsókninni voru tilraunir er gerðar voru í rannsóknastöð

Verkfræðiháskólans í Poitiers í Frakklandi. Loftræstistraumar og annað loftrennsli tengt súrefnislitlum eldi var hermt með tölvuvæddum straumfræðilíkönum, en líkön af ófullkomnum bruna og eldvarnir þar sem eldsvoðar í lokuðum rýmum og súrefnisskorti eiga í hlut eru enn mikið vandamál innan brunavarnarverkfræði.

Tilurð og kraftur reyksprenginga er afleiðing þess þegar opnað er inn á súrefnislítinn eld og þyngdarstraumur veitir lofti inn í rýmið og blandar það eldfimu gasi sem fyrir er. Í ritgerðinni er beitt aðferðum stærðfræðigreiningar og tölulegum reikningum sem gefa glögga mynd af straumum sem geta leitt til reyksprenginga og niðurstöðurnar bornar saman við tilraunir.

ACKNOWLEDGEMENTS

First of all, I would like to thank Prof. Jónas Elíasson and Dr. Björn Karlsson for their support during these four years of studies. I could not have had a better team of motivated, helpful and friendly supervisors.

To the members of my scientific committee: Prof. Jennifer Wen from the University of Kingston in London and Prof. Jean-Michel Most from the Centre National de la Recherche Scientifique (CNRS) in Poitiers, France: thank you for your expertise and precious collaboration during my thesis research.

I would also like to thank all my friends and colleagues at the University of Iceland for their help and support. Same goes to the colleagues and friends I met via my participation in the Firenet project for all the great and enriching times we spent together.

Prof. Most welcomed me in his research facility for three months, thus offering me the opportunity to carry out the experimental work necessary for my thesis research. Many thanks to him and to Prof. François Penot, Jocelyne, Alain, Jacques and everyone at the CNRS for their assistance during my stay in Poitiers.

Thanks to all the staff and course participants at the University of Ulster for the good times we shared during courses and the (numerous) social events.

I would not have enough space to cite all the people who helped and encouraged me in Iceland and during my travels in Europe, but they know who they are and I send them my regards and thanks.

A big thank you to my family, family-in-law and friends for being there for me during this intense and busy period.

I am especially grateful to my parents who helped and encouraged me during all my school and university years. I still can hardly believe they survived living in the same house as me during the stressful exam periods!

Last but not least, I could not have done this without the help, love and support of my fiancée Elísabet Anna. I'm glad we are the exception to Björn's highly scientific theory…

OVERVIEW OF THE THESIS

This document is divided into two parts. The first part, from Chapter 1 to 10, aims at giving an overview of the work carried out during the PhD project. In the second part, the main papers published during this research project are presented.

Chapter 1 introduces briefly the discipline of Fire Safety Engineering and discusses the contribution to science contained in this thesis with an overview of published papers.

Chapter 2 introduces the problem of enclosure fires and backdrafts, discussing the state of the art, the related terminology and lists the goals of this study.

Chapter 3 describes the means and techniques used in this research, i.e. the analytical approach, the Computational Fluid Dynamics (CFD) model and the experimental flow measurement techniques. Advantages and limitations of these techniques are discussed, and recommendations are presented.

Chapter 4 introduces the problem of the simulation of strongly under-ventilated fires and extinction due to oxygen exhaustion. The limitations and possible improvements are discussed. The use and contribution of CFD is of great importance in Fire Safety Engineering, and 2 examples concerning gravity currents are given to illustrate this interest.

Chapter 5 discusses the analytical model of the gravity wave and the flow at the opening of the compartment, introducing the concept of translatory wave in stratified flow and the critical flow approach for vent flows.

Chapter 6 describes the series of experiments carried out during this PhD project. Firstly, the goal, the apparatus, the control variables and the experimental procedure are described. Secondly, an overview of both qualitative and quantitative results is given, with a discussion concerning the limitations and recommendations.

Chapter 7 describes the CFD model set up to simulate the experiments, using FDS (Fire Dynamics Simulator) and contains some preliminary results from the simulations.

Chapter 8 gives a comparison between the results of the 3 techniques, analytical, experimental and numerical, described in the previous chapters, and discusses the validity of the numerical model. The quantitative results allow comparing important characteristics of the gravity currents, such as the transit time and the flow at the opening and inside the compartment. The qualitative results allow comparing the physics of the phenomena, and especially the turbulent structures.

In Chapter 9, the numerical model is used for a detailed study of the behavior laws of the wave and the mixing between the hot and cold layer. The role in the mixing process of the turbulent coherent structures such as Kelvin-Helmoltz instabilities previously identified in the experiments is highlighted. The mixing and its evolution in time are then quantified by evaluating the mixing fraction in each cell in the symmetry plan.

Chapter 10 concludes the main part of the PhD thesis, and gives recommendations for future research.

LIST OF PAPERS INCLUDED IN THIS DOCUMENT

This thesis is based on the following papers:

Paper A:

G Guigay, B Tómasson, J Bengtsson, B Karlsson, J Elíasson. Using Computational Fluid Dynamics in Fire Safety Engineering of Buildings. Accepted for oral presentation and publication in Proceedings of the 19th International Symposium on Transport Phenomena, Reykjavik, Iceland, Aug. 2008.

The candidate was the main author of this paper.

Paper B:

G Guigay, D Gojkovic, L Bengtsson, B Karlsson, J Elíasson. The Use of CFD Calculations to Evaluate Fire-Fighting Tactics in a Possible Backdraft Situation. Accepted for publication in Fire Technology, DOI:10.1007/s10694-008-0058-4, 2008. In press.

The candidate was the main author of this paper.

Paper C:

J Elíasson, G Guigay, B Karlsson. Enclosure Fires, Gravity Waves and the Backdraft Problem. Accepted for publication in Journal of Fire Sciences, DOI: 10.1177/0734904108092116, 2008. In press.

The candidate wrote most of the paper and performed all the calculations.

Paper D:

G Guigay, J Elíasson, A Horvat, YL Sinai, B Karlsson. Analytic Calculation and Computer Simulation of Gravity Flows in Backdraft Studies. Submitted to Journal of Fire Sciences in May 2008.

The candidate was the main author of this paper.

Paper E:

G Guigay, B Karlsson, J Elíasson. Numerical and Simple Engineering Approach to the Determination of Combustion Products in Strongly Under-ventilated Fires Prior to Backdraft. Presented at the First Workshop on Fires in Enclosures, Jordanstown, Ulster, May 2006.

The candidate was the main author of this paper.

TABLE OF CONTENTS

Paper [B]

Paper [C]

Paper [D]

Paper [E]

LIST OF FIGURES

LIST OF TABLES

1 INTRODUCTION, CONTRIBUTION TO SCIENCE AND OVERVIEW OF THE THESIS

1.1 Fire safety engineering

Fire Protection Engineering is a developing discipline; it includes material science, structure strength, chemistry, fluid mechanics and touches many other domains such as medicine and psychology. Its goals are to reduce the number of deaths and injuries in fire accidents, to educate and train fire-fighters to improve their safety during interventions, and to reduce property damage. To this end, it is important to develop predictive tools, which help engineers with their building designs by simulating complex problems like combustion, heat transfer, smoke spread, human behavior and evacuation. However, despite all these efforts, fire remains one of nature's most hazardous and unpredictable phenomena, and therefore discipline requires continuous research. Classical textbooks describing Fire Protection Engineering have been produced by Karlsson and Quintiere [1] and Drysdale [2]. The Society of Fire Protection Engineers (SFPE) has published a complete handbook [3] which is a key reference within the fire protection community.

1.2 Contribution to science

This thesis' main contribution to science concerns the study of under-ventilated fires, in particular backdraft. The work carried out aims at giving a very complete description of the entire gas dynamic process prior to backdraft ignition, by means of experiments, CFD and analytical studies.

Prediction models that have resulted from this research are described in several research papers (Papers [B] to [E]). In these papers, examples of hydraulic analysis of fresh air inflow into compartments filled with hot gases are presented for the first time and verified against former experimental findings from Fleischman and McGrattan [4].

This research project also considers a new approach for estimating of vent flows based on critical flow conditions, by improving the commonly used formulas based on the Bernoulli's equation.

An experimental series has been carried out to give a very complete description of the hydrodynamic process prior to backdraft. A numerical model of these experiments was set-up and its results are validated against the experimental ones. The combination of these two tools allows identifying the primary mechanisms creating the necessary conditions for a backdraft to occur.

The numerical model allows a detailed investigation of the mixing process, identifying the main sources of mixing and quantifying it by calculating the mixing fraction within the compartment.

In the second part of this PhD thesis, the main papers published during this research are presented, as a contribution to the Fire Safety Science:

Paper [A] discusses the benefits of CFD calculations for Fire Safety Engineering and building design. During the last decades, building codes have been shifting from prescriptive to performance based, permitting the design of modern and complex buildings. Fire safety regulations can have a major impact on the overall design of a building with regard to layout, aesthetics, function and cost. At the same time there has been a rapid progress in the understanding of fire processes and their interaction with humans and buildings. Advancement of CFD modeling of fires has been particularly rapid. This paper gives two design examples of complex buildings; firstly, an office building where occupants' safety and evacuation are the main concerns, and secondly a storage building where the focus is on the fire brigade access to the building and how to prevent damage to the goods inside. In both cases, CFD results show that these design solutions provide an acceptable level of safety.

In Paper [B], several practical fire-fighting tactics commonly used when arriving at the scene of an under-ventilated fire are simulated by CFD calculation. It is shown that CFD has a great potential to estimate the effectiveness of these tactics in mitigating the danger of backdraft. If burning has occurred in an oxygen starved environment for a long time, excessive pyrolysis products may have accumulated in the fire compartment. If air is suddenly introduced into the compartment a backdraft can occur. The CFD code used for the simulations is FDS (Fire Dynamic Simulator). This paper focuses on the conditions that can lead to backdraft, and not the deflagration in itself. Therefore, the simulation focuses on the gravity current and the mixing process between cold fresh air and hot smoke gases by considering, as initial condition, a uniform temperature inside the building. The different fire-fighting tactics studied include natural ventilation, Positive Pressure Ventilation (PPV) and dilution by water mist. Their efficiency is observed by comparison with a reference scenario, where no action is taken. It is shown that usage of PPV is very efficient in evacuating the unburnt gases, but increases the mixing, and consequently the probability of backdraft during the early stage of operation. On the other hand, the addition of water mist can mitigate completely the danger of backdraft, at the condition that the unburnt gases' concentration is below the critical fuel volume fraction. If the dilution level is not sufficient, the danger of backdraft is increased, mainly because the time necessary to empty the rooms of hot gases is longer due to cooling, that reduces the density difference between hot and cold gases. During a fire-fighting operation, the choice of tactic depends mainly on whether there are people left in the building or not, but also on the fire-fighters' knowledge of the building's geometry and the fire conditions. If the situation shows signs of strongly under-ventilated conditions, the danger of backdraft has to be considered and the most appropriate mitigation tactics must be applied.

Paper [C] investigates the characteristics of a gravity wave. This flow, created by fresh oxygen entering a hot compartment is an essential element in the backdraft process. The problem seems to be that the mixing and entrainment between the two layers of hot and cold air has a profound effect on the flow velocities. In this paper an analytical gravity wave model that can calculate the velocities in a simple gravity wave is presented. This model uses the equations of stratified flow hydraulics and the translatory wave solution of the flow equations. It is found that the velocities of the model compare very well to the velocities reported from laboratory tests and numerical simulations. Numerical simulations of stratified flow in a CFD model are discussed with respect to model construction. It is concluded that

the densimetric Froude number is the main parameter for the velocity calculations and the length/height ratio is important for the friction forces.

In **Paper [D]**, the classical hydraulic equations of density driven flows are solved in order to determine the gravity controlled inflow in a shipping container full of hot unburnt gases. For this purpose, a critical flow approach, which is new to Fire Safety Engineering, is considered. 1/3 of the container's height is covered by the horizontal opening. For the initial condition, i.e. just before opening the hatch, zero velocity is prescribed everywhere. When the hatch is opened, the incoming air flows down to the container floor and crosses it without meeting any resistance other than normal frictional resistance. The classical way of estimating vent flows in fire safety engineering is to assume that the gases in the fire compartment are either well-mixed or stratified. In this paper, we take a different approach to estimating vent flows, using the critical flow condition and an alternative velocity profile based on experiments. Two flow correction coefficients are considered at the opening, taking into account the uneven distribution of velocity (α) and the effect of mixing and entrainment (C). These semi-analytical results are then compared with CFD simulations performed for the same geometry. Good agreement is found between semi-analytically calculated and numerically obtained flow characteristics, confirming that the quantitative determination of the α and C correction coefficients was reasonably accurate. This also shows that the proposed semi-analytical method can give a good approximation of average velocities and flow rates in gravity currents, for this geometry.

In **Paper [E]**, methods to determine the gas composition in the case of a strongly under-ventilated fire, i.e. when the flame is dying from lack of oxygen, are developed. The determination of the gas composition is essential in Fire Safety Engineering, as research shows that more of 70 % of casualties in fire are due to CO inhalation. The incompleteness of the combustion, and by consequence the amount of CO produced, is directly related to the amount of oxygen available in the compartment. This study is based on experimental results from backdraft studies in reduced scale and real-scale compartments, as well as in poorly ventilated conditions. Results from computer simulations carried out using Fire Dynamic Simulator (FDS), and analytical calculations are compared to the experimental results and observations. These comparisons are found useful to test the availability of the different methods to describe the combustion products due to strongly under-ventilated fires, as well as the flame behavior in its transition to extinction-free conditions to partial or total quenching. The results point out some difficulties due to the relative unreliability of gas measurements in the experiments, as well as the inaccuracy in the FDS flame extinction model and the necessary assumption made for the analytical calculation.

2 UNDER-VENTILATED FIRES AND BACKDRAFT: THE THEME AND THE OBJECTIVES

2.1 Under-ventilated fires

2.1.1 Generality and background

Researching the area of under-ventilated fires has not been conducted at the same rate as well-ventilated fires. This is partly due to the fact that quite complex physical and chemical processes occur during under-ventilated fires. However, it is under-ventilated fires that fire brigades in most cases face when arriving at the scene of a fire. Research regarding the growth of under-ventilated fires, where a great quantity of unburnt gases accumulates, is of considerable importance since such accumulation can result in severe consequences, both for fire-fighters and civilians.

A fire is characterized by the amount of heat (or energy) [5], [6], [7] it releases and its burning rates [8]. The influence of the enclosure on the fire is mainly due to the radiation from hot gases and walls and to the amount of oxygen available [9]. The hot gases will collect at the ceiling level and heat the ceiling and the walls. The walls and the hot gases layer will radiate towards the fuel surface, thus enhancing the burning rate. The availability of oxygen for combustion depends on the enclosure vents (leakage areas, openings, etc.). The combustion is thus incomplete, with a decrease in fuel burnt and energy release rate [10], and an increase in unburnt fuel and products of incomplete combustion.

Estimating the toxic hazards of combustion gases in a fire compartment is essential to fire safety engineering, as most of the casualties in fire are due to CO inhalation [11]. The incompleteness of the combustion is directly related to the amount of oxygen available [12]. Fires leading potentially to backdraft in a very tight compartment are strongly under-ventilated. Little data is available for such fires, and describing the extinction due to exhaustion of oxygen is still a challenge for computer models, for various reasons [13].

Fires in enclosures can lead to very sudden and hazardous phenomena such as flashover, ghosting flames, backdraft and smoke gas explosions [14]. This is due to the very strong dependence between fire behavior and ventilation, and to the radiative heat transfer between flames, gases, walls and fuel. Understanding the fire behavior and the factors controlling its development is essential for fire brigades, in order to prevent or mitigate the risks linked to compartment fires [15]. By studying backdraft, the most complex and dangerous of these phenomena in details, tools to identify hazards and increase knowledge of dangerous conditions can be developed. Recommendations for fire-fighters to mitigate the danger of backdraft have been reported in this thesis, within the FIRENET project (See Part 2.2 and Annex). A description of the backdraft is given in Part 2.2 below.

2.1.2 Terminology

In order to provide a concise description of the problem, it is essential to define the main terminology generally used in fire safety engineering, and especially in the case of under-ventilated fires. Fires in enclosures can be either well-ventilated or under-ventilated, depending on the amount of fuel and oxygen available and the stage of the fire.

Well-ventilated fire (fuel controlled): After ignition and during the initial fire growth stage, the fire is said to be fuel-controlled, since in the initial stages there is sufficient oxygen available for combustion and the growth of the fire depends entirely on the characteristics of the fuel and its geometry.

Under-ventilated fire (ventilation controlled): As the fire grows it may become under-ventilated, when there is not enough oxygen available to combust most of the pyrolyzing fuel. The energy release rate of the fire is then dependant on the amount of oxygen that enters the enclosure openings.

Diffusion flames: a diffusion flame refers to the case where fuel and oxygen are initially separated, and mix through the process of diffusion. Burning and flaming occurs where the concentration of the mixture is favorable to combustion. Although the fuel and the oxidant may come together through turbulent mixing, the underlying mechanism is molecular diffusion, process in which the molecules are transported from a high to low concentration.

Premixed flames: a premixed flame refers to the case where oxygen has mixed with fuel before it reaches the flame front. This creates a thin flame front as all of the reactants are readily available. If the mixture is rich, a diffusion flame will generally be found further downstream. Flames in accidental fires are nearly always characterized as diffusion flame.

Flashover: the transition from the fire growth period to the fully developed stage in the enclosure fire development. The formal definition from the International Standard Organization is “the rapid transition of a state of total surface involvement in a fire of combustible material within an enclosure”. In fire safety engineering the word is used to indicate the demarcation point between two stages of a compartment fire, i.e., pre-flashover and post-flashover.

Pre-flashover: The growth stage of a fire, where the emphasis in fire safety engineering design is on the safety of human. The design load in this case is characterized by its energy released rate curve, where the growth phase of a fire is of most importance.

Post-flashover: When the objective of fire safety engineering design is to ensure structural stability and safety of fire-fighters, the post-flashover fire is of greatest concern. The design load in this case is characterized by the temperature-time curve assumed for the fully-developed fire stage.

2.2 The backdraft phenomenon

2.2.1 Definition

When an under-ventilated fire dies due to lack of oxygen, the enclosed room can remain full of hot unburnt gases. If an opening occurs, for example a window breaks or fire-fighters open a door to the room, fresh oxygen is carried into it by gravity currents, and mixes with

gases. The mixing of gas with oxygen can create a flammable mixture resulting in ignition and an explosive or rapid combustion called backdraft [16]. The deflagration propagates, causing an extreme pressure build-up. The resulting flame travels at a speed of several meters per second. The occurrence and intensity of a backdraft is directly related to the mixing level and therefore to the characteristics of the gravity wave. This very hazardous and dangerous event has killed many fire-fighters in the past years ([17], [18], [19]).

The backdraft phenomenon is schematized in Figure 1. If there is sufficient ventilation, the fire might grow and reach flashover. On the other hand, in under-ventilated conditions, the burning rate of the fire is affected and the temperature rise is dampened (Point A), until the fire dies from oxygen depletion (Point B) and the temperature starts decreasing, with an atmosphere that remains rich in unburnt gases. If an opening is made, allowing a gravity current to enter and bring in fresh oxygen, the mixing process results in a more or less premixed situation. If this mixture ignites (Point C), the deflagration propagates and the temperature increases suddenly. The temperature increase in the case of backdraft and in the case of flashover is portrayed on the red dashed curve and the dotted curve respectively. The red dashed curve shows the temperature increase in the case of backdraft and the dotted curve in the case of flashover. Comparing the slope of the two curves shows that the temperature increases much faster than when flashover occurs, showing the very sudden and powerful nature of the backdraft.

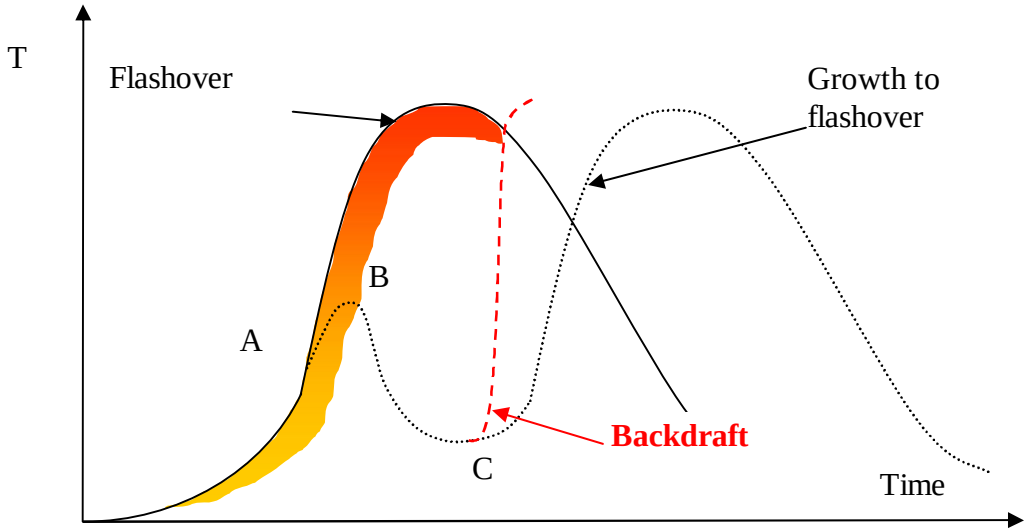

Figure 1: Temperature in an enclosure resulting in flashover or backdraft

2.2.2 Former studies on backdraft, State of the Art and the FIRENET project

Backdraft experiments have been carried out by Gojkovic [20] as a part of the FIRENET project, using methane as fuel and a modified shipping container to create under-ventilated conditions. Figure 2.a shows the container just after ignition of the backdraft. A ball of gases, due to pressure expansion is clearly seen just outside the compartment, shortly followed by the flame (Figure 2.b) spreading through the opening. The backdraft is then at its maximum (Figure 2.c) before decaying, burning the remaining gases (Figure 2.d). The whole process took only 4 or 5 seconds.

Until recently, limited research has been done on backdraft. The pioneer and most complete work on this phenomenon is undoubtedly the work done by Fleischmann [21] in his PhD

thesis. More recent research projects have studied the effect of mass fraction of unburnt fuels and opening on the occurrence of backdraft, and the mitigation effect of water mist (Gottuk et al. [22], Weng and Fan [23]).

Two of the main controlling elements in the study of backdraft are undoubtedly the time that elapses from the opening of the compartment to ignition, and the magnitude of gas mixing. The occurrence and intensity of backdraft is directly related to the intensity of mixing. As a result, one of the key parameters controlling the intensity of a backdraft is the mass fraction of unburnt fuel. Those problems have been studied in laboratory scale experiments ([4], [23], [24]), real scale experiments ([20], [22], [25]), as well as mathematical analysis and numerical modeling ([26], [27], [28]). There are currently several research projects dedicated to the simulation of the combustion and flame spread part of the backdraft ([29], [30], [31]).

During this PhD project, the University of Iceland was a partner in FIRENET, a European project dedicated to the study and understanding of under-ventilated fires and backdraft, coordinated by Prof. Wen from Kingston University (UK). Within this project, the candidate has collaborated with some major research groups, on different issues related to under-ventilated fires: the University of Naples (Italy) studying pyrolysis ([32], [33],[34], [35], [36], [37], [38], [39]), the University of Ulster ([40], [41]) and Kingston University (UK) [42] studying heat transfer and glazing, and the Laboratoire de Combustion et de Détonique in Poitiers (France) [43] and Lund University (Sweden) [20] for ghosting flames and backdraft experiments. The University of Liege (Belgium), Ansys CFX ([29], [44]) and Kingston University ([45], [46], [47], [48]) were mainly involved in the simulation of the flame spread during the deflagration. Within FIRENET, the task of the University of Iceland was mainly the characterization of the hydrodynamic process prior to ignition, i.e. gravity wave and mixing between hot and cold gases ([26], [27], [49], [50]).

Figure 2: Backdraft experiments (Gojkovic [20])

2.3 Objectives

From the works cited in the previous section, the following conditions that may lead to backdraft have been identified:

- Complete extinction by oxygen exhaustion must be achieved.

Backdrafts occur in confined places with very limited leakages, so that the fire consumes all the oxygen available for combustion until reaching the Limiting Oxygen Index (LOI) under which burning cannot occur.

- The mass fraction of unburnt fuel is a key parameter.

Experiments have determined a critical mass fraction value under which backdraft does not occur [23]. This value depends among others on the type of opening. It is also shown that if the mass fraction of unburned fuel increases, the over-pressure in the compartment also increases and the backdraft becomes more severe.

- Opening allowing fresh oxygen.

A sudden opening creates the gravity current that provides fresh oxygen inside the compartment.

- Hot spot or spark for ignition.

The flammable gas must be in contact with an energy source for ignition to occur.

The above mentioned backdraft conditions identified are prior to opening. There has been very little description of the gas dynamics and mixing between opening and ignition, and this is clearly a gap in the identification of the ignition conditions. This project aims to fill this gap, and therefore, analytical, experimental and numerical studies have been carried out, with the following main objectives:

- The development of an analytical model of a gravity wave, based on the translatory wave theory ([51], [52]) and classical fluid mechanics equations adapted to stratified flows [53], with the assumption of a three phase flow.
- The determination of correction factors for the calculation of the flow at the opening of a compartment full of hot gases [4]. These correction factors take into account the uneven distribution of velocity (α) and the effect of mixing and entrainment (C).
- The design, building and running of experiments to investigate in detail the behavior of the gravity wave, by mean of Laser Tomography and Particle Image Velocimetry. The experimental results allow identifying the different turbulent structures recognized from publications on turbulence.
- The development of a CFD model of the experiments using the Fire Dynamic Simulator (FDS) software.

Finally, results from the three methods are compared. Analytical and experimental results are used to calibrate and validate the CFD model. Once validated, this model allows quantifying the wave velocity, estimating the influence of different initial conditions or geometries, and to identify the main sources of mixing and quantification of the mixing intensity. These results will be an essential tool for the development and improvement of future models.

3 MEANS AND TECHNIQUES

3.1 Computational Fluid Dynamics

Computational Fluid Dynamics (CFD) is a modeling technique that uses numerical methods and algorithms to solve and analyze problems involving fluid flows. Programs based on this technique are widely used in the engineering and scientific communities in various disciplines such as aeronautics, medicine, meteorology, fire safety, mechanical engineering, combustion modeling to name only a few. It is not the scope of this thesis to describe CFD software in details, but this chapter will give a short description of its use in the domain of fire safety.

CFD models are based on a complete, time-dependant, three-dimensional solution of the fundamental conservation laws. The studied volume is divided into a multitude of sub-volumes to which the basic laws of mass, momentum and energy conservation are applied. The governing conservation equations for mass, energy and momentum contain the viscous stress components in the fluid flow as further unknowns. Substituting these into the momentum equation yields the Navier-Stokes equations, which are the fundamental basis of any CFD problem [54].

The most common CFD applications involve fluid flow and heat transfer. Applications can also involve other fire related applications such as combustion, phase change, multiphase flow or chemical reactions.

The range of CFD applications is so wide that no single code can incorporate the modeling of all the required physical processes. There are several codes that can be used for fire-involved problems. These, in turn, use a number of different approaches to the sub-processes that need to be modeled. The main sub-processes are:

- Turbulence modeling
- Radiation modeling
- Combustion modeling

3.1.1 Turbulence modeling

There are three different main approaches to turbulence modeling [55]: Direct Numerical Simulation (DNS), Reynolds Average Navier Stokes (RANS) and Large Eddy Simulation (LES).

DNS captures all of the relevant scales of turbulent motion, so no model is needed for the smallest scales. This approach requires extremely fine geometric grid and extremely small time steps. The computing requirements for the direct simulation are thus phenomenal, hence the need for other models to represent the smallest scales of fluid motion.

RANS is the oldest and the most widely used approach to turbulence modeling. With this method, the velocities are split into a mean velocity component and a fluctuating part. The

commercial code Ansys CFX [56] mainly based on a RANS model, has been used during this thesis work (see Paper [D]).

LES is a technique in which the smaller eddies are filtered and are modeled using a sub-grid scale model built on the Smagorinski model [57], while the larger eddies carrying energy are simulated. Fire Dynamic Simulator (FDS) ([57], [58]) is a software developed by the National Institute of Standard and Technology (NIST) [59] which uses LES to model turbulence. FDS is widely used within the Fire Safety community, and was the main simulation tool used during this thesis work. Therefore, the radiation and combustion models described below are the ones featured in FDS.

3.1.2 Radiation modeling in FDS

Radiative heat transfer is included in the radiation model via the solution of the radiation transport equation for a non-scattering gray gas. In a limited number of cases, a wide band model can be used in place of the gray gas model. The radiation equation is solved using a technique similar to a finite volume method for convective transport, hence its name: the Finite Volume Method (FVM). Using approximately 100 discrete angles, the finite volume solver requires about 15 % of the total CPU time of a calculation, a modest cost given the complexity of radiation heat transfer.

3.1.3 Combustion modeling in FDS

The FDS software uses a mixture fraction combustion model for most applications. The mixture fraction is a conserved scalar quantity, defined as the fraction of gas at a given point in the flow field that originated as fuel. The model assumes that combustion is mixing-controlled, and that the reaction of fuel and oxygen is infinitely fast. The mass fractions of all of the major reactants and products can be derived from the mixture fraction by means of "state relations", empirical expressions are obtained by a combination of simplified analysis and measurement.

3.2 Analytical study

One of the goals of this thesis work is to give an analytical description of the gravity wave in the backdraft process. These analytical studies are based on the theory of stratified flow to describe the wave inside the fire compartment and the critical flow approach for the vent flow calculation.

3.2.1 Translatory wave in stratified flows

In order to determine the velocity and the thickness of the gravity wave, we use the translatory wave theory [53], originally developed by Stoker [54]. Pedersen [55] has studied the problem of stratified flows extensively, and stated that the conventional equations of open channel flow can be applied to stratified flow, by exchanging the acceleration of gravity g with a reduced acceleration of gravity Δg. Δ is called the dimensionless reduced mass defined as: $\Delta_c = (\rho_c - \rho_h)/\rho_c$.

This approach is described in details in Paper [C], in the second part of this thesis. An application example is discussed later in Section 5.1 of this document.

3.2.2 Critical flow approach to vent flow calculations and the Froude number

Essential problems such as the state and evolution of the fire or smoke filling and evacuation depend on the flow through the opening to the fire compartment. The first description and modeling of vent flow were carried by Kawagoe [60], assuming a "well mixed" condition. Several studies have found that his model tends to overestimate the actual vent flow, particularly for large opening. Precise descriptions can be found for various shapes of openings, resulting from experiments ([61], [62], [63]) or from numerical simulations [64].

The most widely known methods for calculating vent flows are the ones developed by Emmons [65] which are also cited in the SFPE Handbook [3]. These formulas permit to achieve numerical results in the case of well-mixed conditions, however this is not the case in stratified conditions as the difference in interface elevation between the opening and the room is unknown. This problem is eliminated by using the critical velocity approach.

In the SFPE Handbook [3], there are a few references to literature in hydraulic science. However since their publication there has been some progress in hydrodynamics and hydraulics, which has not found its way into vent flow formulas available to fire safety engineers, especially in stratified flows. Paper [D] therefore introduces the concept of specific energy and critical flow, and applies it to the vent flow in Gojkovic's experiments [19]. This concept assumes that the hot fluid flows freely out of the compartment, and consequently passing the obstacle at the top of the vent requires minimum specific energy. A short description of the theory of critical flow and its application to vent flow is presented at the end of Paper [D].

The concept of specific energy and critical flow has been developed to study open channel flow [66]. For a rectangular channel flow of depth y and discharge per unit width q = Q/b = V.y, the specific energy is:

$$E = y + \frac{q^2}{2gy^2} \tag{1}$$

This energy is minimal for dE/dy = 0, referred as the critical flow condition, and the corresponding depth called the critical depth y_{cr}.

$$\frac{dE}{dy} = 0 = 1 - \frac{q^2}{gy_{cr}^3} \tag{2}$$

$$y_{cr} = \left(\frac{q^2}{g}\right)^{\frac{1}{3}} \tag{3}$$

$$q^2 = gy_{cr}^3 = (gy_{cr})y_{cr}^2 = V_{cr}^2 y_{cr}^2 \tag{4}$$

The combination of Eq. (3) and (4) leads to the Froude number:

$$Fr = \frac{V_c}{\sqrt{gy_{cr}}} = 1 \tag{5}$$

The dimensionless Froude number is the ratio of inertial and gravitational forces that describes the different flow regimes of open channel flow. These flow regimes depend on the value of the specific energy, as shown in Figure 3.

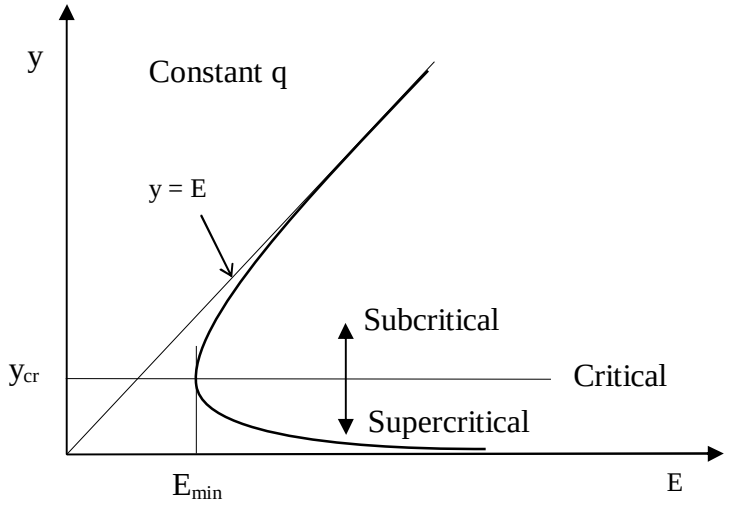

Figure 3: Specific energy E versus depth y. E is minimal at critical depth y_{cr}

For $E < E_{min}$, there are no solutions, and thus such a flow is physically impossible.

For $E < E_{min}$, there are 2 possible solutions:

- Subcritical flow at large depth with $V < V_{cr}$ In this case $Fr < 1$.
- Supercritical flow at small depth with $V > V_{cr}$ In this case $Fr > 1$.

For $E = E_{min}$, the flow is critical and $Fr = 1$. This is an equilibrium state where the flow requires minimum specific energy to pass over an obstacle.

As discussed in [27], the conventional equation of open channel flow can be applied to stratified flow by introducing the reduced acceleration of gravity Δg. This gives the Froude number in its densimetric form, characterizing a stratified flow:

$$Fr_{\Delta} = \frac{V}{\sqrt{\Delta g L}}$$

The densimetric Froude is particularly useful in describing the flow through an opening or the characteristics of the gravity wave. It obeys the same rules for subcritical, critical and supercritical flow described above.

The reduced acceleration of gravity approach is used in Paper [C], in which a theory of a three phases flow behavior for the description of the gravity wave behavior is developed.

3.3 Experimental flow measurement techniques

The variables most commonly measured to describe flow characteristics are pressure, flow rate and velocity. Techniques for pressure and velocity measurements can be divided into

two categories. In the first category, measuring instruments, for examples Pitot tubes or hot-wire anemometers, are placed at certain locations in the flow. The second category is based on marker methods, where identified particles are placed into the stream. By recording and analyzing the motion of these particles, the velocity of the flow itself can be deduced. The major advantage of using marker methods is that the flow field is not disturbed by the presence of a probe or a wire support. A further advantage is that marker methods provide excellent spatial resolution.

In this thesis work, undisturbed flow and excellent spatial resolution are essential requirements. Two different measurements techniques have been used during this research project, Laser Tomography and Particle Image Velocimetry (PIV). These are both optical techniques based on recording movements of particles on a laser sheet. The tomography gives an excellent qualitative description of the flow, while the PIV computes the velocity vectors for each particle, allowing a quantitative description of the flow.

3.3.1 Laser Tomography

The term tomography refers to imaging by sections, which gives a diagnostic in a thin light sheet created by a laser source. The method is used in medicine, archaeology, biology, geophysics, oceanography, material science, astrophysics and other disciplines. In fluid mechanics, tomography is mainly used to visualize the structure of flows.

Principle

The experimental set up typically consists of a laser source creating the light sheet and a high speed camera, linked to a computer, for system control and data acquisition. Images of tracers (seeding particles) are recorded as they cross the light sheet. The movement of the flow is then characterized, providing that the recording between successive images is short enough to show the displacement of particles. A typical layout for tomography is shown in Figure 4.

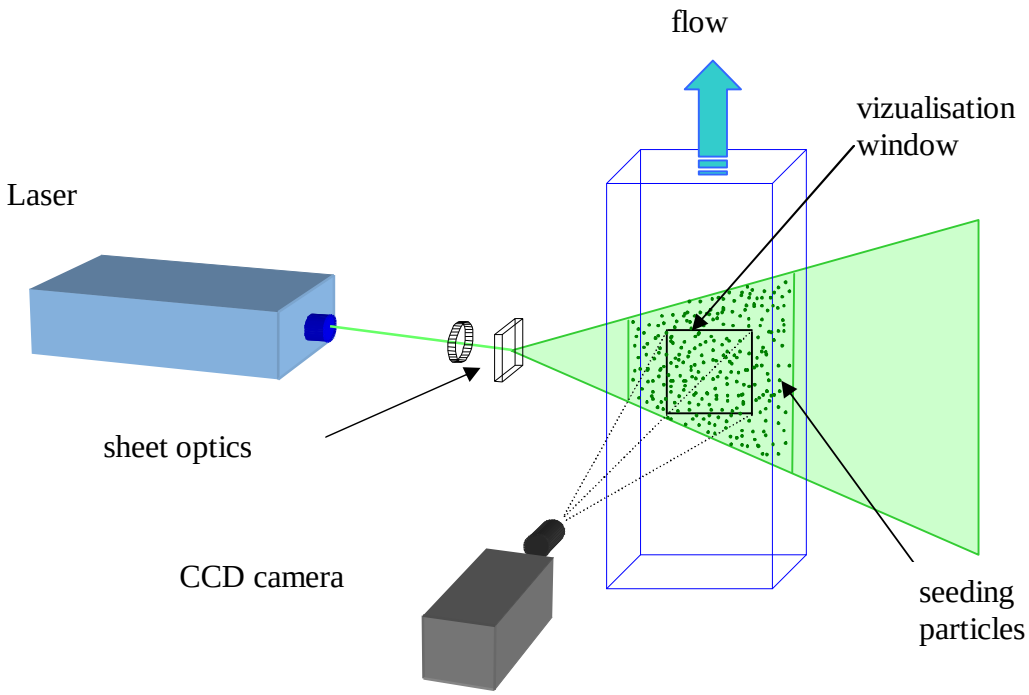

Figure 4: Typical experimental layout for tomography

Advantages and disadvantages

Laser Tomography is a non-intrusive method, as the added tracers (particles) cause negligible distortion to the flow.

The time resolution is very good, allowing the capturing of very fast phenomena such as turbulence and vortex formation. Typically, tomography gives excellent qualitative results, even for very unsteady flow.

The outputs are movies files in .avi format, which are easy to visualize and can be read and modified with various software programs.

The main disadvantage of this method is that it only gives qualitative results. There are some possibilities to extract quantitative values by image treatment using software like matlab, but this requires the use of quite complex programming methods.

3.3.2 Particle Image Velocimetry

Principle

Particle Image Velocimetry is a pattern recognition technique. The set-up typically consists of a laser with sheet optics, one or two digital cameras, and a computer with a timer unit to control the system and store the data. Velocity fields are measured in a planar 2D domain, created by a laser sheet sectioning a flow seeded with particles. The measurement area (visualization window) in this plane is cropped by the field of view of the camera(s). A schematic view of the apparatus and its typical layout is shown in Figure 5.

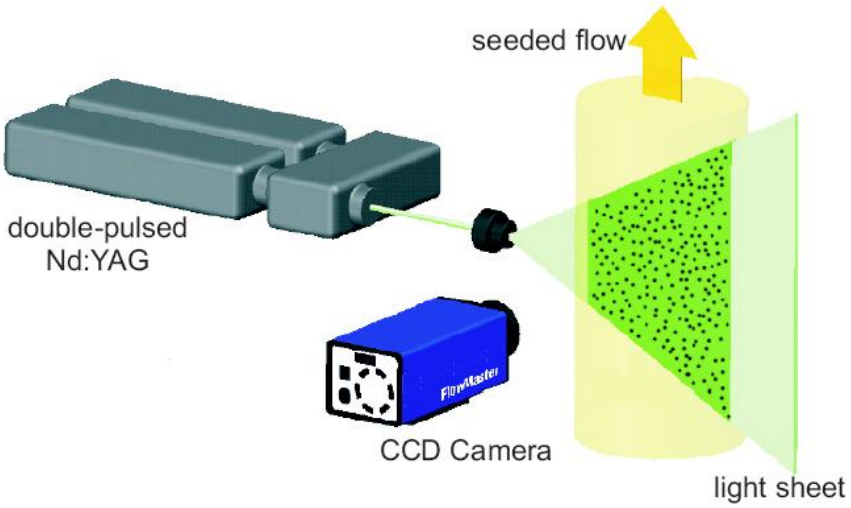

Figure 5: Typical experimental layout for PIV measurements (LaVision Davis [67])

The area of interest (visualization window) is illuminated by two consecutive, short-duration light pulses (typically 10 nanoseconds to 100 microseconds) produced by the laser, and the images are stored in two different frames in the same picture. The frames are then subdivided into a certain number of cells called interrogation windows. The movement of particles is then calculated by cross correlation of the pixel intensity in the interrogation window between the 2 frames.

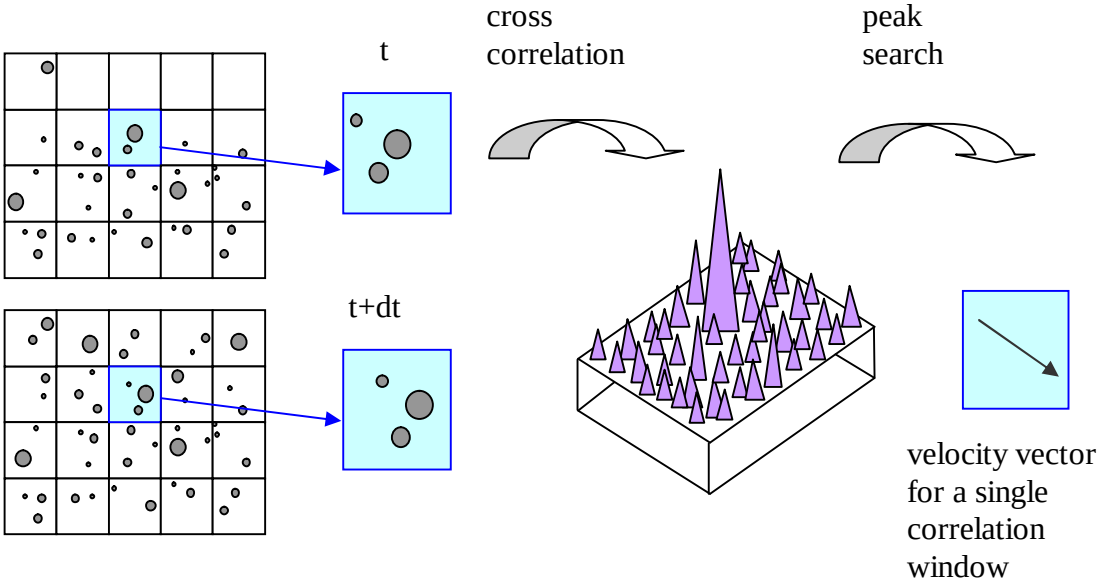

Figure 6: Principle of PIV measurements using cross correlation between successive frames

The correlation function is defined as

$$Cor(dx,dz) = \sum_{x=0,z=0}^{x<n,z<n} I_{pix1}(x,z) \times I_{pix2}(x+dx,z+dz) \qquad (7)$$

$$-\frac{n}{2} < dx < \frac{n}{2}; -\frac{n}{2} < dz < \frac{n}{2}$$

I_{pix1} and I_{pix2} are the image intensity of the first and second interrogation window and the 2D-array, C gives the correlation strength for all integer displacements (dx,dz) between the two interrogation windows, while n is the size of the interrogation window and usually also the size of the correlation plane, i.e. ±n/2 is the maximum displacement computed.

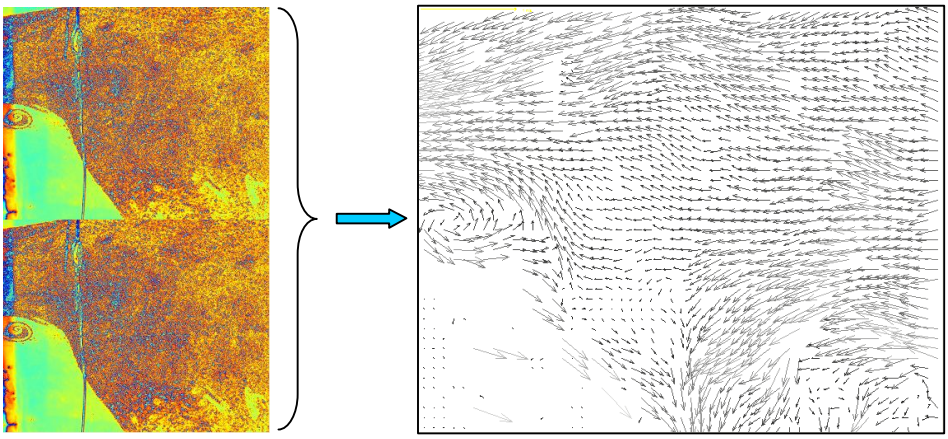

Figure 7: PIV measurements. Successive frames (left) and resulting velocity field after cross correlation

Advantages and disadvantages

As for Laser Tomography, PIV is a non intrusive method, as the added tracers (particles) cause negligible distortion to the flow.

The main advantage of PIV compared to most of the measurements techniques is that this method allows both quantitative and qualitative observations.

PIV measurements give a full description of the velocity field within the desired visualization window. This allows direct comparison with velocity fields obtained by CFD software.

The most significant disadvantage of PIV is the time resolution. The PIV camera used during the experimental series carried out in this PhD work allowed a double frame recording frequency of 2 to 4 Hz. This is sufficient for steady flows, but is clearly unsufficient for unsteady flows. In these cases, an “outerleg” correlation needs to be performed to check that the resolution time scale is smaller than the time scale of turbulence.

Another disadvantage is the huge amount of output data obtained, which requires significant data processing work. However, these results can be easily visualized using the commercial PIV software used in experiments. For advanced post-processing, it is advisable to use more complex mathematical tools, for example in this work the free toolbox PIVmat to extract in Matlab results from Davis [67].

The third disadvantage is that the quality of the output data is strongly dependant on the quality and homogeneity of seeding. Obviously, if there are no particles in an interrogation window at the time of recording, the resulting velocity within this particular window will be zero.

4 CFD SIMULATION APPLIED TO UNDER-VENTILATED FIRES AND BACKDRAFT

As mentioned earlier in Chapter 3, CFD software allow the modeling of most of the sub-processes involved in fires such as combustion, turbulence and radiation. CFD software is very widely used in fire safety for the design of common buildings, in which potential fires should be well-ventilated. A typical example would be the simulation of fire in a shopping mall, in which the fire safety engineer can simulate flame spread, smoke movement, and evacuation to name a few features, as well as test mitigation techniques such as the use of sprinklers, evacuation routes or smoke evacuation by exhaustion system.

The case of under-ventilated fire and backdraft is less common as it involves special and complex features such as incomplete combustion, extinction by oxygen exhaustion and, in the case of backdraft, highly turbulent flow and gas mixing. Until recently, very little research had been done on under-ventilated fires, and CFD software is still unsuccessful in correctly simulating fire behavior in these very complex situations. A part of this thesis work was to test FDS in strongly under-ventilated conditions and suggest recommendations to improve the extinction model; this work is discussed in Paper [E]. Another important part of this thesis work focused on the gravity currents and the mixing of cold and hot gases (Papers [B], [C] and [D]), i.e. the gas dynamics of the backdraft process prior to ignition.

CFD modeling has also been used to test common fire-fighting tactics in a possible backdraft situation, in order to demonstrate the capability of CFD to provide recommendations for backdraft mitigation. Furthermore, CFD models can be a very useful complement to classical fire-fighting training, as they demonstrate complex and dangerous phenomena such as backdraft or flashover.

4.1 Combustion

FDS uses by default the mixture fraction combustion model, which is described in some detail in [59].

At the beginning of this thesis work, the first attempts to simulate a backdraft clearly pointed out that the combustion model would be a problem, as the model assumes that “mixed is burnt”. More precisely, the combustion model is based on a single-step reaction, with the physical limitation that it assumes that fuel and oxygen burn instantaneously when mixed, without the need of an ignition source and irrespective of the amount of available oxygen. This will be discussed in Section 4.3 which discusses the limitations.

In order to suggest solutions for improvements, it is necessary to identify the particularities of under-ventilated fires. These are extracted from literature concerning under-ventilated fires, strongly under-ventilated fires and former backdraft experiments. These particular characteristics are listed below, and are described in greater detail in Paper [E].

- Obs. 1: Heat Release Rate is irregular ([68], [69]).
- Obs. 2: The flame is “crawling” for oxygen ([70], [71], [72]).

- Obs. 3: The hot layer interface, calculated using the idealized 2-zone approximations [73], is situated slightly above the burner surface ([4], [23]).
- Obs. 4: The flame is completely extinguished after a certain time, depending on the available amount of oxygen. This is always observed in every backdraft experiments ([4], [22], [23]). Moreover, there is a Limiting Oxygen Index, noted LOI, concentration level under which methane cannot burn (about 15 mol %).

Once these characteristics are identified, a first FDS model is set-up and results are then compared to the previous observation. It appeared that the fire behavior in FDS didn't match these observations, resulting in a non natural fire behavior.

Various solutions were tested to improve the basic model, by creating successive models, M0, M1 and M2, with the following improvements:

- Model M0: Basic model.
- Model M1: improvement step 1: Introduction of leakages.
- Model M2: improvement step 2: Introduction of leakages and forced extinction.

The following table shows the evolution of these FDS model, depending if their results match to some degree the observations described above or not:

Table 1: Evolution of the FDS model

Model	Obs. 1	Obs. 2	Obs. 3	Obs. 4
M0	no	no	no	no
M1	yes	yes	yes	no
M2	yes	yes	yes	yes

The study by Sinai [74] highlights how leakages affect the fire behavior. They are very important and should not be omitted by engineers or researchers while simulating a fire in a confined area. Currently, the only way to control the extinction is to modify manually the Limiting Oxygen Index when a certain level of oxygen is reached closed to the burner. A possible solution could be to create a variable (LOI), that will automatically change for certain conditions with respect to temperatures and oxygen concentration.

4.2 Gas dynamic and gravity currents

The major effort of this thesis work was concentrated on the study of gravity currents and gas dynamic inside a building. This concerns movements of smoke and hot vitiated gases, or how to prevent the formation of explosive atmospheres. Smoke venting is of major concern in every fire situation, and especially in public buildings, where evacuation could be compromised due to lack of visibility and the public therefore be in danger of inhaling vitiated gases. The degree of difficulty of a fire-fighting intervention may also depend, among other things, on the degree of visibility. The prevention of the formation of explosive

atmosphere generally concerns industrial plants with potential explosive hazards such as chemical plants, but also air-tight buildings or rooms open to the public such as saunas, in which smoke gas explosions were reported to happen.

Several mitigation techniques of explosion hazards are based on forced or natural ventilation. In the following section, we will discuss this matter by giving two examples, one concerning the storage of hydrogen in an industrial plant, the other one concerning fire-fighting tactics in a possible backdraft situation.

4.2.1 Hydrogen storage and mitigation techniques

The storage of hazardous substances is a major safety issue. A typical example is the storage of hydrogen [75]. No CFD calculation for this situation has been carried out during this thesis work. However, the author has obtained a postgraduate degree in hydrogen safety from the University of Ulster, as part of his thesis work. Moreover, the use of hydrogen is rapidly increasing as it has the potential to be a long-term alternative to petroleum-based liquid fuels in some transportation applications, and Iceland has the ambition to become the first hydrogen based economy. Hence, problems with hydrogen storage will become more and more common, and design engineers should be aware of these mitigation methods and be able to simulate their effect by means of CFD calculation.

Hydrogen brings together three major factors in the creation of explosive atmosphere (ATEX), i.e wide flammability range, small minimum ignition energy and low density. Prevention of damage by explosions in case flammable gases are released unintentionally is regulated by the ATEX directive 1999/92/CE, relative to minimum requirements for improving the safety and health protection of workers potentially at risk from explosive atmospheres (ATEX).

Hydrogen removal techniques must be used whenever hydrogen is stored in a confined place, to prevent the formation of an explosive atmosphere. These techniques are either ventilation or inerting.

Ventilation is the most useful and common safety barrier to prevent the formation of explosive atmospheres in such environments. The basic principle of ventilation is to bring fresh air into a room and to remove the inside air (this aspect is sometimes called extraction), thereby preventing the accumulation of explosive substances. The benefits of ventilation with respect to control of explosive atmospheres are threefold:

- Ventilation prevents the accumulation of explosive gas, by removing it.
- Ventilation limits the size of explosive volumes by dilution with fresh air. In that case it is sometimes called dilution ventilation.
- Ventilation limits the resident time of explosive atmospheres, since it is active for a longer time than the duration of a leak of combustible gases.

Ventilation can be either forced (mechanical) or natural. The performance of natural ventilation fluctuates since it depends heavily on climatic conditions, whereas mechanical ventilation can provide a constant and controlled ventilation flow, and can be sized appropriately. For natural ventilation to be effective, openings at ground and ceiling levels should be provided, as it is driven by temperature differences, i.e. gravity currents similar to the case of backdraft, and by wind or draughts.

As far as mechanical ventilation is concerned, the main question to be answered when using this measure as a protection barrier is how to size the ventilation rate, so that hazardous explosive atmospheres cannot be formed in the event of non-catastrophic accidental leaks. Sizing can be determined using “best practice” documents; or calculations based on assumed leakage rates or based on the hydrogen leak detection sensitivity.

These best practices are always related to the volume of the room, but not the value of the leak rate. Ventilation rates of 10 a.c.h (air changes per hour) are generally considered adequate ventilation rates in normal conditions, and they should be increased to about 20 a.c.h in the event of an emergency (hydrogen detection).

Ventilation rates can also be calculated assuming a credible, non-catastrophic, leak rate, for example by using the formula below, where hydrogen concentrations are assumed homogeneous in the compartment:

$$Q_{vent} = \frac{100}{LFL} Q_{leak} K_{safety} \quad (8)$$

where Q_{vent} is the flow rate through the ventilation system and Q_{leak} is the flow rate through leakages. LFL is the Lower Flammability Limit (25% in the case of hydrogen), and K_{safety} is a safety factor, which in the case of hydrogen, should be either 4 to ensure that the steady state concentration is 25% of the LFL, or 10 to ensure a steady state concentration level of 10% LFL.

In order to be effective, the ventilation rate needs to be adequately designed in terms of technique and performance. CFD has proven to be very efficient for this purpose.

Inerting is an important way to prevent the formation of explosive atmosphere. It is defined as the replacement of a sufficient proportion of oxygen contained in a gaseous atmosphere by an inert gas, to make it impossible for the atmosphere to be ignited or a flame to propagate. There are several methods of inerting systems where hydrogen is to be used and the main ones are:

- Pressure swing or vacuum swing method: This involves pressurizing the system with inert gas, and relieving the system back to atmospheric pressure. Vacuum swing is based on the same principle, but involves the evacuation of a closed system and restoration to atmospheric pressure by the admission of inert gas. It is useful where a system can withstand vacuum but cannot withstand pressure.
- Flow-through method: this method is used where systems can be neither evacuated nor pressurized, a flow-through technique can be used, it involves the replacement of an oxidant by a continuous flow of inert gas into a system which is vented to atmosphere. This is less efficient than the pressure swing or vacuum swing method, and great care is required to ensure that adequate purging is achieved. A high flow rate is required to ensure adequate mixing.
- Displacement method: this method relies on using an inert gas of significantly different density to that which is to be purged, and where significant mixing does not take place. It is used typically on the inerting of very large vessels, where it would not be possible to ensure adequate mixing if an inert gas of substantially the same density were to be used.

As for ventilation, the efficiency of the inerting method depends on gas movements, and CFD calculations are very useful in its design.

Natural ventilation is an application of the gravity currents, widely studied in this project. Both methods are typical fluid mechanic problems that are worth being simulated using CFD. Readers can find examples of CFD calculation concerning hydrogen safety in tunnels or parking lots [76].

4.2.2 Evaluation of Fire-fighting tactics in a possible backdraft situation

A study was made to evaluate classical fire-fighting tactics in a possible backdraft situation while arriving at the scene of an under-ventilated fire. The goal was both to present recommendations for fire-fighters in a particular backdraft situation, and to demonstrate the potential use of CFD simulation for evaluation or fire-fighters' training. This study is described in Paper [B]. The choice of tactics was based on the experience of one of the co-authors, who has worked as a fire officer for over a decade. Then, the effectiveness of these tactics in mitigating the danger of backdraft was estimated.

A basic scenario in a 3 room building is created and simulated. It is assumed that at the time of the fire-fighters arrival, the fire has burnt for quite a long time and has died from lack of oxygen. However, hot unburnt gases remain inside the building and the temperature and the gas concentrations are uniformly distributed within the 3 rooms. When fire-fighters open the front door, they allow fresh oxygen carried by the gravity current to enter and mix with the hot gases thus creating a flammable mixture. If the flammable region reaches an ignition source, a backdraft may occur. The danger of backdraft then depends on the thickness of this flammable region and on the time it takes for the gases to be vented out of the building. The effectiveness of each tactic regarding the mitigation of backdraft is estimated by comparing these two parameters, thickness and venting time, with the basic scenario where fire-fighters just open the door but do not take other actions. The chosen scenarios are:

- Scenario 1: Reference scenario where no action is taken.
- Scenario 2: A life saving operation where fire-fighters enter the building.
- Scenario 3: Natural ventilation of the building by opening a window at the back of the building.
- Scenario 4A: Ventilation of the building using Positive Pressure Ventilation (PPV) at low flow rate 3.73 m^3/s.
- Scenario 4B: Ventilation of the building using PPV at high flow rate 5.38 m^3/s.
- Scenario 5: Incorrect use of PPV at high flow rate 5.38 m^3/s (No discharge opening).
- Scenario 6: Dilution of the unburnt gases, by use of water spray before opening the door. Four different levels of dilution are simulated, from 25% to 10% of unburnt gases.

The flammability envelope is bounded by the Upper (UFL) and Lower (LFL) Flammability Limit. The limits considered in this study are assumed to be similar to those of methane's, i.e. LFL = 5 (vol. %) and UFL= 15 (vol. %). In Figure 8, the red isosurface corresponds to UFL and the blue to LFL, and the volume in between is the flammable region. Vertical animated planar slices passing through the middle of each room display the values of unburnt fuel concentration.

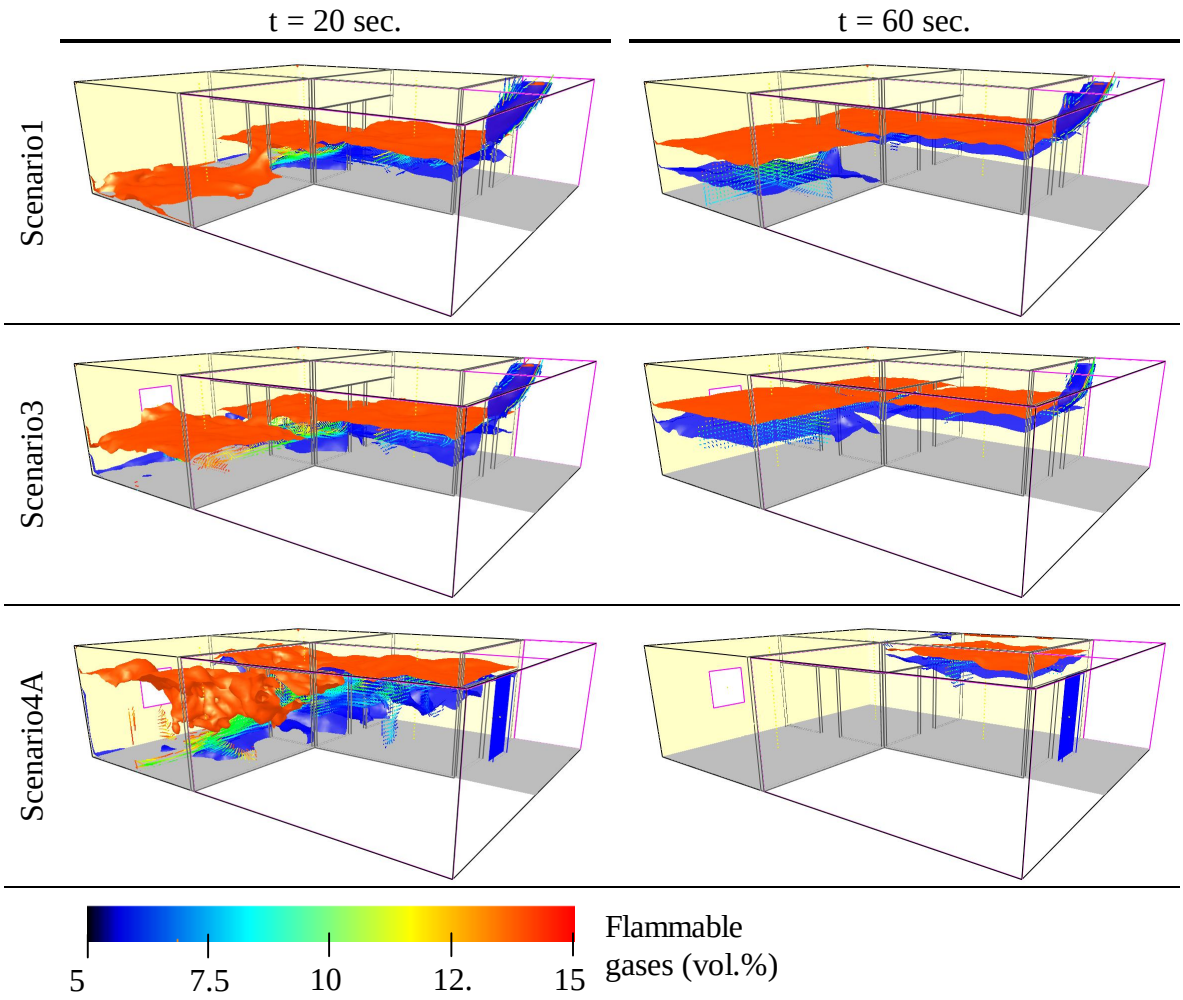

Figure 8: Flammability envelope at 20 and 60 seconds after opening for scenarios 1 (reference), scenario 2 (natural ventilation) and scenario 3(ventilation with PPV)

Here, only an example of the effectiveness comparison of the three scenarios is given. The comparison shows that natural venting (scenario 1) is rather efficient as the volume of the flammability envelope has reduced after 60 seconds, when compared to scenario 1. This comparison shows that PPV is very efficient in venting out gases (the building is almost empty of flammable gases after 60 sec.) but induces a high level of mixing due to forced flow during the first seconds. We can then conclude that using PIV increases the danger of backdraft at the beginning but creates a safe situation within a short time. This information can be crucial for fire-fighters.

4.3 Limitations and recommendations

The most important limitation to simulating the whole backdraft process with CFD software comes from the combustion model, with the “mixed is burnt” process which assumes that fuel and oxygen burn instantaneously when mixed. This is of course a huge problem when trying to simulate backdraft. What happens is that prior to opening, the fire has died out of oxygen, and the oxygen concentration in each cell inside the compartment is below the Limiting Oxygen Index (LOI), below which combustion can not occur. When an opening is

created, fresh oxygen will enter and its concentration in the first cell which receives this fresh oxygen will rise above the LOI, creating a flammable mixture. The combustion model will automatically assume burning in this particular cell. This process will occur in every cell receiving fresh oxygen, and the flame will spread cell by cell. Consequently, when simulating backdraft using the conventional FDS code, the burning will start right at the opening, and move toward the compartments, without any ignition source. This "mixed is burnt" problem hasn't been solved yet, and researchers at NIST and in other research groups are looking for improvements. Specialists and developers agree that actual computer capacities are not sufficient enough to solve this problem in a satisfactory way at this point in time.

Sub-grid simulation of extinction due to oxygen starvation or by introduction of a suppression agent is still an area of research within the fire community. Ideas for improvements have been discussed in the previous paragraph and in Paper [E], but the development of a combustion model suitable for under-ventilated fires is still a challenge. A detailed description of the combustion model is given in [57].

One of the particularities of under-ventilated fires is the incomplete combustion. The production of unburnt gases, soot and dangerous products, such as carbon monoxide are strongly dependant on the degree of incompleteness. Comparisons of various CFD calculations with experiments give deceptive results, especially concerning gases having a very small contribution in the mass balance. The reliability of gas measurements in the experiments is often questionable as they are very sensitive to the measuring locations and combustion conditions. It is consequently difficult to conclude on the CFD capability in predicting accurately concentrations of combustion products in the case of strongly under-ventilated fires. As inhalation of carbon monoxide is the main source of casualties in fire, engineers and scientists should take special caution, considering for example very conservative safety factors, while estimating combustion product from numerical simulations.

FDS allows only rectilinear geometry, and therefore the shape and position of features such as obstacles, probes or vent must match the rectangular mesh, otherwise FDS will automatically adapt the size of the features component to the closest grid size. This might require smaller or multiple meshes in case some features are small compared to the global geometry, which often has to be approximated to fit the rectangular mesh size. Non-rectangular features also have to be approximated to fit the mesh, for example a cylindrical column will have to be divided into rectangles matching the mesh.

The use of FDS is limited to low-speed, with a Mach number smaller than 0.3. This assumption rules out using the model for any scenario involving flow speeds approaching the speed of sound, such as explosions, choke flow at nozzles, and detonations. In the case of backdraft, the overpressure will make it possible for the flames to reach speeds up to 15 to 20 m/s. The speed of sound depends in dry air is given approximately by $V_{sound} = 331.4 + 0.6T$. If T = 100°C, so the Mach number will be roughly between 0.038 and 0.051. FDS should then be suitable to model the flame spread during a backdraft, but this assumption should be kept in mind while modeling complex fire related phenomena.

5 THE ANALYTICAL MODEL

The goal of this chapter is to develop two analytical models that help describing density driven flows in backdraft studies. The first model calculates the head velocity of the gravity wave on a flat bottom within a compartment, and the second develops equations at the opening, applying the critical flow theory to vent flow calculations. The results will be compared in Chapter 8 to experimental results and results from a CFD model. Developing analytical models has the advantage of presenting simple results that can easily be used for engineering purposes and for fast estimation of the velocity of the wave, and consequently the duration of the risk of backdraft after creating an opening in case of fire-fighting operations. Simple analytical models also allow direct quantification of the main variables driving the processes and therefore give an indication of the importance of each variable.

5.1 Gravity wave on a flat bottom

The model described here is based on classic hydraulic equations for two layer flows, preliminarily developed to describe two layer flows in estuaries and fjords [51]. Pedersen [53] stated that formulas from conventional open channel flows also apply to stratified flows just by exchanging the acceleration of gravity g with a reduced acceleration of gravity Δg.

The compartment is closed at the beginning, but then suddenly a window or door opens. Cold air flows in and an equal amount of hot air flows out. When the door opens, the initial pressure surge will quickly settle down and a neutral plane will develop near the middle of the opening, with inflowing air below and outflowing air above it. The gravity wave will then develop in three phases, provided the compartment is long enough. A time history of the flow velocity is schematically shown in Figure 9.

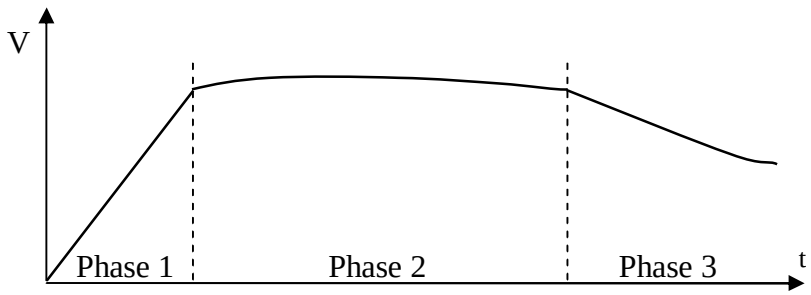

Figure 9: Time history of the flow velocity when air enters a flat bottom compartment

The evolution of the flow can be divided in three different phases. During Phase 1, the wave accelerates from zero to full velocity. According to Stocker's theory in [52], the second phase is the translatory wave, moving with almost constant velocity. Finally, the third phase is the retarding wave, when it looses momentum and slows down. During the first phase, the friction is neglected, so the acceleration is linear. The average velocity is consequently half of the maximum velocity, at the beginning of the second phase.

During the second phase, the dense bottom current is treated as an open channel flow in a gravity field Δg instead of g. Open channel flow equations have, as a solution, a translatory wave with constant wave velocity equal to the water velocity. In this phase, we have a translatory wave pushing the light fluid out, and slowly pushing the interface upwards. The three following equations are used to analyze the flow:

- The depth integrated energy equation for the upper layer.
- The momentum equation for both layers.
- The momentum equation for the lower layer.

The solutions of these equations and the explanation of the symbols are described in detail in Paper [C]. The outcome is a graphical method to determine the dimensionless wave velocity C_Δ and the dimensionless gravity current thickness on depth ratio ψ, knowing the friction coefficients f_i or C_f or vice versa.

We consider the following dimensionless coefficients A and B, which represent the frictional effect:

$$A = \frac{\ell}{h} f_i \,, \quad B = 2\frac{\ell}{h} C_f \text{ with } \psi = \frac{y_{c,n}}{h}$$

$$\frac{V_c}{\sqrt{\Delta g h}} = C_{a,\Delta} = \sqrt{\frac{\psi^2}{\left(\frac{\psi}{1-\psi}\right)^2 - \frac{2\psi}{1-\psi} + \frac{A}{(1-\psi)^2} + B}} \tag{9}$$

$$\frac{V_c}{\sqrt{\Delta g h}} = C_{b,\Delta} = \sqrt{\frac{\psi^2 - 2}{2\left(A\left(1 - \frac{2}{\psi^4}\left(\frac{\psi}{1-\psi} + \mathrm{Ln}(1-\psi)\right)\right) - \frac{B}{\psi^2} - \frac{\psi}{1-\psi}\right)}} \tag{10}$$

Eq. (9) and (10) are both expressions of the dimensionless wave velocity, so this set of equations has to satisfy the condition $C_{a,\Delta} = C_{b,\Delta}$ and can be solved by iteration and used to produce Figure 10:

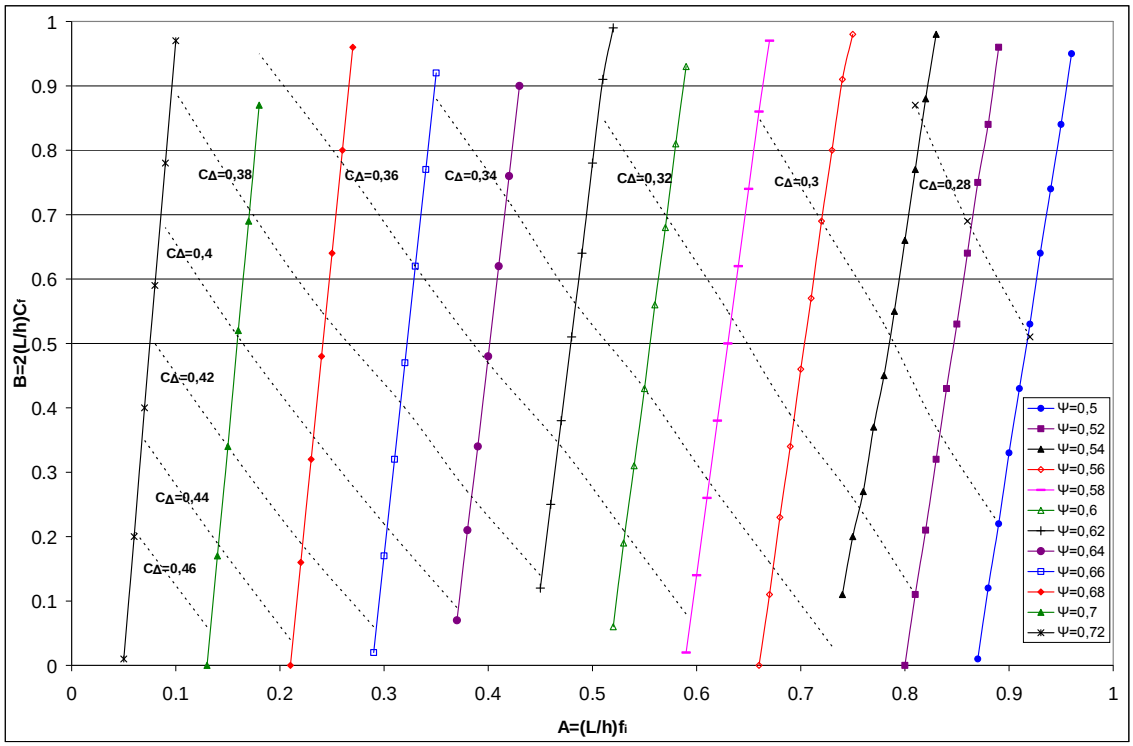

Figure 10: Couple (A,B) solution, and iso-values of C_{Δ} satisfying the condition: $C_{a,\Delta} = C_{b,\Delta}$

Figure 10 can be used to determine the velocity and the neutral height in the opening when A and B is known, or to estimate A and B in experiments where the velocity and the neutral plane position is observed.

As an example, let us consider a 50 m long corridor, 2.8 m high, filled with hot gas with density 75% of air. A glowing wire acts as an ignition source at the far end. We want to estimate the travel time of the wave from the opening to the ignition source, to check if there is sufficient time for the fire-fighters to escape the fireball. From tables, we can estimate $C_f = 0.003$, $f_i = 0.013$. The time to ignition of the fireball can be estimated as follows:

$$B = 2\frac{\ell}{h}C_f = 2\frac{50}{2.8}0.003 = 0.11$$

$$A = \frac{\ell}{h}f_i = \frac{50}{2.8}0.013 = 0.23$$

Figure 10 gives approximately $\psi = 0.68$ and $C_{\Delta} = 0.43$

$$t = \frac{\ell}{C_{\Delta}\sqrt{\Delta g h}} = \frac{50}{0.43\sqrt{0.25 \times 9.82 \times 2.8}} = 44\,\text{sec.}$$

This is a very rough estimation, but gives the fire-fighters idea of the time they have to open the door and run for cover.

5.2 Flow at the opening

When the air wave comes flowing through a door or a window driven by a fixed density difference, we have a situation where the opening regulates the flow into the room through

formation of critical velocities in the opening. The inflow also depends on flow coefficients that are due to boundary layer mixing and friction at the interface between the two fluids. Such coefficients have to be extracted from experiments or numerical studies and generally, one global correction factor between 0.6 and 0.7 is admitted in literature without further research [77]. In this thesis work, a particular effort was made to discuss the physical meaning and to determine the flow coefficients that suit our geometry and boundary conditions. Our primary results were adjusted by comparing them with the data from Fleischmann and McGrattan [4], who conducted experimental and numerical analysis of gravity current prior to backdraft. In these experiments, the velocity profile was found very different from the profiles based on pressure difference calculation [65].

The coefficients considered are α, due to uneven distribution of velocities, and C due to the mixing and entrainment. By solving the depth-integrated energy equation for the hot layer and considering the continuity equation, the average velocities $V_{op,h}$ and $V_{op,c}$ can be expressed as:

$$V_{op,h} = C_h \sqrt{\frac{1}{\alpha_h} \Delta_h g \left(1 - \frac{1}{1 + (\rho_h / \rho_c)^{1/3}} \right) h} \quad \text{with} \quad \Delta_h = \frac{\rho_C - \rho_h}{\rho_h} \tag{11}$$

$$V_{op,c} = C_c \sqrt{\frac{1}{\alpha_c} \Delta_c g \left(\frac{1}{1 + (\rho_h / \rho_c)^{1/3}} \right) h} \quad \text{with} \quad \Delta_c = \frac{\rho_C - \rho_h}{\rho_C} \tag{12}$$

Where Δ_h and Δ_c are the reduced acceleration of gravity for the hot and cold layer respectively.

The detailed discussion concerning the correction coefficients are given in Paper [D]. A reasonable estimation for α is found to $\alpha_h = \alpha_c = 1.2$. C is found to be a function of Δ_h, that can be approximated by (with max. error = 3.2 %):

$$C_c = C_h = 0.6641 \Delta_h^{-0.1955} \tag{13}$$

A simulation is made with results from a simulation of Gojkovic's experiments [20] performed using Ansys CFX. These results are presented in Paper [D] and show that it is of interest to determine these correction coefficients.

6 EXPERIMENTS

This chapter describes experimental series carried out by the author at the Laboratoire de Combustion et de Détonique of the CNRS in Poitiers, France. The goal of these experiments was to characterize the gravity wave in detail, which has never been done in backdraft studies before. An overview of the results is presented and discussed in this chapter, and more complete results are compared directly with other methods in Chapter 8 of this thesis.

6.1 Goal of the experiments

Very few experimental studies on the backdraft phenomena have been carried out, due to its complexity and dangerous character. Previous experiments have described the process of the phenomena, relating the conditions prior to opening (temperatures, gas concentrations) to the occurrence and intensity of backdraft, for various geometries ([19], [20], [22]). Apart from the work of Fleischmann [21], who used probes to register velocities at the opening and gave a qualitative description of the gravity wave, there has been very little description of the gas dynamics and the mixing between opening and ignition, and this is clearly a gap in the identification of the ignition condition. The experimental series aim to fill this experimental gap and is the first one to study the gravity current leading to backdraft in details by using state of the art experimental techniques such as Particle Image Velocimetry or Laser Tomography. A reduced scale compartment was specially designed and built by the author, and 87 experiments were carried out, testing two different opening geometries. The temperature build-up inside the compartment is not performed by combustion but by heating the air using a resistance, which allows a good control of the initial temperature. A second set of experiments with combustion and backdraft is planned within the next months using the same or similar apparatus.

This experimental work gives a very detailed picture of the gravity current, using two non intrusive complementary techniques discussed in Chapter 3, the Laser Tomography for qualitative results and the PIV mainly for a quantitative description. The goal of these experiments is mainly:

- To validate experimentally the 3 phases flow theory assumed by the authors and the average velocities of the flow (Papers [C] and [D]).
- To identify different turbulent structures, recognized from papers on turbulence [33] from the pictures. This has not been done before in backdraft studies.
- To obtain a qualitative and quantitative description of the flow, which can be used to calibrate and validate the results of the CFD modeling of these experiments. Once validated against these results, the CFD model will be useful for more detailed analysis and to estimate the efficiency of the mixing.

6.2 Experimental design and procedure

6.2.1 Description of the experimental apparatus

The configuration of the experimental apparatus is shown in Figure 11. The experimental apparatus is a reduced scale compartment, insulated using ISOFRAX panels and blankets, and sealed with a refractory mastic and glass fiber braid seal. For flow visualization, VITROCERAM heat resistant windows are on one side of the box and on the floor. This has also the advantage of reducing friction. The compartment is small compared to apparatus used in former backdraft experiments ([20], [21], [22], [23]). The choice for this size was motivated by the spatial resolution capacities of the PIV camera. With these dimensions, the entire opening and the thickness of the gravity current can be recorded by the camera. The light sheet from the laser source goes though the middle of the compartment, using the symmetry of the compartment.

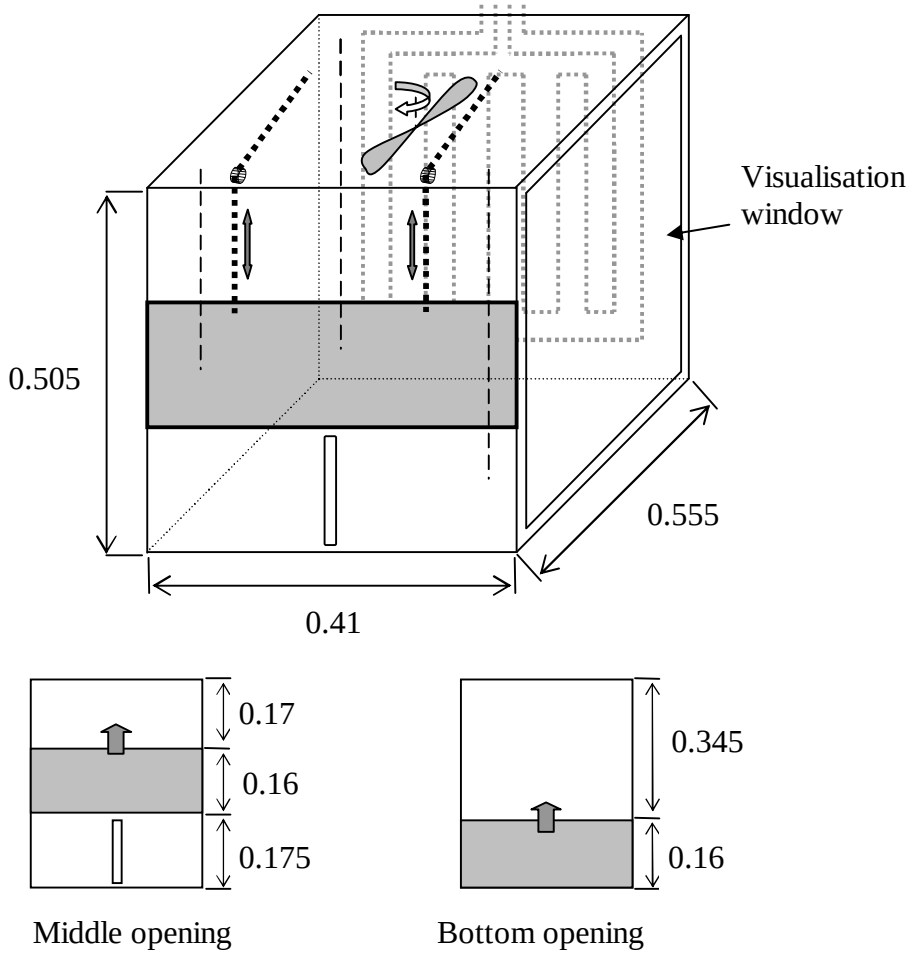

Figure 11: Sketch of the experimental compartment with different opening configurations

The two different opening configurations are described in Figure 11, with the removable plate colored in grey. The opening covers the entire width of the front wall. In order to visualize the gravity current, the light sheet must illuminate the lower part of the compartment. Therefore, for the middle slot opening configuration, a slot covered by a quartz window allows the light to go through the lower plate.

A sketch of the complete experimental set-up is shown in Figure 12, with the temperature, fan, opening, seeding control and the Argon continuous laser forming a light sheet. The camera and the acquisition system are triggered simultaneously with the hatch opening.

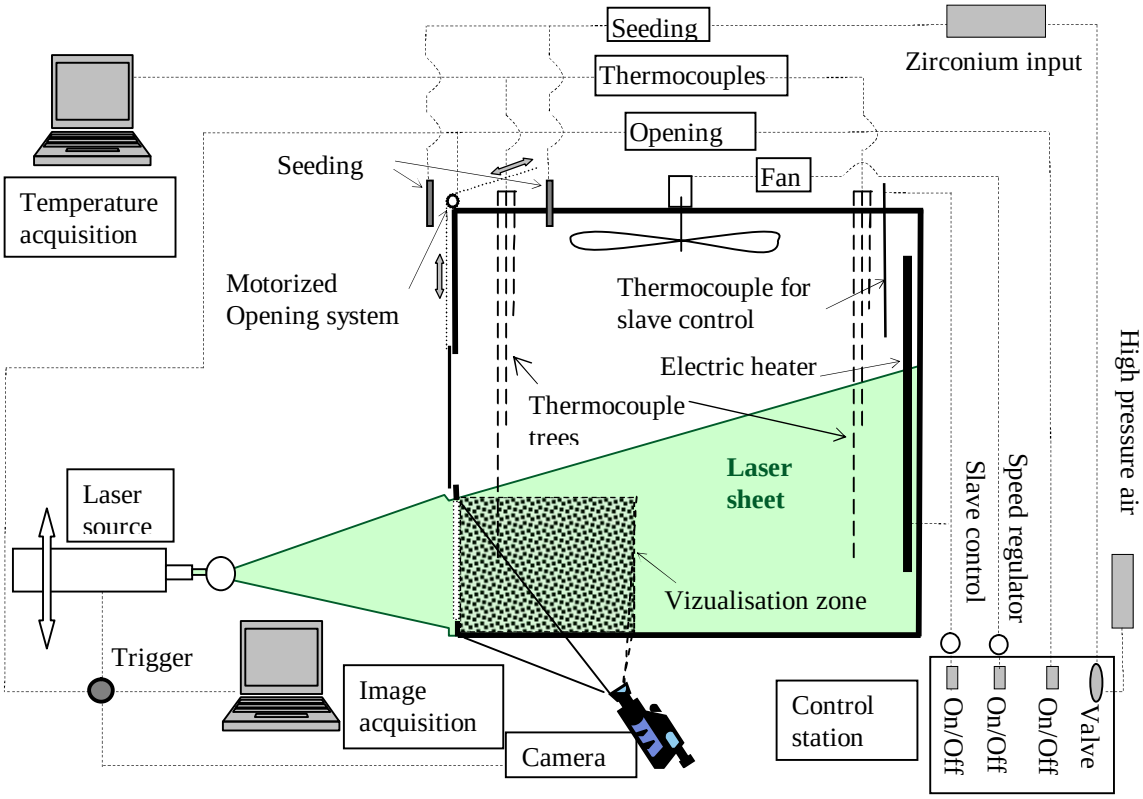

Figure 12: Schematic of the backdraft experimental apparatus

Table 2: Laser sources and acquisition systems

Vizualisation	Laser source	Camera	Freq.	Software
PIV	Quantel Ultra PIV30	Lavision Flowmaster	2 to 4 Hz	Lavision Davis 6.2
Tomography	Coherent Verdi	Redlake Motionscope PCI	128 Hz	Motionscope PCI

The compartment is heated with a 3.2 kW electric heater automatically-controlled with a thermocouple. A fan is installed on the ceiling, in order to homogenize the gas temperature. There are two trees composed of three K-type thermocouples each, one near the window/opening wall corner and one near the diagonally opposed corner, respectively at 0.100, 0.250 and 0.400 m below the ceiling, and at 0.1 m from the walls. A third thermocouple tree is in the other corner near the opening, at 0.250 m below the ceiling. This configuration allows checking the homogeneity of the temperature in both vertical and horizontal direction. The thermocouple signals are acquired with a Keithley 2700/2701/2750 Multimeter.

Figure 13 shows the front wall with the laser source and opening system. The plate covering the opening is lifted by means of a system of chain and counterweight controlled remotely by a step by step motor. The disadvantage of this system is the opening length time, which is 1 second. The advantage is that the disturbance on the outside flow is limited compared to a pivoting system. It was also necessary to lift the plate instead of dropping it in order to allow the light sheet to enter through the quartz window, and to permit the bottom opening configuration.

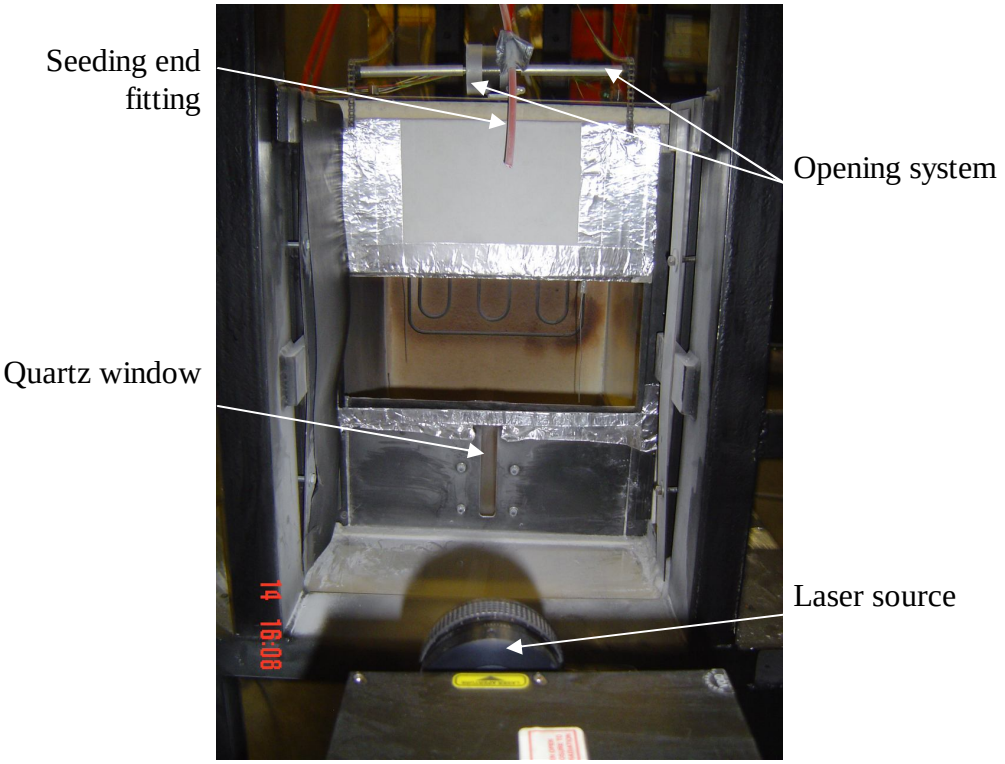

Figure 13: Front view of the experimental compartment (middle opening configuration)

Figures 14 and 15 show the other essential elements of the compartment apparatus, with connections. Note that the apparatus was designed to be used also with combustion, therefore, the top plate is not strongly fixed to serve as a pressure relief panel, and the rear wall is in fact a methane burner covered by an isofrax plate. This plate and the heater could easily be removed for a combustion configuration, which could be studied in future work.

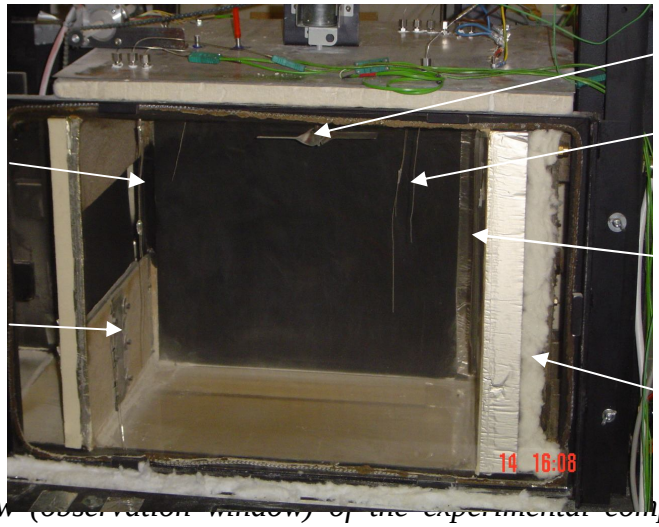

Figure 14: Right view (observation window) of the experimental compartment (middle opening configuration)

PIV requires the seeding of the flow by micrometrical particles. Due to the fact that some temperatures in the enclosure are higher than the boiling temperature of most liquids, zirconium oxide powder is used (see paragraph 6.2.2 below). The particle seeder uses an endless screw to push powder in the air flow.

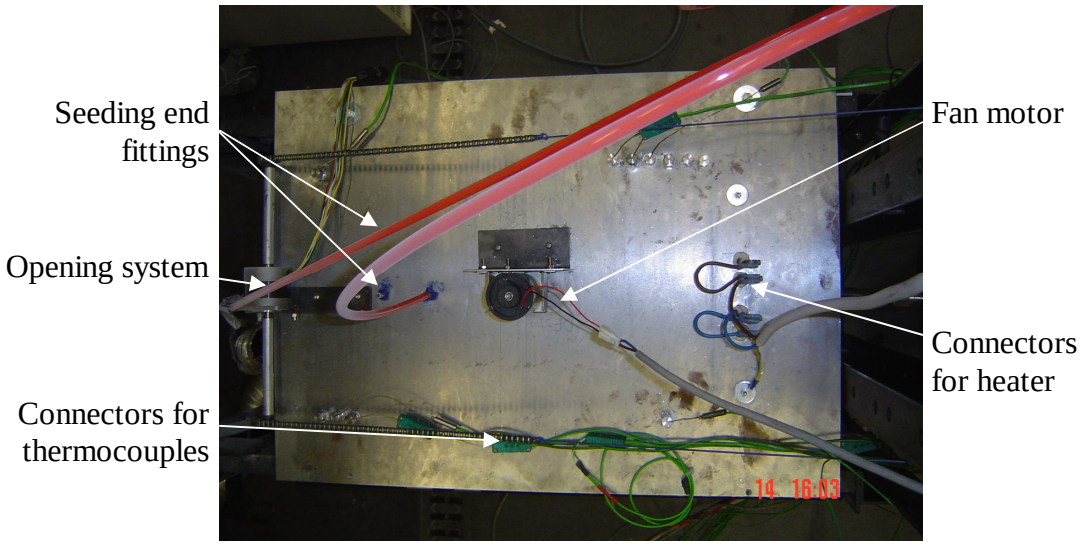

Figure 15: Top view of the experimental compartment (middle opening configuration)

6.2.2 Choice of seeding

The choice of seeding is a delicate and crucial problem faced in measuring methods based on particles. The quality of the results depends strongly on the seeding quality, which should be carried by the flow and disturb it as little as possible, but still be thick enough to be visualized and radiate the light from the laser. Depending on the visualization case, it is necessary to seed the incoming flow, the outcoming flow or both. Several methods were discussed or tested, and finally zirconium oxide powder was selected. Table 3 shows the advantages and disadvantages of different seeding materials.

Table 3: Advantages and disadvantages of different seeding materials

Material	Advantages	Disadvantages
Cigarette smoke	- Easy to implement - Negligible flow disturbances	- Particles are too thin to radiate light
Sawdust	- Easy to implement	-Risk of particles ignition
Water Droplets	- Easy to implement - Homogeneous seeding	-High absorption level of laser light -Behavior strongly dependant on temperatures. Evaporation at temperature >100°C.
Zirconium powder	- Easy to implement - Excellent resistance to high temperatures	- Process of injection can induce disturbances (necessity of delay between injection and opening)

After an initial investigation, both cigarette smoke and sawdust were eliminated, as the disadvantages cited in Table 3 made their usage either impossible to this kind of study or hazardous. Water droplets were tested, but due to evaporation, it was only possible to seed the incoming cold flow. Moreover, even if the temperature of the gravity current is below the evaporation temperature, it is not necessarily the case of the mixed flow at the interface, which could consequently not be characterized. Furthermore, the absorption level of water droplets made them impossible to be visualized everywhere in the compartment, as shown in Figure 16 where the waterfall is visualized for the same inner initial temperature. In Figure 16.a, the incoming flow is seeded with water droplets. It is clear that all the light close to the front wall, is absorbed and half the visualization window is just dark. As a consequence, the wave moving towards the compartment cannot be observed. In Figure 16.b, the hot inside air is seeded with zirconium powder. In this case, the wave is observed on the entire window. Observations of the flow at different positions inside the compartment confirmed that seeding the hot air with zirconium was the most suitable way to visualize the gravity wave in the entire compartment. Therefore, this method was used during all the experiments.

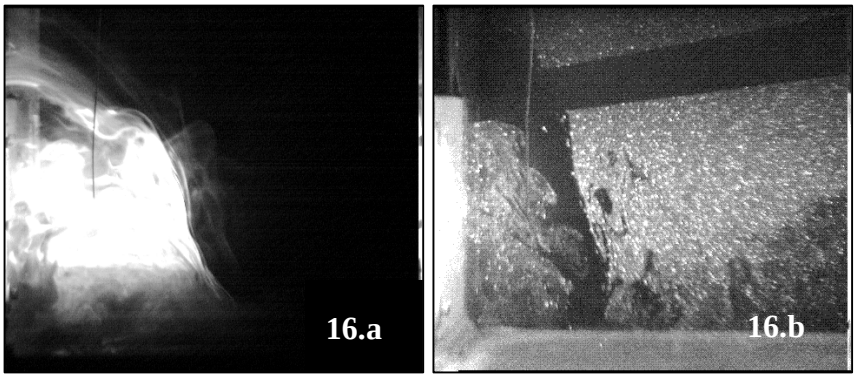

Figure 16: Visualization of the waterfall in middle opening configuration and T_h = 150°C 2 seconds after opening, with the cold flow seeded with water droplets (16. a, left) and hot flow seeded with Zirconium powder (16. b, right)

6.2.3 Control variables and visualization windows

The control variables of these experiments are two different openings and eight different initial temperatures inside the compartment.

The two openings that are studied are middle slot and bottom slot opening, 160 mm high and 410 mm wide. Openings that cover the entire width of the compartment were chosen to avoid transversal flow that could be created by the boundary layer of the vertical sides of the openings and thus affect the movements of particles through the light sheet. With this geometry, the light sheet is the symmetry plane of the compartment, and the flow is mainly longitudinal.

The initial (hot) temperatures inside the compartment noted T_h that are tested are 50, 75, 100, 125, 150, 175, 200 to 225°C. The ambient (cold) temperature T_c in the laboratory is 20°C. This is quite a wide range of temperatures, and despite all the efforts to seal the compartment, it was very difficult to reach homogeneous temperatures higher that 225°C.

The characteristics of the different runs are described in Table 4 for the middle opening configuration and in Table 5 for the bottom opening configuration.

Table 4: Characteristics of the experimental runs in middle opening configuration

run	name	T_h (°C)	visu	window	time (s)	Freq. (Hz)	Seeding	
							in	out
1	Tom-M-OP_T50	50	tomo	OP	10	125	yes	no
2	Tom-M-OP_T100	100	tomo	OP	10	125	yes	no
3	Tom-M-OP_T150	150	tomo	OP	10	125	yes	no
4	Tom-M-OP_T200	200	tomo	OP	10	125	yes	no
5	Tom-M-OP_T225	225	tomo	OP	10	125	yes	no
6	Tom-M-BA_T50	50	tomo	BA	10	125	yes	no
7	Tom-M-BA_T100	100	tomo	BA	10	125	yes	no
8	Tom-M-BA_T150	150	tomo	BA	10	125	yes	no
9	Tom-M-BA_T200	200	tomo	BA	10	125	yes	no
10	Tom-M-BA_T225	225	tomo	BA	10	125	yes	no
11	PIV-M-OU_T50	50	PIV	OU	15	4	yes	yes
12	PIV-M-OU_T75	75	PIV	OU	15	4	yes	yes
13	PIV-M-OU_T100	100	PIV	OU	15	4	yes	yes
14	PIV-M-OU_T125	125	PIV	OU	15	4	yes	yes
15	PIV-M-OU_T150	150	PIV	OU	15	4	yes	yes
16	PIV-M-OU_T175	175	PIV	OU	15	4	yes	yes
17	PIV-M-OU_T200	200	PIV	OU	15	4	yes	yes
18	PIV-M-OU_T225	225	PIV	OU	15	4	yes	yes
19	PIV-M-OP_T50	50	PIV	OP	10	2	yes	yes
20	PIV-M-OP_T75	75	PIV	OP	10	2	yes	yes
21	PIV-M-OP_T100	100	PIV	OP	10	2	yes	yes
22	PIV-M-OP_T125	125	PIV	OP	10	2	yes	yes
23	PIV-M-OP_T150	150	PIV	OP	10	2	yes	yes
24	PIV-M-OP_T175	175	PIV	OP	10	2	yes	yes
25	PIV-M-OP_T200	200	PIV	OP	10	2	yes	yes
26	PIV-M-OP_T225	225	PIV	OP	10	2	yes	yes
27	PIV-M-WF_T50	50	PIV	WF	12.5	2	yes	yes
28	PIV-M-WF_T75	75	PIV	WF	12.5	2	yes	yes
29	PIV-M-WF_T100	100	PIV	WF	12.5	2	yes	yes
30	PIV-M-WF_T125	125	PIV	WF	12.5	2	yes	yes
31	PIV-M-WF_T150	150	PIV	WF	12.5	2	yes	yes
32	PIV-M-WF_T175	175	PIV	WF	12.5	2	yes	yes
33	PIV-M-WF_T200	200	PIV	WF	12.5	2	yes	yes
34	PIV-M-WF_T225	225	PIV	WF	12.5	2	yes	yes
35	PIV-M-FL_T50	50	PIV	FL	10.8	3.7	yes	yes
36	PIV-M-FL_T75	75	PIV	FL	10.8	3.7	yes	yes
37	PIV-M-FL_T100	100	PIV	FL	10.8	3.7	yes	yes
38	PIV-M-FL_T125	125	PIV	FL	10.8	3.7	yes	yes
39	PIV-M-FL_T150	150	PIV	FL	10.8	3.7	yes	yes
40	PIV-M-FL_T175	175	PIV	FL	10.8	3.7	yes	yes
41	PIV-M-FL_T200	200	PIV	FL	10.8	3.7	yes	yes
42	PIV-M-FL_T225	225	PIV	FL	10.8	3.7	yes	yes
43	PIV-M-BA_T50	50	PIV	BA	15	2	yes	yes
44	PIV-M-BA_T75	75	PIV	BA	15	2	yes	yes
45	PIV-M-BA_T100	100	PIV	BA	15	2	yes	yes
46	PIV-M-BA_T125	125	PIV	BA	15	2	yes	yes
47	PIV-M-BA_T150	150	PIV	BA	15	2	yes	yes
48	PIV-M-BA_T175	175	PIV	BA	15	2	yes	yes
49	PIV-M-BA_T200	200	PIV	BA	15	2	yes	yes
50	PIV-M-BA_T225	225	PIV	BA	15	2	yes	yes

Table 5: Characteristics of the experimental runs in bottom opening configuration

run	name	T_h (°C)	visu	window	time (s)	Freq. (Hz)	Seeding in	Seeding out
51	Tom-B-OP_T50	50	tomo	OP	10	125	yes	no
52	Tom-B-OP_T75	75	tomo	OP	10	125	yes	no
53	Tom-B-OP_T100	100	tomo	OP	10	125	yes	no
54	Tom-B-OP_T125	125	tomo	OP	10	125	yes	no
55	Tom-B-OP_T150	150	tomo	OP	10	125	yes	no
56	Tom-B-OP_T175	175	tomo	OP	10	125	yes	no
57	Tom-B-OP_T200	200	tomo	OP	10	125	yes	no
58	Tom-B-BA_T50	50	tomo	BA	10	155	yes	no
59	Tom-B-BA_T75	75	tomo	BA	10	125	yes	no
60	Tom-B-BA_T100	100	tomo	BA	10	125	yes	no
61	Tom-B-BA_T125	125	tomo	BA	10	125	yes	no
62	Tom-B-BA_T150	150	tomo	BA	10	125	yes	no
63	Tom-B-BA_T175	175	tomo	BA	10	125	yes	no
64	Tom-B-BA_T200	200	tomo	BA	10	125	yes	no
65	PIV-B-OU_T50	50	PIV	OU	10	4	yes	yes
66	PIV-B-OU_T75	75	PIV	OU	10	4	yes	yes
67	PIV-B-OU_T100	100	PIV	OU	10	4	yes	yes
68	PIV-B-OU_T125	125	PIV	OU	10	4	yes	yes
69	PIV-B-OU_T150	150	PIV	OU	10	4	yes	yes
70	PIV-B-OU_T175	175	PIV	OU	10	4	yes	yes
71	PIV-B-OU_T200	200	PIV	OU	10	4	yes	yes
72	PIV-B-FL_T50	50	PIV	FL	14.3	2.8	yes	yes
73	PIV-B-FL_T75	75	PIV	FL	14.3	2.8	yes	yes
74	PIV-B-FL_T100	100	PIV	FL	14.3	2.8	yes	yes
75	PIV-B-FL_T125	125	PIV	FL	14.3	2.8	yes	yes
76	PIV-B-FL_T150	150	PIV	FL	14.3	2.8	yes	yes
77	PIV-B-FL_T175	175	PIV	FL	14.3	2.8	yes	yes
78	PIV-B-FL_T200	200	PIV	FL	14.3	2.8	yes	yes
79	PIV-B-FL_T225	225	PIV	FL	14.3	2.8	yes	yes
80	PIV-B-BA_T50	50	PIV	BA	14.3	2.1	yes	yes
81	PIV-B-BA_T75	75	PIV	BA	14.3	2.1	yes	yes
82	PIV-B-BA_T100	100	PIV	BA	14.3	2.1	yes	yes
83	PIV-B-BA_T125	125	PIV	BA	14.3	2.1	yes	yes
84	PIV-B-BA_T150	150	PIV	BA	14.3	2.1	yes	yes
85	PIV-B-BA_T175	175	PIV	BA	14.3	2.1	yes	yes
86	PIV-B-BA_T200	200	PIV	BA	14.3	2.1	yes	yes
87	PIV-B-BA_T225	225	PIV	BA	14.3	2.1	yes	yes

Figure 17 shows the location of the visualization panels, outside (OU), opening (OP), waterfall behind the middle slot (WF), floor (FL) and back of the enclosure (BA) for the middle opening configuration. Figure 18 indicates the panel for the bottom opening configuration. The subscripts indicate the type of visualization, i.e. PIV (p) or tomography (t) or both (p,t) for each window. Their coordinates, relative to the origin situated at the front on the compartment on floor level are shown in Table 6. The panels are visualized from the side of the compartment, through the visualization window (see Figure 11).

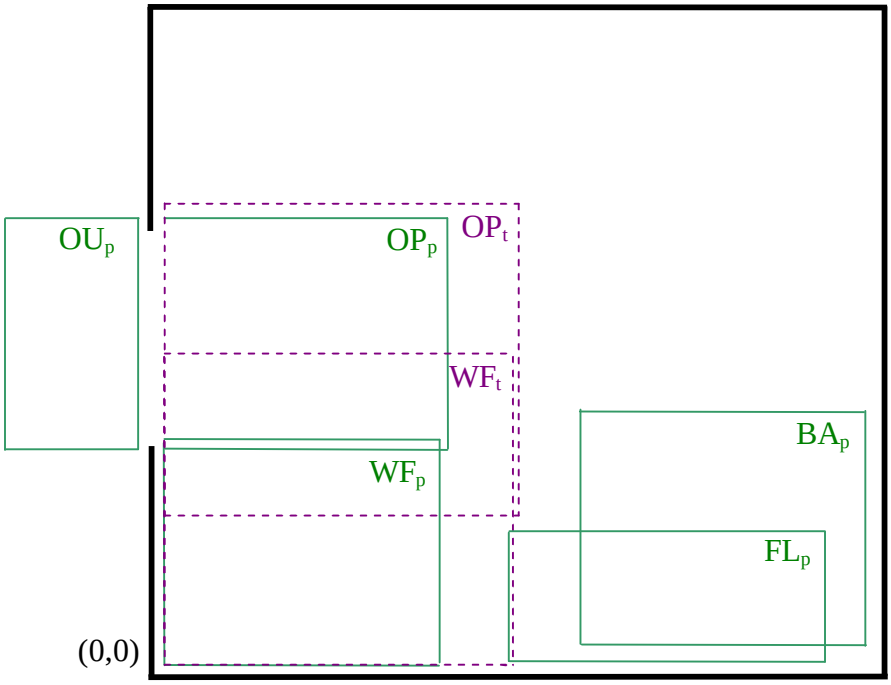

Figure 17: Position of the visualization windows in the middle opening configuration

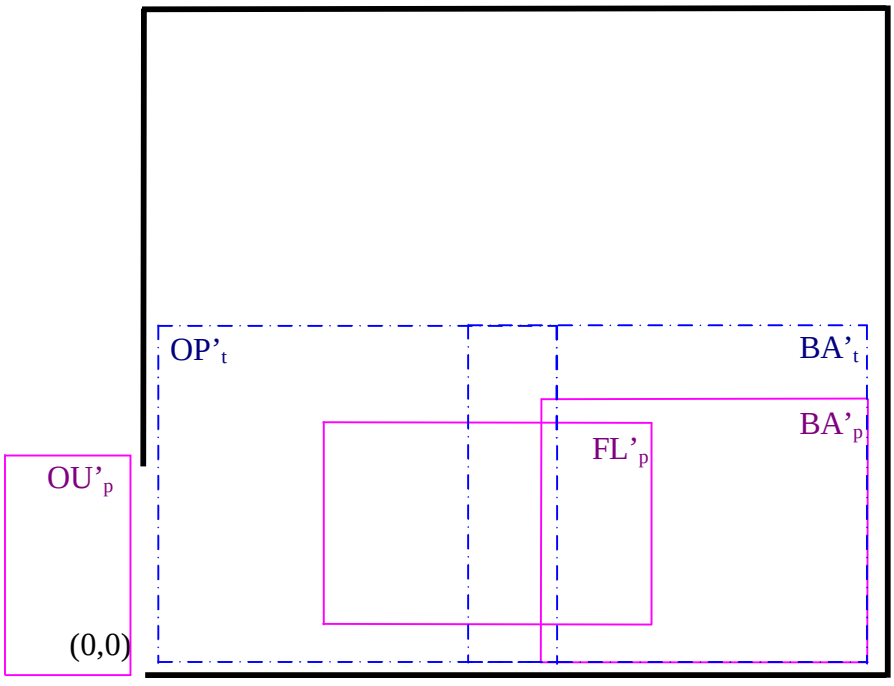

Figure 18: Position of the visualization windows in the bottom opening configuration

Table 6: Position and size of the visualization windows

Case	window	position	visu	X_{min} (mm)	Z_{min} (mm)	X_{max} (mm)	Z_{max} (mm)
Middle	OU_p	outside	PIV	-121	170	-10	345
	OP_p	opening	PIV	10	172	224	345
	WF_p	waterfall	PIV	10	10	219	179
	FL_p	floor	PIV	271	10	510	104
	BA_p	back	PIV	323	22	540	197
	OP_t	opening	tomo	10	120	279	355
	WF_t	waterfall	tomo	10	10	276	243
Bottom	OU'_p	outside	PIV	-103	0	-10	165
	FL'_p	floor	PIV	139	40	381	194
	BA'_p	back	PIV	298	10	540	206
	OP'_t	opening	tomo	10	10	308	270
	BA'_t	back	tomo	241	10	540	270

6.2.4 Experimental procedures

For temperature build-up, the desired initial hot temperature inside the compartment T_h is entered into the slave command, and both heater and fan are turned on. The temperature homogeneity is considered acceptable when all of the 7 thermocouples are within a range of T_h ± 10 %. The heater and fan are turned off and a 10 second delay is given to get a damping of the convective flow. A puff of air is injected into the seeding system during 2 seconds to form a cloud of particles at the enclosure entrance. The hatch is then opened, triggering the laser source and the image acquisition.

6.3 Experimental results

The experimental results discussed in this section are mainly qualitative, as the main interest of quantitative results is to compare them directly to the CFD and analytical models. However, some examples of results for both tomography and PIV are shown and discussed.

6.3.1 Qualitative results

As discussed in the previous sections, the main advantage of tomography is that it gives excellent qualitative results. Generally, these results show that the flow is very unsteady with a lot of turbulent structures, and the same type of structures can be observed for all the different temperatures. Typically, we can observe the same structures and entrainment process as are observed in fjords or deltas [53]. The most interesting features enhancing the mixing between the hot and cold layer are detailed in Figures 19 to 21.

Figures 19 to 21 show instantaneous tomography images respectively on panels OP_t and WF_t and OP_t' for experiments performed with T_h = 100°C. The observed main characteristics will be referred to as Obs. in the figures and text. In Figure 19, only the inside flow is seeded. This figure shows the formation of small scale pair of counter rotating vortices (Obs 19.1) between cold entering air and hot inside air. The time resolved

sequences of images shows successive vortex coalescence process where pairs of Van Karman vortices are ingested in a single large vortex [53]. Other visualizations have shown pulsating disturbances at the opening despite minimizing air disturbance in the room. Figure 20 shows the evolution of the waterfall. A 3D recirculation zone is formed behind the step (Obs 20.1), and two different free boundary layers creating vortex entrainments can be observed. One is due to the shear friction between the cold layer and the recirculation zone (Obs 20.2) and the other one is due to shear friction between hot and cold layers (Obs. 20.3). The disturbances are very similar to vortices in turbulent coaxial jets [78].The wave detaches itself from the waterfall in a pulsating mode which enhances the flow mixing (Obs. 20.4). Figure 20, for hatch at the floor level, shows the formation of a more standard and steady wave with vortices (Obs 21.1) with different stages of cusp entrainment (Obs 21.2). These vortices are typical of Kelvin–Helmholtz instabilities [79] where two fluids in parallel motion with different velocities and densities will yield an unstable interface. This flow phase is rapidly affected by the rebounded wave on the rear panel (Obs 21.3).

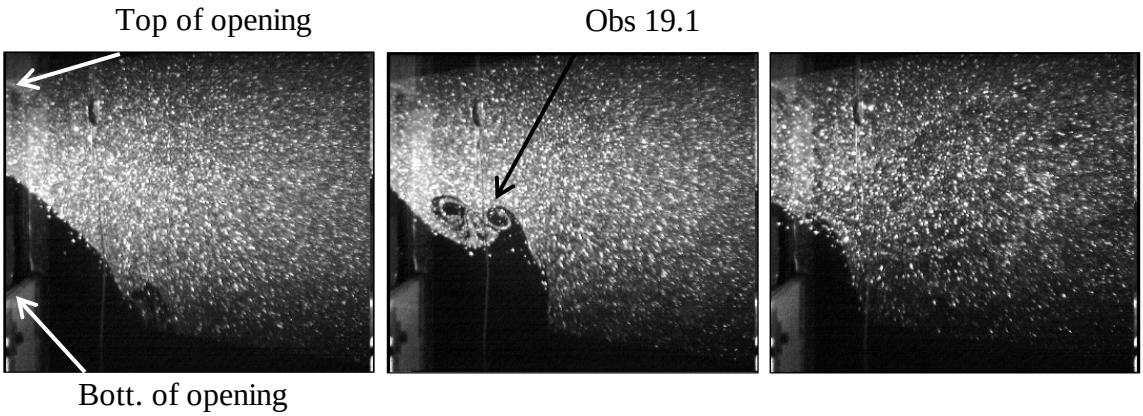

Figure 19: Tomography Tom-M-OP_T100 at t = 2, 4.2 and 6.4 sec. after opening (left to right)

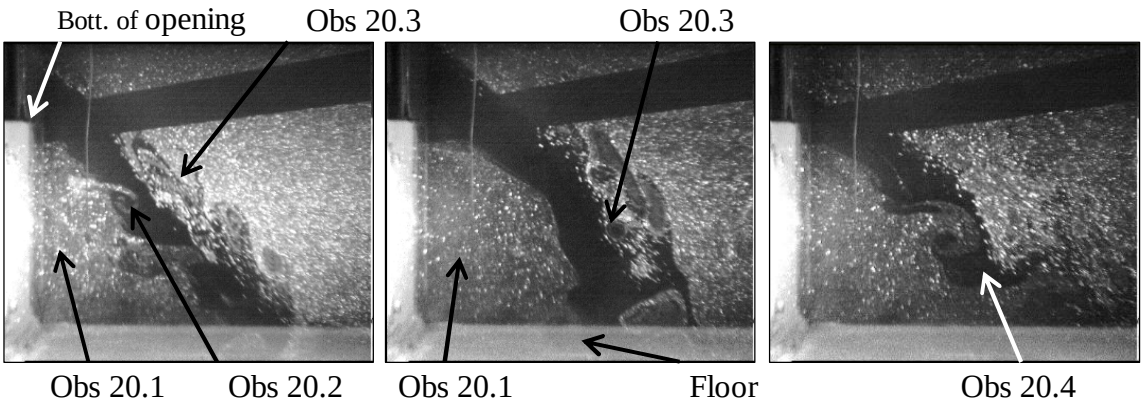

Figure 20: Tomography Tom-M-WF_T100, t = 2.2, 4.6 and 6.4 sec. after opening (left to right)

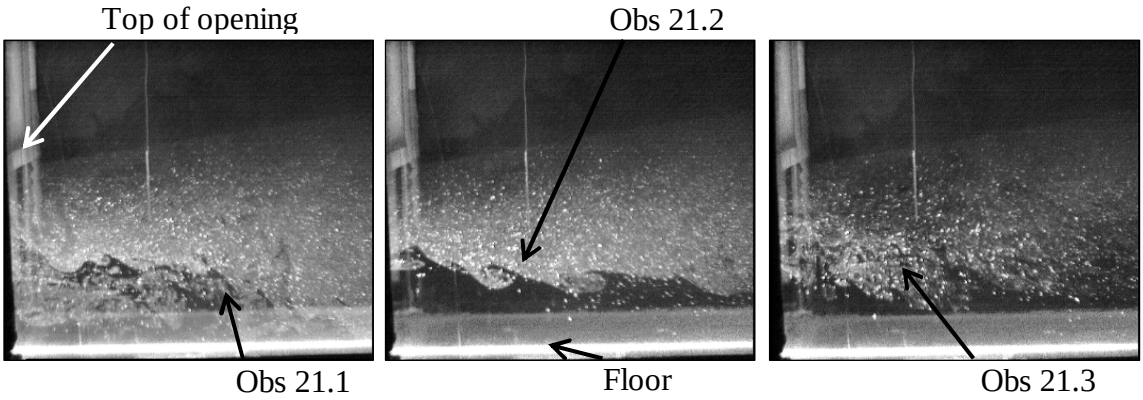

Figure 21: Tomography Tom-B-OP_T100, t = 1.2, 2.4 and 4.2 sec. after opening (left to right)

6.3.2 Quantitative results

The following PIV results show the velocity fields at the opening for T_h = 100°C (Figure 22) and T_h = 200°C (Figure 23), from 3 to 10 seconds after hatch opening, in middle opening configuration (cases PIV-M-OP_T100 and PIV-M-OP_T200). The velocities of the cold fluid are roughly between 0.4 at 0.6 m/s in Figure 22 and 0.5 to 0.8 m/s in Figure 23. A clear mixing zone can be observed in both cases at the interface, with entrainment and recirculation, as indicated by the oval shape on the figures. This zone seems wider with higher temperatures.

Generally, PIV results confirm the very turbulent behavior of the gravity wave. The most interesting results to be extracted from these experiments are the flow at the opening and the velocity of the head of the gravity wave. These results will be displayed and compared directly with CFD and analytical results in Chapter 8 of this thesis document.

6.3.3 Discussions and recommendations

These experiments give a complete picture of the flow driven by density difference in a reduced scale compartment. The advantage of choosing a small scale apparatus and to choose to heat the compartment with a heater instead of combustion is that it allows an important number of experiments, with well-defined initial conditions to be carried out.

The quantitative results can be easily compared to CFD models and are essential for their improvement, as well as for the development, calibration and validation of future CFD models. However, the main limitation comes from the time resolution of the PIV used in this study. As the phenomenon is very unsteady, the evolution of turbulent structures cannot be easily described in a quantitative way. New experiments using fast PIV are scheduled by Professor Most at the Laboratoire de Combustion et de Détonique within the next few months, with a time resolution comparable to one used with the tomography.

The description of the velocity field is strongly dependant on the quality of seeding. As shown in Figures 22 and 23, the cold flow is seeded only during the first seconds. A method for continuous seeding outside the compartment that does not disturb the flow should be investigated for improvements. However, at least the hot flow is well described, which allows a good estimation of the flow rates as a function of the temperature difference.

The fast tomography allows a good qualitative description of the gravity currents, showing turbulent structures that have not be studied and observed in backdraft studies before.

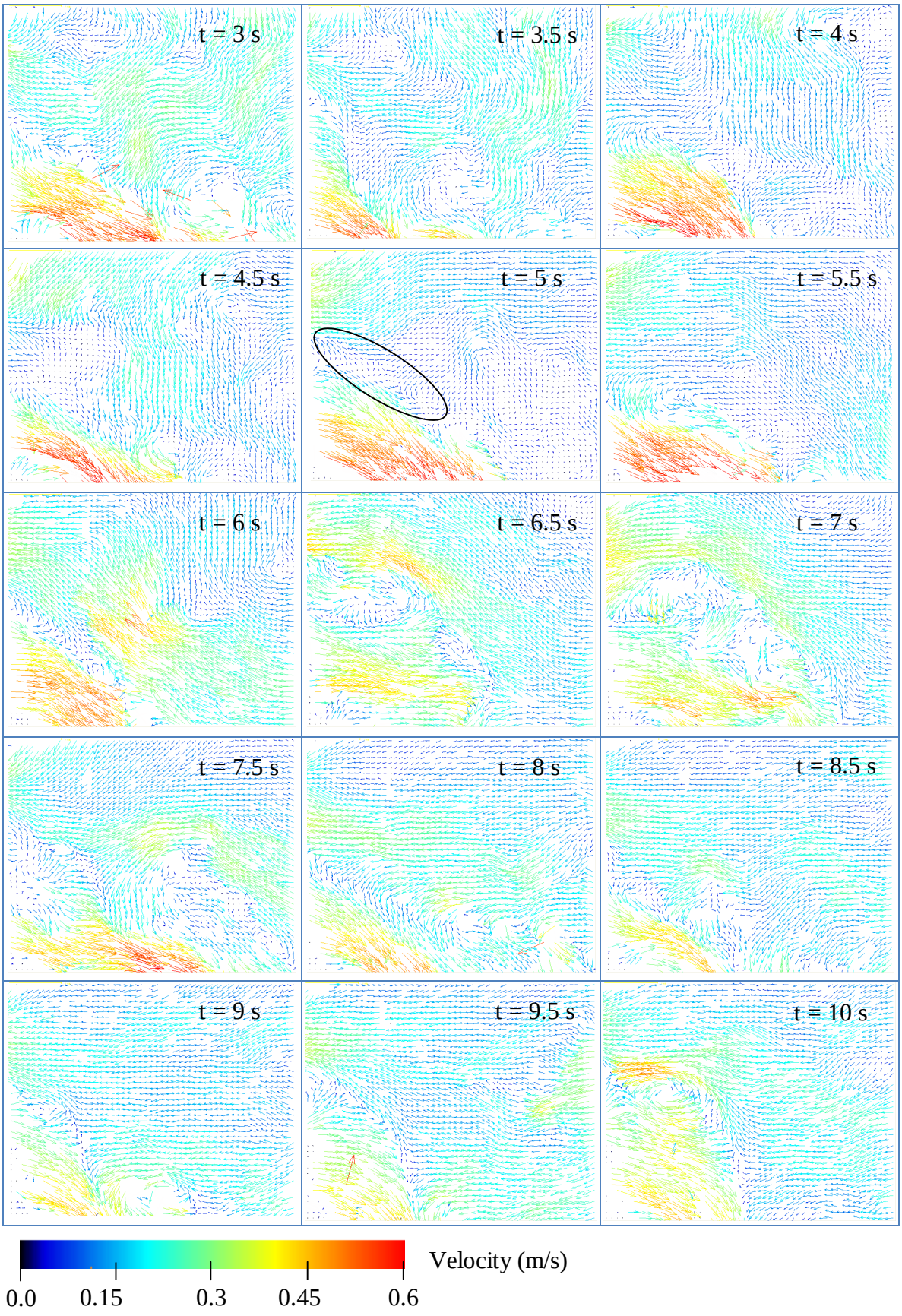

Figure 22: PIV results PIV-M-OP_T100, from 3 to 10 seconds after hatch opening

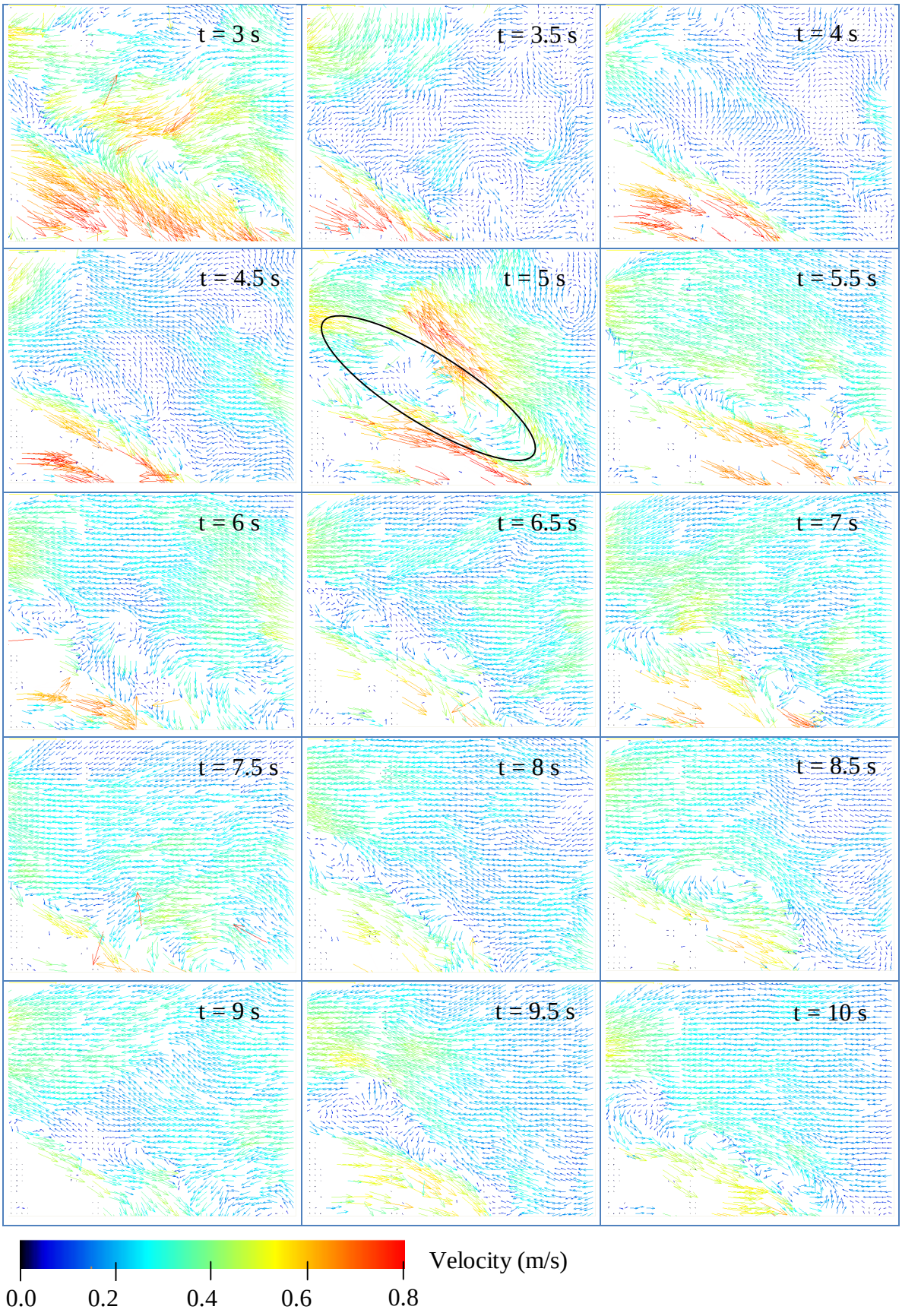

Figure 23: PIV results PIV-M-OP_T200, from 3 to 10 seconds after hatch opening

7 DESCRIPTION OF THE FDS NUMERICAL MODEL

In this chapter, a numerical model of the experiments discussed earlier in this thesis is described. The results will be mainly described and discussed in Chapter 9, where they are compared to both experimental and analytical methods developed in the previous sections.

7.1 Description of the model

A numerical model of the experiments was set-up using Fire Dynamic Simulator (FDS). The geometry of the model is shown in Figure 24. The dimensions of the domain are 0.8x0.205x0.7 m^3 (LxWxH) with a mesh composed of 160x41x140 = 918400 cells regularly spaced (spatial resolution = 5 mm). The domain is extended in front and on top of the compartment, in order to simulate the flow correctly and prevent the pressure boundary conditions from influencing the flow inside the compartment. Only half of the compartment is modeled by using the symmetry of the compartment, applying the "MIRROR" function to the plan y = 0.205 m, the same plan as the laser sheet in the experiments.

In order to simulate the opening, the hatch is composed of 32 removable obstacles. One obstacle is removed every 0.032 seconds, from the bottom to the top of the opening. The total opening time is 1.024 seconds, which is very similar to the experiments

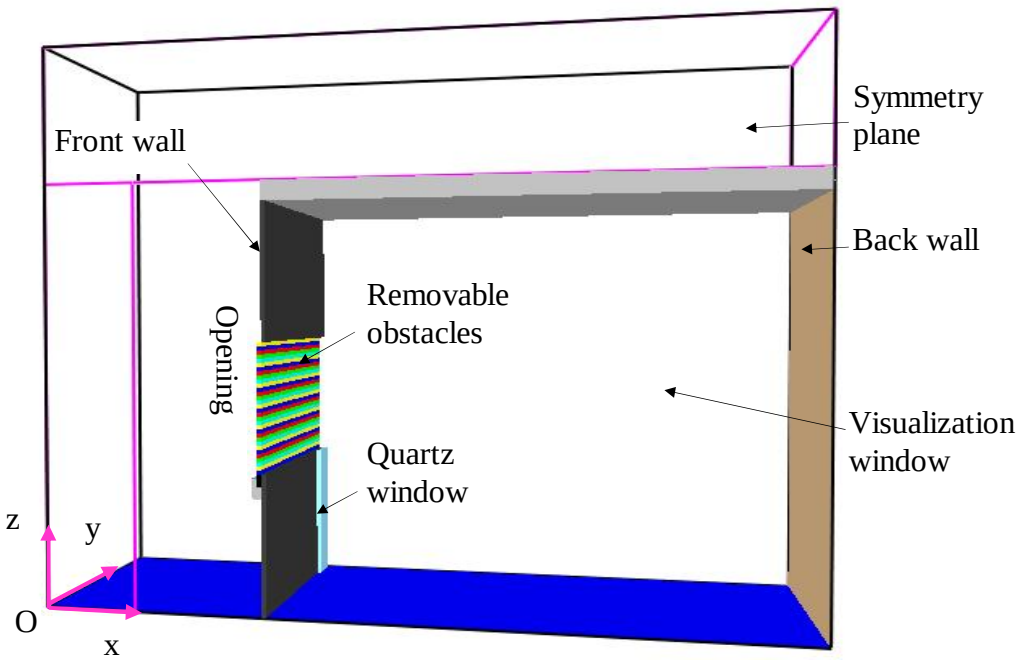

Figure 24: FDS model of the experimental apparatus (middle opening configuration)

The initial conditions specified are the required hot temperature inside the compartment and ambient (20°C) outside.

The same control variables (i.e. opening configuration and inner temperatures) and the same referencing system as in the experiments is used, e.g FDS-B-_T100 stands for the FDS run in bottom configuration and T_h = 100°C.

7.2 Visualization and measuring probes

The visualization software Smokeview [80] can display results from FDS, showing quantities such as temperatures, densities, velocities, visibility, to name only a few. It also allows shows 3D isosurfaces, boundary files and smoke movements.

It is also possible to record physical quantities at precise positions using the "devices" that are similar to probes in experiments. The results from the devices can be opened in Microsoft Excel. This allows a fast and easy comparison with experimental results.

In this model, the choice was to visualize the velocities, temperatures, densities and the concentration of the hot fluid, on symmetry plan y = 0.205 m, which corresponds to the visualization laser sheet in the experiments.

The fluid mixing is studied through the mixing fraction, defined as the ratio between the mass concentration of hot and cold air $f = Y_h / Y_c$. Mixing fraction f = 1 corresponds to the zones where there is only hot air, and f = 0 corresponds to the inflow and ambient fluid.

Displaying the 3D isosurface for f = 1 allows the visualization of the the progression of the gravity wave. Figure 25 shows this isosurface for cases FDS-M-_T150 and FDS-M-_T150 at 3 and 4.5 seconds after opening. In the middle opening configuration (Figure 25.a), the progression of the wave is slower and more turbulent. The rebound on the back wall clearly induces more turbulence and consequently more mixing in the middle than in the bottom opening configuration (Figure 25b), where it behaves more as a classical hydraulic jump.

Figures 26 and 27 show the concentration of hot fluid in both configurations and for three different temperatures. They clearly show that the traveling velocity of the wave increases with increased temperature. However, viewing these figures, it is difficult to conclude on the influence of density difference on the mixing. This will be discussed in detail in Chapter 9. The level of turbulence clearly increases in middle the opening configuration, due to the disturbance created by the waterfall, and also the effect of the sharp boundary of the bottom of the opening in this configuration.

The devices are specified in the FDS script before running the calculation. They are positioned to record the velocity profiles at the opening and inside the compartment, on the symmetry plane. This set-up allows making direct comparisons with the experiments. The positions of these devices are indicated in Figures 32 and 37 in the Chapter 9 of this thesis.

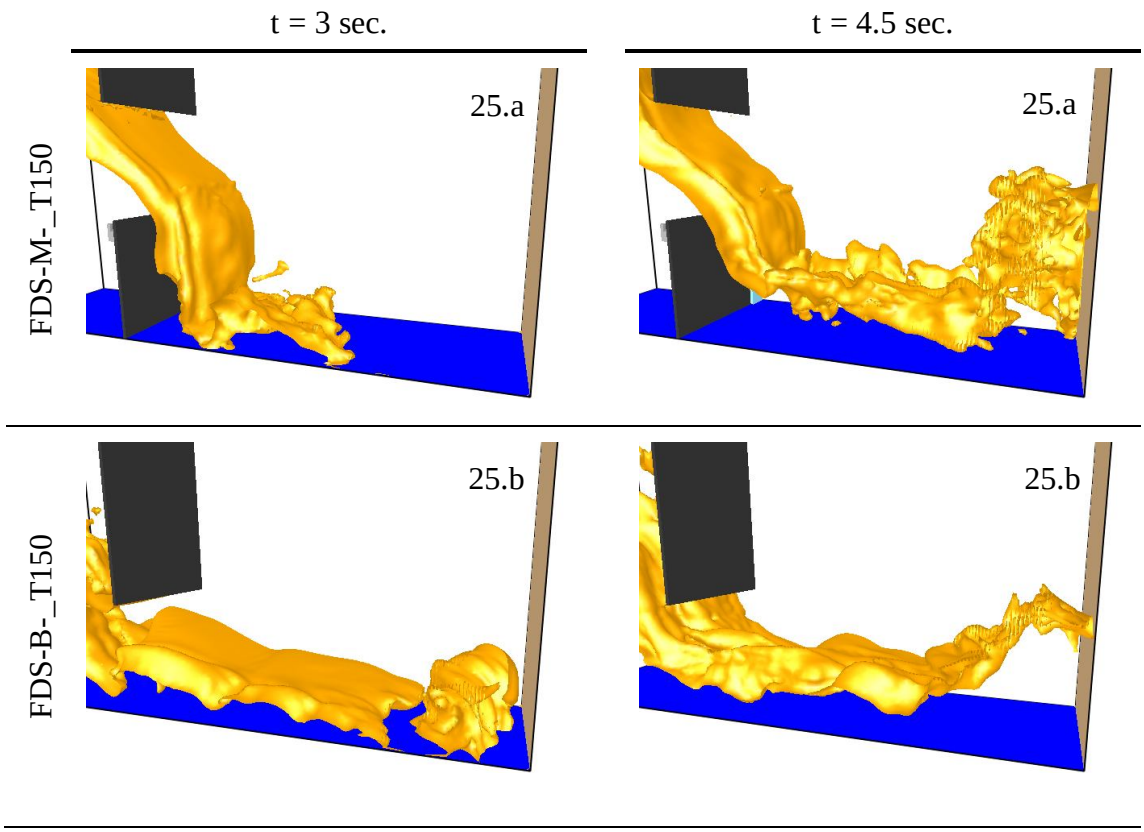

Figure 25: Isosurface of mixing fraction f = 1, at 3 and 4.5 seconds after opening, in the middle opening configuration (Figure 25. a) and in the bottom opening configuration (Figure 25. b)

7.3 Advantages, disadvantages and recommendations

In this section, we will not discuss the accuracy of the numerical model, as this requires comparison with experimental results, which will be the subject of Chapter 8. However, it is interesting to discuss the possibilities offered by the numerical model, as well as its limitations.

The major advantage offered by the numerical simulation is that is allows to make many runs within a short time, thus testing various scenarios for example by changing the initial conditions or the geometry. This takes little time and is not costly compared to experimental studies. Another advantage is the possibility to record and display multiple scalar quantities at every desired position within the numerical domain. In FDS, however, the quantities that are to be computed must be specified before running the simulation.

A major limitation is due to the restriction of the rectangular mesh. In this case, the geometry is rather simple and square, so this restriction does not have a major effect on the model. It is worth noting that neither the electric heater nor the fan are modeled, as they do not interact directly, in terms of obstacles, with the wave, except maybe the lower part of the resistance with the rebound of the wave on the back wall. However, its influence is considered negligible.

A more general discussion on the advantages, limitations and recommendations concerning CFD models is presented in Section 4.3 of this thesis.

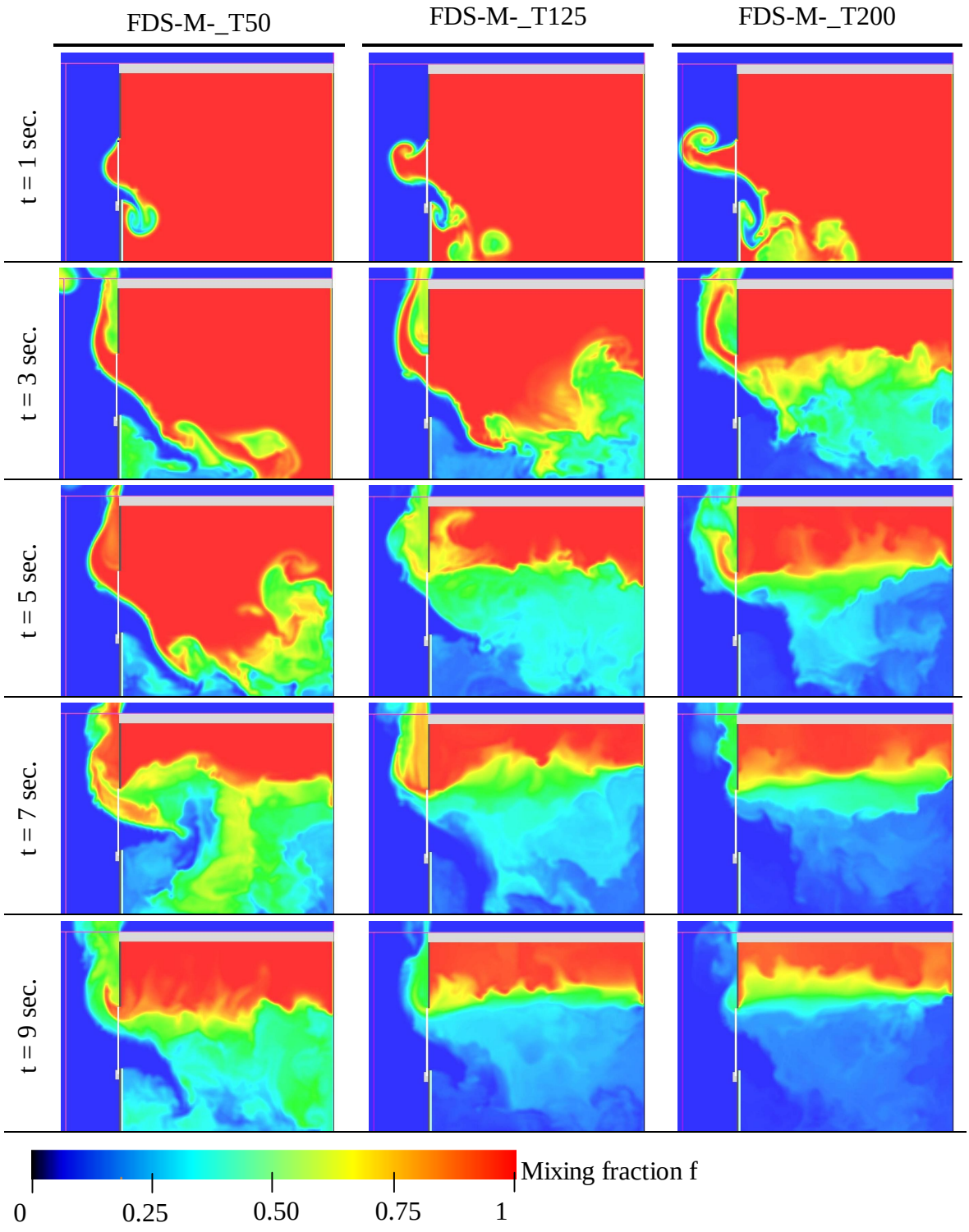

Figure 26: Concentration of hot fluid from 1 to 9 seconds after opening in the middle opening configuration, for T_h = 50°C (left), T_h = 125°C (center), T_h = 200°C (right)

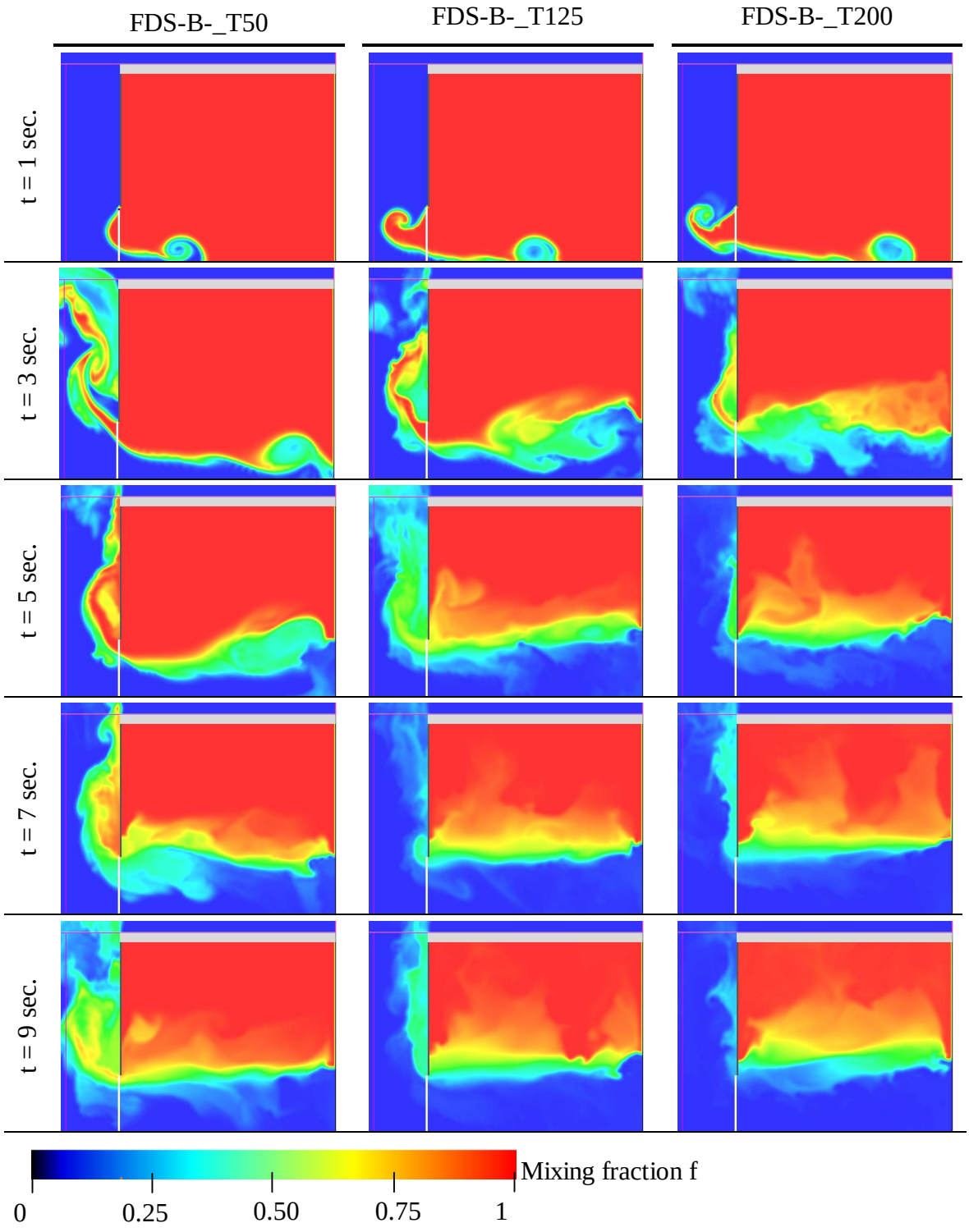

Figure 27: Concentration of hot fluid from 1 to 9 seconds after opening in the bottom opening configuration, for T_h = 50°C (left), T_h = 125°C (center), T_h = 200°C (right)

8 COMPARISON OF CFD, ANALYTICAL AND EXPERIMENTAL RESULTS

In this chapter, three methods will be compared: experimental, analytical and numerical.

8.1 Qualitative results

Qualitative results for experiments and simulation have been discussed separately in the previous chapters. In this chapter a direct comparison of all three methods will be presented.

Qualitative results discussed in chapter 6.3.1 concerning tomography permitted the identification of very characteristic turbulent structures. The simulation shows the same vortex coalescence process where a pair of counter rotating vortices are ingested by a single large vortex discussed earlier (see Figure 28). These vortices are roughly the same size, although, in the simulation, they first appear further inside the compartment, as indicated by the distances from the bottom of the opening to the center of the structure. In both cases, these vortexes are then ingested into a single larger vortex.

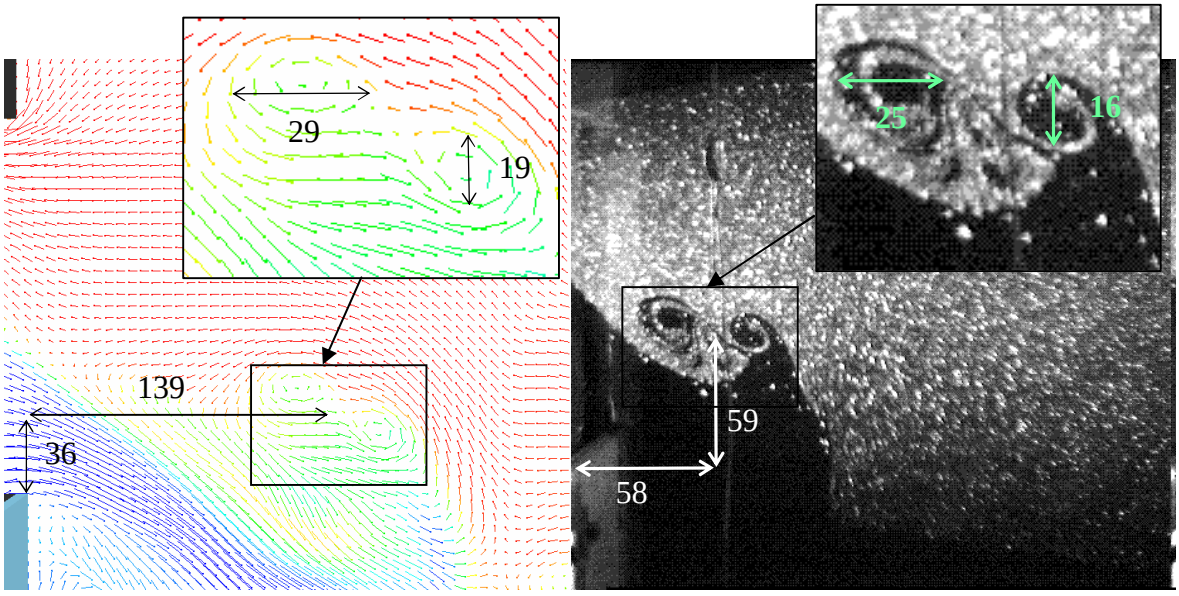

Figure 28: View of the flow on panel OP for T_h = 100°C, for simulations after 3.5 sec. (left), and tomography after 2.05 sec. (right). The position of the pair of vortices is shown relative to the bottom of opening, and their sizes are indicated on the zoomed views

An interesting structure shown by both simulations and experiments is the “mushroom head” shape of the head of the current before it hits the bottom of the box, on the waterfall visualization panel WF (see Figure 29). On each side of the head is a rotating structure creating this particular shape, characteristic of a stationary jet flow. The vortex on the internal side of the waterfall is roughly the same size in simulation and experiments. On the external side of the waterfall, the simulation shows cusp entrainment with a well mixed

structure which is a bit different from the vortex entrainment shown with the experiments. In this case, as the cold fluid is going up, its kinetic energy is transformed in potential energy. The cold fluid has then less kinetic energy for mixing, which explains the very clear boundary between hot and cold fluid within the vortex. The vortex entrainment creates a significantly smaller structure that the cusp entrainment, which is due to the difference in the mixing efficiency. However, both types of entrainment create significant momentum exchange and mixing. The flow of the wave immediately after the head and up to the opening is significantly wider in the experiments. There is a strong entrainment of hot fluid into these originally cold vortices. The behavior and the influence of these turbulent structures will be discussed in detail in Chapter 9.

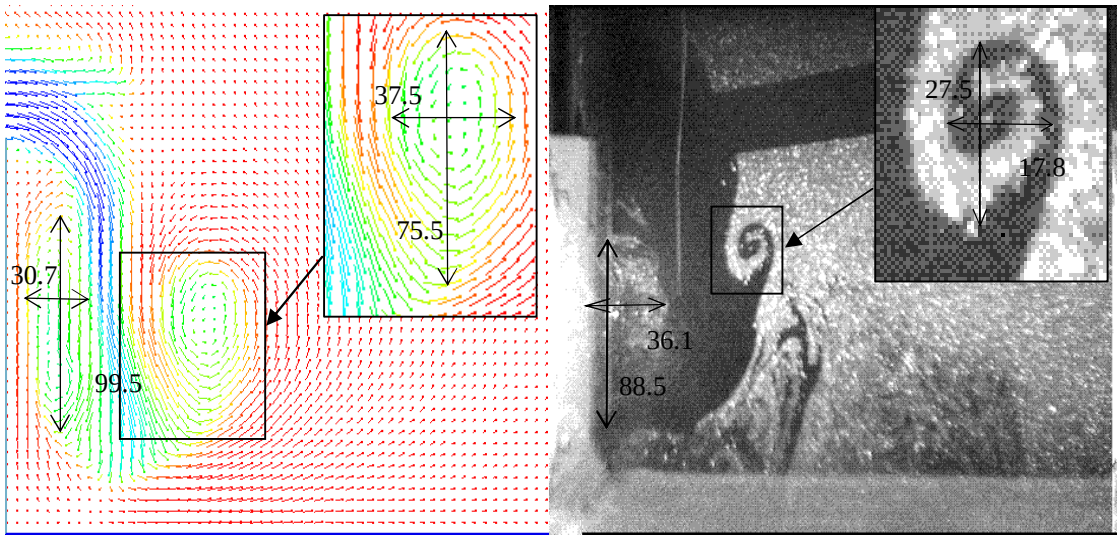

Figure 29: View of the flow on panel WF for T_h = 50°C, after 1.45 sec. for simulations (left) 2 sec. for tomography (right). The position of the pair of vortices is shown relative to the bottom of opening, and their sizes are indicated on the zoomed views

Figure 30 shows results from tomography and FDS simulation, on 3 different panels (OP_t, WF_t and OP'_t) from 0.5 to 5 seconds after opening, every 0.5 seconds. The hot fluid corresponds to the light grey seeded part on tomography and the red part on the FDS slides, showing the temperatures. These results agree generally quite well together, at least for the largest turbulent structures. These structures seem more coherent in the simulated flow, especially at the beginning of the waterfall, where some parts of the cold flow are detached from the head of the current. The mixing seems generally more efficient in the experiments. For the bottom opening, the wave develops faster than in the experiments, with a wide head, as in the case of a forced flow.

Experiments and simulations show similar characteristic turbulent structures, as shown in Figures 28 and 29. The evolution in time also shows a similar behavior between experiments and simulations. From a qualitative point of view, it can be concluded that there is a fair comparison between experiments and simulation.

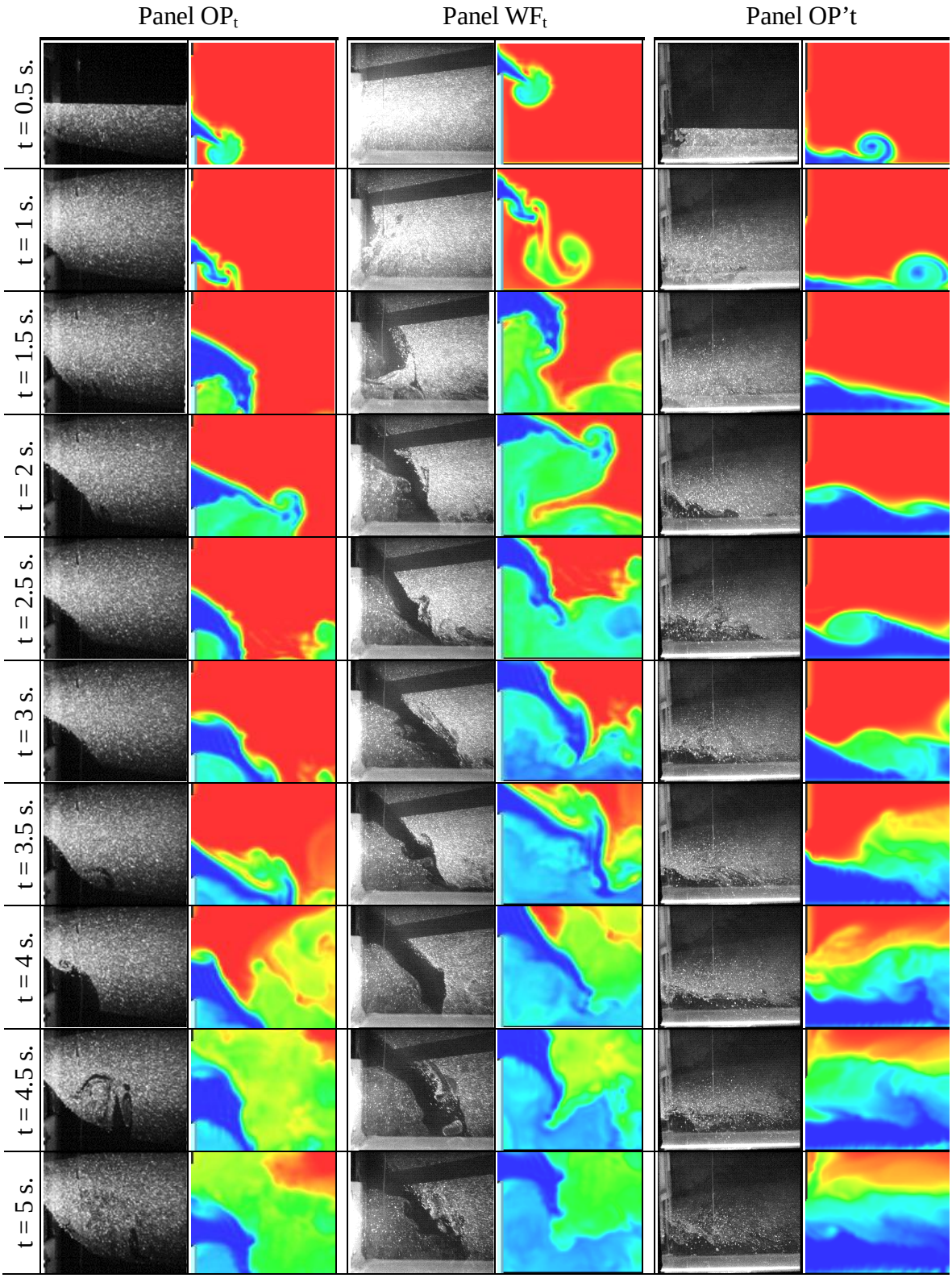

Figure 30: Experimental and corresponding FDS results (temperatures) from 0.5 to 5 seconds after opening for different panels (see Figure 4) and T_h = 100°C

8.2 Quantitative results

8.2.1 Transit time

The transit time is defined as the time for the leading edge of the gravity current to reach the wall opposite the opening. This is evaluated by observing pictures from PIV and FDS in the middle opening configuration and, from PIV, FDS and tomography in the bottom opening configuration. The results generally agree quite well together. In both the middle and the bottom opening configuration, the transit time is shorter in the simulations. This difference might be due to the higher mixing level in the experiments, consequently slowing the gravity current. It might also be due to the fact that the temperatures are not perfectly homogeneous in the experiments, with colder gases at the bottom, reducing the density difference.

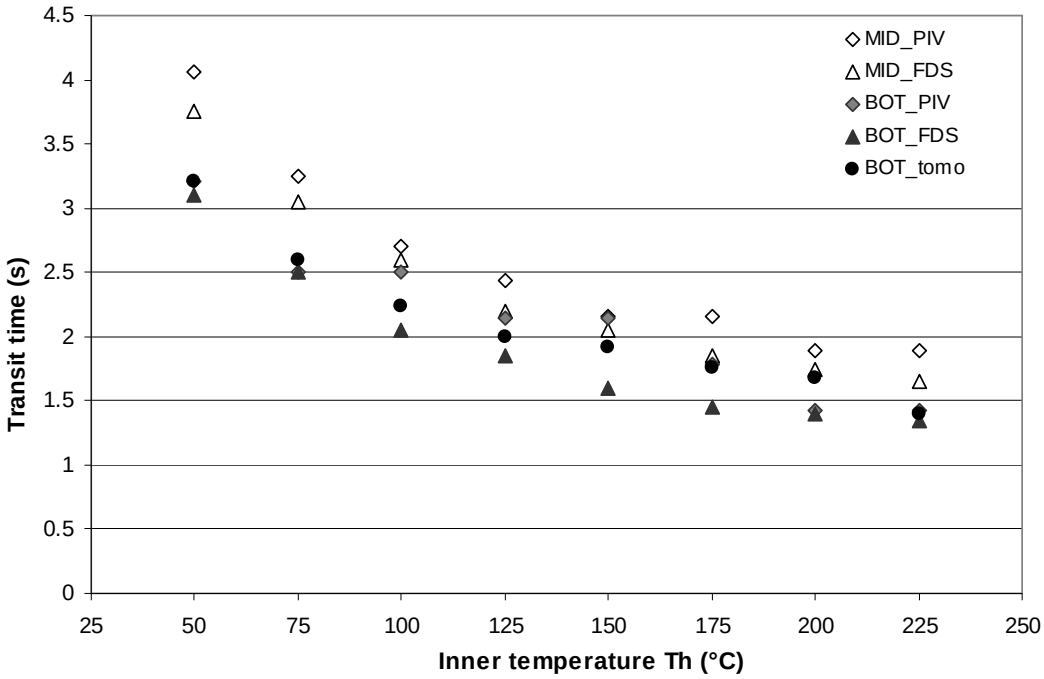

Figure 31: Transit time for middle (PIV and FDS simulation) and bottom opening configuration (PIV, FDS simulation and tomography)

8.2.2 Wave velocity inside the compartment

The velocity of the wave inside the compartment is recorded by a column of pixels in PIV measurements creating a velocity profile and a thermocouple tree in FDS. The position and spatial step of these measurement points are described in Figure 32 and Table 7 below.

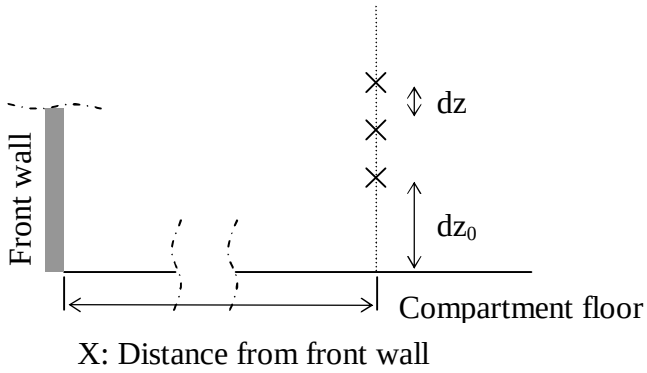

Figure 32: Position of measurement devices on Thermocouple tree THCP

Table 7: Position and spatial step of measurement points for wave velocity inside the compartment

case	step ref	Step (mm)	
		PIV	FDS
Mid	X (m)	0.305	0.305
	dz_0 (mm)	10	10
	dz (mm)	4.7	5
Bot	X (m)	0.205	0.205
	dz_0 (mm)	12	10
	dz (mm)	4.7	5

Figures 33 and 34 show the profile of the maximum horizontal velocity component from z = 0 to z = 0.24 m (see Figure 32), for middle and bottom opening configuration respectively. The time when the maximum U component is recorded by the THCP is shown on the legend of each profile. This occurs faster in the FDS simulation than in the experiments, which agrees with the observations from transit time. The width of the wave can be determined by considering the point when the U velocity component becomes negative. In the middle configuration, the width was found quite similar in both experiments and simulations. However, in the bottom configuration, this width is significantly smaller in the simulations (see Figure 33) and the boundary of the wave is more defined then in the experiments. At this particular time step, the FDS model does not catch the unstable interface with Kelvin-Helmholtz instabilities shown in Figure 21.

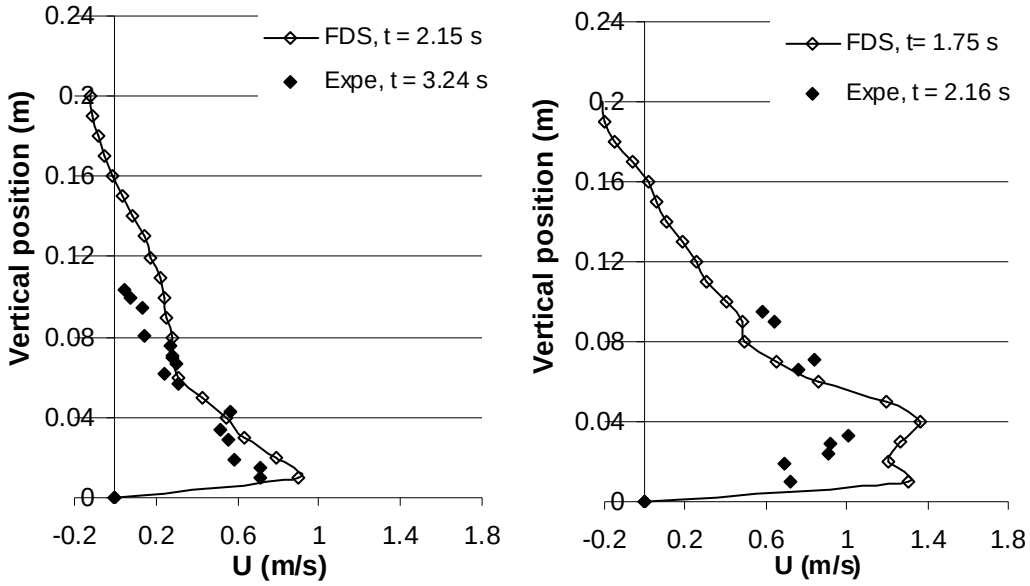

Figure 33: Max. velocity profile on THCP, middle opening configuration, for T = 100°C (left) and T = 150°C (right)

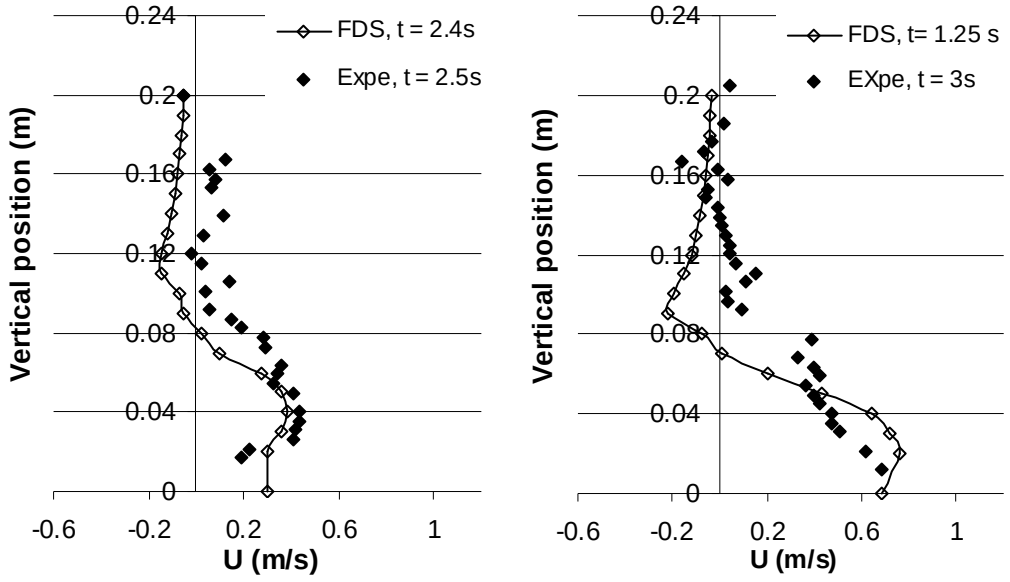

Figure 34: Max. velocity profile on THCP, bottom opening configuration, for T_h = 100°C (left) and T_h = 150°C (right)

We can observe that the maximum velocity is between z = 0 to 0.04 m from bottom, corresponding to the leading edge of the wave. An average of the velocities on this vertical range is considered in order to plot the velocity history of the wave, shown in Figures 35 and 36. The comparison of the numerical and experimental values shows that the velocity amplitudes are in good agreement, although a time offset of approximately 0.7 seconds is shown by the position of the maximum values.

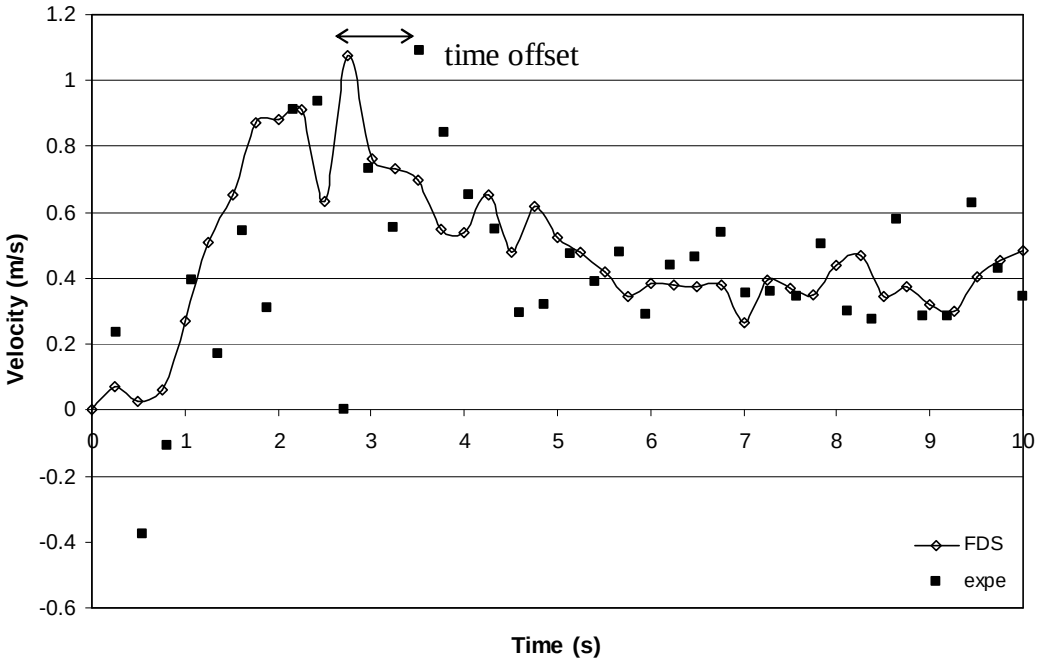

Figure 35: Velocity history, THCP 1 average from z = 0 to 0.04 m, middle opening configuration, for T_h = 175°C

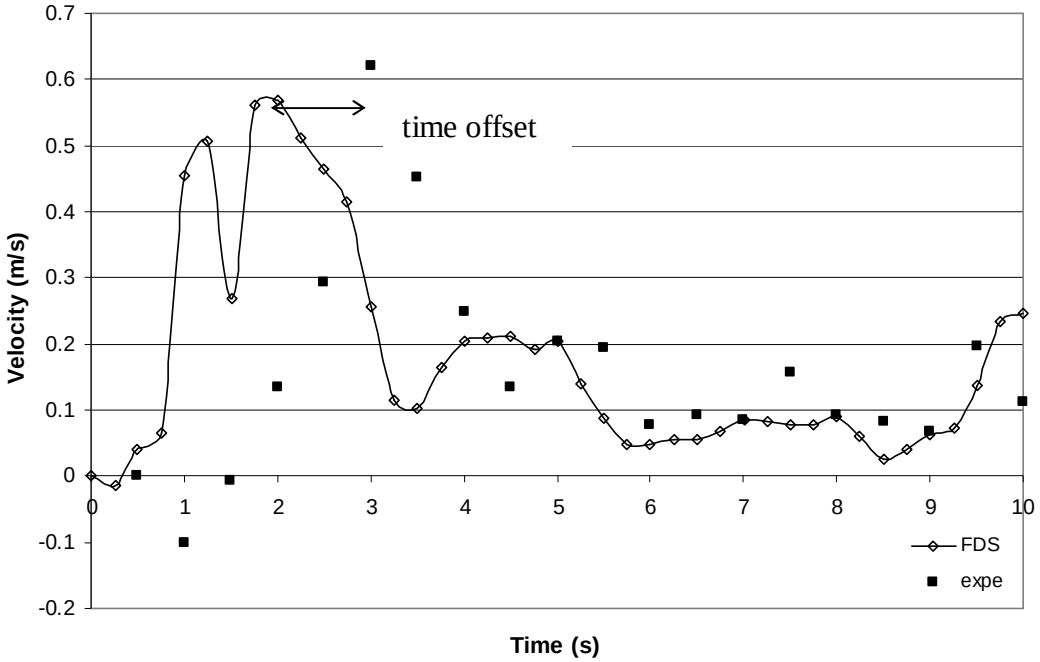

Figure 36: Velocity history, THCP 1 average from z = 0 to 0.04 m, bottom opening configuration, for T_h = 150°C

8.2.3 Interface and velocity at the opening

The velocity at the opening of the compartment is recorded by a column of pixels in PIV measurements and thermocouple trees in FDS creating velocity profiles. The position and

spatial step of these measurement points are described in Figure 37 and Table 8. In order to overcome the problem due to non homogeneous seeding, the velocities in this part are taken to be an average of the 3 pixel rows that are closest to the opening.

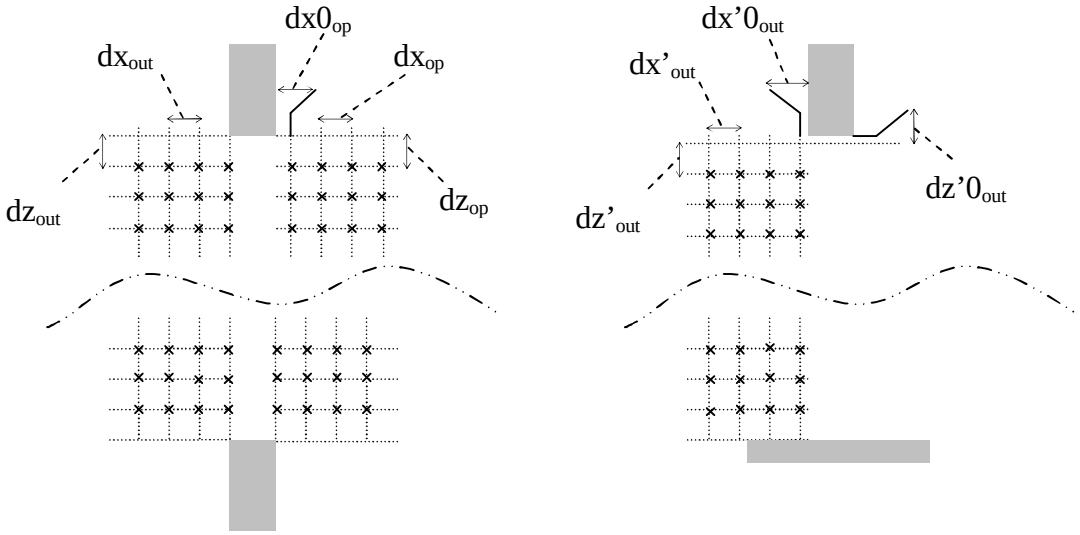

Figure 37: Position of measurement points at the opening of the compartment in the middle (left) and in the bottom (right) opening configuration

Table 8: Position and spatial step of measurement points for wave velocity inside the compartment

case	panel	step ref.		step (mm)	
				PIV	FDS
Middle	OU_p	dx_{out}		4.2	5
	OU_p	dz_{out}		4.2	5
	OP_p	dx_{op}		4	5
	OP_p	dz_{op}		4	5
	OP_p	$dx0_{op}$	offset	2	0
Bottom	OU'_p	dx'_{out}		4.4	5
	OU'_p	dz'_{out}		4.4	5
	OU'_p	$dx'0_{out}$	offset	1	0
	OU'_p	$dz'0_{out}$	offset	2	0

As shown by the qualitative results, the flow at the opening is very unsteady. The height of the interface depends on the influence of the opening, on the turbulent structures formed by the friction between hot and cold flow, and the oscillating effect of the wave inside the compartment.

FDS can estimate the layer height on a continuous vertical profile. The method is based on the consideration of average temperatures from a continuous vertical profile of temperature. If we consider a continuous function T(z) defining temperature T as a function of height z, where z = 0 being the bottom of the opening and z = H its top, the conservation equation gives:

$$(h - z_{int})T_h + z_{int}T_c = \int_0^h T(z)dz = I_1 \quad (14)$$

where T_h and T_c the upper and lower layer temperature respectively, and z_{int} is the interface height.

The conservation of mass (assuming perfect gas) gives:

$$(h - z_{int})\frac{1}{T_h} + z_{int}\frac{1}{T_c} = \int_0^h \frac{1}{T(z)}dz = I_2 \quad (15)$$

The interface can thus be expressed as:

$$z_{int} = \frac{T_l(I_1 I_2 - h^2)}{I_1 + I_2 T_c^2 - 2T_c h} \quad (16)$$

By letting T_c be the temperature in the lowest grid cell and using Simpson's Rule to perform the numerical integration of I_1 and I_2, T_h can be defined as the average upper layer temperature via:

$$(h - z_{int})T_h = \int_{Z_{int}}^h T(z)dz \quad (17)$$

Further discussion concerning the determination of interface height can be found in [81].

Because of the unsteady behavior of the flow and the somewhat low frequency of the PIV, the results from tomography will be compared with the experiments. To achieve this, the images are treated in Matlab. The column of pixels at the opening is selected and converted into a binary black and white picture, the white pixels being the particles in the hot flow. Then, the program browses the entire column and computes the distance between the bottom of the opening and the lower white pixels, corresponding to the lower particle.

The results from FDS and tomography images treatment are compared in Figure 38, for T_h = 150°C. The interface height is constantly varying, confirming the unsteady behavior of the flow. The effect of the opening is observed from 0 to 2 seconds, with important variations. Then, the interface height is oscillating, but with a rather steady average on the period between 2.5 and 7 seconds. This average value is shown in Figure 39 on the entire temperature range. It shows that the interface height is significantly lower in the experiments, which is also observed in Figure 38. This difference might be explained by the calculation method used in FDS and where the software considers the boundary between each layer, but it can also show that the mixing at the opening is more important in the experiments. Particles are entrained from the hot flow into the cold flow, showing an important mixed zone. The image treatment in Matlab considers that the lower part of the mixed zone indicates the position of the interface. In reality, the interface should be in the middle of this mixed zone.

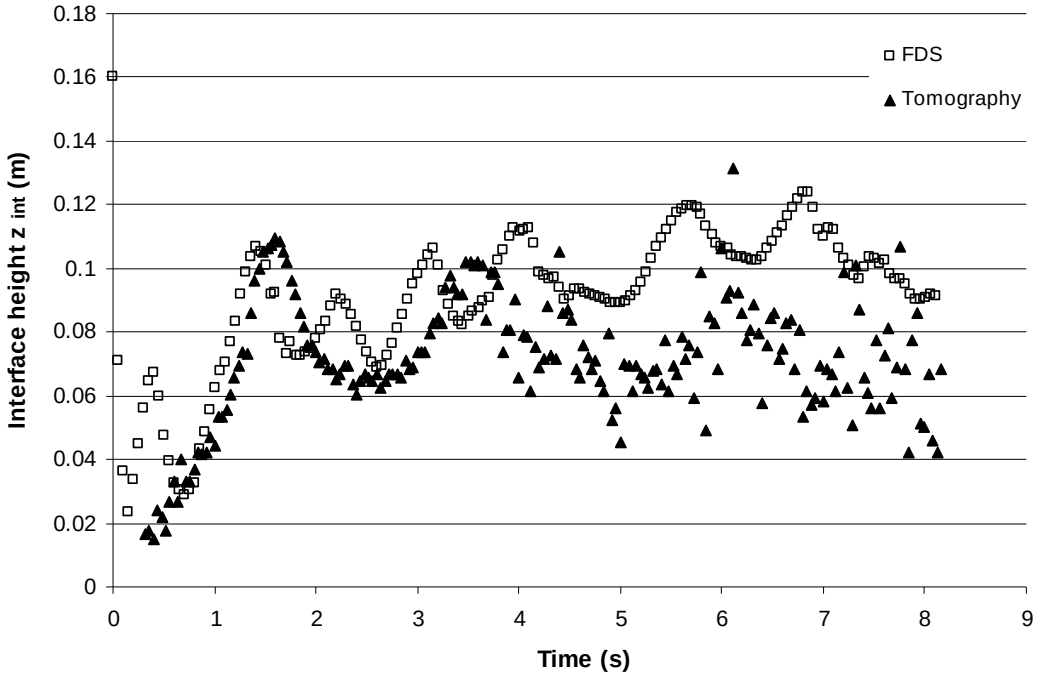

Figure 38: Interface height z_{int} history for T_h = 150°C

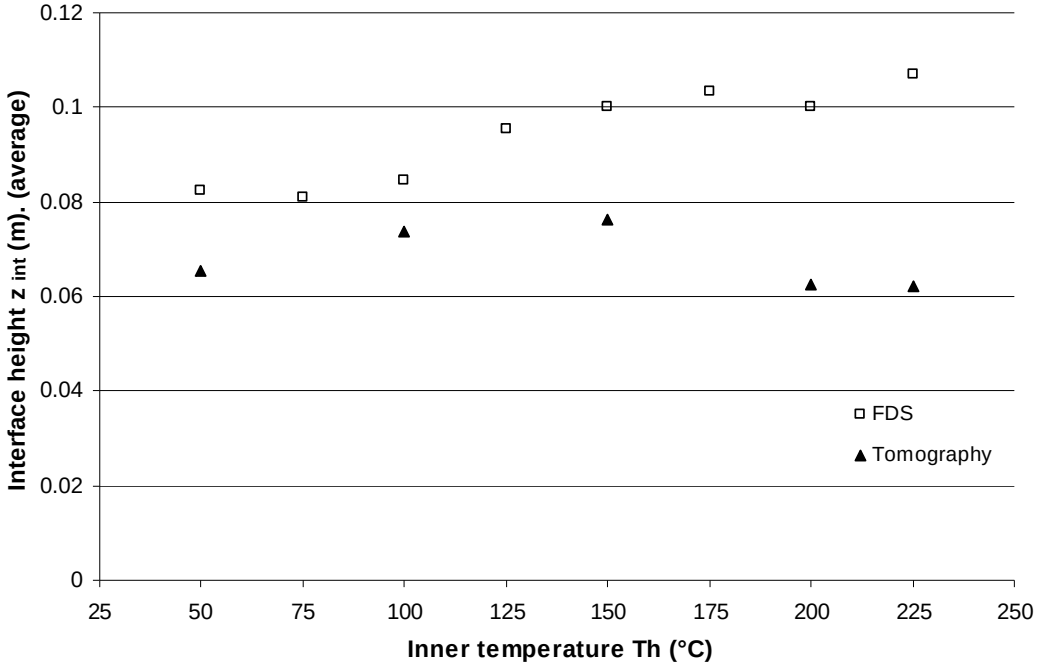

Figure 39: Average interface height z_{int} for various temperatures (average from t = 2.5 to 7 sec.)

Figure 40 shows the evolution and mean longitudinal component of the velocity (U and W stand for the horizontal and vertical velocity respectively and Vel stands for its norm) of the hot layer at the opening for T_h = 200°C. It shows an accelerating phase just after full opening (from 3 to 7 sec. for T_h = 75°C and 3 to 5 sec. for T_h = 200°C). The velocity fluctuations are damped after a few seconds and reach a constant value function of the T_h

values which allows the comparison of analytical and experimental average velocities. Figure 41 compares these average velocities for various temperature differences. There is a fair agreement between the results for the three methods, and tends to confirm the three phases flow theory developed in Paper [C].

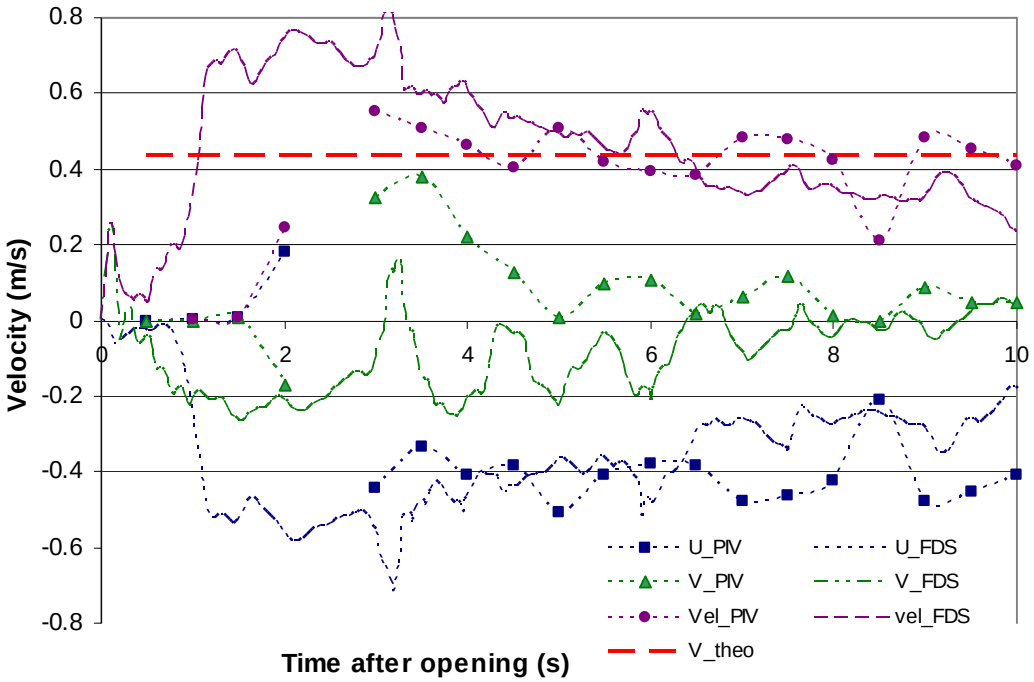

Figure 40: Velocity history at the opening for T_h = 200°C. Results from PIV measurements (average on probes 6 to 10), FDS simulation (probes 4 to 8) and average velocity from analytical study

Figure 41 shows the time average (on the steady period i.e. from t = 2.5 to 7 sec.) of the norm of velocity in the hot layer. This norm is spatially averaged considering a fixed value of the hot layer.

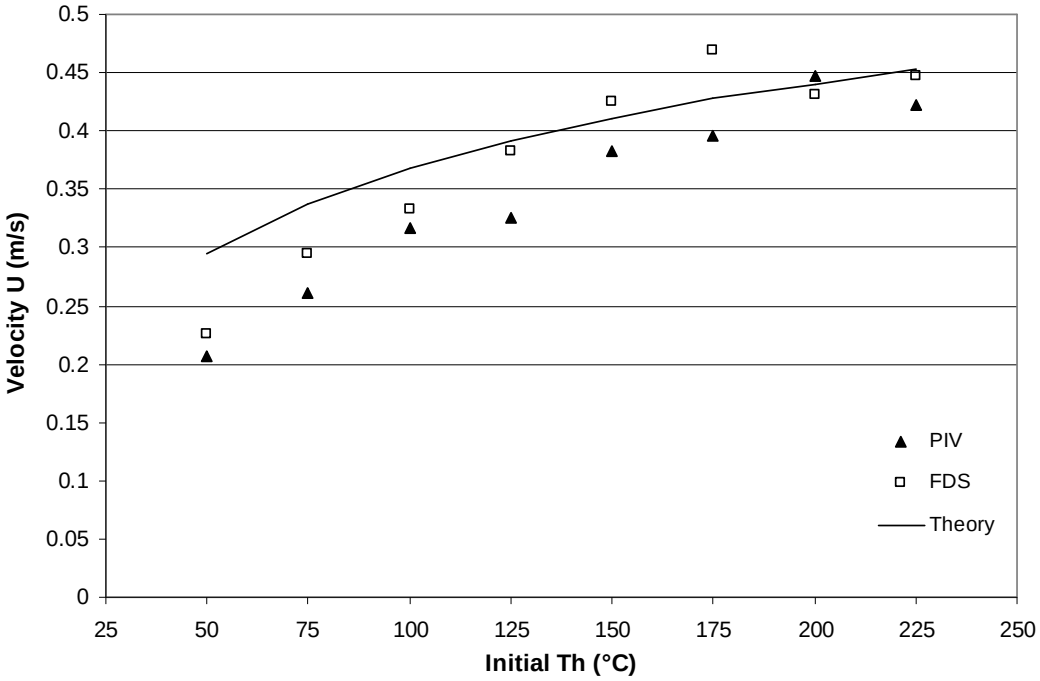

Figure 41: Average velocity as a function of the inner temperature. Average from t = 2.5 sec. and 7 sec.)

Figures 42 and 43 show the velocity profiles for the hot layer at the opening, using results from panel OP in Figure 16, at different times after opening. Fleischmann et al [21] first observed a particular shape of the velocity profile. Guigay et al. suggested a profile similar to potential flow in a 180 degree bend around a wall end (See Paper [D]). In that situation the velocity obeys the relation $V_{pf} \sim 1/r$. The equation for the potential flow equation follows thus:

$$V_{pf} = \frac{A}{r} + V_{min} \qquad (18)$$

The empirical constant A and the minimum velocity V_{min} have to be determined. Therefore, they are calibrated by optimization of the variance between the experimental profiles obtained by PIV. The same principle could be applied with numerical results from FDS, giving another profile.

After calibration with experimental data, the following profiles shown in Figures 42 and 43 are obtained:

For T_h = 75°C and t = 3.75 s, V_{pf} = -0.0051/r – 0.150

For T_h = 75°C and t= 6.5 s, V_{pf} = -0.0046/r – 0.110

For T_h = 200°C and t = 3 s, V_{pf} = -0.0042/r – 0.260

For T_h = 200°C and t = 6.75 s, V_{pf} = -0.0046/r – 0.260

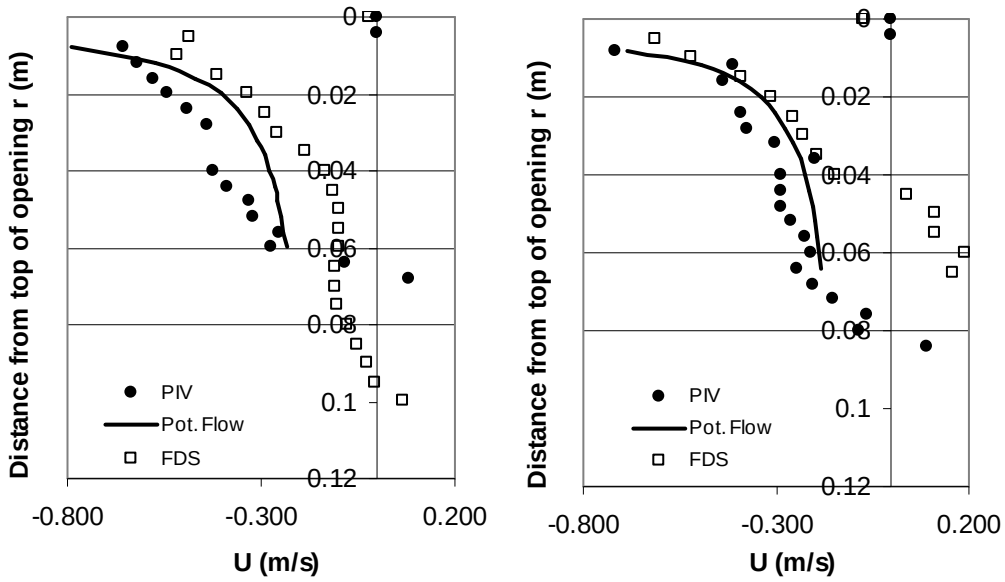

Figure 42: Velocity profile at the opening (panel OP) for T_h = 75°C after t = 3.75 sec. (left) and t = 6.5 sec. (right)

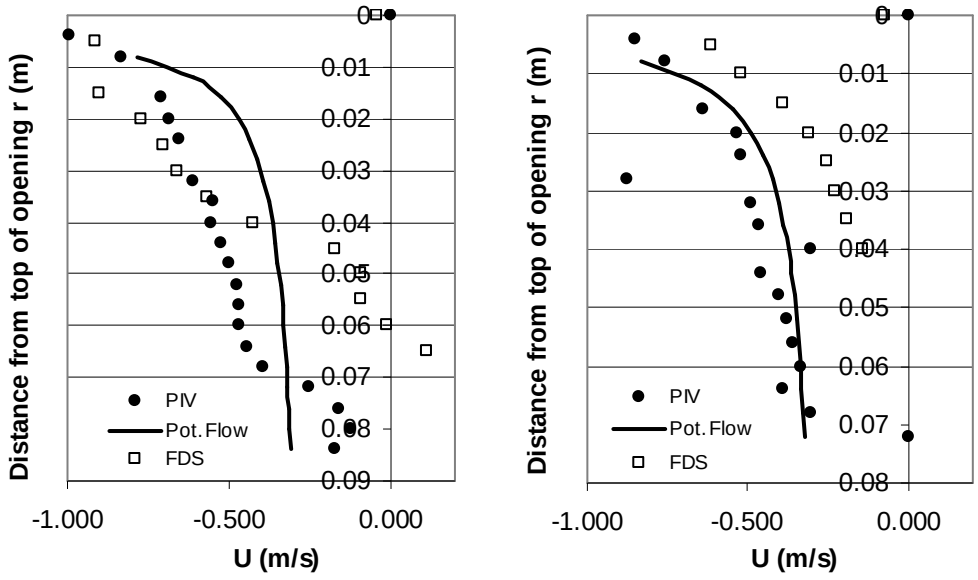

Figure 43: Velocity profile at the opening (panel OP) for T_h = 200°C after t = 3 sec. (left) and t = 6.75 sec. (right)

Results show that the shape of the velocity profiles changes significantly during the period between 3 to 6.75 seconds after opening, for both the experimental and numerical studies, confirming the very unsteady behavior of the flow. Experimental and numerical data does not agree very well, especially considering the width of the hot layer, i.e. from the top to the point where the profiles cross the vertical axis. However, Figures 42 and 43 are snapshots at particular times, and the time offset shown in Figures 35 and 36 can explain this difference, along with the width difference shown previously in Figure 33.

The potential flow profiles do not compare very well with the ones from the experiments, especially 3 sec. after opening. However, this is improved after 7 seconds, where the potential flow profiles are in good agreement with the profiles described by Fleischmann et al. [4]. Nevertheless, in [4], velocities were measured using only 6 fixed probes for a 40 cm opening, while using PIV allows such measurements at 40 positions for a 16 cm opening. Additionally, results using PIV allows the variation of the interface position to be taken into consideration. Consequently, it is difficult to conclude on an analytical description of the velocity profile at the opening.

8.3 Discussion

In this chapter, both qualitative and quantitative results from the FDS numerical model are compared to the experimental results from both PIV and fast tomography. In addition, quantitative results are also compared with an analytical description of the flow at the opening.

Qualitative observations of results from tomography and from the numerical model show that the flow is very unsteady, with turbulent structures creating an offset in both time and position of the interface. These structures are very similar, even though tomography shows vortex entrainment when simulations also show cusp entrainment (see Figure 59). Both create a momentum exchange, but cusp entrainment is more efficient in the mixing process. There is a very slight difference between cusp and vortex entrainment, and there have been very few publications differentiating these two processes. The interested reader is referred to Pedersen [55]. In order to avoid confusion, we will not differentiate the two processes and only refer to vortex entrainment.

Quantitatively, the unsteady behavior, shown by the variation of interface position (Figure 38), velocity histories both at the opening (Figure 40) and inside the compartment (Figures 35 and 36), makes it difficult to consider velocities averaged over a certain range of time after opening. However, these velocity histories seem to confirm a three phase behavior of the flow, with an accelerating phase, followed by a quasi steady phase and finally a decaying phase. It is possible to extract a significant mean longitudinal velocity for experimental, numerical and analytical results. The agreement between the three methods is considered to be fair concerning this mean longitudinal velocity at the opening. Comparison of experiments and simulations of the wave velocity inside the compartment is also carried out. Results agree generally well together, showing nevertheless a time offset of approximately 0.7 second. This offset is also shown by the comparison of transit times. The experimental quantitative results are strongly dependant on the seeding quality and the low frequency of PIV images, which limits the possibilities and the number of relevant mean velocity measurements. This limitation is enhanced by the very unstable behavior of the flow. However, there is generally a fair agreement between analytical, experimental and numerical quantitative results.

Concerning the qualitative comparison, both experiments and simulations show the same physical characteristics of the flow, with similar complex turbulent structures. The level of turbulence is higher than anticipated, especially in the experiments. The friction between the two layers seems therein somehow higher, with higher level of entrainment, which has the tendency to slow the progression of the wave.

From this comparison, it can be concluded that the physics of the phenomena is consistent between the FDS model and experiments, despite the slight differences cited above. The FDS model could be of course improved, but in general we can conclude that the FDS results are validated by the experimental results. As discussed in Chapter 7, the advantage of the numerical methodology is that it allows various visualizations and a more complex diagnostic. Consequently, in the next chapter, the FDS model will be used to study the turbulent structures previously identified and their role in the mixing process, in greater details.

9 ANALYSIS AND QUANTIFICATION OF THE MIXING PROCESS

The previous chapter has shown that the physics in the turbulent and mixing process on the numerical model (FDS) is consistent with experimental observations. In this chapter, the mixing induced by the turbulent structures and the vortices in the mixing process will be discussed in detail using the numerical results.

9.1 Middle opening configuration

In this part, we follow the evolution of the flow just after the opening. In the case shown in the following figures, the initial hot temperature is T_h = 125°C, but note the same structures and the same behavior law are observed with for every run within the studied temperature range.

Just after the opening, at t = 0.7 sec., the head of the flow entering the compartment is a mushroom shaped structure typical of a stationary jet (see Figure 44). This structure, sometimes also referred to as “sinking bubbles” in fluid mechanics, is composed of two counter-rotating coherent structures, one on each side of the flow. Figure 44 shows the velocity vectors colored by the temperature. The 2 x zoom on the head (Obs. 44.1) shows the hot fluid being entrained inside the vortices, creating important mixing. The temperature in the core of the vortices is already close to $(T_h-T_c) / 2$ = 62.5°C conforming this important mixing.

When the wave reaches the floor of the compartment, at t = 1 sec. (see Figure 45), the head is broken, with the inner vortex (Obs. 45.1) moving toward the opening wall. At this time, the outer vortex has already detached and created a coherent structure moving towards the back wall (Obs. 45.2). This highly mixed vortex could be a real ignition threat, if it hits an ignition source such as an electric spark or a hot surface.

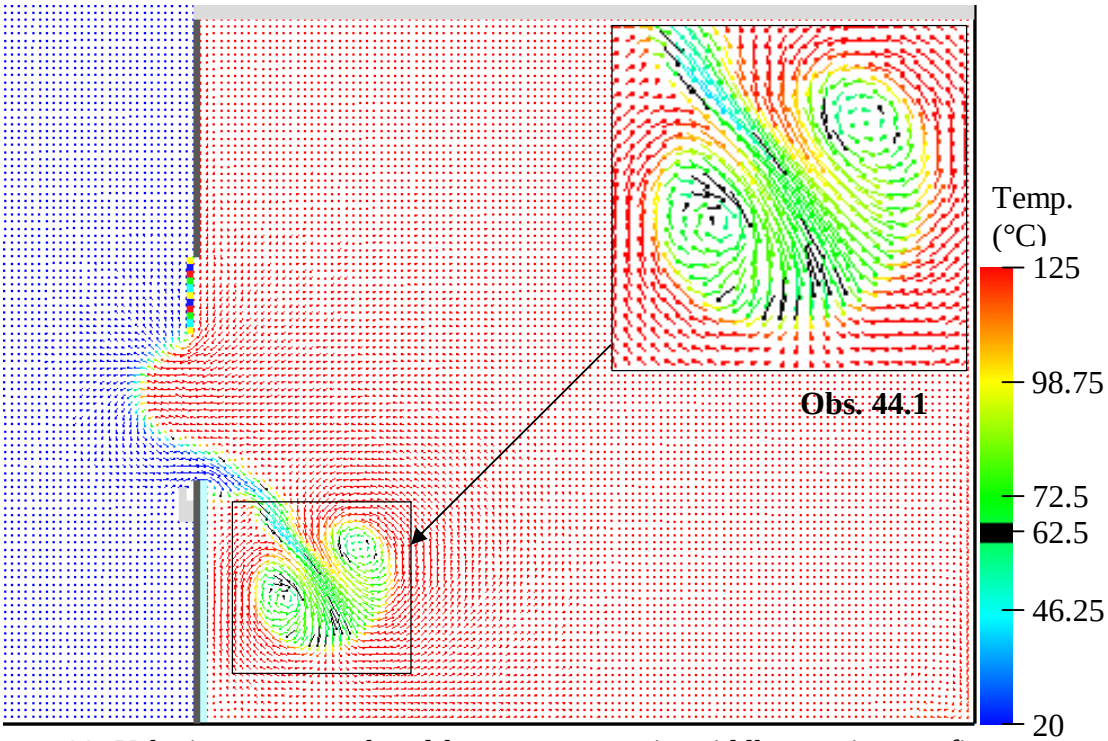

Figure 44: Velocity vectors colored by temperature in middle opening configuration and T_h = 125°C, at t = 0.7 sec. after opening, with 2 x *zoom on the head of the wave*

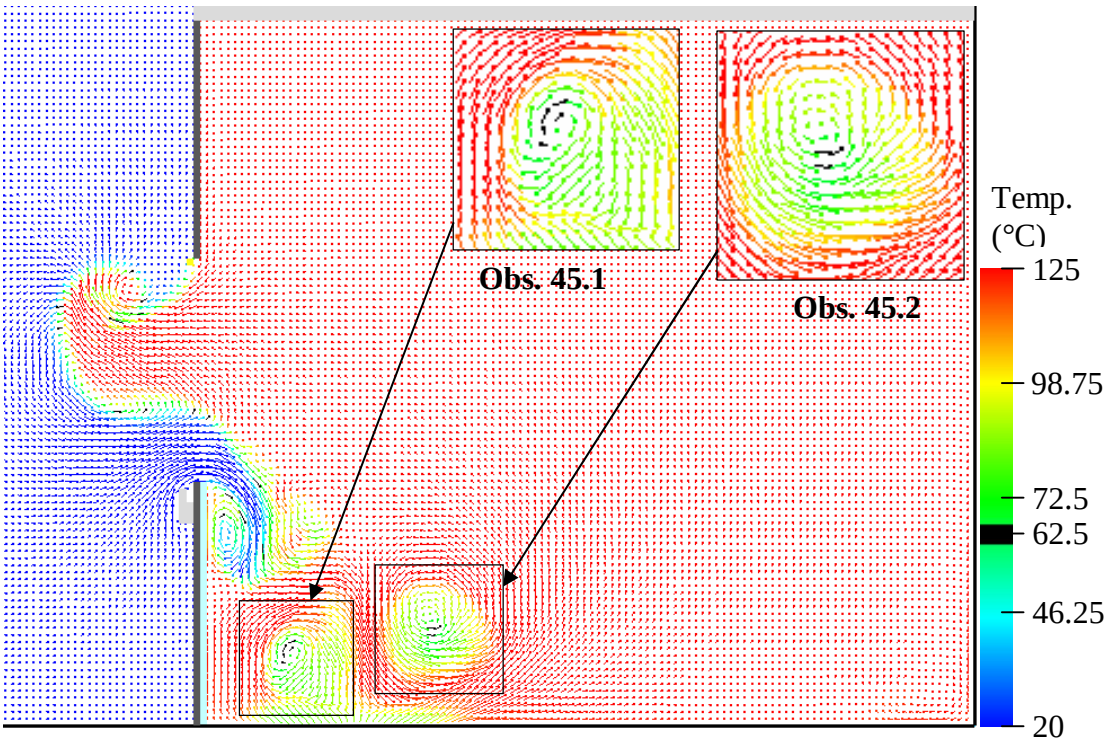

Figure 45: Velocity vectors colored by temperature in middle opening configuration and T_h = 125°C, at t = 1 sec. after opening, with 2 x *zoom on the inner and outer vortices detaching from the wave*

After t = 1.3 sec. (see Figure 46), the inner vortex moves up along the front wall creating a recirculation zone where cold air is entrained from the main flow, cooling this zone (Obs.

45.1). The outer vortex continues its way toward the back of the compartment, increasing its core temperature by entraining hot fluid.

After t = 1.7 seconds (see Figure 47), the inner vortex hits the incoming flow and splits the wave (with a detached pocket of cold air, Obs. 47.1), enhancing the mixing and the cooling of the recirculation zone between the waterfall and the front wall. Meanwhile, the head of the wave has gained in temperature and has almost reached the back wall.

The behavior of the wave after the rebound is shown in Fig, 25 in Chapter 7. It shows that if the rebound creates an important mixing zone, there is a fast dilution in the lower part of the compartment, creating a cold zone, while the upper part is still filled with hot fluid. Following is a rather stable two-zone situation, with the hot fluid flowing out of the compartment with critical condition at the opening.

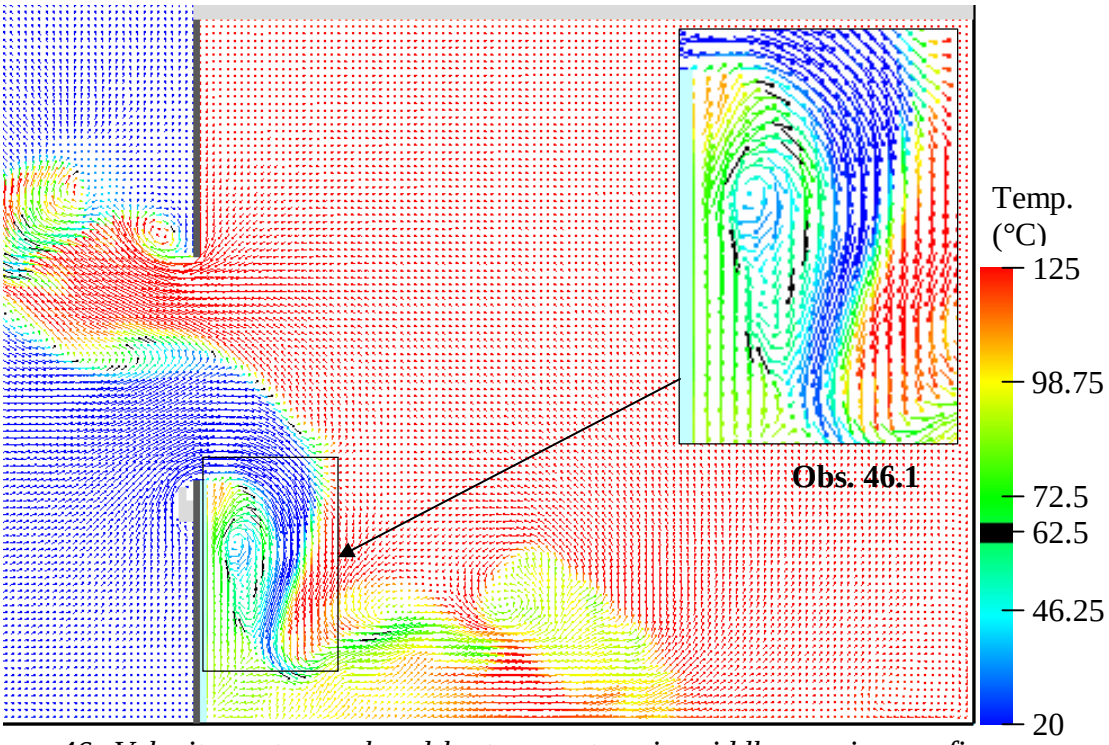

Figure 46: Velocity vectors colored by temperature in middle opening configuration and T_h = 125°C, at t= 1.3 sec. after opening, with 2 x *zoom on the recirculation created by the inner vortex*

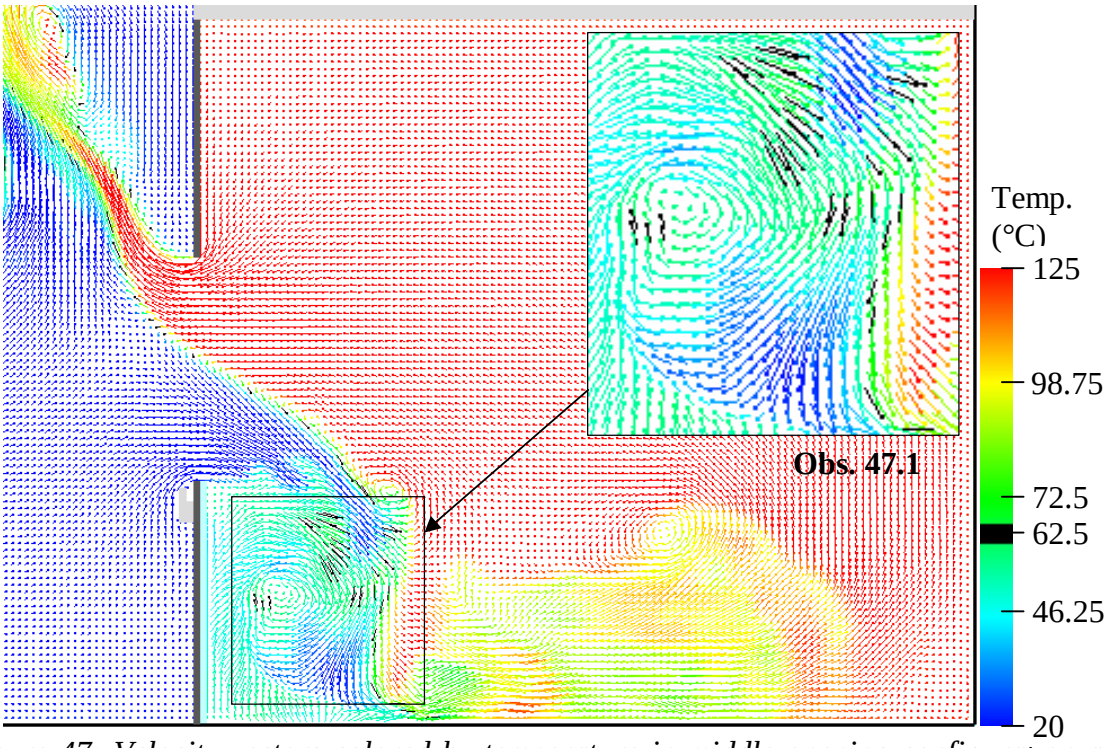

Figure 47: Velocity vectors colored by temperature in middle opening configuration and T_h = 125°C, at t= 1.7 sec. after opening, with 2 x *zoom on the recirculated inner vortex breaking the main flow*

9.2 Bottom opening configuration

In this section, we will discuss the flow after the opening. Figure 48 shows the temperature contours at t = 1.6 sec. The head of the gravity wave is formed by a wide counter rotating vortex, similar to the shape of the head of a forced flow (Obs. 48.1). The isotemperature T = 40°C is shown in black. It indicates that the head remains rather cool until the wave hits the back wall.

Figure 49 shows the wave when it reaches the back wall. Some mixing is created by the rebound. Here we notice some Kelvin-Helmholtz instabilities (Obs. 49.1) observed by tomography in Chapter 7, also responsible for some mixing. However, the mixing seems generally less important than in the middle opening configuration.

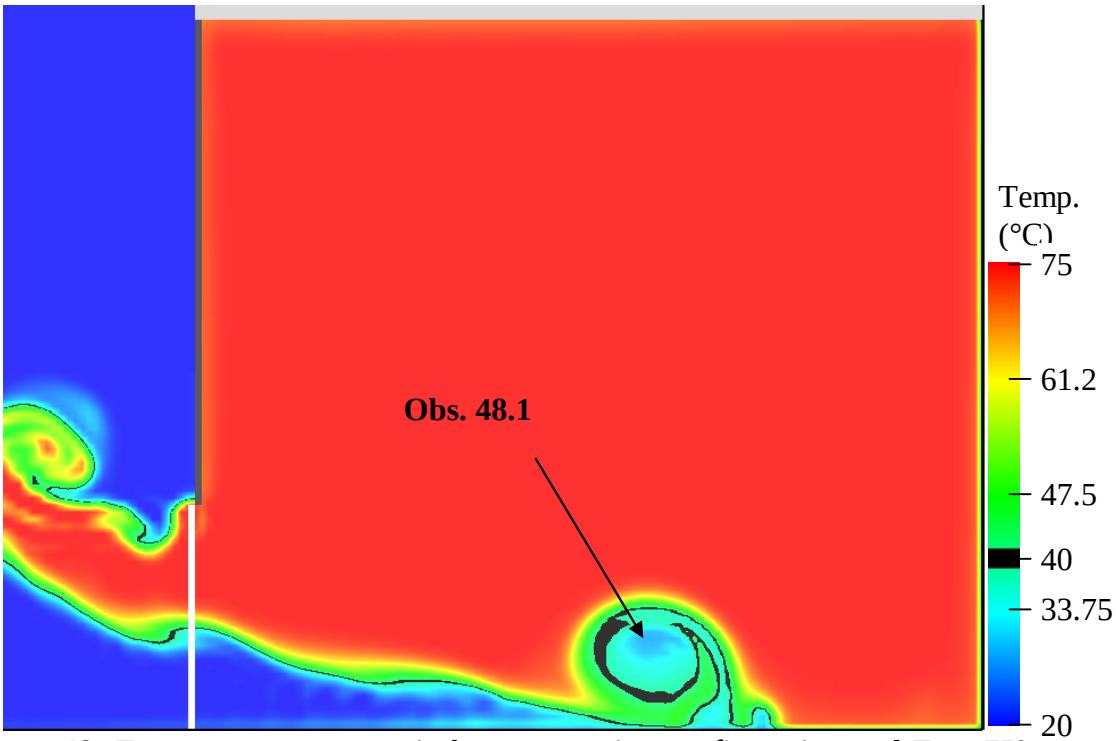

Figure 48: Temperature contours in bottom opening configuration and T_h = 75°C, at t= 1.6 sec. after opening

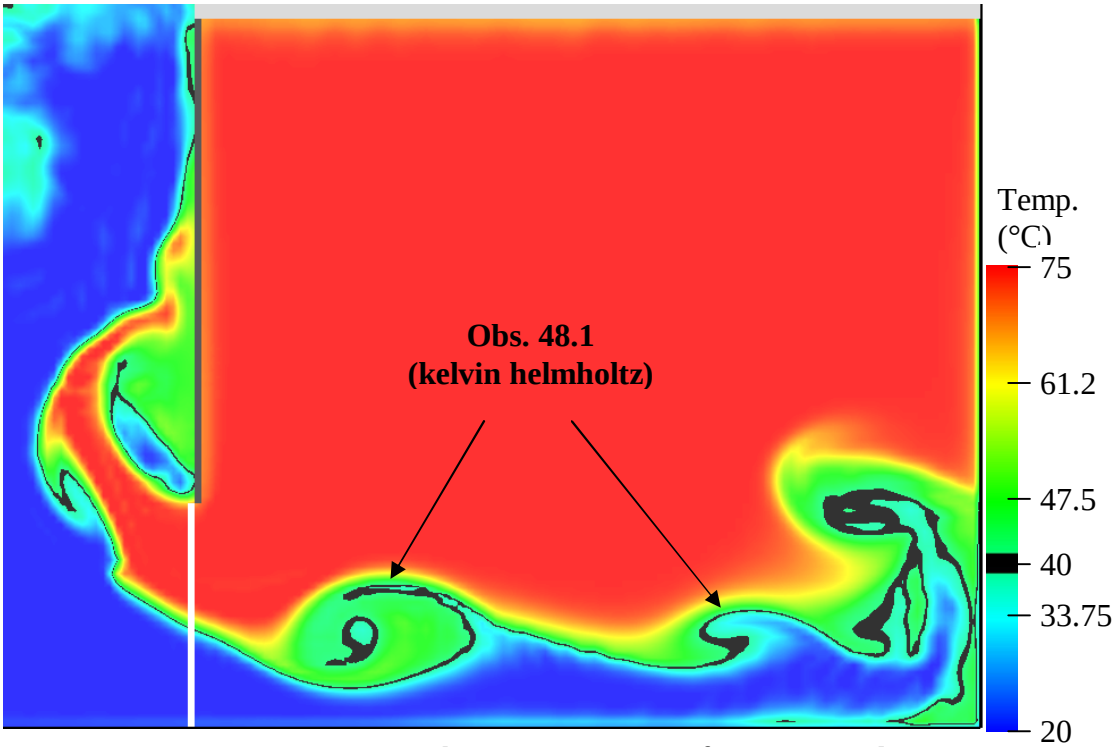

Figure 49: Temperature contours in bottom opening configuration and T_h = 75°C, at t= 3 sec. after opening

9.3 Quantification of the mixing

In this section, an attempt is made to estimate the mixing inside the compartment. To this purpose, the values of the mixing fraction recorded in the FDS slice file .sf is extracted using a short Fortran program fds2ascii.f which accompanies the FDS software. The values of mixing fraction in every cell of the symmetry plane are extracted every 0.2 sec.

Here, in order to estimate the mixing efficiency, we study the number of cells N (%) inside the compartment in which the mixing fraction f is between 0.4 and 0.6. This condition will be referred to as N[0.4 <f < 0.6].

9.3.1 Middle opening configuration

Figure 50 shows the evolution of this number of cells as a function of time, for different initial hot temperatures. The time when the wave hits the back wall (rebound) and when it reaches the opening (back wave) is shown by the vertical lines, for T_h = 100°C. The intensification of mixing (max. slope of N(t)) is maximum between the rebound and the back wave, and the peak value of mixing is just after the back wave, when the wave has just bumped into the inflow, and enhanced the mixing. Figure 51 shows the time average on 10 sec. and maximum number of cells N[0.4 < f < 0.6]. It also shows the time the maximum is reached, the time to rebound and the time to back wave. It shows that the mixing level is maximum when the wave comes back. The maximum and average value of N show that the mixing level is decreasing (except for T_{init} = 75°C) when the density difference increases. It seems that the dominating cause for mixing enhancing is the effect of the 2 waves, inflow and back wave, crossing and bumping into each other close to the opening rather than the rebound on the back wall. Shortly after the time when the back wave occurs, the mixing level drops and then oscillates around N = 5%.

It is interesting to note that the mixing process is much more intense and slower for T_h = 50°C. In the case of higher temperatures, the mixing level reaches its maximum value between rebound and back wave, showing that the rebound has more effect on mixing than for higher temperature differences. The slow motion of the gravity wave gives more time for the hot and cold layer to mix together and consequently the wave becomes thicker before hitting the back, which explains the more effective role played by the rebound on the mixing for this case.

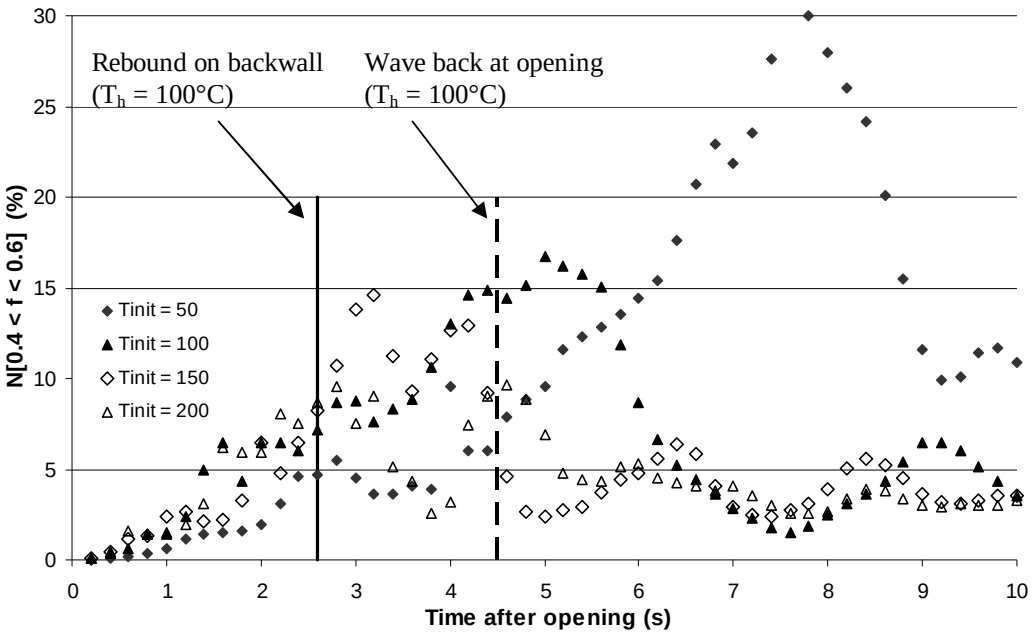

Figure 50: Time evolution of the number of cells N[0.4 < f < 0.6], for different initial temperature (middle opening configuration)

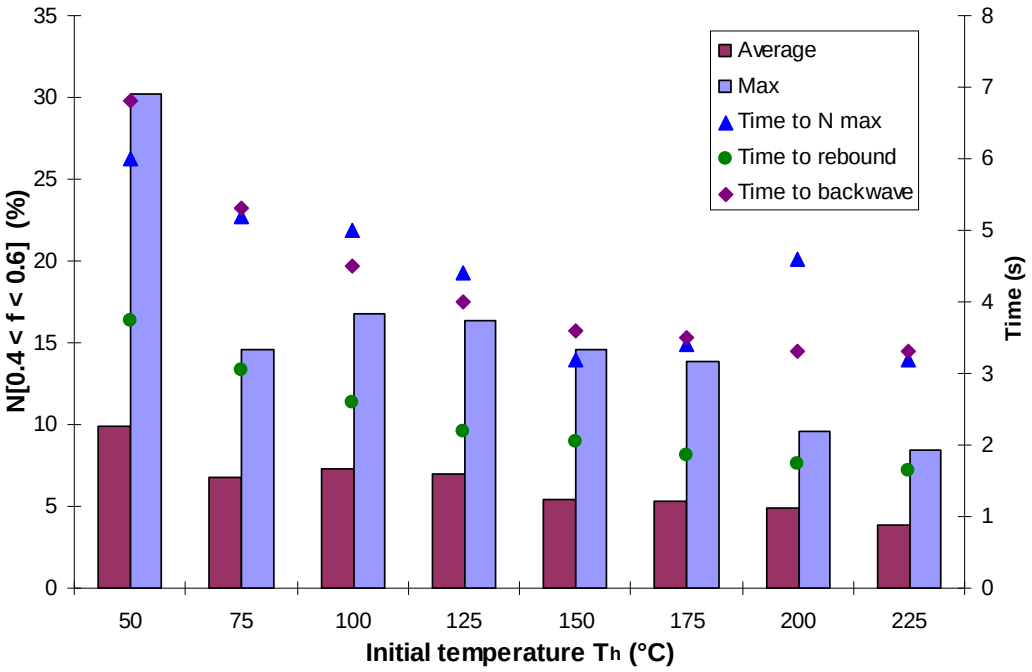

Figure 51: Average and maximum values of N[0.4 < f < 0.6] with the time to reach this maximum, the time to rebound and back wave for different initial temperature (middle opening configuration)

9.3.2 Bottom opening configuration

As previously for the middle opening configuration, Figure 52 shows the evolution of the number of cells N as a function of time, for different initial temperatures. The time when the

wave hits the back wall (rebound) and when it reaches the opening (back wave) is shown by the vertical lines, for T_h = 100°C. Figure 53 shows the average over 10 sec. and maximum number of cells N[0.4 < f < 0.6]. It also shows the time the maximum is reached, the time to rebound and to back wave. From Figure 52, we can observe that N is quickly oscillating, and that its maximum value is not necessarily reached at the first peak. Therefore, the time to first peak is added in Figure 53. The time to N max (or to first peak) is closer to the time to rebound, which is the dominating cause for mixing enhancing in this configuration. Comparing Figures 51 and 53 shows that the mixing level is much lower in the bottom opening configuration.

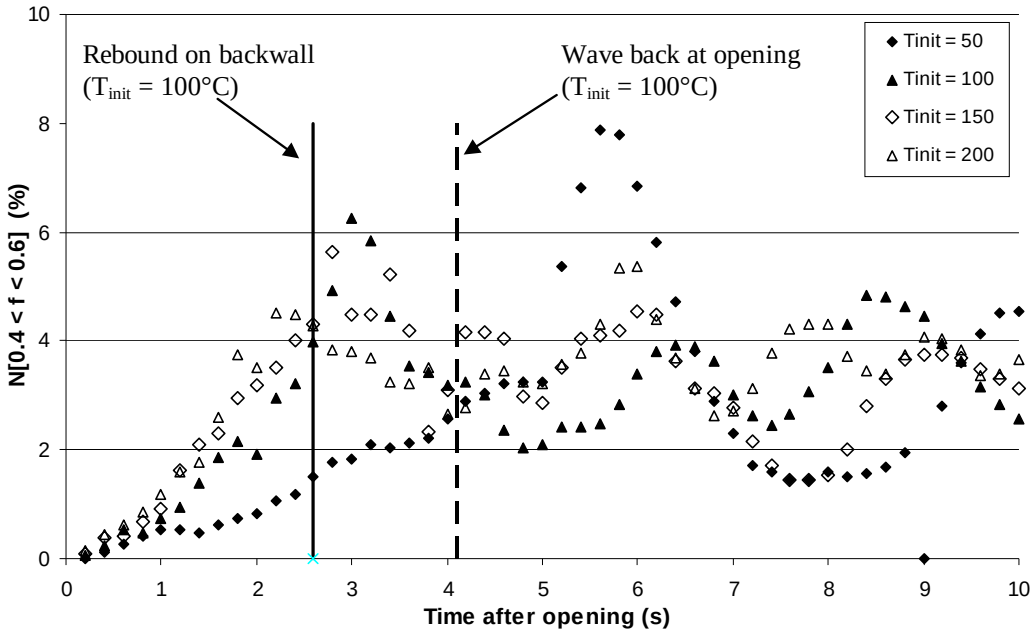

Figure 52: Time evolution of the number of cells N[0.4 < f < 0.6], for different initial temperature (bottom opening configuration)

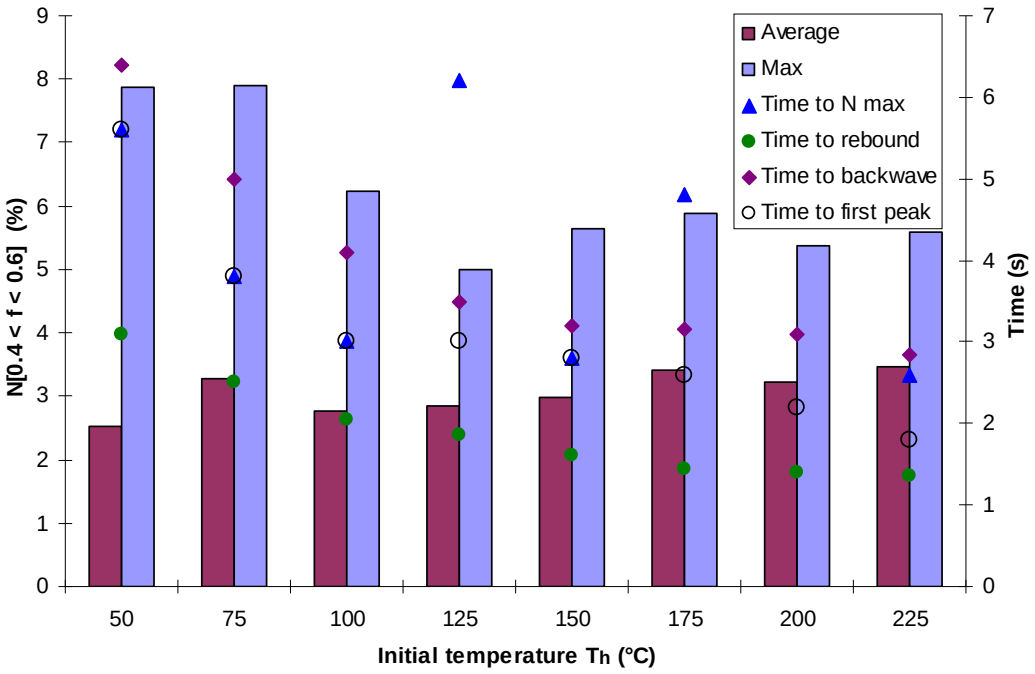

Figure 53: Average and maximum values of N[0.4 < f < 0.6] with the time to reach this maximum, the time to rebound and back wave for different initial temperature (bottom opening configuration)

9.3.3 Discussion

The evolution of the flow a short time after opening is studied in both the middle and bottom opening configuration. In the middle opening configuration, the head of the cold flow shows highly mixed turbulent coherent structures forming a mushroom or sinking bubble-like shape. When the cold flow hits the floor, highly mixed vortices detach from the flow and moving towards the compartment. These detaching vortices cold ignite in the back of the compartment event though the wave still hasn't reached the back wall. The recirculation zone below the opening is quickly filled with cold fresh oxygen and should not develop into a potential backdraft ignition region.

By studying the value of the mixing, the mixing intensity between the hot and cold layer and its evolution in time can be estimated and quantified. With FDS, we can observe the evolution of the mixed regions and determine where backdraft might occur.

The first observation is that the mixing level is significantly higher in the middle opening configuration (N= 10 to 30 %) than in the bottom opening configuration (N=5 to 8%). The time to maximum mixing is rather similar, roughly between 3 to 7 seconds depending on density differences, in both configurations. The mixing level then drops, and, in a last phase when the compartment is emptying, the mixing level oscillates. This oscillation period is roughly 2 sec., which corresponds to the oscillating period of the wave with the maximum value corresponding to the wave reaches the back wall.

The dominant source of mixing is depends on the opening configuration. When the opening is at the bottom, the main source is the rebound of the wave on the back wall. In the middle opening configuration, it is the bumping between the wave coming back from the wall after rebound and the inflow that causes a great deal to the mixing.

The mixing level is lower with higher density differences, as shown in Figures 51 and 53. It can be concluded that mixing is damped by acceleration.

In this case, we chose to simulate the experiments exactly, i.e. using hot and cold air as initial condition. A second model is created with a certain percentage of hot unburnt and inert gases as initial condition. After the opening allowing fresh oxygen to enter, the flammability envelope (where the concentration of unburnt gas is between its flammability limits) and its evolution can be studied with the same principle as with the mixing fraction applied in this section. Studying the evolution of the flammability envelope has been applied to test fire-fighting tactics in Paper [B].

10 CONCLUSION AND RECOMMENDATION FOR FURTHER WORK

During this thesis work, experiments, CFD and analytical calculation were carried out to study compartment fires and especially to characterize the gravity current and mixing process that may lead to backdraft. The following are the main conclusions:

- Under-ventilated compartment fires can lead to very sudden and hazardous phenomena, such as flashover, smoke gas explosion or backdraft. The last mentioned phenomenon is probably the most complex. Previous studies have identified the following conditions for backdraft to occur:
    - Complete extinction of the fire by oxygen starvation.
    - Mass fraction of unburnt fuel above a certain critical mass fraction (approximately 10 %, depending on the type of opening).
    - Sudden opening allowing fresh oxygen to enter carried by gravity current and subsequent mixing with unburnt gases creating a flammable mixture.
    - Presence of an ignition source.

  From these observations and reviews of actual and former studies on backdraft, it was decided to concentrate the research efforts mainly on the gravity currents and the mixing process.
- In order to investigate the hydrodynamic process leading to backdraft, numerical (CFD), analytical and experimental studies were carried out during this PhD work. The CFD software used in this thesis work was Fire Dynamic Simulator (FDS), the most widely used software for fire modeling. The analytical study was based on equations from classical hydraulics and densimetric Froude number condition. State of the art measurement methods such as Particle Image Velocimetry (PIV) and tomography were used for the first time in backdraft studies to characterize the gravity wave and the mixing process.
- The CFD technique has proven to be very useful when designing safer building or when testing the effectiveness of fire-fighting tactics, as discussed in Papers [A] and [B]. However, it is still not possible to correctly model incomplete combustion and extinction due to oxygen starvation and there is still room for improvement. This work has shown that by considering leakages and by forcing the extinction at a certain oxygen concentration level (LOI), the strongly under-ventilated fire experiments conducted within this work can be simulated in a reasonable manner. In FDS, the combustion model assumes that fuel and oxygen burn instantaneously when mixed and does therefore not allow the ignition and flame spread to be simulated well in the backdraft process.
- An analytical model based on classical hydraulic equations for two layer flows was set-up. It was developed from the open channel flow theory considering a reduced acceleration of gravity. The gravity wave inside the compartment was characterized by assuming a three-phase flow, acceleration, translatory and decay phase. A graphical method is obtained by solving the depth integrated equation for both layers, the momentum equation for both layers and for the lower layer, which allows

estimating the travel speed of a gravity wave on a flat bottom. The flow at the opening is calculated by considering the critical flow condition. This approach, developed from the open channel flow theory, is new to the fire community. It adds a new equation to the classical approach based on the Bernoulli equations and consequently gives an explicit solution for vent flow for the stratified case, which could not be achieved analytically without this additional equation.

- Previous findings from Fleischmann and Mc Grattan [4] showed that the shape of the flow at the opening was very different than the one suggested by Emmons [65] or Karlsson [1] based on pressure difference calculation. This observation was confirmed by series of experiments and CFD calculations carried out by the author during this thesis work. He also suggested a description based on potential flow theory, as shown in Figures 42 and 43. This particular shape of the flow is considered by introducing two correction coefficients which take into account the mixing and entrainment at the interface (C), as well as the uneven distribution of velocity (α). The coefficients are calibrated using results from [4] and are validated by comparing the flow characteristics obtained semi-analytically with simulations of Gojkovic's experiments [20]. This shows that the quantitative description of these correction coefficients was reasonably accurate (see Paper [D]).
- Experimental work was carried out during this PhD work to characterize the gravity wave in detail. The flow was measured for various temperature differences and two types of openings using PIV and tomography, which are complementary non intrusive measurement methods. The combination of these two methods gives a good qualitative and quantitative description of the velocity field and the wave behavior. The results show a very unsteady flow and a turbulence level higher than anticipated, especially in the middle opening configuration. Different types of turbulent structures or entrainment processes were observed for the first time in backdraft studies. Special attention has to be given to the choice of the seeding, as it has a great influence on the quality of the results. However, to obtain a more detailed quantitative description of the coherent turbulent structures, it would be advisable to increase the PIV frequency further than the 2 to 4 Hz, which was the maximum frequency allowed by the experimental apparatus used by the author in the present work.
- A CFD model of the experiments was set up using FDS. The main advantage of a CFD model is that it allows running many cases at little cost compared to experiments, and allows the measuring and visualizing of multiple scalar quantities. However, it is essential to validate numerical results against experiments, which was done in this work, by comparing with different experiments carried out by the author and other researchers.
- The results from the three methodologies, analytical, numerical and experimental, were compared and they generally showed a good agreement. Qualitatively, the results from the FDS model showed the same type of turbulent coherent structures observed in the experiments, as shown in Figures 28, 29 and 30. Quantitatively, there is a good agreement between the three methodologies concerning the mean longitudinal velocity, as shown in Figure 40. The velocity of the wave inside the compartment is slightly higher in the simulation than in the experiments, resulting in a shorter transit time. However, as shown in Figure 31, this difference is quite small, and might be due to the higher mixing level in the experiments, which slows the progression of the wave. Differences in quantitative measurements are probably due

to the very unsteady behavior of the flow and the low frequency of the PIV images. Despite some differences, it was concluded that the physics of the phenomena was consistent between the FDS model and experiments, thus validating the numerical results.

- Once validated, the FDS model was used to investigate the mixing process between the two-layers in greater detail, as well as ways to quantify this mixing were considered. Results showed that coherent turbulent structures, such as counter rotating vortices detaching from the waterfall in the middle opening configuration and Kelvin-Helmoltz instabilities in the bottom opening configuration, played an essential role in the mixing process. However, the mixing appeared generally less important in the bottom opening configuration than in the middle opening configuration. In the latter the first highly mixed detaching vortex could be a real ignition threat, if it were to hit an ignition source. The mixing quantification showed a higher mixing level in the middle opening configuration and that he dominant source of mixing was different depending on the configuration. It also showed that the mixing level is lower with higher density differences, as shown in Figures 51 and 53. It can be concluded that mixing is damped by acceleration.

The particular problem of extinction and its numerical modeling is currently studied by several research groups, and especially by the FDS group led by Kevin McGrattan at NIST. The ignition and the spread of the backdraft are also studied by different groups. On the other hand, the complex hydrodynamic process of the gravity wave and the mixing between hot and cold fluid prior to backdraft still requires further efforts. Here is therefore a list of possible orientations and recommendations for future research:

- New experiments should be conducted, with fast PIV (frequency 100 Hz), to get a complete quantitative description of the turbulent structures observed qualitatively. It should be kept in mind, however, that PIV creates a huge amount of data (the PIV experiments presented in this document gave more than 20 Gbytes of data with a frequency between 2 to 4 Hz only). It should therefore be recommended to limit the number of runs to keep the amount of data to a reasonable minimum. The experience gained from the first experimental series described in this thesis leads to the following recommendations:
    - A longer experimental compartment could be used, where the phenomenon lasts longer without being disturbed by the rebound and the returning wave, that disturb the inflow.
    - The seeding of the flow should be improved and tested using fast PIV. New types of particles and seeding procedures should be tested.
    - Some experiments could include combustion and backdraft ignition. However, for a matter of personal and material safety, it will not be possible to observe any flow details, and such experiments will require considerable financial efforts to satisfy the safety requirements for explosive experiments.
- Experimental results using fast PIV will permit statistical studies to be made as well as measurements of the turbulence spectrum. An attempt to develop an interfacial shear stress model has been carried during this thesis work, but due to the unsteadiness of the flow, a better time resolution is required to collect sufficient data.
- A study of the gas concentration in each cell at every time step of the simulation could determine where and when the highest probability of ignition is. However, a good

mesh resolution and a small time step would be necessary to obtain significant results; therefore this study will require some important computing efforts and capacities.

- The numerical model can be used to test the influence of the initial conditions or the geometry on the gravity wave behavior and the resulting mixing by changing for example the type of opening.

The field of under-ventilated fires still needs considerable amount of work with regards to various areas such as combustion, turbulence and radiation to name a few. The conclusions and recommendations for future work discussed above are given in respect to the work carried out in this thesis.

NOMENCLATURE

Latin letters

A	Dimensionless coefficient. $A=(L/h)f_i$
b	Width of channel
B	Dimensionless coefficients. $B=2(L/h)C_f$
C	Velocity correction factor due to mixing and entrainment
C_c	Velocity correction factor due to mixing and entrainment (cold layer)
C_f	Bottom friction factor
C_h	Velocity correction factor due to mixing and entrainment (hot layer)
Cor	Correlation function (PIV measurements)
C_Δ	Non dimensional wave velocity
dt	Time step between consecutive light pulse
dx	Displacement in horizontal direction
dx_{op}	Displacement in horizontal direction (Panel OP)
dx_{out}	Displacement in horizontal direction (Panel OU)
dx0	Original displacement in horizontal direction
$dx0_{op}$	Original displacement in horizontal direction (Panel OP)
dx'_{out}	Displacement in horizontal direction (Panel OU')
$dx'0_{out}$	Original displacement in horizontal direction (Panel OU')
dz	Displacement in vertical direction
dz_{op}	Displacement in vertical direction (Panel OP)
dz_{out}	Displacement in vertical direction (Panel OU)
dz0	Original displacement in vertical direction
dz'_{out}	Displacement in vertical direction (Panel OU')
$dz'0_{out}$	Original displacement in vertical direction (Panel OU')
E	Specific energy
E_{min}	Minimum specific energy
f	Mixing fraction. $f = Y_h / Y_c$
f_i	Interfacial friction factor
Fr	Froude number
g	Acceleration of gravity
h	Height of the opening
I	Integration function
I_{pix}	Intensity of a pixel
K_{safety}	Safety factor
n	Size in pixels of the interrogation window
N	Number of cells (Mixing fraction condition)
q	Discharge per unit width
Q	Discharge
Q_{vent}	Flow rate through ventilation system
Q_{leak}	Flow rate through leakages
r	Distance to the top of the opening for potential flow theory
t	Time
T	Temperature

T_c	Temperature of the cold layer
T_h	Temperature of the hot layer
U	Horizontal component of velocity
V	Velocity of the flow
V_{cr}	Critical velocity of the flow
V_{min}	Minimum velocity in potential flow
V_{sound}	Speed of sound depends in dry air
$V_{op,c}$	Average velocity of the cold layer at the opening
$V_{op,h}$	Average velocity of the hot layer at the opening
V_{pf}	Velocity in potential flow
Vel	Norm of velocity
W	Vertical component of velocity
x	Horizontal coordinate
y	Depth of channel flow, lateral coordinate
$y_{c,n}$	Thickness of the cold layer at point n
y_{cr}	Critical depth
Y_c	Mass concentration of cold air
Y_h	Mass concentration of hot air
z	Vertical coordinate

Greek letters

α	Velocity correction factor due to uneven distribution of velocity
α_c	Velocity correction factor due to uneven distribution of velocity (cold layer)
α_h	Velocity correction factor due to uneven distribution of velocity (hot layer)
Δ	Dimensionless reduced mass function
Δ_c	Dimensionless reduced mass. $\Delta_c = (\rho_c-\rho_h)/\rho_c$
Δ_h	Dimensionless reduced mass. $\Delta_h = (\rho_c-\rho_h)/\rho_h$
ρ_c	Density of the cold layer
ρ_h	Density of the hot layer
ψ	Dimensionless gravity current thickness over depth ratio. $\psi = y_{c,n}/h$

Abbreviations

ATEX	Explosive atmosphere
B	Bottom
BA	Back
CFD	Computational Fluid Dynamics
DNS	Direct Numerical Simulation
FDS	Fire Dynamics Simulator
FL	Floor
FVM	Finite Volume Method
LES	Large Eddy Simulation
LFL	Lower Flammability Limit
LOI	Limiting Oxygen Index
M	Middle
NIST	National Institute of Standard and Technology
Obs	Observation
OP	Opening

OU	Outside
PIV	Particle Image Velocimetry
PPV	Positive Pressure Ventilation
RANS	Reynolds Average Navier Stokes
SFPE	Society of Fire Protection Engineers
THCP	Thermocouple
Tom	Tomography
UFL	Upper Flammability Limit
WF	Waterfall

REFERENCES

[1] Karlsson, B., Quintiere, J.G. 1986, *Enclosure Fire Dynamics*, CRC press, New York.

[2] Drysdale, D. 1992, *An Introduction to Fire Dynamic*, 2nd edn, Wiley-Interscience, Chichester.

[3] *SFPE Handbook of Fire Protection Engineering*, 2nd edn, 1995, National Fire Protection Association, Quincy, MA.

[4] Fleischmann, C.M., McGrattan, K.B. 1999, 'Numerical and Experimental Gravity Currents Related to Backdrafts', *Fire Safety Journal*, vol. 33 pp. 21-34.

[5] Babrauskas, V. 1994, 'Heat Release Rate – Comment', *Fire Technology*, vol. 30, no. 4, pp. 478-479.

[6] Babrauskas, V., Peacock, R.D. 1992, 'Heat Release Rate - The Single Most Important Variable in Fire Hazard', *Fire Safety Journal*, vol. 18, no. 3, pp. 255-272.

[7] Babrauskas, V., Grayson, S.J. 1992, *Heat Release in Fires*, Elsevier Applied Science Publishers, London.

[8] Babrauskas, V., 'Burning rates', *SFPE Handbook of Fire Protection Engineering*, 2nd edn., 1995, National Fire Protection Association, Quincy, MA.

[9] Tewarson, A., 'Generation of Heat and Chemical Compound in Fires', *SFPE Handbook of Fire Protection Engineering*, 2nd edn., 1995, National Fire Protection Association, Quincy, MA.

[10] Hugget, C. 1980, 'Estimation of Rate of heat Release by means of Oxygen-Consumption Measurements', *Fire and Materials*, vol. 4, no. 2, pp. 61-65.

[11] Pitts, V.M. 1995, 'The Global Equivalence Ratio Concept and the Formation Mechanisms of Carbon Monoxide in Enclosure Fires', *Progress in Energy and Combustion Science*, vol. 21, no. 3, pp. 197-237.

[12] Gottuk, D.T., Roby, R.J., 'Effect of Combustion Condition on Species Production', *SFPE Handbook of Fire Protection Engineering*, 2nd edn., 1995, National Fire Protection Association, Quincy, MA.

[13] Floyd, J.E., McGrattan, K.B. 2007, 'Multiple Parameter Mixture Fraction with Two-step Combustion Chemistry for Large Eddy Simulation', *Proceedings of 10th Interflam conference*, London.

[14] Bengtsson. L.G., Karlsson, B. 2000, 'An Experimental and Statistical Study of the phenomenon Flashover, Backdraft and Smoke Gas Explosion', *Proceedings of the 3rd international seminar on Fire and Explosion Hazards*, Lancashire, 2000.

[15] Bengtsson, L.G. 2001, *Enclosure fires*, Swedish Rescue Services Agency.

[16] Chitty, R. 1994, *A Survey on Backdraught*, Pub No 5/94, Fire Research Station.

[17] Fahy, R.F., LeBlanc, P.R. 2005, *Fire-Fighters Fatalities in the United States*, Fire Analysis and Research Division, National Fire Protection Association.

[18] Zalosh, A., 2007, 'Analysis of a New York City Flammable Liquids Fire Leading to a Backdraft Explosion', *Proceedings of the 5th international seminar on Fire and Explosion Hazards*, Edinburgh.

[19] Bukowski, R.W. 1995, 'Modeling a Backdraft: The Fire at 62 Watts Street', *NFPA Journal*, vol. 89, no. 6, pp. 85-89.

[20] Gojkovic, D. 2001, *Initial Backdraft Experiments*, Report 3121, Department of Fire Safety Engineering, Lund University, Sweden.

[21] Fleischmann, C.M.1993, *Backdraft Phenomena*, Doctoral thesis, NIST –GCR-94-646, University of California, Berkley.

[22] Gottuk, D.T., Peatross, M.J., Farley, J.P., Williams, F.W. 1999, 'The development and mitigation of backdraft: a real-scale shipboard study', *Fire Safety Journal*, vol. 33, pp. 261-282.

[23] Weng, W.G., Fan, W.C. 2002, 'Experimental Study on the Mitigation of Backdraft in Compartment Fires with Water Mist', *Journal of Fire Sciences*, vol. 20, no. 4, pp. 259-278.

[24] Weng, W.G., Fan, W.C. 2003, 'Critical Condition of Backdraft in Compartment Fires: a Reduced-Scale Experimental Study', *Journal of Loss Prevention in the Process Industries*, vol. 16, pp.19-26.

[25] Zhou, F., Wang, D. 2005, 'Backdraft in Descensionally Ventilated Mine Fire', *Journal of Fire Sciences*, vol. 23, no. 3, pp.261-271.

[26] Elíasson. J., Guigay. G., Karlsson. B. 2008, 'Enclosure Fires, Gravity Currents and the Backdraft Problem', *Journal of Fire Sciences*, DOI: 10.1177/0734904108092116, JFS 092116, in press.

[27] Guigay, G., Elíasson, J., Horvat, A., Sinai, Y., Karlsson, B. 2008, 'Semi-Analytic and CFD Calculation of Gravity Flows in Backdraft Studies', *Submitted for publication in Journal of Fire Sciences.*

[28] Chow. W.K., Zou, G.W. 2005, 'Correlation Equations on Fire-Induced Air Flow Rates through Doorway Derived by Large Eddy Simulation', *Building and Environment*, vol. 40, pp.897-906.

[29] Horvat, A., Sinai, Y. 2007, 'Numerical Simulation of Backdraft Phenomena', *Fire Safety Journal*, vol. 42, no. 3, pp. 200-209.

[30] Ferraris, S.A., Wen, J.X. 2007, 'Dembelle S. Large Eddy Simulation of the Backdraft Phenomenon', *Fire Safety Journal*, DOI:10.1016, in press.

[31] Yang, R., Weng, W.G., Fan, W.C., Wang, Y.S. 2005, 'Subgrid Scale Laminar Flamelet Model for Partially Premixed Combustion and its Application to Backdraft Simulation', *Fire Safety Journal*, vol. 40, no. 2, pp. 81-98.

[32] Branca, C., Di Blasi, C. 2008, 'Oxidative Devolatilization Kinetics of Wood Impregnated with two Ammonium Salts', *Fire Safety Journal*, DOI: 10.1016/j.firesaf.2007.11.004, in press.

[33] Di Blasi, C., Branca, C., Galgano, A. 2008, 'Thermal and Catalytic Decomposition of Wood Impregnated with Phosphorous- and Sulfur-containing Ammonium Salts', *Polymer Degradation and Stability*, vol. 93, no. 2, pp.335-346.

[34] Di Blasi, C., Branca, C., Galgano, A. 2008, 'Products and Global Weight Loss Rates of Wood Decomposition Catalyzed by Zinc Chloride', *Energy & Fuels*, vol. 22, pp.663-670.

[35]Di Blasi, C., Branca, C., Galgano, A. 2007, 'Flame Retarding of Wood by Impregnation with Boric Acid - Pyrolysis Products and Char Oxidation Rates', *Polymer Degradation and Stability*, vol. 92, pp. 752-764.

[36] Di Blasi, C., Branca, C. 2007, 'Oxidation characteristics of chars generated from wood impregnated with (NH4)2HPO4 and (NH4)2SO4', *Thermochimica Acta*, vol. 456, pp. 120-127.

[37] Di Blasi, C., Branca, C., Galgano, A. 2007, 'Effects of Diammonium Phosphate on the Yields and Composition of Products from Fire Wood Pyrolysis', *Industrial & Engineering Chemistry Research*, vol. 46, pp. 430-438.

[38] Galgano, A., Di Blasi, C., Horvat, A., Sinai, Y. 2006, 'Experimental Validation of a Coupled Solid- and Gas-phase Model for Combustion and Gasification of Wood Logs', *Energy & Fuels*, vol. 20, pp. 2223-2232.

[39] Galgano, A., Di Blasi, C. 2006, 'Coupling a CFD Code with a Solid Phase Combustion Model', *Progress in Computational Fluid Dynamics*, vol. 6, pp. 287-302.

[40] Tofilo, P., Delichatsios, M.A. 2004, 'Heat Fluxes to the Walls in Enclosure Fires', *Proceedings of the 6th Asia – Oceania Symposium for Fire Safety and Technology*, Daegu, South Korea.

[41] Tofilo, P., Delichatsios, M.A., Silcock, G.W.H, 2005,'Effect of fuel sootiness on the heat fluxes to the walls in enclosure fires', *Proceedings of the 8th IAFSS Symposium*, Beijing.

[42] Rosario, R.A.F., Dembele, S., Wen, J.X. 2007, 'Investigation of Glazing Behaviour in a Fire Environment using a Spectral Discrete Ordinates Method for Radiative Heat Transfer', *Numerical Heat Transfer*, vol. 52, no. 6, pp. 489-506.

[43] Most, J.M., Pearson, A., Ferraris, S. 2006, 'Caractérisation du Mécanisme de Stabilisation d'une Combustion Diluée', *10ème Congrès Francophone de Techniques Laser*, Toulouse, France.

[44] Horvat, A., Sinai, Y., Gojkovic, D., Karlsson, B. 2008, 'Numerical and Experimental Investigation of Backdraft', *Combustion Science and Technology*, vol. 180, no. 1, pp 45-63.

[45] Ferraris, S.A., Wen, J.X., Dembele, S. 2007, 'Large Eddy Simulation of the Backdraft Phenomena', *Fire Safety Journal*. In Press, available online in Sept. 2007.

[46] Magda, S.I., Ferraris, S.A., Dembele, S., Wen, J.X., Karwatzki, J. 2005, 'LES Simulation of a Backdraft with Water Mist', *Journal of Applied Fire Science*, vol. 13, no. 3.

[47] Ferraris, S.A., Wen, J.X. 2007, 'Large Eddy Simulation of a Lifted Turbulent Jet Flame', *Combustion and Flame*, vol. 150, no. 4, pp. 320-339.

[48] Ferraris, S., Dembele, S. ,Wen, J.X. 2005, 'Large-Eddy Simulation of a Large-scale Methane Pool Fire', *Accepted by the 9th Int. Symp. On Fire Safety Science.*

[49] Guigay, G., Gojkovic, D., Bengtsson, L.G., Karlsson, B., Elíasson, J. 2008, "Evaluation of Firefighting Tactics in a Possible Backdraft Situation Using CFD

Calculation", *Fire Technology* (FIRE 93R1), DOI:10.1007/s10694-008-0058-4, 2008, in press.

[50] Guigay, G., Most, J.M., Karlsson, B., Elíasson, J., Penot, F. 2007, 'Experimental Investigation of the Influence of Gas Hydrodynamics on Backdraft Studies', *Poster and paper in proceedings of the 11th Interflam conference*, London.

[51] Elíasson, J., Kjaran, S.P., Holm, S.L., Gudmunsson, M.T., Larsen, G. 2007, 'Large Hazardous Floods as Translatory Waves', *Environmental Modeling and Software*, vol. 22 pp. 1392/1399.

[52] Stoker, J.J. 1992, *Water Waves. The Mathematical Theory with Applications*, Interscience Publishers, London.

[53] Pedersen, F.B. 1986, *Environmental Hydraulics: Stratified Flows*, Springer-Verlag Editions, Berlin Heidelberg.

[54] Anderson, J.D. 1995, *Computational Fluid Dynamics*, McGraw-Hill, New-York.

[55] Davidson, P.A. 2004, *Turbulence*, Oxford University Press, New York.

[56] ANSYS CFX, 1998, [online] http://www.ansys.com/products/cfx.asp and documentation [online] http://www-waterloo.ansys.com/community/

[57] McGrattan, K., Hostikka, S., Floyd, J., Baum, H., Rehm, R. 2008, *Fire Dynamics Simulator (Version 5) Technical Reference Guide*, NIST Special Publication 1018-5.

[58] McGrattan, K., Klein, B.K., Hostikka, S., Floyd, J. 2008, *Fire Dynamics Simulator (Version 5) User's Guide*, NIST Special Publication 1019-5.

[59] National Institute of Standards and Technology, 2005, [online] http://www.nist.gov.

[60] Kawagoe, K. 1958, *Fire Behaviour in Rooms*, Report No. 27, Building Research Institute, Japan, pp. 1–72.

[61] Steckler, K.D., Quintiere, J.G., Rinkinen, W.J. 1982, *Flow Induced by a Fire in a Compartment*, US Department of Commerce, NBSIR 82-2520.

[62] Rockett, J. 1976, 'Fire Induced Gas Flow in an Enclosure', *Comb. Sci. Tech.*, vol. 12, pp. 165–175.

[63] Babrauskas, V., Williamson, R.B. 1978, 'Post-Flashover Compartment Fires: Basis of a Theoretical Model', *Fire and Materials*, vol. 2, no. 2, pp. 39–53.

[64] Chow, W.K., Zou, G.W. 2005, 'Correlation Equations on Fire-Induced Air Flow Rate Through Doorway Derived by Large Eddy Simulation', *Building and Environment*, vol. 40, pp. 897-906.

[65] Emmons, H.W. 1995, 'Vent Flows', *SFPE Handbook of Fire Protection Engineering*, 2nd edn., 1995, National Fire Protection Association, Quincy, MA.

[66] White, F.M. 1999, *Fluid Mechanics*, 4th edn., WCB McGraw-Hill.

[67] Lavision Product information [online] http://www.lavision.de/

[68] Pretrel, H., Querre, P., Forestier, M. 2005, 'Experimental Study of Burning Rate Behavior in confined and Ventilated Fire Compartments', *Proceedings of the 8th IAFSS Symposium*, Beijing.

[69] Hu, Z., Utiskul, Y., Quintiere, J., Trouve, A. 2005, 'A Comparison between Observed and Simulated Flame Structures in Poorly Ventilated Compartment Fires', *Proceedings of the 8th IAFSS Symposium*, Beijing.

[70] Utiskul, Y., Quintiere, J., Rangwala, A., Ringwelski, B., Wakatsuki, K., Naruse, T. 2005, 'Compartment fire phenomena under limited ventilation', *Fire Safety Journal*, vol. 40, pp.367-390.

[71] Utiskul, Y., Quintiere, J., Naruse, T. 2004, 'Wall-Vent Compartment Fire Behavior Under Limited Ventilation', *Proceedings of 10th Interflam conference*, Edinburgh.

[72] Most, J.M., Pearson, A., Guigay, G., Karlsson, B. 2006, 'Transition to an underventilated compartment fire to the backdraft phenomenon', *Congres Francophone de Techniques Laser,* Toulouse.

[73] Quintiere, J., Steckler, K., Corley, D. 1984, 'An assessment of Fire Induced Flows in Compartments', *Fire Sciences and Technology*, vol. 4, no.1. pp. 1-14.

[74] Sinai, Y.L. 1999, 'Comments on the Role of Leakages in Field Modeling of Underventilated Compartment Fires', *Fire Safety Journal*, vol. 33, pp. 11-20.

[75] The Biennial Report on Hydrogen Safety, 2007 [online], www.hysafe.org/brhs

[76] Mukai, S., Suzuki, J., Mitsuishi, H., Oyakawa, K., Watanabe, S. *CFD Simulation of Diffusion of Hydrogen Leakage Caused by Fuel Cell Vehicule Accident in Tunnel, Underground Parking Lot and Multistory Parking Garage*, Japan Automobile Research Institute, Japan, Paper Number 05-0293.

[77] Titus, J.J. 1995, 'Hydraulics', *SFPE Handbook of Fire Protection Engineering*, 2nd edn., 1995, National Fire Protection Association, Quincy, MA.

[78] Balarac, G., Si-Ameur, M. 2005, 'Mixing and coherent vortices in turbulent coaxial jets', *C. R. Mecanique*, vol. 333 pp. 622–627.

[79] Cushman-Roisin, B. 2005, 'Kelvin–Helmholtz Instability as a Boundary-value Problem', *Environmental Fluid Mechanics*, vol. 5 pp.507-525.

[80] Forney, G.P. 2008, *User's Guide for Smokeview (Version 5) Technical Reference Guide*, NIST Special Publication 1017-1.

[81] He, Y.P., Fernando, A., Luo, M.C. 1998, 'Determination of interface height from measured parameter profile in enclosure fire experiment', *Fire Safety Journal*, vol. 31, pp.19-38.

Annex 1

Firenet project: Completion of the recommendations

Firenet project

Final report

Completion of the recommendations

Iceland Fire Authority
July 2006

Definition of a backdraft

There exists often some confusion among firefighters and fire safety engineers when distinguishing between the different explosive phenomena that can occur in enclosure fires, especially the phenomena called flashover, backdraft and smoke gas explosion. Since we shall concentrate on the backdraft phenomena in this report, it is important to give a definition of the term backdraft:

Limited ventilation can lead to a fire in a compartment producing fire gases containing significant proportions of products of pyrolysis and of partial combustion. If these accumulate then the admission of air when an opening is made to the compartment can lead to a sudden deflagration. This deflagration moving through the compartment and out of the opening is a ***backdraft***.

Note that under-ventilated fires can lead to other dangerous phenomena that are worth mentioning, even if they are not the subject of this report:

- Flashover, defined as a sudden transition to a state of total surface involvement in a fire of combustible materials within a compartment.
- Smoke gas explosions, which may occur in compartments or sealed spaces at a distance from the original fire compartment.
- The "blowtorch effect", when a window breaks and flames are pushed out through a vent at the other side of the compartment.
- Spontaneous fireballs and other such phenomena that may or may not fall in with the definitions of the terms mentioned above.

A thorough survey of the literature concerning these phenomena has been carried out by Chitty [1]. Dangerous phenomena in enclosure fires are described by Bengtsson [2].

Warning signs indicating imminent risk of backdraft occurrence

The task of IFA is to spread the knowledge on backdraft for fire brigades, and elaborate recommendations for mitigating backdraft. Below are listed some indicators which, taken together, should be regarded as warning signals of conditions which can produce a backdraft:

Before a firefighter opens the door to the fire room, he should look for signs of an underventilated fire. Therefore, the following points need to be taken into consideration:

- Fires in enclosed spaces with minimal ventilation, for instance, closed rooms or spaces under the roof.

- Oily deposits on window panes, which is a sign that pyrolysis products have condensed on cold surfaces.
- Hot doors and windows, indicating that the fire has been burning a while, perhaps with limited ventilation.
- Pulsating fire gases from small openings in the room, which are a sign of under-ventilated conditions. When the air enters the room combustion takes place, which means that the oxygen runs out as the temperature rises. Then the temperature falls slowly and when the pressure has dropped slightly the air can be sucked into the room.
- A whistling sound in openings, which may be related to the fire pulsating.

If the decision is made to enter, the firefighter must be on the lookout for the following signs, particularly at the moment when he has opened the door to the fire room and looks into the room. These signs, along with the others, can provide warning signals for an imminent backdraft:

- An orange glow or a fire which is not visible can indicate that the fire has been burning a long time with a lack of oxygen.
- Fire gases drawn back through the opening, indicating that an air current has entered the room. Hot fire gases will leave the room, perhaps through another opening and replacement air will be drawn in through the opening. It may seem as if the fire gases are being drawn towards the fire.
- The neutral plane is close to the floor.
- A whistling sound may occur due to air being drawn in through small openings at high speed.

<u>Recommendations for the mitigation of a backdraft</u>

The course of action to be taken during an ongoing operation is described below. The firefighters must estimate the risks by thinking carefully about the following points:

- Available manpower.
- Available equipment for ventilation - both low-tech (e.g. axes) and high-tech (e.g fans), both built-in installations (fans and roof vents) and equipment brought on fire engines.
- Accessibility of fire compartment - too high to be reached by ladders, in basement, with or without windows to the outside world, on top floor of building.
- Likelihood of people being trapped inside the compartment (and of such people still being alive)
- How airtight is the structure? Are there any leaks at floor level? Is the room well insulated?
  What stage is the fire at? Fuel controlled or ventilation controlled? How long has the fire been burning for?

- How big is the fire load? The quantity of combustible material available and its arrangement can determine the quantity of combustible gases. What type of material are we dealing with?
- Where is the air inflow coming from during an operation? Has much turbulence been generated? Turbulence can affect the fire's development.

Depending on the risk and the operation's objectives, fire fighters might adopt defensive tactics, by either ventilation or gas cooling.

Ventilation must be facilitated as high up as possible to force out any unburnt fire gases. As there is a build-up of positive pressure, it is important that there is a "clear path" out for any backdraft which occurs. Otherwise, there can be a very large increase in pressure. Another option is to cool down the fire gases. The best way to do this is without opening the room, for instance, by using water mist or a cutting extinguisher.

In other situations, such as in a life-saving situation, rapid internal operations may be necessary and rooms may have to be opened. In these scenarios there are two alternative approaches:

- Open the door quickly. Cool down. Close the door quickly. Repeat this procedure until the temperature and pressure in the room have dropped. One should note that if the door is opened just for a couple of seconds this is enough for too much air to get in, which could cause a backdraft.
- The BA (Breathing apparatus) firefighters crawl in and close the door behind themselves as quickly as possible and cool down the fire gases. This method can entail major risks for the firefighters. It is important not to get caught in the open doorway. Apart from the risks being greater, it also helps to generate more turbulence.

In some cases a positive pressure fan can be used for ventilation-controlled fires. But there is still a great risk of the heat of the fire increasing as air can enter the room. Fans should be used with great caution in a backdraft situation. Fans generate powerful turbulence, which can cause the fire gases to mix, making then ignitable. The fire gases must be cooled down before ventilation. Otherwise, there is a great risk that they will ignite. Using a fan can also cause fire gases to be quickly removed from a room. Firefighters need to assess whether fans should be used on a case-by-case basis. There is no definite answer on which choice to make.

References:

[1] Chitty B., "A Survey of Backdraught", FRDG Fire Research Reports and Memoranda, 5/94.

[2] Bengtsson L.G., "Enclosure Fires" Swedish Rescue Services Agency, 2001.

Paper [A]

Using Computational Fluid Dynamics Fire Safety Engineering of Buildings

Accepted for oral presentation and publication in Proceedings of the 19th International Symposium on Transport Phenomena, Reykjavik, Iceland, Aug. 2008.

USING COMPUTATIONAL FLUID DYNAMICS IN FIRE SAFETY ENGINEERING OF BUILDINGS

Georges Guigay[1], Bödvar Tómasson[2], Jens Bengtsson[2], Björn Karlsson[3], Jónas Elíasson[1]

[1] Department of Environmental and Civil Engineering, University of Iceland, Reykjavik, ICELAND

[2] Linuhönnun Consulting Engineers, Reykjavik, ICELAND

[3] Iceland Fire Authority, Reykjavik, ICELAND

ABSTRACT

During the last decades, building codes have been shifting from prescriptive to performance based, in order to comply with the evolution of modern building design. This approach strongly relates on the development and performance of Computational Fluid Dynamics (CFD) codes. This article introduces briefly the fundamental principles of Fire Safety Engineering and gives examples of CFD use in the design of modern buildings.

INTRODUCTION

Fire safety regulations can have a major impact on the overall design of a building with regard to layout, aesthetics, function and cost. In the the last decades, the rapid development within modern building technology has resulted in unconventional structures and design solutions; the physical size of buildings is continually increasing; there is a tendency to build large underground car parks, warehouses and shopping complexes. The interior design of many buildings with large light shafts, patios and covered atriums inside buildings, connected to horizontal corridors or malls, introduces new risk factors concerning spread of smoke and fire. Past experiences or historical precedents (which form the basis of current prescriptive building codes and regulations) rarely provide the guidance necessary to deal with fire hazards in new or unusual buildings.

At the same time there has been a rapid progress in the understanding of fire processes and their interaction with humans and buildings. Advancement has been particularly rapid where analytical fire modeling is concerned. Several different types of such models, with a varying degree of sophistication, have been developed in recent years and are used by engineers in the design process.

As a result, there is a worldwide movement to replace prescriptive building codes with ones based on performance. Instead of prescribing exactly which protective measures are required (such as prescribing a number of exits for evacuation purposes), the performance of the overall system is presented against a specified set of design objectives (such as stating that satisfactory escape should be effected in the event of fire). Fire modeling and evacuation modeling can often be used to assess the effectiveness of the protective measures proposed in the fire safety design of a building. This paper will give a brief introduction to the fundamental principles of fire safety engineering design, describe how CFD models have been developed to simulate fires in buildings and give examples of how CFD have been used when designing relatively complex buildings with respect to fire safety.

The need to take advantage of the new emerging technology, both with regards to design and regulatory purposes, is obvious. However, the increased complexity of the technological solutions requires higher levels of academic training for fire protection engineers and a higher level of continuing education during their careers. Some excellent textbooks ([1], [2]), and design guides [3] have been produced for this purpose. The National Fire Protection Association (NFPA) has published a complete handbook [4] which is a reference within the fire protection community.

FUNDAMENTAL PRINCIPLES OF FIRE SAFETY ENGINEERING

The field of Fire Safety Engineering encompasses topics from a wide range of engineering disciplines as well as material of unique interest to fire safety engineering. The fundamental topics of interest have been divided into the following five modules [5]:

- Fire fundamentals. This module provides the basic chemistry and physics for the understanding of fire.
- Enclosure fire dynamics. This module gives an understanding of room fire growth and spread mechanisms. It is of particular interest in regards to fluid mechanics as it deals among others on vent flows, heat flow, ceiling flames and jets, smoke filling and evacuation and venting.
- Active fire protection. This module deals with the analysis and design of active fire protection fires such as detection system, automatic and manual suppression system and smoke management system.
- Passive fire protection. This module develops an understanding of the traditional practices of the code approach to the structural aspect of passive fire protection for building.
- Interaction between fire and people. People can interact with fire in many different ways, e.g. they can cause fire ignition. The movement of people and access of fire-fighters are essential concerns to Fire Safety Engineer.

It is not the scope of this paper to discuss in details these different modules. The performance based approach with respect to building design will mainly deal with the enclosure fire dynamics.

ENGINEERING MODELS FOR ENCLOSURE FIRES

The rapid progress in the understanding of fire processes and their interaction with buildings has resulted in the development of a wide variety of models which are used to simulate fires in compartments. The models can be classified as being either deterministic or probabilistic. Probabilistic models do not make direct use of the physical and chemical principles involved in fires, but make statistical predictions about the transition from one stage of fire growth to another. Such models will not be discussed further here. The deterministic models can roughly be divided into three categories; CFD models; zone models; and hand-calculation models.

CFD models for fire safety

The most sophisticated of the enclosure fire models are the models based on Computational Fluid Dynamics, often termed CFD models. Engineering applications of CFD involve not only fluid flow and heat transfer, but can also involve features such as combustion, phase change, multiphase flow and chemical reactions. Classical examples are furnaces or combustion engines.

The very wide range of application that can be addressed by CFD is such that no single CFD code can incorporate all the physical and chemical processes of importance. There exist therefore only a few CFD codes that can be used for problems involving fire. These, in turn, use a number of different approaches to the subprocesses that need to be modeled. Some of the most important of these subprocesses are:

- Turbulence modeling
- Radiation and soot modeling
- Combustion modeling

This article will not describe in further details the technique of CFD modeling. The most widely used CFD code within the fire research and engineering community is FDS [6] (Fire Dynamic Simulator), a model for fire-driven fluid flow developed by NIST [7] (National Institute of Technology), appropriate for low-speed, thermally-driven flow with an emphasis on smoke and heat transport from fires, which treats turbulence by means of a LES (Large Eddy Simulation). However, other CFD codes based on a RANS (Reynolds Averaged Navier-Stokes) approach of turbulence modeling are also use in fire modeling.

Two-zone models

A second type of deterministic fire models is those that divide the room into a limited number of control volumes or zones. The most common type is termed “two-zone models” where the room is divided into an upper, hot zone and a lower, cold zone. These are not discussed further here, but are described in details in [8].

FIRE SIMULATIONS IN COMPLEX BUILDINGS

In this section, two examples of CFD modeling in complex buildings will be described, to demonstrate the interest and the necessity of CFD in performance based modeling, allowing much complex design than when the prescriptive approach is used. These two buildings, an office and a storage building, have different requirements in term of design fire, visibility, evacuation, etc. which require different design solutions.

Fire Simulation in an office building

The building shown in this example is an eleven floor office building, with a particular and complex design. Its main feature is an atrium linking the floors 1 to 9 creating a huge open space. There is an offset in the opening to the atrium (white part in the middle of the building in Fig. 1) from floor to floor. The 10th and 11th floors are separated from the 1st to 9th floor, and are modeled for visual perspective. There are no smoke hatches in this simulation.

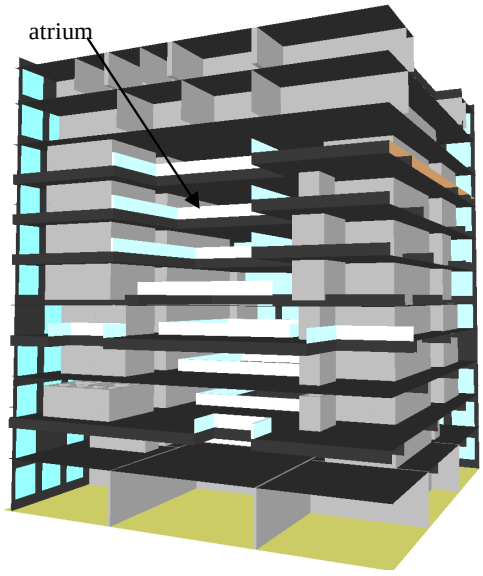

Fig. 1: The 3D model with removed outer walls

The structure is divided into a total of 6 different grids to make it possible to run the simulations on multiple processors and thus reducing the calculation time. The finer grids, close to the fire, are composed of 0.25 m long cells and the coarser grids, close to the top are composed of 0.5 m long cells. The total mesh in this simulation is thus composed of almost 4.5 millions (4 499 200).

The fire is designed as a fast fire with the maximum energy release rate assumed to be 15 MW, which is a conservative choice for an office building. In a real fire the initial growth is nearly always accelerating. A simple way to describe this accelerating growth is to assume that the energy release rate $\dot{Q}$ increases as the square of time. By multiplying the time squared by a factor of α various growth velocities can be simulated, and $\dot{Q}$ as a function of time could be expressed as:

$$\dot{Q} = \alpha \cdot t^2 \quad (1)$$

The values of α for different growth rates with corresponding type of occupancies recommended by NFPA 204 [9] are shown in Table 1.

Table 1: Fire growth rates for various occupancies

Growth rate	α (kW/s^2)	*Type of occupancy*
Ultra fast	0.19	Shopping and entertainment centers
Fast	0.047	Schools, offices, nursing homes, hotels, etc.
Medium	0.012	Dwellings, etc.
Slow	0.003	

The evolution of a fire can be described as shown in Fig. 2:

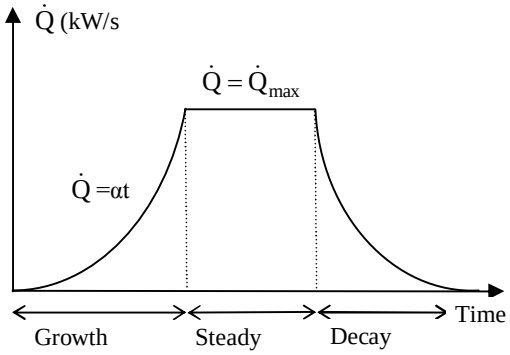

Fig. 2: A simple design fire curve

In our design fire, using Eq. (1) and the growth rate for fast fire from Table 1, a $\dot{Q}_{max}$ of 15 MW is reached approximately after 9.5 minutes. The fire is placed on the 1st floor, by the opening between the floors. The substance supposed to be on fire is a plastic material and thus the yields of soot and carbon monoxide are relatively high. The soot yield is set to 0.05 and the carbon monoxide is set to 0.06.

Figures 3 and 4 show the visibility after 6 and 8 minutes respectively. In this project, the acceptable minimum visibility is set to be 16.4 meters (corresponding to the black contours in the figures). After 6 minutes (Fig. 4), the smoke has spread on the right part of floors 3 and 4, in the atrium, and closed to the ceiling of floor 5, reducing the visibility to this minimum in these areas. After 8 minutes (Fig.

5), the visibility is considered poor in a wide part of the building, especially on floors 1 to 5. It is interesting to couple the CFD results with an evacuation model. Models for simulating evacuation of humans from buildings can be probabilistic, deterministic or both. The deterministic type of model will typically include little or no physics and will to considerable extent be based on information collected from statistics and evacuation experiments. Some will only attempt to describe the movements of humans; others will attempt to link movements with behavior ([10], [11], [12]). In this project, the evacuation is simulated using the software STEPS [13].

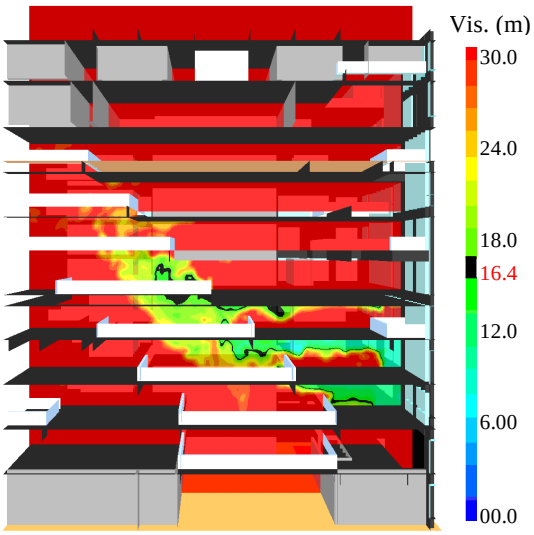

Fig. 3: Visibility in the middle of the structure after 6 minutes

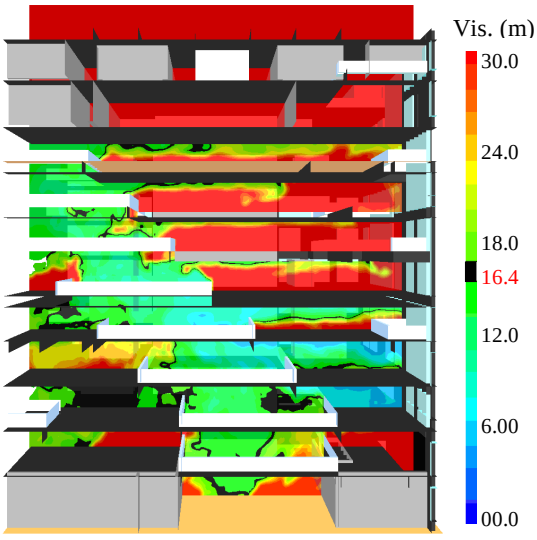

Fig. 4: Visibility in the middle of the structure after 8 minutes

Figures 5 and 6 show the evacuation simulation after 1 and 6 minutes respectively. There are 100 people on each floor at the beginning of the simulation. After 1 minute, there are still people waiting to reach the stairs. There are many people waiting on the 2 top floors (10th and 11th), but these are not part of the open space and are consequently not exposed to the smoke. On the other floors, however, Fig. 3 shows that the visibility is still acceptable except close to the fire source and in the atrium itself. After 6 minutes (Fig. 6), when visibility becomes critical in a wide part of the building (Fig. 4), everyone is in the stair case, which, as required for evacuation routes, is fire and smoke protected.

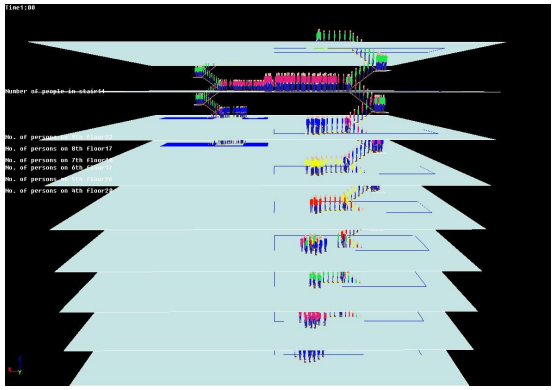

Fig. 5: Evacuation simulation after 1 minute, with 100 people per floor

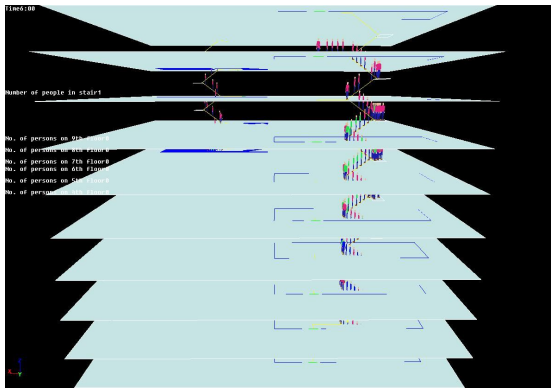

Fig. 6: Evacuation simulation after 6 minutes, with 100 people per floor

By comparing results from fire simulation and evacuation, we see that, even considering a conservative choice for the fire design and the number of people (100) on each floor, all the occupants are safe at least 2 minutes before the situation becomes dangerous because of the visibility.

Fire Simulation in a storage building

The building shown in this example (Fig. 7) is a classical storage building. In the simulations 10 smoke hatches of 2 m2 each are assumed to be installed evenly spread in the roof. The smoke hatches are simulated to be opened after 5 minutes since they are expected to be activated manually, when the first people from the fire department are expected to arrive at the fire scene. In addition to the smoke hatches, all loading doors are expected to be opened during the fire, which will create a well ventilated fire.

The calculation domain is 120 x 60 x 20 meters. The size of the mesh is homogeneous within the whole domain, with 0.4 meters spatial resolution, so the grid is 300 x 150 x 50 = 2250000 cells.

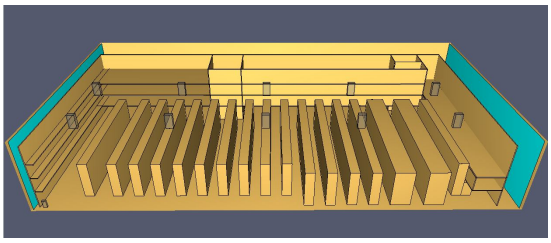

Fig. 7: 3D model of the storage building seen from the back with wall and roof removed for visualization

The fire in this simulation is designed as ultrafast αt^2 (see Eq.(1) and Table 1), since the design fire is assumed to be in the rack storage. The fire reaches a maximum energy release rate of 15 MW after 5 minutes, and after that the Energy Release Rate is constant. The properties of the materials stored in the storage are unknown at the moment of the simulation and thus a conservative fire development has been assumed. The same is true about the yields from the simulated fire since the yields are very conservative with a carbon monoxide yield of 0.1 and a soot yield of 0.1. In this case, the simulated fire is modeled as a 10 m2 large patch with a maximum energy release rate per unit area of 1500 kW/m2 and is placed partly under the office part. The location is chosen to create a maximum spread of the smoke because empty pallets were planned to be stored there, and a fire in these could potentially have a development similar to the simulated fire.

Fig. 8 shows the visibility after 4, 6 and 10 minutes. Note that the acceptable minimum visibility is set to be 10 meters, when it was set to be 16.4 meters for an office building, where the main concern was human life saving and safe evacuation while the concern in the storage building is more about property saving, making a lower visibility level acceptable.

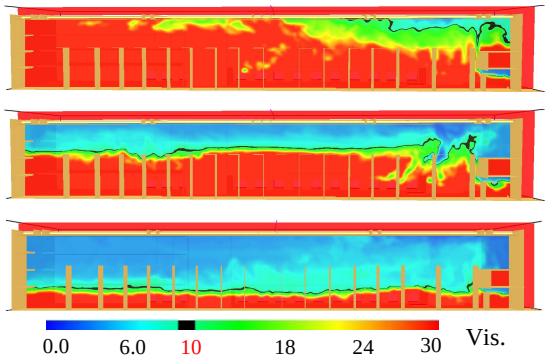

Fig. 8: Visibility after 4, 6 and 10 minutes (from top to bottom)

Fig. 9 shows the temperature after 5 minutes, which is essential information in fire-fighting operation.

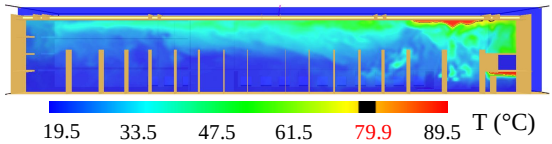

Fig. 9: Temperature in the storage after 5 minutes

The simulations showed that the parameter that first becomes critical is the visibility and this was also expected considering the high soot yield of the fire. Critical conditions for visibility are when the visibility is less than 10 meters and these conditions start to arise after approximately 3 minutes, but at this point the critical conditions only arise at heights above where people are present and it takes long time before critical conditions arise at levels where people are stationed. The simulation also shows that the temperature remains rather low except at very precise locations close to the fire source, so the conditions are good for fire-fighting operations inside the building. In this case, the CFD simulation has proved that the 10 smoke hatches placed in the roof are sufficient to keep acceptable conditions for a sufficient time for the fire-fighters to access the fire.

CONCLUSION

During the last decades, important efforts have been carried out to shift from prescriptive to performance based design of building with respect to fire safety, allowing the construction of more complex, open-spaced and modern buildings, than the prescriptive approach would allow. Still, it is essential that these new buildings meet an acceptable level of public and property safety in the event of fire. CFD codes allow designers to verify that fire safety precautions are sufficient and comparable to demands made by prescriptive codes and allow more creative and innovate design such as buildings with open-spaces or large atriums.

In this paper, two examples of CFD calculations with very different fire conditions and design, geometry, recommendations and safety concerns have been discussed.

The first example was a complex and modern office, where the main concern is protection of human life. Simulation after 6 minutes (Fig. 3) shows clearly that the visibility will be under the minimum 16.4 m required, when all the occupants are in the fire protected evacuation stairs (Fig. 6).

The second example was a storage building. In this case, as there is generally no public and very few occupants, the main concern is securing property. The CFD calculations allowed the designer to test the efficiency of smoke hatches. The simulation clearly demonstrates that the visibility will be under the required minimum 10 meters under 5 meters height (Fig. 8) for a long time, and that the temperature conditions are acceptable for fire-fighters to access the fire (Fig. 9).

Furthermore, the CFD model can test, by achieving different runs with various parameters such as fire conditions or geometry, the effect and efficiency of additional safety features such as smoke vents or water sprinklers.

In this article, we have provided a very brief introduction of the discipline of Fire Safety Engineering and the role of CFD calculations in building design. However, CFD can assess various problems like smoke toxicity, two-phases flows, heat transfer, material flammability and resistance, flame spread, as well as complicated and dangerous phenomena such as flashover, backdraft and smoke gas explosions. With the development and improvement of models and computer capacity, as well as CFD education for engineers, the role of CFD codes in Fire Safety Engineering must be said to be very important and will keep growing.

NOMENCLATURE

t	Time (s)
$\dot{Q}$	Energy release rate (kW)
α	Growth rate
Subscripts	
max	maximum

REFERENCES

[1] Karlsson B., Quintiere J.G. (2000): “Enclosure Fire Dynamics”, CRC Press.

[2] Drysdale D.D. (1992): ”An Introduction to Fire Dynamics”, Wiley-Interscience.

[3] Klote, J. H., Milke J.A. (1992): “Design of Smoke Management Systems”, American Society of Heating, Refrigerating & Air-Conditioning Engineers.

[4] SFPE Handbook of Fire Protection Engineering, 2nd ed. (1995): National Fire Protection Association.

[5] Magnusson, S.E., Drysdale, D.D., Fitzgerald, R.W., Mowrer, F., Quintiere, J.G., Williamson, R.B., Zalosh, R.G. (1995): "A Proposal for a Model Curriculum in Fire Safety Engineering", Fire Safety Journal, Vol. 25.

[6] McGrattan, K., Hostikka, S., Floyd, J., Baum, H., Rehm, R., (2008): “Fire Dynamics Simulator (Version 5) Technical Reference Guide“, NIST Special Publication 1018-5.

[7] National Institute of Standards and Technology, Gaithersburg, Maryland. http://www.nist.gov

[8] Quintiere, J.G. (1995): “Compartment Fire Modeling”, SFPE Handbook of Fire Protection Engineering”, 2nd ed., National Fire Protection Association.

[9] NFPA 204M (1991): “Guide for smoke and heat venting”, National Fire Protection Association.

[10] Bryan J.L. (1995): “Behavioural response to fire and smoke”, SFPE Handbook of Fire Protection Engineering”, 2nd ed., National Fire Protection Association.

[11] Pauls J. (1995): “Movement of people”, SFPE Handbook of Fire Protection Engineering”, 2nd ed., National Fire Protection Association.

[12] Nelson H.E, MacLennan H.A. (1995): “Emergency movement”, SFPE Handbook of Fire Protection Engineering”, 2nd ed., National Fire Protection Association.

[13] STEPS software, Mott MacDonald. http://www.mottmac.com/skillsandservices/software/stepssoftware/

Paper [B]

The Use of CFD Calculations to Evaluate Fire-Fighting Tactics in a Possible Backdraft Situation

Fire Technology

DOI:10.1007/s10694-008-0058-4

Received: 20 September 2007/Accepted: 2 May 2008

Georges Guigay[a], Daniel Gojkovic[b], Lars-Göran Bengtsson[c], Björn Karlsson[d], Jónas Elíasson[a].

AFFILIATIONS:

a- Civil and Environmental Department, Faculty of Engineering, University of Iceland, Reykjavik, Iceland

b- Øresund Safety Advisers ltd, Malmö, Sweden

c- Helsingborg Fire Department, Sweden

d- Iceland Fire Authority, Reykjavik, Iceland

CORRESPONDING AUTHOR: Georges Guigay

Tel: 00 354 525 5882

Fax: 00 354 525 4632

E-mail: gjg3@hi.is

Abstract

This paper is an attempt to integrate theoretical Computational Fluid Dynamics (CFD) calculations with practical fire-fighting tactics commonly used when arriving at the scene of an underventilated fire. The paper shows that CFD has a great potential in improving understanding and creating better effectiveness in the estimation of fire-fighting tactics. If burning has occurred in a lack of oxygen for a long time, excessive pyrolysis products may have accumulated in the fire compartment. If air is suddenly introduced in the compartment a backdraft may occur. The CFD code used for the simulations is Fire Dynamics Simulator (FDS). In this paper, we focus on the conditions that can lead to backdraft, and not the deflagration or rapid combustion in itself. Therefore, the simulations focus on the gravity current and the mixing process between cold fresh air and hot smoke gases by considering a uniform temperature inside the building as initial condition.

The different tactics studied include natural ventilation, Positive Pressure Ventilation (PPV) and dilution by water mist. Their effectiveness is observed comparing them with a reference scenario, where no action is taken. The main objective of natural ventilation is to find the fire source, and the venting is more effective with several openings. Tactics involving PPV are very effective in evacuating the unburnt gases, but increases the mixing, and consequently the probability of backdraft during the early stage of operation. On the other hand, the addition of water mist can reduce the danger of backdraft by reducing the concentration of unreacted combustible gases below the Critical Fuel Volume Fraction (CFVF), where ignition cannot occur. If the dilution level is insufficient the danger of backdraft is increased, mainly because the process of gases evacuation is longer due to cooling, which reduces the density difference between hot and cold gases.

During a fire-fighting operation, the choice of tactic depends mainly on whether there are people left in the building or not, but also on the fire-fighters' knowledge of the building's geometry and the fire conditions. If the situation shows signs of strongly underventilated conditions, the danger of backdraft has to be considered and the most appropriate mitigation tactics must be applied.

KEYWORDS: Fire-fighting tactics; Computational Fluid Dynamics; Backdraft.

1. Introduction

The purpose of this paper is to show how theoretical CFD calculations can be integrated with practical procedures that are normally used by the rescue services at the scene of a fire and to gain understanding of the best way to deal with a backdraft situation. This knowledge and the understanding of the warning signs identified just before backdraft occurs will lead to a more successful result in handling such situations.

Until recently little research has been done on backdraft [1, 2, 3, 4, 5], except the work done by Fleischmann [2, 3], in spite of how hazardous and dangerous this phenomenon is to fire-fighters. When an under-ventilated fire dies from a lack of oxygen, the enclosed room can remain full of hot unburnt gases. If an opening occurs, for example a window breaks or fire-fighters open a door to the room, fresh oxygen is carried by gravity currents, and mixes with gases. The mixing of gas with oxygen can create a flammable mixture resulting in ignition and a deflagration or rapid combustion called backdraft. The deflagration

propagates, causing an extreme pressure build-up. The resulting flame may travel at a speed of several meters per second. The occurrence and intensity of a backdraft are directly related to the mixing level and therefore to the properties of the gravity wave.

Knowledge of the underlying processes that control the three phenomena flashover, backdraft and smoke gas explosion is of great importance. Backdraft is especially important as many fires are ventilation controlled when the fire services arrive and open up an access route in order to fight the fire. According to the statistics [6], backdraft does not occur very often. However, since a backdraft is a very rapid and sudden event, its consequences may be rather severe. Therefore is it of great importance that the main physical and chemical processes that control the backdraft phenomena are elucidated [7, 8, 9, 10, 11, 12].

Fire tactics are widely discussed in magazines or books mainly written for fire-fighters [13], but very few scientific articles have been published on the subject. Some experimental studies have been carried out [14]. This paper aims to extend, by means of CFD techniques, this practical and experimental knowledge by integrating CFD techniques, and widen the discussion on fire tactics to scientists and engineers.

During an intervention on a strongly underventilated fire, fire-fighters must be aware of the danger of backdraft and its warning signs [15].To estimate the effect of different tactics on backdraft mitigation, the flammable region obtained in CFD simulations is plotted at different times in both defensive tactics, e.g. natural ventilation, or offensive tactics, such as using PPV fans [16, 17, 18] or dilution by water mist.

A special effort is dedicated to the effect of water mist. Experimental research on backdraft mitigation [1, 5] has shown that its effectiveness is due to dilution and reduction of the fuel volume fraction, rather than a thermal mechanism of cooling. CFD calculation allows a rough quantification of the effect of the water mist.

Finally, some conclusions are drawn regarding how currently used tactics can influence the risk of backdraft, discussing their advantages and disadvantages in regards to this particularly dangerous phenomena.

One of the co-authors has worked as a fire brigade officer for over a decade, and based on his experience, several tactics commonly used in fire-fighting operations in Sweden were chosen for analysis in this paper. Then, we look at the effectiveness of these tactics in mitigating a particular danger that is backdraft.

2. Modelling with CFD

The CFD code used in this investigation is Fire Dynamics Simulator (FDS) [19]. This software uses Large Eddy Simulation (LES) developed by the National Institute of Standard and Technology (NIST). Some of the scenarios in this paper have already been modeled [20] using Simulation Of FIres in Enclosures (SOFIE) [21], another CFD software which uses Reynolds Average Navier-Stokes (RANS) turbulence model. It is interesting to see if the different models allow the same conclusions, even though it is not the purpose of this paper to compare the performance of these softwares. LES models are known to be more adapted to simulate the mixing, which is essential in the backdraft phenomena while RANS models may simulate gradient flows better.

It is actually not possible to model the whole backdraft scenario in CFD since proper sub-models that handle the premixed burning and the deflagration have not yet been developed.

Therefore, the flammable region, created by this mixing will be modeled as a mixture of methane and air that does not burn because it is never ignited. To achieve this, the combustion module in the FDS simulator is shut off from so that there is no burning in any of the simulations. By diminishing the possibility of a rapid combustion, or its force, should a deflagration occur, it is possible to estimate the effect of the different tactics used in the mitigation of backdraft. The method used is to simulate different mitigation scenarios and compare them to the basic scenario when nothing is done, as is described in the next chapter. Therefore, no combustion modeling by FDS is used in this paper.

3. Geometry and scenarios

3.1. General

When the fire-fighters arrive at the scene of a fire that involves a possible backdraft situation their actions can depend on several factors. Different tactics may be used depending on whether there are people left in the building or not, what resources are available, the accessibility of the building or the fire room, what stage the fire is in, the commanding officer's level of knowledge of the situation, etc. What this means is that there are special conditions at a fire scene that determine which tactics can be used, rather than the technical properties of the fire as such. This fact induces a certain difficulty in the CFD simulations. In this paper, these difficulties are circumvented by choosing six different tactics that are all evaluated, but there may be situations where none of them can be applied to that particular event due to other reasons than the technical properties of the fire itself. There may also be situations where tactics other than the six discussed in this paper should rather be applied.

In this paper, we address the gas temperature, unburnt fuel concentration and density in various geometries, which are some of the essential parameters for the triggering of a backdraft. However, there are many other parameters that can have an influence on backdraft potential (e.g.: geometry, leakages, wind, etc…), but these are not addressed in this paper.

3.2. Geometry

A basic scenario has been created for easier evaluation of the different tactics. This scenario consists of a 3 room apartment. Each room measures 4 x 4 m and is 2.8 m high. There are 3 doors that measure 0.80 x 2.0 m, 2 connect the different rooms, and one front door connects room 1 to the outside. Its opening corresponds to the start of the simulation. Room 3 has a window that is opened in Scenarios 3 and 4. The geometry is shown on Figures 1 and 2.

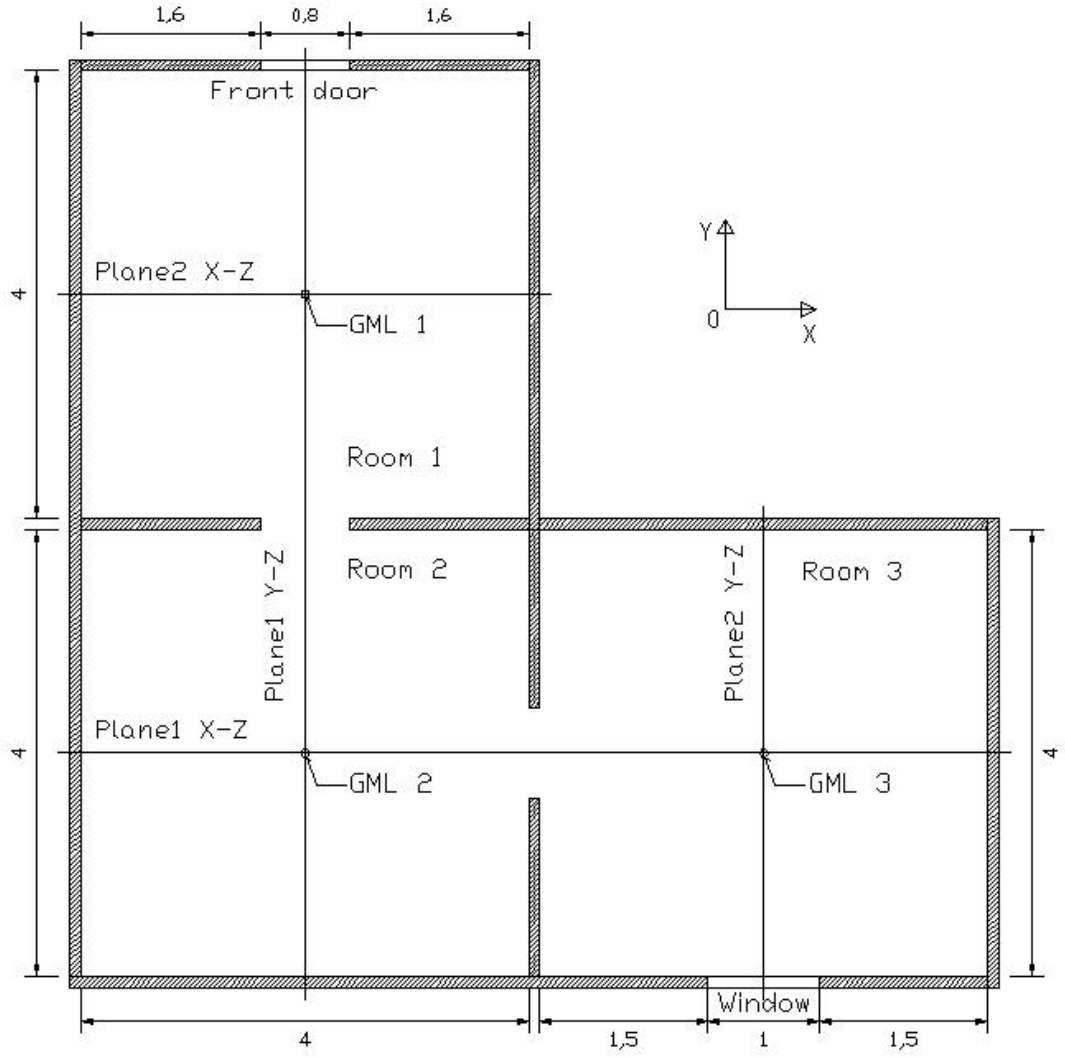

Figure 1: Plane view of the apartment

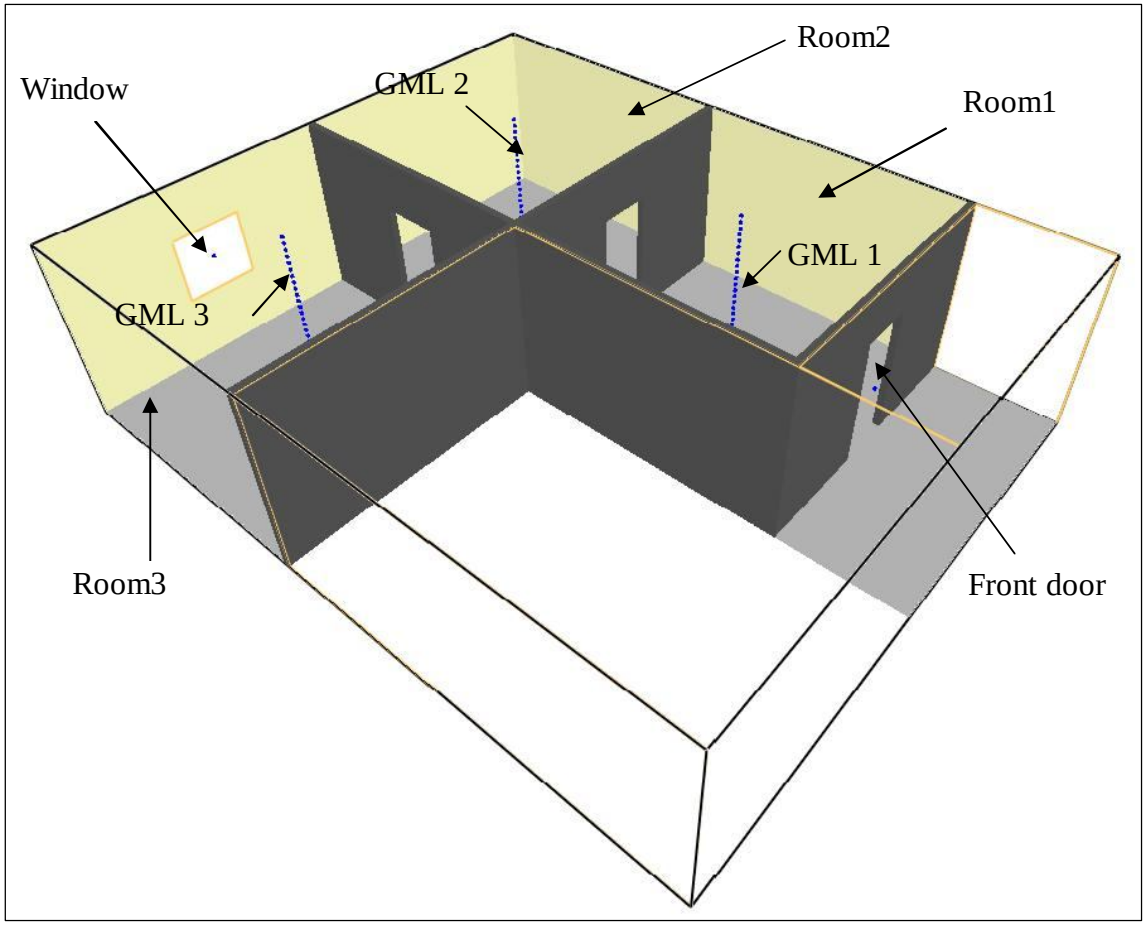

Figure 2: 3D view of the apartment

3.3 Scenarios

The studied tactics are:

- Scenario 1: Reference scenario where no action is taken.
- Scenario 2: A life saving operation where fire-fighters enter the building.
- Scenario 3: Natural ventilation of the building by opening a window at the back of the building.
- Scenario 4A: Ventilation of the building using PPV at low flow rate 3.73 m3/s.
- Scenario 4B: Ventilation of the building using PPV at high flow rate 5.38 m3/s.
- Scenario 5: Incorrect use of PPV at high flow rate 5.38 m3/s (No discharge opening).
- Scenario 6: Dilution of the unburnt gases, by use of water spray before opening the door. 4 different levels of dilution are simulated, from 25% to 10% of unburnt gases.

3.4. Initial conditions and measurements

The CFD-calculations have been carried out with a computational grid containing 226800 cells (10 cm of mesh resolution). All walls are modeled adiabatic. Consequently, the wall temperatures are the same as the local gas temperature. This choice is motivated by the fact

that the initial temperature is assumed to be homogeneous, and that the heat transfer should not have a significant influence on a short simulation time.

As mentioned earlier the combustion is not modeled due to the lack of sub-models that handle the premixed burning. Instead of modeling the whole combustion process and the smoke spread it is assumed that the burning has lasted a long time, and the temperatures as well as the gases concentrations are uniformly distributed in the three rooms. The initial temperature in the three rooms has been raised to 573 K. These values and this kind of modeling are selected in order to describe a room where a fire has burnt for a long time. The flame has died out due to under ventilation since no doors or windows are open. The apartment is also well insulated so there is still some heat kept within the apartment. Radiation from the hot gases has been pyrolysing combustible material, such as furniture. After a while a high concentration (in this case 30%) of combustible gases is reached in the apartment.

The initial conditions specified in the FDS script file are:

Table 1: Initial conditions for FDS calculations

	scenario	T (°K)	ρ* (kg/m^3)	CH4 conc. (% Kg)
Inside	1 to 5	573	0.616	30
Inside	6	373	0.946	Depends on dilution level
Outside	all	293	1.204	0

*Perfect gas law $\rho = 353/T$

Comparison of the different scenarios is carried out by means of 4 visualization planes and 3 Gas Measurement Lines (GML). The visualization planes are vertical animated planar slices passing through the middle of each room (see plane 1 X-Z, plane 2 X-Z and plane1 Y-Z, plane 2 Y-Z on Figure 1). These slices allow the display of quantities such as temperatures, velocities or gas concentrations. In our case, comparison will be made by displaying the flammable region, i.e. the unburnt gas concentration within the range of its flammability limits, and comparing its width and position for every chosen scenario at the same time after opening the door. The GML are vertical lines of probes, placed in the middle of each room (see Figure 1 and 2), that are used to record various quantities at certain points as a function of time, similarly to a classical thermocouple tree. In our case, the recorded quantity is the gas concentration. Each vertical line is composed of 27 probes regularly spaced, allowing measurements every 10 cm. This allows both a good qualitative and quantitative description of the time evolution of the flammability region for each investigated scenario.

In the following sub-chapters each of the six chosen scenarios will be described. These scenarios are selected because they are anticipated to be useful to fire-fighters in their evaluation of tactics used in fighting the potentially underventilated fire.

4. Qualitative results

4.1. Scenario 1: Reference scenario

Scenario 1 is a reference scenario, to which the other five scenarios are compared. This scenario describes what happens when the fire-fighters arrive at the scene of a fire where burning has occurred for a long time. The apartment is rather airtight, no doors or windows are open. In this scenario the fire-fighters open the front door in order to vent out the hot gases. The fire-fighters stay low and aside. This is where the simulation starts. Due to the buoyancy differences between the hot smoke gases and the cold fresh air, a gravity current enters the apartment. To allow better visualization, only the flammable region will be shown along four planes that pass through the center of the rooms, as indicated on Figure 2. The lower (LFL) and upper (UFL) flammability limits considered in this study are assumed to be similar of methane's, i.e. LFL = 5 (vol. %) and UFL= 15 (vol. %). Figure 3 shows the flammable region at 2 different time steps, after 20 and 60 seconds. The volume concentration within the flammable region varies between 5 % displayed in blue (corresponding to LFL) and 15 % displayed in red (corresponding to UFL). The color bar on the left indicates the gas concentration. Note, if the pictures are printed in grey scale, that the blue part corresponds in fact to the darkest region in the lower part of the flammability envelope. The red part is slightly darker and is in the upper part of the flammability envelope.

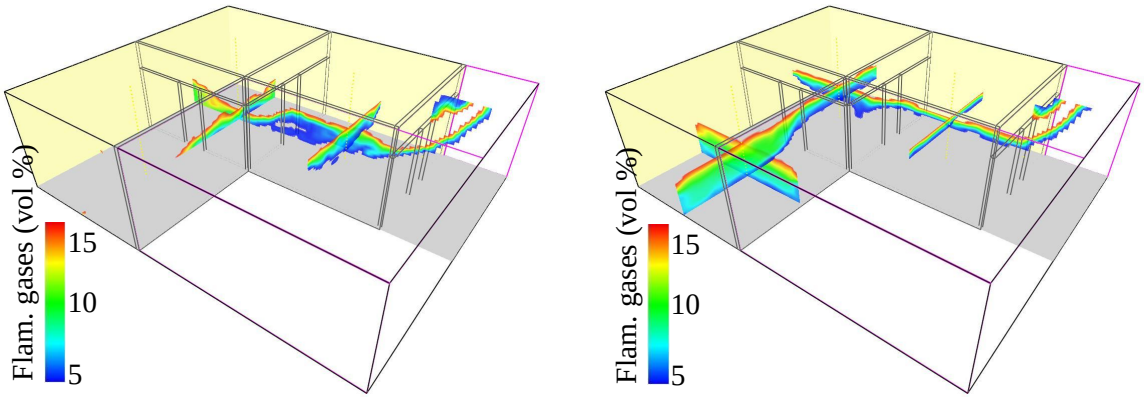

Figure 3: Scenario 1 - Flammable region after 20 sec. (left) and 60 sec. (right)

We can see that between 20 and 60 seconds, the flammability region has propagated into the 3 rooms, and has reduced in width and moved towards the ceiling in room 1. The wider the flammability region, the more likely it is that flammable gas could come in contact with an ignition source (e.g. electric spark, smoldering fire) and creates a backdraft.

4.2. Scenario 2: Offensive attack through the front door by BA team

In this scenario, the rescue services have arrived at the scene of the fire and found out that there are people inside the apartment. Time is a critical factor in this case and is not sufficient to evaluate all possible measures. The commanding officer decides to send in a BA (Breathing Apparatus) team through the front door. By choosing this tactic the fire-fighters will be exposed to a high risk. The fire-fighters will have to be careful and cool the

hot gases with water as soon as they have opened the door. Knowledge of time it takes for the gravity current to mix with the hot gases is essential, since this time determines how long a time slot the fire-fighters have to cool the hot gases with water spray and thus minimize the risk of ignition. Fire-fighters open the door slightly, spray short pulses of water and close the door again to let the spray vaporize inside the apartment. This is repeated until the situation is considered safe. However, the door closing and the spray are not modeled, as the goal is to observe the influence of an even small opening during a short time can have on the situation.

This scenario is modeled very similarly to Scenario 1. The only difference is that two blockages have been placed at the door opening. The blockages are supposed to simulate the influence of the fire-fighters on the stream.

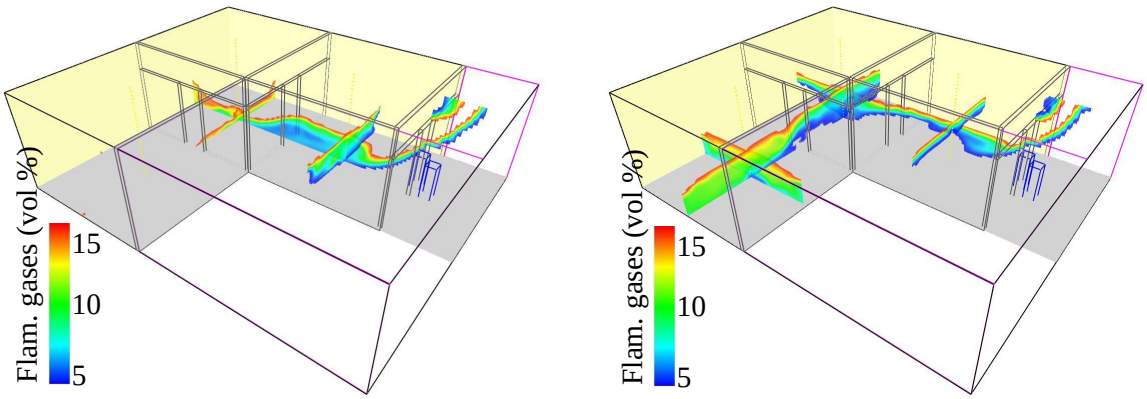

Figure 4: Scenario 2 - Flammable region after 20 sec. (left) and 60 sec. (right)

There is very little difference between results from Scenario 1 and 2. The only conclusion that can be drawn is that the gravity current seems to travel slower in Scenario 2. This is due to the blockages in the opening, which are obstructing the flow, as shown by comparing the Figures 3 and 4 (left), which show the results 20 seconds into the simulation. Moreover, the blockages may create mixing, and thus increase the risk of backdraft. However, this should not have a huge influence and the main lesson learned from the simulation is that it only takes a few seconds for the gravity current to create a flammable region large enough to generate hazardous conditions. In this scenario, the gravity current travels approximately at 1.7 m/s.

4.3. Scenario 3: Defensive attack with natural ventilation

In this scenario, it is clear that there is no-one left inside the apartment, and consequently time is not as critical as in Scenario 2. The conditions at the fire scene are such that it is possible to open up a vent, e.g. a window, to the apartment at the back of the building. The commanding officer has also enough personnel to perform this operation. The vent at the back must be protected with water in case a backdraft or flashover occurs; otherwise the fire may spread over the façade. This method of attacking the fire is defensive. The fire-fighters do not need to take any unnecessary risks in case the situation becomes menacing.

The modeling of this scenario differs from Scenario 1 due to the opening (1x1 m horizontally centered and 1m from the floor in Room 3).

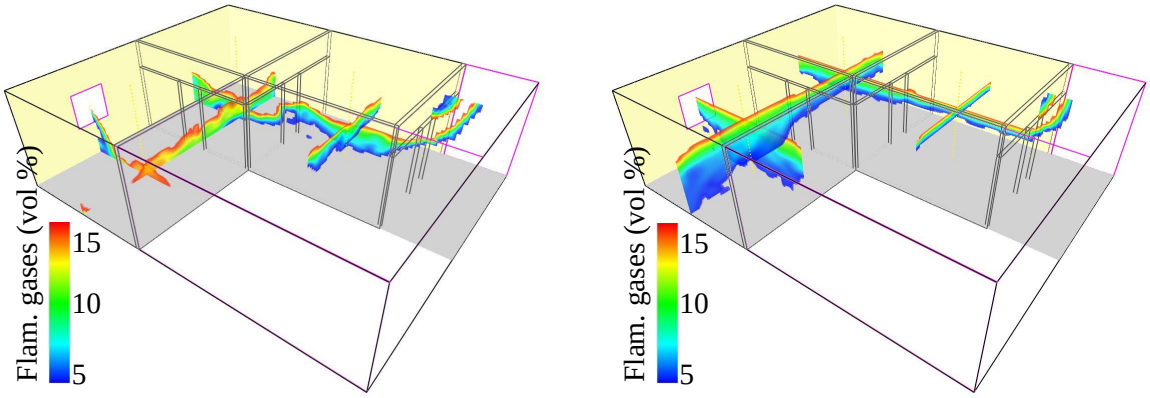

Figure 5: Scenario 3 - Flammable region after 20 sec. (left) and 60 sec. (right)

The results show that a flammable region is created in room 3 almost immediately, as shown by comparing Figures 3 and 5. This is expected since fresh air is allowed to enter room 3 through the window opening. The smoke gases are also vented out faster in Scenario 3.

By comparing Figures 4 and 5, we see that the flammability region is wider in this scenario, especially in room 3. However, in this scenario, the flammability region has moved faster towards the ceiling, showing a faster evolution in the venting process. Moreover, the main purpose of the venting is to find the fire source, which is of course beneficial. However, if ignition occurs, fire-fighters must be prepared for rapid flame spread.

4.4. Scenario 4: Offensive attack using Positive Pressure Ventilation

In several countries like Sweden, it is becoming more common to use PPV at an early stage of an operation. This is a very offensive way of attacking the fire and some rescue services even use this technique in life saving situations. It is important to remember that more resources, i.e. more personnel, are necessary so that the fan can be placed at the correct location. In some cases, e.g. when a fire occurs at the fourth floor of a building, it is not necessary to carry the fan all the way up to the floor where the fire is. It is quite adequate to place the fan on the ground floor, e.g. at the door to the stairwell. In this case the whole stairwell would be pressurized.

Venting a fire, especially by using PPV, may increase the potential for flashover. However, venting is common practice in fire-fighting operations, and fire-fighters are aware of and prepared for a potential increase in fire growth.

This scenario has been modeled in CFD by putting an inflow boundary in front of the door.

This does not simulate the characteristics of a fan very well, e.g. the swirl created by the fan is not correctly modeled. However, the main purpose is still fulfilled, as a great amount of air is forced inside the apartment. The inflow boundary is wider than the door to be sure that its flow covers the entire door, as the cone of air from the fan should do (see recommendations in [16]). The research described in [17] has investigated optimal airflows when utilizing PPV against hot-fire conditions and suggested an ideal flow based upon a minimum value of 1000 m^3/hour and maximum value of 1440 m^3/hour per 10 m^3 of space. With our geometry, we have:

Volume of hot gases (volume of the enclosure): V_{gas} = 4 x 4 x 2.8 x3 = 134.4 m^3.

Table 2: Recommended air flow for PPV

Air flow	Q_{fan} (m3/s)	v_{fan} (m/s)
Minimum air flow	3.73	3.5
Maximum air flow	5.38	5

The flow rate through the door is calculated by FDS, and the velocity at the inflow boundary V_{fan} is obtained by iteration to obtain the desired value of Q_{fan}. This boundary is placed 20 cm in front of the door, in order to keep the possibility to have an outflow forcing throughout the door.

The window in room 3 is opened and will function as a discharge opening. Information about the usage of PPV in fire-fighting is detailed in [18].

4.4.1. Scenario 4A: PPV at minimum recommended air flow

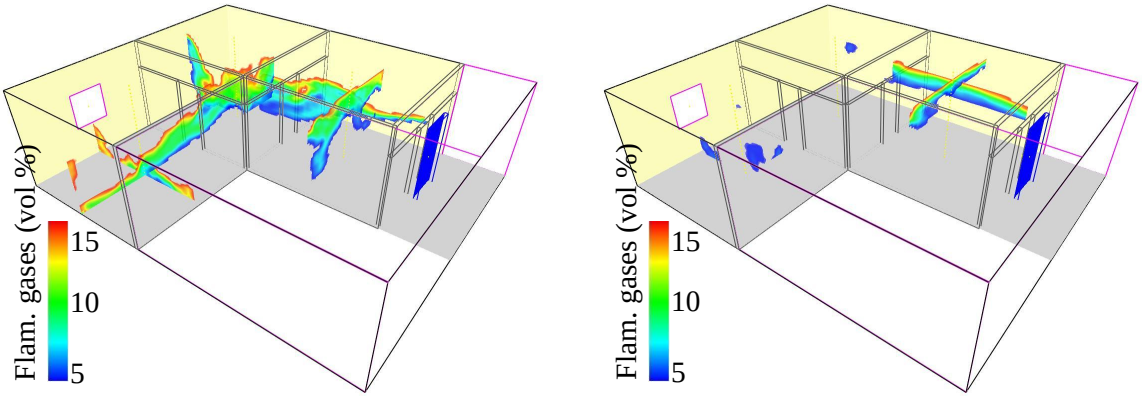

Figure 6: Scenario 4A - Flammable region after 20 sec. (left) and 60 sec. (right)

4.4.2. Scenario 4B: PPV at maximum recommended air flow

By comparing Figures 3, 6 and 7, we see that a lot of mixing is created in Room 1 and Room 2, during the first seconds after opening, consequently creating a wide flammability region. However, the flammable gases are vented very quickly. The quantitative study detailed later shows that the apartment is almost empty of smoke gases, after around 60 seconds for low flow rate (Figure 16), and 40 seconds for high flow rate (Figure 15).

From these observations, we can say that the higher the PPV flow rate is, the higher the level of mixing and consequently the probability of backdraft will be during the early moments of operation. On the other hand, the danger will be eliminated sooner.

The conclusions are that if PPV is used in a correct way, it will very effectively clear the apartment of smoke gases. The possibility of ignition must be kept in mind and it is important that the discharge opening be protected with water.

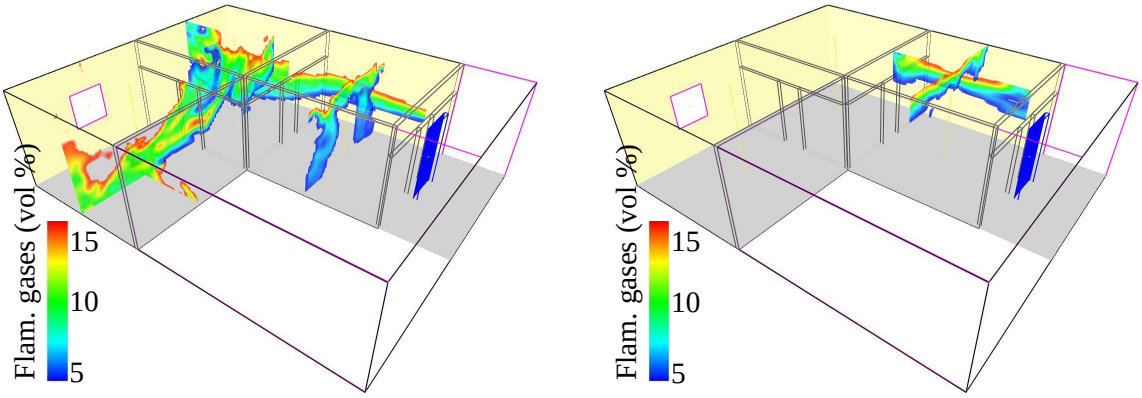

Figure 7: Scenario 4B - Flammable region after 20 sec. (left) and 60 sec. (right)

4.5. Scenario 5: Incorrect use of PPV

Using PPV requires knowledge of how the intake opening and the discharge opening function together. Even though the use of PPV seems to work properly, a door between the intake and the discharge opening may close due to the air stream created by the PPV fan.

Scenario 5 investigates how such a blocked discharge opening influences the probability of a backdraft occurrence. Scenario 5 is modeled as Scenario 4 with Q_{fan} = 5.38 m^3/s, except for the window opening, which is closed in this scenario.

Comparison of the Scenario 4 and Scenario 5 simulations results shows that there is very little difference between the two, as long as the gravity current does not reach the back wall of Room 2.

Figure 8 shows that a large flammable region is remaining in the apartment for a long time.

In this scenario, the risk of backdraft is highly increased due to forced mixing, and lasts a long time, as gases are not evacuated correctly This is of course an extremely hazardous situation for the fire-fighters. Another problem could be that smoke gases are forced into areas that are not yet damaged from smoke, due to the positive pressure created by the PPV. This is highly unwanted and therefore it is recommended not to use PPV if the apartment geometry is not known.

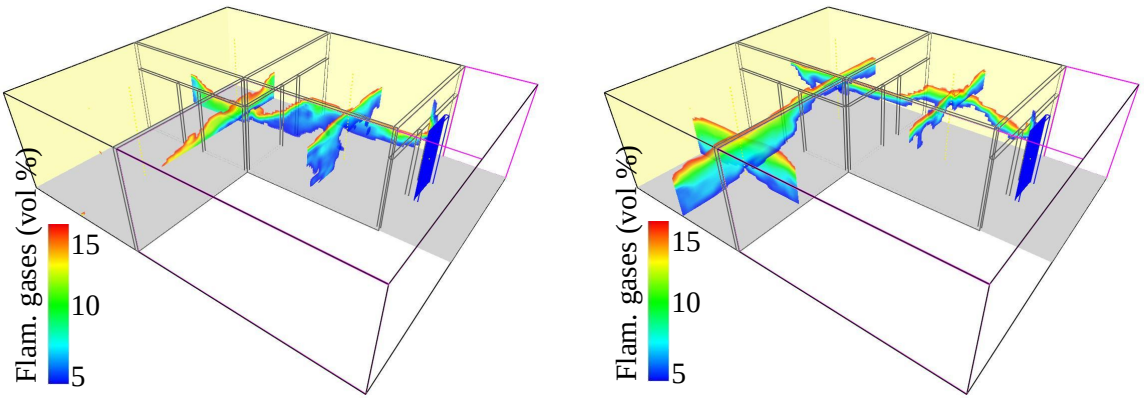

Figure 8: Scenario 5 - Flammable region after 20 sec. (left) and 60 sec. (right)

4.6. Scenario 6: Dilution of unburnt gases by introduction of water spray

This scenario is an attempt to simulate the effect of tools such as piercing nozzles or cutting extinguishers, which spray water before opening the door. The process of dilution is not modeled in itself by FDS but its consequences on initial conditions are considered. It is assumed that dilution has been achieved and that temperatures and gas concentrations are homogeneous when the simulation starts. Different dilution levels will be considered, from a mass concentration of 25% to 10% of unburnt gases. The geometry is the same as in the reference Scenario 1, only the initial conditions change.

Experimental research on backdraft mitigation [1, 5] has shown that its effectiveness is due to the dilution and reduction of the fuel mass fraction, rather than a thermal mechanism of cooling.

Nevertheless, the thermal cooling reduces the density difference and will therefore decrease the speed of the gravity wave [10, 11]. Consequently the evacuation of hot gases will take longer. Both effects will be considered in the simulation.

4.6.1. Effect of dilution

By diluting the hot gases with water spray, the mass fraction of the initial components is reduced. Figure 9 shows a classical flammability diagram for the three-component system methane/oxygen/nitrogen. Details about the usage of flammability diagram can be found in [22] and [23]. Note that the use of flammability diagrams like Figure 9 is only valid for well mixed cases, which might not be the case in every parts of the compartment in a real situation.

The ‘air’ line C-A goes from 100% (point C) to 0% (point A) of methane in air. Its intersection with the flammable region gives the Upper (UFL) and Lower (LFL) Flammability Limit. In the case of methane, UFL = 15% and LFL =5%.

In the first five scenarios, the mass concentration of methane was 30% (Kg/Kg). However, a volume percent flammability diagrams will be used as these are more common. A conversion from mass to volume percent is therefore necessary. As shown in Table 2, this will correspond to 43.6% of methane, 44.7% of nitrogen and 11.7% of oxygen. This initial gases composition point is noted D(30) on the flammability diagram. In the rest of the article, the notation D(X) will correspond to the scenario with X % mass concentration of fuel. In a more realistic case where actual combustion is taken into account, the flammability diagrams will change somewhat, since CO, CO2 and H2O have been introduced into the mixture. However, for backdraft conditions to arise requires that much of the unburnt fuel (methane) remains, which is the situation we are concerned within this paper. Therefore, the contribution to the mass balance of the products of combustion will be small compared to the contribution of the main species, nitrogen, oxygen and methane and will not have a major influence on the flammability of the mixture.

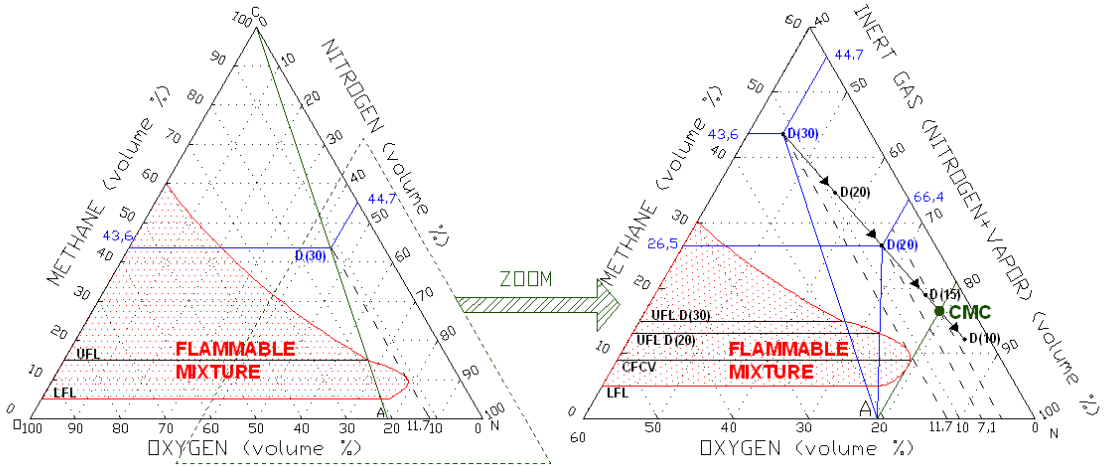

Figure 9: Methane flammability diagram with dilution point (detailed part on the right)

The intersections of line D(30)-A with the flammable region limits are the same as with the air line, D(30) being on this line, which is logical as there is the same ratio 21:79 of O2 relative to N2 as in air. Dilution will affect this ratio and the initial gases composition will not be on the air line CA anymore. Here, the assumption is that the diluting gases, in this case water vapor, are inert gases (with the same molecular weight as vapor) and their concentrations are added to the nitrogen concentration.

Consequently the flammability limits will change, as shown on the zoomed part (right) of Figure 9, which is detailing the lower right part of the flammability diagram, indicating all the dilution point (called D(25), D(20),…) studied.

In order to avoid to complicating Figure 9, only the concentration, UFL and LFL for D(30) and D(20) are indicated on it. The concentration for points D(25), D(15) and D(10) as well as their UFL and LFL are shown in Table 2. These concentrations are calculated as follows:

With the initial condition of the problem, the mass without dilution of the total gaseous mixture inside the building M_0 and the mass of unburnt gases (methane) M_{CH4} are:

$$M_0 = \rho_{in} V_{gas} \quad (1)$$

$$M_{CH4} = (30/100) M_o \quad (2)$$

Considering M_{vap}, mass of vapor to be added so that M_{CH4} is (30-y)% of the new total mass of gases, y being the dilution factor to obtain the desired gas composition, i.e. D(30-y), this gives:

$$M_{CH4} = ((30 - y)/100)(M_0 + M_{vap}) \quad (3)$$

With Equations (2) and (3), we have:

$$M_{vap} = (y/(30 - y)) M_0 \quad (4)$$

Introducing the dilution ratio χ:

$$M_{vap} = \chi M_0 \text{ with } \chi = y/(30 - y) \quad (5)$$

Knowing the initial mass M_0, we obtain the mass of vapor M_{vap} necessary for the desired dilution, the mass concentration (% Kg), and, by conversion, the volume concentration (% mol). These values are then used in the flammability diagram, giving graphically the corresponding LFL and UFL.

Table 3: Concentration and flammability for different mass concentration of unburnt gases

					Mass conc. (% Kg)				Vol. conc. (% mol)						
X	M_0	y	χ	M_{vap} (Kg)	CH_4	vap	N_2	O_2	CH_4	vap	N_2	O_2	Vap $+N_2$	LFL	UFL
30	80.5	0	0	0.0	30.0	0.0	53.9	16.1	43.6	0.0	44.7	11.7	44.7	5	15
25	80.5	5	0.2	16.1	25.0	16.7	44.9	13.4	34.6	20.5	35.6	9.3	56.1	5	14
20	80.5	10	0.5	40.2	20.0	33.3	35.9	10.7	26.5	39.2	27.2	7.1	66.4	5	12.9
15	80.5	15	1	80.5	15.0	50.0	27.0	8.1	19.0	56.4	19.5	5.1	75.9	5	10
10	80.5	20	2	160.9	10.0	66.7	18.0	5.4	12.2	72.1	12.5	3.3	84.6	-	-
13.2 (CFVF)	80.5	16.8	1.3	102.4	13.2	56	23.7	7.1	16.5	62.2	16.9	4.4	79	9	9

In Figure 9, the addition of vapor is shown by the arrows, as it is equivalent to moving down from D(30) to D(10) towards other concentration point. Line A-F shows that below this line, the mixture won't be flammable. The intersection of this line with the flammable region corresponds to the Critical Fuel Volume Fraction (noted CFVF) and the corresponding mixture is the Critical Mixture Composition CMC (see Table 3).

4.6.2. Effect of cooling

The major problem when performing an operation involving an underventilated fire is that somehow an opening must be made to the fire compartment, either is by using PPV or normal ventilation. The problem with making an opening is that oxygen is allowed to enter the apartment, which may cause ignition of the smoke gases, as shown in Scenario 2. It would be preferable to inert the smoke gases without making an opening, by using equipments such as piercing nozzles or cutting extinguishers. Once the door has been penetrated the water is distributed in the room. If the water distribution is effective the smoke gases are cooled and the risk of ignition is minimized.

The cooling capacity of such tools and the new initial temperature condition that will be used in the dilution simulations are calculated as follows:

If all the water evaporates, the cooling capacity is:

$$\Delta H_w \rho_w V_w = (T_{in} - T_{final}) C_{air} \rho_{gas} V_{gas} \quad (6)$$

The necessary water volume V_w necessary to cool V_{gas} of hot gases down from T_{in} to T_{final} will be:

$$V_w = \frac{(T_{in} - T_{final}) C_{air} \rho_{gas} V_{gas}}{\Delta H_w \rho_w} \quad (7)$$

In this problem, to cool all the hot gases to the temperature of vaporization T_{final} =100°C, the amount of water calculated using Equation (7) is V_w=7.3 liters. Table 3 shows that 16.1 liters are necessary to obtain the desired minimum dilution D(25), so 100°C will be the

initial temperature in the dilution calculations. Here, we make the reasonable assumption that vaporization will still occur after 7.3 liters by contact of additional water with hot surfaces.

It is interesting to note that below 100°C, there is no risk of autoignition, but gases could still ignite by contact to a source, e.g. an electrical spark or a smoldering surface.

The conditions described above are quite idealized. In reality, the water added will not vaporize instantaneously, but over time, and much of the water will not be used effectively in the dilution or cooling process but will collect in puddles and on surfaces. The reader should keep this in mind when considering the quantities mentioned above.

As no new air is forced into the apartment, and no natural ventilation is used, the venting of gases takes much longer than in other scenarios. Therefore, comparisons will be made with the reference scenario over a five minute period.

4.6.3. Scenario 1 (reference scenario)

The flammability zone for this scenario over a long period is shown on Figure 10 below.

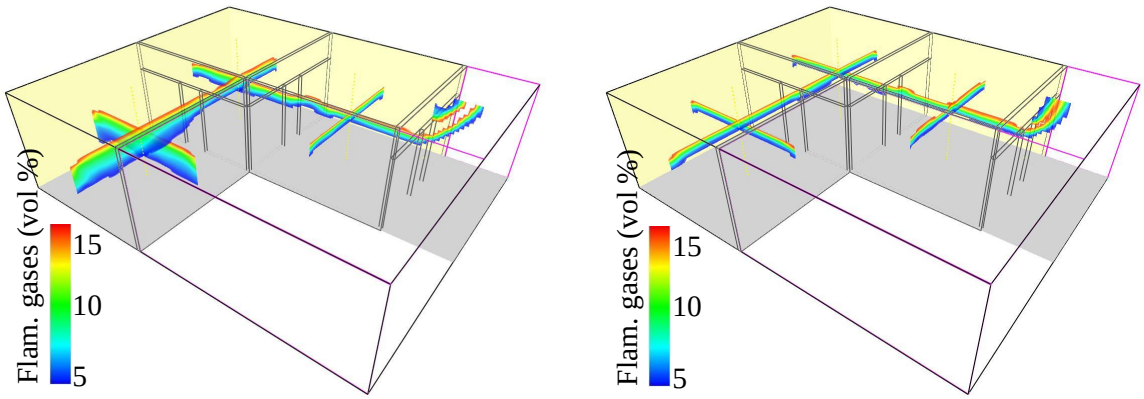

Figure 10: Scenario 1 - Flammable region after 100 sec. (left) and 200 sec. (right)

4.6.4. Dilution D(25)

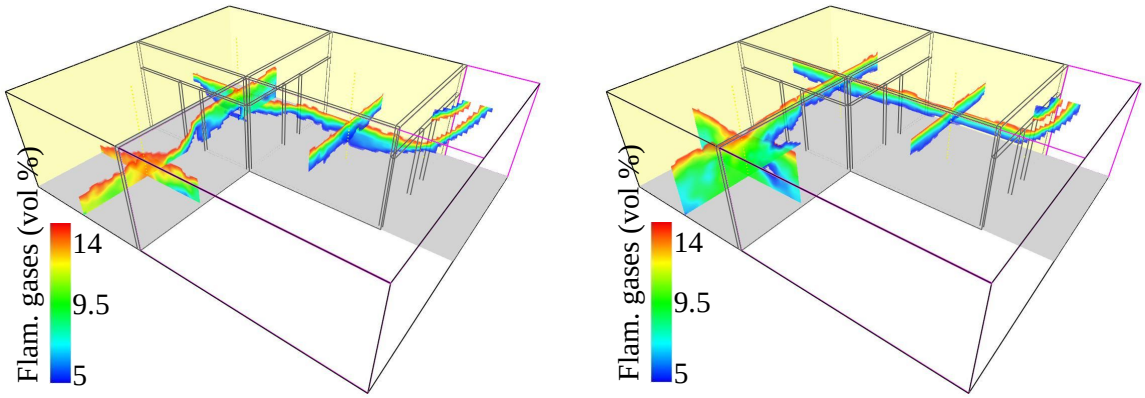

Figure 11: Dilution D(25) - Flammable region after 100 sec. (left) and 200 sec. (right)

4.6.5. Dilution D(20)

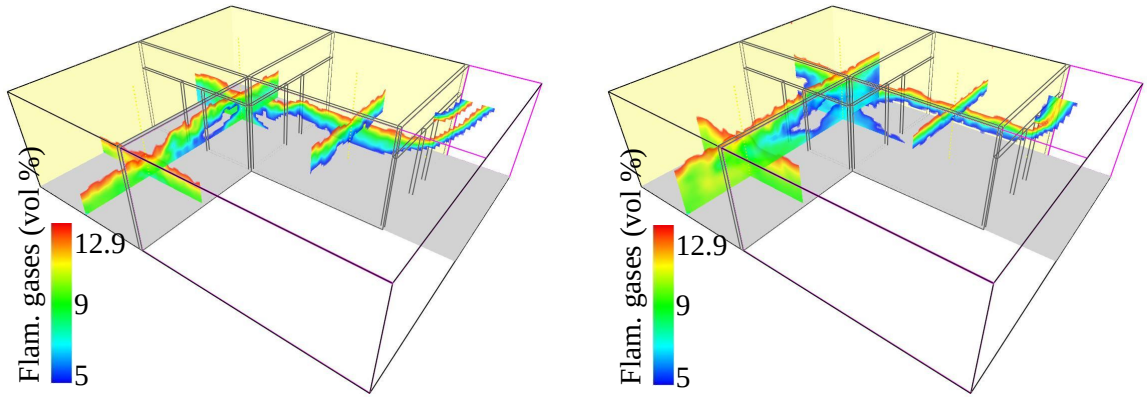

Figure 12: Dilution D(20) - Flammable region after 100 sec. (left) and 200 sec. (right)

4.6.6. Dilution D(15)

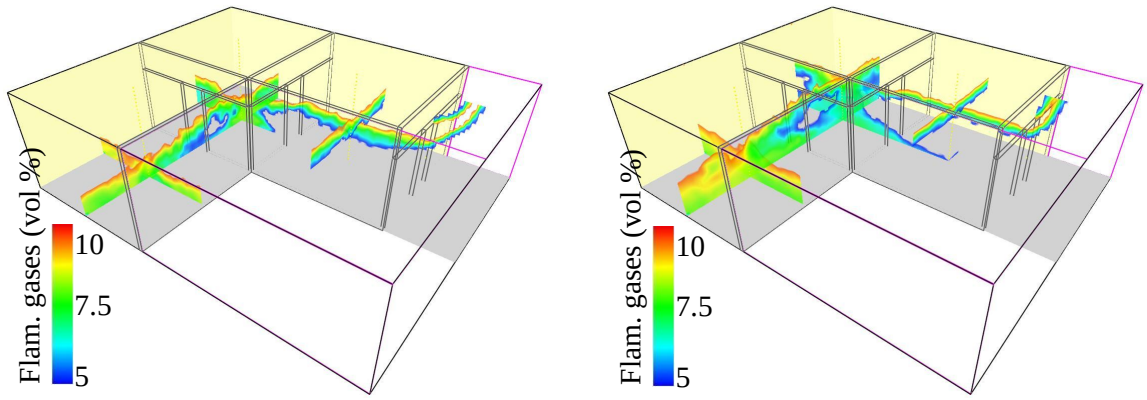

Figure 13: Dilution D(15) - Flammable region after 100 sec. (left) and 200 sec. (right)

The results show that the gravity current is strongly decelerated because of the cooling effect. Without dilution, it is traveling at roughly 2 m/s, hitting the back wall of room 2 after 8 seconds, while its travel time is 1 m/s seconds at 100°C. Moreover, the equilibrium of densities is reached rather quickly, creating a stagnant condition much sooner than in scenario1 (Figure 10).

This qualitative analysis shows that, when compared to the other scenarios, the values of CH4 concentration within the flammability region are often close to the LFL, especially after 200 seconds. However, if the concentration values are small, the situation remains dangerous.

This will be studied more into details in the next quantitative chapter. Yet, we can already say that dilution should be carried until the minimum volume fraction of fuel is reached (point CVC) on Figure 9. It is worth noting that with a piercing nozzle or a cutting extinguisher at 50 l/min, it will only take 55 seconds to reach complete backdraft elimination. If this sufficient dilution is not reached, the danger of backdraft lasts longer.

5. Quantitative results

The qualitative results gave a good description of the effectiveness of the different scenarios. In this part, this effectiveness is quantified by comparing the vertical position and width of the flammable region at the 3 Gas Measurements Lines (GML) indicated on Figures 1 and 2. The vertical position of the flammable region is an indication of the evolution of the venting. In fact, the flammable region starts by progressing at floor level into the building, then move toward the ceiling under the effect of venting, until all flammable gases are finally evacuated.

Table 4 presents the results for every scenario studied, at every 10 seconds. Table 5 shows expanded results up to 300 seconds for Scenario 1 and the various levels of dilution. The results are then displayed graphically. (e.g. on Figure 16 are shown the lower and upper limit of the flammability region, respectively noted Z_{low} and Z_{up} as well as its width for scenario 4B, room 2 and t = 10 s. These values are in bold in Table 4).

When studying the values over the first eighty seconds (Table 4, Figures 14 to 16), we see that there is very little evolution in the reference Scenario 1, as the flammability region width in the 3 rooms does not reduce quickly, and is mostly centered (e.g. in room2, Δz = 0.66 m at t = 30 sec., and Δz = 0.44 m at t = 70 sec.). On the other hand, the effect of the natural ventilation (Scenario 3) is that the flammability region is slowly reducing and moving towards the ceiling. This evolution shows that the gases venting will be significantly shorter with natural ventilation.

Using PPV, the rooms 2 and 3 are completely empty of flammable gases (after 40 sec. for Scenario 4B and 60 sec. for Scenario 4A), with a wide flammability region (approx. 1.5 meters) quickly moving towards the ceiling. This shows a swift evolution in the gases evacuation, but also an important mixing in these first seconds. If PPV is incorrectly used (Scenario 5), there is very little evolution in both the size and the position of the flammability region, showing a stagnant situation, with mixing and ineffective ventilation.

For the dilution case, a thin flammability region is still growing after 80 seconds, thus showing a slow gravity current. This demonstrates that the dilution is a slow process compared to other tactics. When studying the dilution effect over 5 minutes (Table 5 and Figure 18), we see that there is a very wide flammability region, even after 300 sec. This is due to the fact that the initial gases composition is closed to the flammability limit, and that the cooling effect reduces the density difference. Consequently, density equilibrium is reached before the flammable gases are evacuated. This shows that the dilution is very effective if the Critical Fuel Volume Fraction (CFVF) is reached, as the backdraft will be completely eliminated, but has the opposite effect if the dilution is not sufficient, due mainly to slower gases velocities.

Table 4: Vertical position and size of the flammability region in each room for all scenarios

		t = 10 seconds			t = 20 seconds			t = 30 seconds		
		Z_{low} (m)	Z_{up} (m)	Δz (m)	Z_{low} (m)	Z_{up} (m)	Δz (m)	Z_{low} (m)	Z_{up} (m)	Δz (m)
Room 1 GML 1	scen1	0.11	0.6	0.49	0.45	1	0.55	0.87	1.12	0.25
	scen2	0.03	0.17	0.14	0.07	0.89	0.82	0.22	1.07	0.85
	scen3	0.16	0.82	0.66	0.37	1.1	0.73	0.88	1.39	0.51
	scen4A	0.46	1.4	0.94	1.44	1.95	0.51	1.7	2.26	0.56
	scen4B	1.07	1.92	0.85	1.95	2.37	0.42	1.95	2.56	0.61
	scen5	0.42	1.08	0.66	1.07	1.65	0.58	1	1.66	0.66
	scen D(25)	0.04	0.12	0.08	0.13	0.63	0.50	0.2	0.98	0.78
	scen D(20)	0.07	0.25	0.18	0.07	0.67	0.60	0.17	0.79	0.62
	scen D(15)	0.1	0.24	0.14	0.08	0.68	0.60	0.18	0.84	0.66
Room 2 GML 2	scen1	0.02	0.08	0.06	0.05	0.28	0.23	0.1	0.76	0.66
	scen2	0.02	0.07	0.05	0.05	0.38	0.33	0.09	0.58	0.49
	scen3	0.02	0.08	0.06	0.07	0.67	0.60	0.22	1.02	0.80
	scen4A	0.08	0.45	0.37	0.37	1.57	1.20	1	2.25	1.25
	scen4B	**0.23**	**0.95**	0.72	0.67	2.26	1.59	1.5	2.8	1.30
	scen5	0.03	0.09	0.06	0.07	0.6	0.53	0.25	1.1	0.85
	scenD (25)	0.02	0.05	0.03	0.02	0.07	0.05	0.03	0.13	0.10
	scenD (20)	0.02	0.06	0.04	0.03	0.08	0.05	0.04	0.17	0.13
	scenD (15)	0.03	0.06	0.03	0.04	0.08	0.04	0.05	0.24	0.19
Room 3 GML 3	scen1	0.02	0.04	0.03	0.02	0.06	0.04	0.03	0.09	0.06
	scen2	0.01	0.03	0.02	0.02	0.05	0.03	0.03	0.08	0.05
	scen3	0.02	0.05	0.03	0.03	0.25	0.22	0.04	0.94	0.9
	scen4A	0.02	0.06	0.04	0.04	0.42	0.38	0.07	2.28	2.21
	scen4B	0.02	0.07	0.05	0.04	0.99	0.95	0.04	2.8	2.76
	scen5	0.01	0.05	0.04	0.02	0.07	0.05	0.03	0.17	0.14
	scen D(25)	0.01	0.03	0.02	0.01	0.04	0.03	0.02	0.05	0.03
	scen D(20)	0.02	0.04	0.02	0.02	0.05	0.03	0.02	0.06	0.04
	scen D(15)	0.02	0.05	0.03	0.03	0.05	0.02	0.03	0.06	0.03

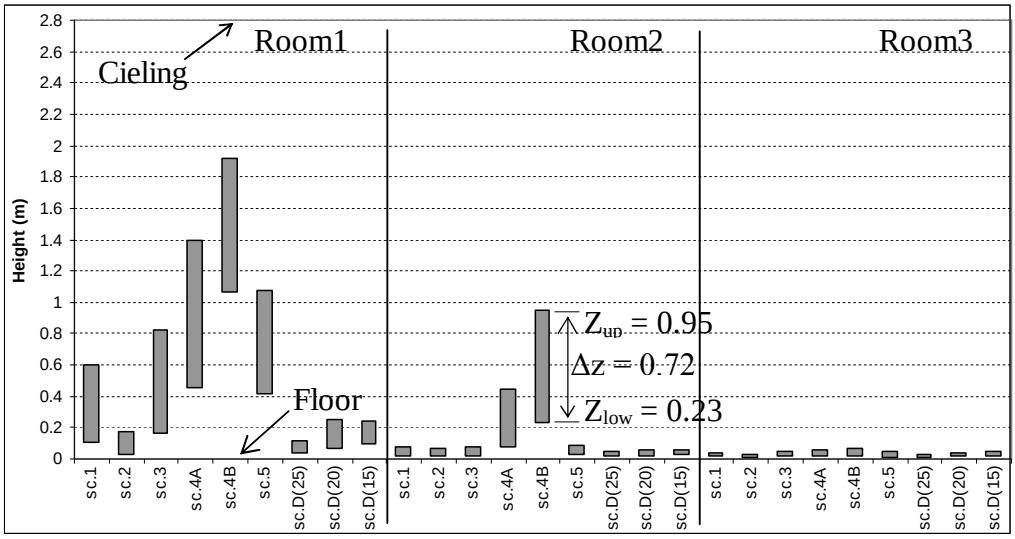

Figure 14: Flammability vertical width (GML 1 to 3) and position after 10 sec.

Table 4 (continued 1)

		t = 40 seconds			t = 50 seconds			t = 60 seconds		
		Z_{low} (m)	Z_{up} (m)	Δz (m)	Z_{low} (m)	Z_{up} (m)	Δz (m)	Z_{low} (m)	Z_{up} (m)	Δz (m)
Room 1 GML 1	scen1	0.99	1.24	0.25	1.1	1.31	0.21	1.21	1.36	0.15
	scen2	0.33	1.15	0.82	0.75	1.16	0.41	0.96	1.25	0.29
	scen3	1.23	1.53	0.30	1.32	1.6	0.28	1.43	1.68	0.25
	scen4A	1.98	2.33	0.35	1.94	2.36	0.42	2.06	2.44	0.38
	scen4B	2.27	2.55	0.28	2.1	2.62	0.52	2.13	2.63	0.50
	scen5	1.46	1.84	0.38	1.69	1.89	0.20	1.62	2.3	0.68
	scen D(25)	0.18	1.07	0.89	0.25	1.07	0.82	0.73	1.22	0.49
	scen D(20)	0.29	0.98	0.69	0.48	1.1	0.62	0.51	1.06	0.55
	scen D(15)	0.5	0.99	0.49	0.57	1.1	0.53	0.57	1.08	0.51
Room 2 GML 2	scen1	0.13	0.94	0.81	0.42	1.13	0.71	0.74	1.18	0.44
	scen2	0.12	0.87	0.75	0.14	1.03	0.89	0.22	1.13	0.91
	scen3	0.37	1.44	1.07	0.81	1.54	0.73	1.09	1.66	0.57
	scen4A	0.94	2.4	1.46	2.02	2.65	0.63	-	-	-
	scen4B	-	-	-	-	-	-	-	-	-
	scen5	0.51	1.3	0.79	0.95	1.38	0.43	1.1	1.57	0.47
	scenD (25)	0.04	0.2	0.16	0.08	0.59	0.51	0.11	0.7	0.59
	scenD (20)	0.06	0.4	0.34	0.09	0.63	0.54	0.05	0.72	0.67
	scenD (15)	0.08	0.39	0.31	0.05	0.55	0.50	0.05	0.6	0.55
Room 3 GML 3	scen1	0.04	0.32	0.28	0.04	0.84	0.8	0.08	1.07	0.99
	scen2	0.04	0.12	0.08	0.05	0.53	0.48	0.07	0.89	0.82
	scen3	0.06	1.44	1.38	0.08	1.63	1.55	0.6	1.74	1.14
	scen4A	0.18	2.8	2.62	0.08	2.8	2.72	-	-	-
	scen4B	-	-	-	-	-	-	-	-	-
	scen5	0.06	0.75	0.69	0.07	1.08	1.01	0.27	1.37	1.1
	scen D(25)	0.02	0.06	0.04	0.02	0.07	0.05	0.03	0.11	0.08
	scen D(20)	0.03	0.07	0.04	0.03	0.08	0.05	0.03	0.1	0.07
	scen D(15)	0.04	0.08	0.04	0.04	0.1	0.06	0.05	0.21	0.16

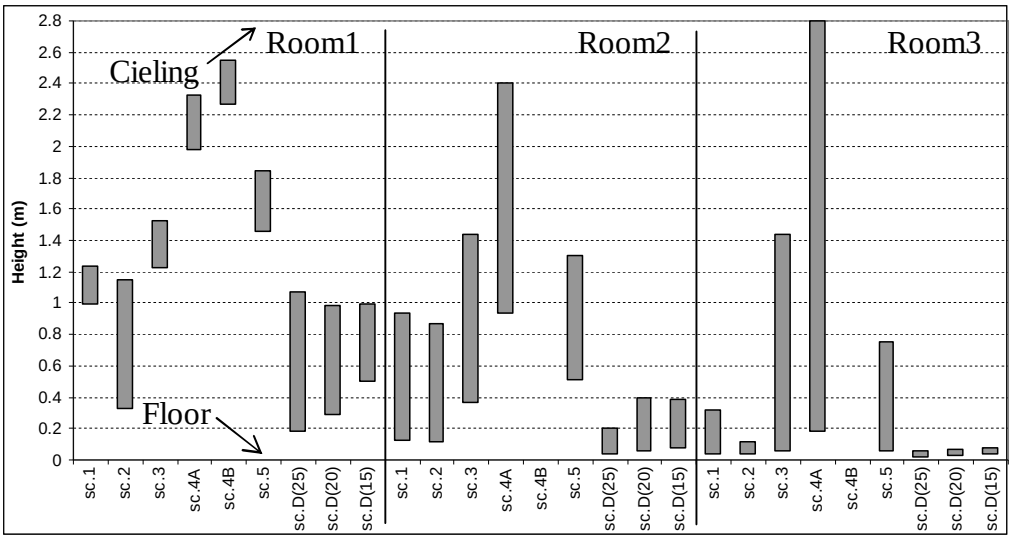

Figure 15: Flammability vertical width (GML 1 to 3) and position after 40 sec.

Table 4 (continued 2)

		t = 70 seconds			t = 80 seconds		
		Z_{low} (m)	Z_{up} (m)	Δz (m)	Z_{low} (m)	Z_{up} (m)	Δz (m)
Room 1 GML 1	scen1	1.24	1.42	0.18	1.26	1.46	0.20
	scen2	1.07	1.3	0.23	1.11	1.38	0.27
	scen3	1.46	1.74	0.28	1.52	1.76	0.24
	scen4A	2.18	2.45	0.27	2.15	2.47	0.32
	scen4B	2.25	2.8	0.55	2.57	2.8	0.23
	scen5	1.66	2.45	0.79	1.87	2.65	0.78
	scen D(25)	0.72	1.2	0.48	0.67	1.26	0.59
	scen D(20)	0.5	1.18	0.68	0.5	1.2	0.70
	scen D(15)	0.66	1.21	0.55	0.65	1.25	0.60
Room 2 GML 2	scen1	0.84	1.28	0.44	1.03	1.35	0.32
	scen2	0.55	1.17	0.62	0.79	1.24	0.45
	scen3	1.21	1.7	0.49	1.35	1.78	0.43
	scen4A	-	-	-	-	-	-
	scen4B	-	-	-	-	-	-
	scen5	1.19	1.65	0.46	1.42	1.76	0.34
	scenD (25)	0.21	0.82	0.61	0.41	1.06	0.65
	scenD (20)	0.05	0.8	0.75	0.05	0.74	0.69
	scenD (15)	0.05	0.66	0.61	0.06	0.72	0.66
Room 3 GML 3	scen1	0.11	1.24	1.13	0.18	1.38	1.2
	scen2	0.07	1.12	1.05	0.09	1.21	1.12
	scen3	0.97	1.78	0.81	1.18	1.84	0.66
	scen4A	-	-	-	-	-	-
	scen4B	-	-	-	-	-	-
	scen5	0.31	1.55	1.24	0.62	1.67	1.05
	scen D(25)	0.04	0.23	0.19	0.03	0.71	0.68
	scen D(20)	0.04	0.33	0.29	0.04	0.49	0.45
	scen D(15)	0.05	0.37	0.32	0.05	0.64	0.59

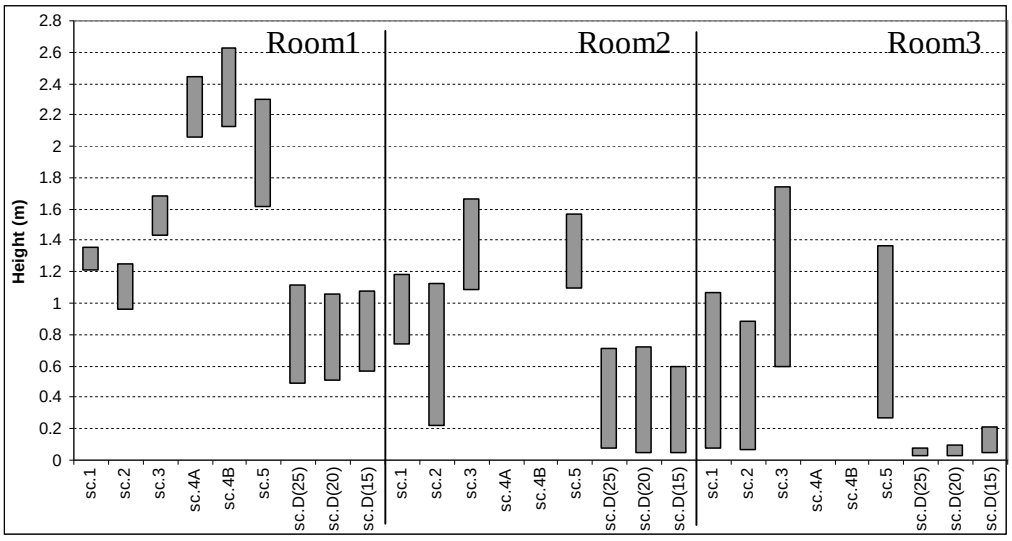

Figure 16: Flammability vertical width (GML 1 to 3) and position after 60 sec.

Table 5: Vertical position and size of the flammability region in each room for all Scenario1 and dilution

		t = 100 seconds			t = 200 seconds			t = 300 seconds		
		Z_{low} (m)	Z_{up} (m)	Δz (m)	Z_{low} (m)	Z_{up} (m)	Δz (m)	Z_{low} (m)	Z_{up} (m)	Δz (m)
Room 1 GML 1	scen1	1.37	1.56	0.19	1.61	1.82	0.21	1.68	1.92	0.24
	scen D(25)	0.67	1.26	0.59	1.29	1.67	0.38	1.54	1.87	0.33
	scen D(20)	0.67	1.3	0.63	1.39	1.76	0.37	1.59	1.95	0.36
	scen D(15)	0.92	1.37	0.45	1.48	1.8	0.32	1.66	2.02	0.36
Room 2 GML 2	scen1	1.11	1.55	0.44	1.55	1.77	0.22	1.67	1.86	0.19
	scenD (25)	0.41	1.06	0.65	1.1	1.6	0.5	1.44	1.75	0.31
	scenD (20)	0.05	0.98	0.93	0.07	1.62	1.55	0.05	1.88	1.83
	scenD (15)	0.06	0.87	0.81	0.07	1.65	1.58	0.07	1.92	1.85
Room 3 GML 3	scen1	0.73	1.53	0.8	1.55	1.76	0.21	1.69	1.85	0.16
	scen D(25)	0.03	0.71	0.68	0.05	1.3	1.25	0.05	1.76	1.71
	scen D(20)	0.05	0.77	0.72	0.05	1.4	1.35	0.06	1.77	1.71
	scen D(15)	0.05	0.74	0.69	0.05	1.12	1.07	0.06	1.67	1.61

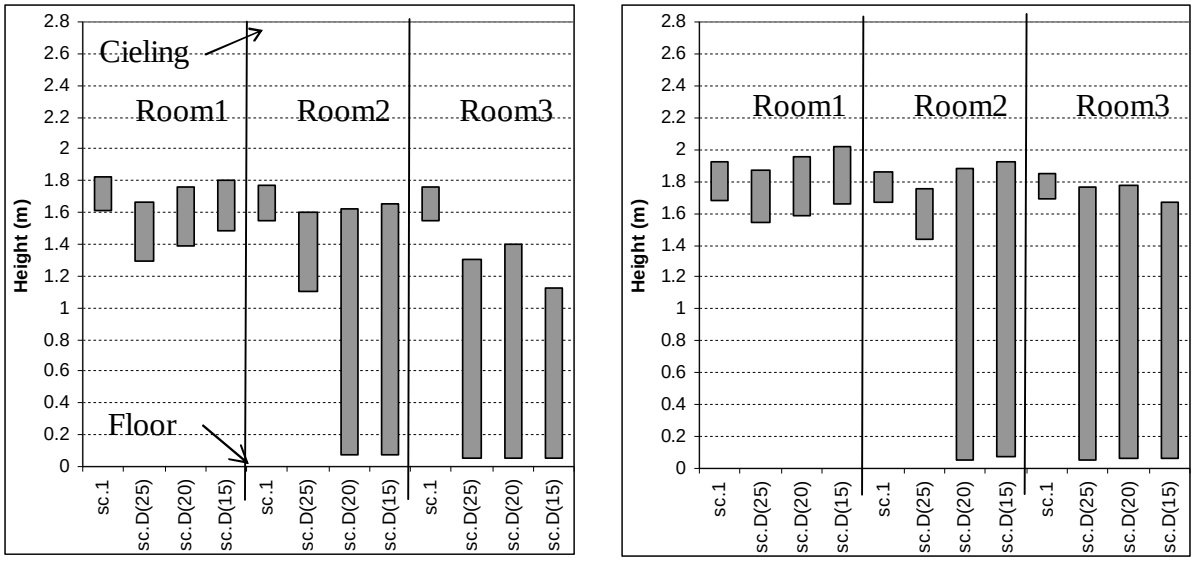

Figure 17: Flammability vertical width (GML 1 to 3) and position after 200 sec. (left) and 300 sec. (right)

6. Conclusions

The choice of fire-fighting tactics to use at the scene of a fire depends a lot on the situation the fire-fighters will face upon arrival there. In this paper, commonly used tactics were selected, based on one of the co-author's experience as a fire officer. Depending on the conditions, the particular risk of backdraft had to be considered, and CFD calculations were used to characterize the effects of these tactics on backdraft mitigation.

To estimate this risk, the warning signs that can be observed are [15]:

- Pulsating gases in small gaps and openings.
- Hot windows and doors indicate that temperatures are still high in the apartment allowing pyrolysation to take place.
- No visible flame in the fire room.
- Whistling sounds around doors and windows.

If there is a serious risk of backdraft, the following factors will influence the choice of tactics:

- The most critical factor is whether there are people left inside the apartment or not. In a life saving operation the time factor is critical, and the fire-fighters will have to use the less time consuming measures. In this situation the personnel is usually taking a higher risk since the attack is made with Breathing Apparatus (BA) team. The most important thing for the BA team is to cool the smoke gases as soon as fresh air is introduced in the apartment. The introduction of water spray has the effect of cooling the gases, creating a better environment for fire-fighters.
- Positive Pressure Ventilation may also be used in a life saving operation. However, it is very important that the air stream generated by the PPV fan has a clear path to the discharge opening. Nevertheless, Scenario 4 shows that the use of PPV can be very effective for the venting of flammable gases. The danger of backdraft will increase significantly during the first seconds, but decrease very quickly.

The use of PPV requires good knowledge and utilization experience. Scenario 5 clearly shows that incorrect use of PPV can highly increase the risk of backdraft due to a long-lasting highly mixed situation.

- In a situation where it has been confirmed that there is no-one left in the building, the use of a defensive tactic such as natural ventilation is very beneficial. This is clearly shown in the CFD calculations. The apartment can be vented both through the front door and e.g. a window on the back. There is a risk that the smoke gases may ignite outside the building and therefore, water extinguishing methods should be ready outside the opening. However, in defensive tactics, there is very low risk of human injuries.

Dilution is the dominant extinguishing mechanism, and the method of spraying water mist has proved very effective, provided that the dilution is sufficient. This means that the volume fraction of the unburnt gases is below the critical fuel volume fraction, as the danger of backdraft will be completely eliminated. It is important that as little fresh oxygen as possible is introduced during the water mist spraying, and therefore it is very beneficial to use tools such as piercing nozzles or cutting extinguishers. These tools have sufficient rates (typically around 70 l/min.) to reach the required dilution level rather quickly, i.e. approximately one minute for a classical size apartment. Nevertheless, if the volume fraction

is still above this critical value, the danger of backdraft lasts much longer. Yet, fire-fighting manuals recommend dilution as a tactic to use on underventilated fire.

The CFD calculations are proven to be very useful to estimate the effectiveness of the different fire-fighting tactics. As they are a good complement to the fire-fighters' experience, they can also be used for training and recommendations.

Acknowledgement

The present work was performed as a part of the project "Under-Ventilated Compartments Fires (FIRENET)" (Co. No. HPRN-CT-2002-00197). The project is supported by the EU Research Training Network FP5, which is gratefully acknowledged.

Nomenclature

C_{air}	The heat capacity of air (approximately 1 kJ/(kgK))
CFVF	Critical Fuel Volume Fraction
CMC	Critical Mixture Composition
D(X)	Dilution level, corresponds to a scenario with X % mass concentration
GML	Gas Measurements Line
LFL	Lower Flammability Limit
M_o	Initial mass of hot gases
M_{vap}	Mass of vapor added to obtain the desired dilution
M_{CH4}	Mass of unburnt gases (methane)
Q_{fan}	Flow rate of the PPV fan
t	Simulation time
T	Temperature
T_{final}	Temperature of hot gases after dilution
T_{in}	Temperature of hot gases inside the compartment
T_{out}	Temperature of cold gases outside the compartment (ambient)
UFL	Upper Flammability Limit
v_{fan}	Velocity at the inflow boundary, due to PPV fan
V_{gas}	Volume of hot gases in the enclosure
V_w	Volume of water to cool the gases from T_{in} to T_{final}
X	Mass concentration of unburnt gases (methane)
y	Dilution factor (%)
Z_{low}	Lower vertical limit of the flammability region
Z_{up}	Lower vertical limit of the flammability region

ΔH_w Heat of vaporization for water (2260 kJ/kg)

Δz Vertical width of the flammability region. $\Delta z = Z_{up} - Z_{low}$

ρ_{gas} Density of gases

ρ_{in} Density of hot gases inside the compartment (approximately $353/T_{in}$)

ρ_{out} Density of cold gases outside the compartment

ρ_w Water density in kg/liter (1 kg/l)

χ Dilution ratio

References

[1] Weng WG, Fan WC (2002) Experimental Study on the Mitigation of Backdraft in Compartment Fires with Water Mist. J Fire Sci Vol. 20, No. 4, 259-278.

[2] Fleischmann M, McGrattan KB: “Numerical and Experimental Gravity Currents Related to Backdrafts”, Fire Safety Journal 33 (1999) 21-34.

[3] Fleischmann CM: “Backdraft Phenomena”, University of California, Berkley,

1993.

[4] Gojkovic D: ”Initial Backdraft Experiments”, Report 3121, Department of Fire

Safety Engineering, Lund University, Sweden, 2001.

[5] Gottuk DT, Peatross MJ, Farley JP, Williams FW: ”The development and mitigation of backdraft: a real-scale shipboard study”, Fire Safety Journal 33 (1999) 261-282.

[6] Fahy RF, LeBlanc PR: “Fire-fighters fatalities in the United States – 2005”. Fire Analysis and Research Division, National Fire Protection Association. June 2006.

[7] Bengtsson LG, Karlsson B, "An Experimental and Statistical Study of the Phenomena Flashover, Backdraft and Smoke Gas Explosion" 3rd International Seminar on Fire and Explosion Hazards, 10-14 April, 2000, The University of Central Lancashire, England.

[8] Chitty R: ”A Survey on Backdraught”, Fire Research Station, Pub No 5/94, 1994.

[9] Guigay G, Karlsson B, Elíasson J: “Numerical and analytical determination of combustion products in strongly underventilated fires prior to backdraft**.** Presented in Workshop in Enclosure Fires, FIREsert, 2006.

[10] Elíasson J, Guigay G, Karlsson B (2008) Enclosure fires, gravity currents and the backdraft problem. J Fire Sci, JFS 092116. In Press.

[11] Guigay G, Elíasson J, Horvat A, Sinai Y (February 2006) Semi-analytic and CFD calculation of gravity flows in backdraft studies. Intended for publication in J Fire Sci.

[12] Gojkovic D, Karlsson B, "Describing the Importance of The Mixing Process in a Backdraft Situation Using Experimental Work and CFD Simulations" 3rd International Seminar on Fire and Explosion Hazards, 10-14 April, 2000, The University of Central Lancashire, England.

[13] Bengtsson LG, “Enclosure fires”: Swedish Rescue Services Agency (2001).

[14] Svensson S: “A study of tactical patterns during fire fighting operations”, Fire Safety Journal 37 (2002) 673-695.

[15] Iceland Fire Authority: “Completion of the recommendations”, Firenet project report (2006).

[16] Kerber: “Evaluation of the Ability of Fire Dynamic Simulator to simulate Positive Pressure Ventilation in the Laboratory and Practical scenarios”, NIST report NISTIR 7315, April 2006.

[17] Tuomisaari: “Smoke Ventilation in operational fire fighting”, VTT Publication 326, 1997.

[18] Positive pressure ventilation; PPV in firefighting (2006): http://www.firetactics.com/PPV.htm.

[19] FDS-fire dynamics simulator, NIST (2008): http://fire.nist.gov/fds/

[20] Gojkovic D, Bengtsson LG: ”Some theoretical and practical aspects on fire fighting tactics in a backdraft situation”, Proceedings of the 9th conference, Interflam 2001.

[21] SOFIE homepage (2005): http://www.cranfield.ac.uk/sme/sofie/

[22] Drysdale D: “An Introduction to Fire Dynamics”, Second edition, Wiley, 1998.

[23] Beyler B: “Flammability Limits of Premixed and Diffusion Flames”, chapter 2-19 of SFPE Handbook of Fire Protection Engineering, 2nd edition, NFPA Publication, 1995.

Paper [C]

Enclosure Fires, Gravity Waves and the Backdraft Problem

Journal of Fire Sciences

DOI: 10.1177/0734904108092116

Received: 16 May 2006/Accepted: 29 August 2007

Jónas Elíasson[a], Georges Guigay[a,*], Björn Karlsson[b].

AFFILIATIONS:

a- Civil and Environmental Department, Faculty of Engineering, University of Iceland, Reykjavik, Iceland

b- Iceland Fire Authority, Reykjavik, Iceland

CORRESPONDING AUTHOR: Georges Guigay

Tel: 00 354 525 5882

Fax: 00 354 525 4632

E-mail: gjg3@hi.is

Abstract

The air flow to an underventilated compartment fire often depends on the flow velocities in the gravity wave of cold air that feeds the fire with oxygen. This problem has been studied in laboratory experiments and by CFD simulations. The main problem seems to be whether mixing and entrainment between the two layers of hot and cold air has profound effect on the flow velocities. In this article, an analytical gravity wave model that can calculate the velocities in a simple gravity wave is presented. This model uses the equations of stratified flow hydraulics and the translatory wave solution of the flow equations. It is found that the velocities of the model compare very well to the velocities reported from laboratory tests and numerical simulations. Numerical simulations of stratified flow in a CFD model are discussed with respect to model construction. It is concluded that the densimetric Froude number is the main parameter for the velocity calculations and the length/height ratio is important for the friction forces.

KEYWORDS: Backdraft, gravity wave, density driven flow.

1. Introduction

Until recently, little research had been done on backdraft [1-4] in spite of how dangerous this phenomenon is to firefighters. This event is very hazardous and dangerous and has killed many firefighters in the past years [5]. The reason is undoubtedly the great difficulty in understanding this complicated process: first the accumulation of gases from an underventilated flame, then the gravity wave that carries oxygen into the compartment, and finally the ignition and the backdraft explosion itself. When an underventilated fire dies from a lack of oxygen, the enclosed room can remain full of hot unburned gases. If firefighters enter through a door, a window breaks or an opening occurs, fresh oxygen is carried in by gravity currents, and mixes with the gases. The crucial element is this wavelike gravity current, i.e. whether its dilution with gases and smoke into a flammable mixture results in backdraft or not.

The single most difficult detail in backdraft study is undoubtedly the time that elapses from the opening of the compartment until the occurrence of the explosion, which is the time it takes for the gravity wave to roll in and create the explosive mixture. This problem is highly fluid mechanical in character and is therefore best studied by the classical methods of fluid mechanics, reduced scale experiments [1-3], [6-8], CFD numerical modeling [9,10] and mathematical analysis. Successful backdraft mitigation demands an understanding of the gravity wave.

This study focuses on the velocity and thickness of the gravity wave that causes backdraft. Stratified fluid dynamics are applied to find the thickness (height) and the velocity of the gravity wave that carries fresh air into the compartment. The travel time of the wave from the opening to the point of possible ignition and the oxygen carrying capacity of the wave may thus be estimated. To do this, the translatory wave theory [11] is used, originally developed by Stoker [12] and adapt it to stratified flow using [13], which is a very complete and detailed work on gravity waves, describing in detail the theory of non-miscible and miscible stratified flow, as well as wind-driven and buoyant flow. The fluid mechanical part of the analysis is enclosed in the Appendix and will be referred to as necessary.

2. Gravity wave on a flat bottom

A gravity wave is studied here, which progresses at a velocity V (see Figures 1 and 2). At first the compartment is closed, but then suddenly a wall opens. Cold air flows in and an equal amount of hot air flows out.

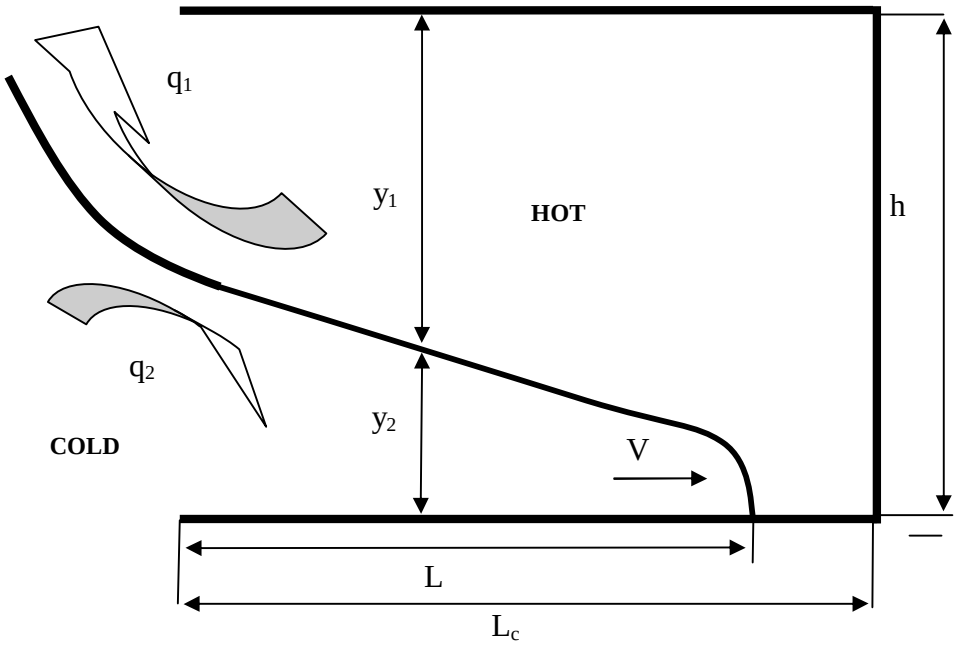

Figure 1: Definition sketch of a gravity wave flowing through a full opening

When the door opens, the initial pressure surge will settle down quickly and a neutral plane will develop near the middle of the opening, with inflowing air below and outflowing air above. The gravity wave will then develop in three phases, provided the compartment is long enough. A time history of the flow will look like Figure 2.

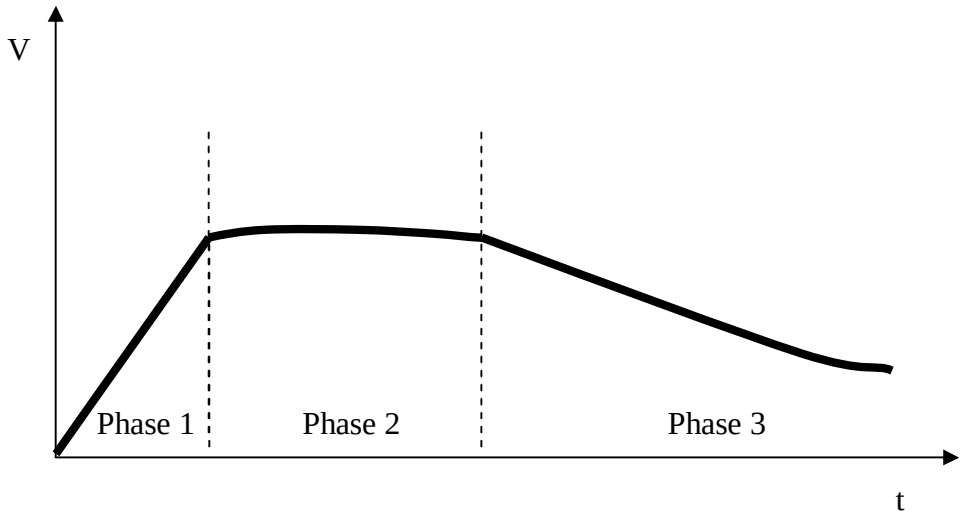

Figure 2: Time history of the flow entering a flat bottom compartment

One can see that the evolution of the flow can be divided in 3 different phases. During Phase 1, the wave accelerates from zero to full velocity. The second phase is the translatory

wave, moving with almost constant velocity (see Stoker's theory described in [12]). Finally, the third phase is the retarding wave, when it looses momentum and slows down.

2.1. Phase 1: The accelerating phase

Just after the opening is lifted, the flow velocities are small, the friction negligible, and one can use the unsteady Bernoulli equation.

$$\frac{\partial}{\partial t}\rho\phi + P + \rho g z + \frac{1}{2}\rho V^2 = Cst \qquad (1)$$

Taking the gradient of this equation, one obtains:

$$\frac{\partial}{\partial t}(\rho\vec{\nabla}\phi) + \vec{\nabla}(P + \rho g z + \frac{1}{2}\rho V^2) = 0 \qquad (2)$$

Multiplying by $\overline{dS} = \overline{(dx.dy)}$ and integrating along a closed curve that is a fluid pathline, one gets:

$$\frac{\partial}{\partial t}\oint \rho(V_x dx + V_y dy) = \frac{\partial}{\partial t}\oint |V| dS \qquad (3)$$

$$\frac{\partial}{\partial t}\oint |V| dS + \oint d(P + \rho g z + \frac{1}{2}\rho V^2) = 0 \qquad (4)$$

or

$$\rho_2 \frac{\partial}{\partial t}\overline{V}\ell = \Delta\rho_2 g h \qquad (\overline{V}: \text{average velocity over } \ell) \qquad (5)$$

If one lets the pathline touch the floor and the surface, with, $\ell \approx (L + h)$, $\partial\overline{V}/\partial t$ will be nearly constant until $L \approx h$.

In an accelerating translatory wave, one will have:

$$\rho_2 \frac{DV}{Dt} = \rho_2 \frac{\partial V}{\partial t} \text{ as } \frac{\partial V}{\partial x} \approx 0 \qquad (6)$$

$\partial\overline{V}/\partial t$ is higher in the wave than elsewhere on a closed path line and proportional to the average acceleration. Now, by using the proportionality factor obtained from the unsteady Bernoulli equation and including the acceleration forces in the depth integrated energy equation for the gravity wave as an unknown inertial force, one gets:

$$\rho_2 \frac{\partial V}{\partial t} y_2 = -\Delta\rho_2 g \frac{\partial y_2}{\partial x} y_2 - \tau \qquad (7)$$

where τ is the combined interfacial and bottom shear stress. Equation (7) shows how the acceleration term on the left hand side is balanced by the pressure gradient in Phase 1 if the friction τ is almost zero. Later, in Phase 2, the acceleration term becomes zero and shear stress and pressure gradient will balance each other. When the acceleration term becomes zero, Equation (2) turns into the Bernoulli equation. It will approximately hold for the flow outside the box in the cold fluid as velocities are low here. This gives an estimate of the

maximum velocity of the flow into the box. A neutral plane at y = h/2 is estimated. Applying Bernoulli's equation to a streamline, close to the bottom, one obtains:

$$V = \sqrt{\Delta g h} \text{ with } \Delta = \frac{\rho_2 - \rho_1}{\rho_2} \tag{8}$$

Assuming linear acceleration (no friction) as shown in Figure 2, the average velocity is:

$$V_{av} = \frac{1}{2} V_{max} \tag{9}$$

Equation (5) can be used to estimate roughly the time necessary to accelerate the fluid up to the Bernoulli velocity. One gets:

$$t_a = \ell / \sqrt{\Delta g h} \tag{10}$$

2.2. Phase 2: The translatory phase

In air, only confined (closed) flow is possible, but in mixing zones of salt and fresh water, unconfined (free surface) flow is the rule. With hydrostatic pressure distribution everywhere in the compartment one would have:

$$\rho_1 h = \rho_1 y_1 + \rho_2 y_2 \tag{11}$$

It is easy to see that the pressure gradient alongside the bottom is zero for this pressure distribution, and therefore no fluid would flow into the compartment. This is the case when dealing with stationary salt water wedges, that can be regarded as translatory waves with zero wave velocity. Behind the salt water wedge where $y_2 = 0$, one has $y_1 = (1+\Delta)h$, so fluid will be flowing out under the action of a pressure head Δh. This extra fluid depth behind the wedge does not exist in confined flows, where $y_1+y_2 = h$ always holds. But by using Boussinesq's approximation, one can exclude Δ everywhere except in pressure gradient (buoyancy) terms, and then proceed to treat confined and unconfined flow the same way.

It is noted that the dense bottom current is treated as an open channel flow in a gravity field Δg instead of g. Equations (A1) to (A7) in Appendix 1 are for stationary flow, but the open channel flow equations have another solution, a translatory wave with constant wave velocity equal to the water velocity [12]. In this phase, one has a translatory wave pushing the light fluid out, and slowly pushing the interface upwards.

2.2.1. Derivation of the basic equation

The continuity equation for the lower flow (see Appendix 1) will be:

$$\frac{\partial q_2}{\partial x} + \frac{\partial y_2}{\partial t} = 0 \Rightarrow \frac{\partial q_2}{\partial x} - V_2 \frac{\partial y_2}{\partial x} = 0 \tag{12}$$

The similar continuity equation for the upper flow gives directly:

$$q_2 = V_2 y_2 = q_1 \Rightarrow V_2 = V_1 \frac{y_1}{y_2} \tag{13}$$

By definition, the effect of mixing and entrainment on the overall densities will be small in this phase and will thus be disregarded. One can use three equations to analyze the flow:

- The depth integrated energy equation for the upper layer (Equation (A6)).
- The momentum equation for both layers.
- The momentum equation for the lower layer.

a) The depth integrated energy equation for the upper layer.

$$I = -\frac{d}{dx}\left[y_2 + y_1 + \frac{V_1^2}{2g} \right] \tag{14}$$

To evaluate the headloss term I, Equation (A7) is used with ρ as the reference density ρ_R, and then one gets:

$$\tau_i = \rho g y_1 I = \frac{f_i}{2}\rho (V_1 + V_2)^2 = \frac{f_i}{2}\rho V_2^2 \left(\frac{h}{y_1} \right)^2 \tag{15}$$

Equation (15) is derived from the more general Equation (A5) by using Boussinesq's approximation mentioned earlier.

By identification between Equations (14) and (15), one obtains:

$$\left[y_2 + y_1 + \frac{V_1^2}{2g} \right]_0^L = \frac{f_i}{2g} V_2^2 \int_0^L \frac{h^2}{y_1^3} dx \tag{16}$$

Assuming that y_2 is a parabola, it has the equation:

$$\frac{y_2}{h} = \frac{y_{2,0}}{h}\sqrt{1-\frac{x}{L}} = \psi\sqrt{1-\frac{x}{L}} \tag{17}$$

The integral in Equation (16) is solved as:

$$\int_0^L \frac{h^2}{y_1^3} dx = \frac{1}{h}\int_0^L \frac{dx}{\left(1-\frac{y_2}{h}\right)^3} = \frac{1}{h}\int_0^L \frac{dx}{\left(1-\psi\sqrt{1-\frac{x}{L}}\right)^3} = \frac{1}{h(1-\psi)^2} \tag{18}$$

Substituting this result in Equation (16), one obtains:

$$y_L - y_{2,0} - y_{1,0} = \frac{V_2^2}{2g}\left(\frac{\psi}{1-\psi}\right)^2 + \frac{f_i}{2g}\frac{L}{h}\frac{V_2^2}{(1-\psi)^2} \tag{19}$$

b) The momentum equation for both layers. This equation results in:

$$y_L - y_{2,0} - y_{1,0} = \frac{1}{2}\Delta h \Psi^2 + \frac{V_2^2}{2g}\frac{2\psi}{1-\psi} - C_f \frac{V_2^2}{g}\frac{L}{h} \tag{20}$$

Combining one gets:

$$\frac{V_2}{\sqrt{\Delta g h}} = C_\Delta = \sqrt{\frac{\psi^2}{\left(\frac{\psi}{1-\psi}\right)^2 - \frac{2\psi}{1-\psi} + \frac{L}{h}\left(\frac{f_i}{(1-\psi)^2} + 2C_f\right)}} \tag{21}$$

c) The momentum equation for the lower layer. This equation results in:

$$\left(\Delta h - y_L + y_{2,0} + y_{1,0}\right)\frac{1}{2}\psi^2 g \rho_2 h = \int_0^L (\tau_i + \tau)dx = \frac{f_i}{2}\rho_2 V_2^2 L \frac{2}{\psi^2}\left(\frac{\psi}{1-\psi} + \ln(1-\psi)\right) + C_f \rho_2 V_2^2 L$$

or

$$y_L - y_{2,0} - y_{1,0} = \Delta h - \frac{V_2^2}{g}\frac{L}{h}\frac{1}{\psi^2}\left(\frac{2f_i}{\psi^2}\left(\frac{\psi}{1-\psi} + \ln(1-\psi)\right) + 2C_f\right) \tag{22}$$

These are equations for V_2, Y_2 and Y_L. Then f_i and C_f have to be estimated. Pedersen ([13], Figure 7.2) suggests for f_i:

$$\sqrt{2/f_i} = 2.45\left(\ln(R_{e,i}\sqrt{f_i/2}) - 1.3\right) \text{ with } R_{e,i} = \frac{(U_m - U_i)(y - y_0)}{\nu} \tag{23}$$

The theory for the growing boundary layer can be used to estimate C_f. According to Prandtl (chapter 7 in [14] R_{eL} based on boundary layer length), one has:

$$C_f = \frac{1.310}{R_{eL}^{1/2}} \tag{24}$$

2.2.2. Graphical method to find CΔ in the Phase 2 equations.

The set of Equations (19), (20) and (22) needs to be solved in order to determine C_Δ and ψ knowing the friction coefficients f_i or C_f or vice versa. The following dimensionless coefficients A and B are considered, which represents the frictional effect:

$$A = \frac{L}{h} f_i \text{ and } B = 2\frac{L}{h} C_f \tag{25}$$

With these coefficients, Equation (21) reduces to:

$$\frac{V_2}{\sqrt{\Delta g h}} = C_{a,\Delta} = \sqrt{\frac{\psi^2}{\left(\frac{\psi}{1-\psi}\right)^2 - \frac{2\psi}{1-\psi} + \frac{A}{(1-\psi)^2} + B}} \tag{26}$$

Combining Equations (20) and (22), one obtains:

$$\frac{V_2}{\sqrt{\Delta g h}} = C_{b,\Delta} = \sqrt{\frac{\psi^2 - 2}{2\left(A\left(1 - \frac{2}{\psi^4}\left(\frac{\psi}{1-\psi} + \mathrm{Ln}(1-\psi)\right)\right) - \frac{B}{\psi^2} - \frac{\psi}{1-\psi}\right)}} \tag{27}$$

This set of equations has to satisfy the condition $C_{a,\Delta} = C_{b,\Delta}$.

This equation set is solved by iteration and used to produce Figure 3. It can be used to find the velocity and the neutral plane height in the opening when A and B are known, or to estimate A and B in experiments where velocity and neutral plane position are observed. Then, the two nondimensional numbers C_Δ and ψ can be determined. For example, taking A = B = 0.1 one finds the values $C_\Delta = 0.46$ and $\psi = 0.7$. It may be noted that the $C_\Delta = 0.50$ is the highest possible value in Figure 3, which is then the terminal velocity for Phase 2 for frictionless flow. How much C_Δ is below 0.5 can therefore be considered a tool to measure the influence of bottom friction and turbulent shear stress in the interface between the inflowing and outflowing liquids.

2.2.3. Discussion of the analytical results.

The equations leave us with implicit expressions for the depths of fluid 2 (the inflow), the adverse pressure at the wave head and finally the inflow velocity. To complete the calculation, the length of the gravity wave L must be known. In Phase 2, this is $L = V_2 t$ where t is the elapsed time, but as the wave has acquired some length as Phase 2 starts, estimating L can be more complicated.

Friction is not very important for Phase 2 waves but plays a part. Pedersen [13] has investigated many results and come up with the formula for the interfacial friction factor f_i (Equation (23)), which is based on 9 experimental series in a laboratory and 4 field study series by various researchers. The results show a great scatter, especially the experimental series. This is natural, as the velocity formulas clearly show that when they are used to calculate the friction factor, only a small deviation in y_2 creates a large deviation in the friction factor. In the same way, a small acceleration force will render a large deviation in the friction factor, but by using Pedersen's Figure (7.2), one finds that 0.01 is a fair estimate of f_i for clearly subcritical flows. In near-critical flows ($F_\Delta \leq 1$) the momentum exchange by increased entrainment can change this friction factor, as discussed in [13].

2.3. Phase 3: The retarding wave

When the L/h ratio grows large enough the friction term will dominate C_Δ, which becomes smaller and smaller, whatever the value of ψ is. At the same time, turbulent mixing and entrainment will change the density on both sides of the interface. In these processes, the entrainment velocity should be taken into account, but that depends on the Bulk Flux Richardson's number [13]. Such gravity waves have to be very long and they are therefore very difficult to reproduce in the laboratory. In short compartments, the wave will hit the back wall and get reflected before Phase 3 starts. Therefore, the interest in Phase 3 waves from a fire protection engineering viewpoint is debatable. In situations leading to backdraft, it is more likely that the gravity wave will hit the opposite wall and be reflected from it before going into Phase 3. Therefore, one will not consider the analytical treatment of Phase 3 waves at this point.

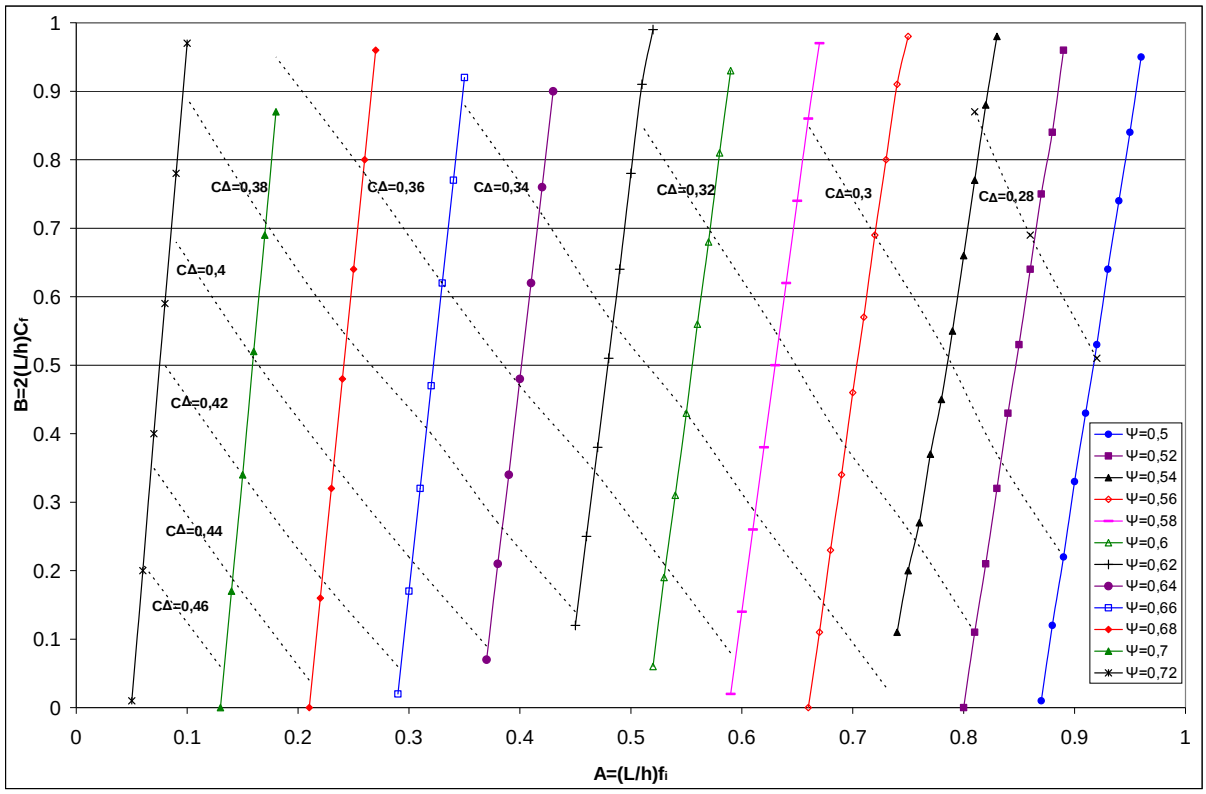

Figure 3: Couples (A,B) solutions, and isovalues of CΔ satisfying the condition: Ca,Δ = Cb,Δ

3. Comparison with experimental values

Here one shall compare the theoretical results to three experiments. Two apply to the confined case and one to the unconfined case.

3.1. Experiments of Fleischman and McGrattan [1] (confined)

They conducted salt water experiments in their backdraft study and simulated the flow with a Large Eddy Simulation turbulence model in a compartment [1]. This article gives a remarkable qualitative observation of the gravity wave, as well as detailed quantitative results on the propagation time of the wave and velocity field in the compartment, with a good agreement between salt water experiments and CFD simulations. The following experimental values for Δ and t* are taken from Figure 5 in [1]. The velocities are then calculated using Equation (5) in [1] (L is here the total length of the compartment, t travel time across) $t = t^*L/(\Delta g h)^{1/2}$ and $V_{ex} = L/t$.

From this, one has $C_\Delta = 1/t^* = 0.43$ with 2 significant digits. By using Figure 3, one gets ψ between 0.67 and 0.72. This result may be accurate enough, but if one has the friction data (not published in [1]), the complete theory of phase 2 flow analytical results can be used to analytically determine ψ and C_Δ by using Equation (27). When one assumes $C_f = 0.003$, $f_i = 0.013$, one gets A= 0.225, B = 0.107, $\psi = 0.68$ and $C_\Delta = 0.43$.

Table 1 below shows the experimental and analytical values for the terminal velocity.

Table 1: Theory compared to Fleischmann and McGrattan results

	Fleishmann and McGrattan - Experiments			Theory Phase 2
Δ	t*	t (s)	V_{ex} (m/s)	V_{an} (m/s)
0.01	2.3	5.69	0.053	0.052
0.018	2.2	4.06	0.074	0.070
0.04	2.25	2.78	0.108	0.104
0.07	2.3	2.15	0.140	0.137
0.1	2.2	1.72	0.174	0.164

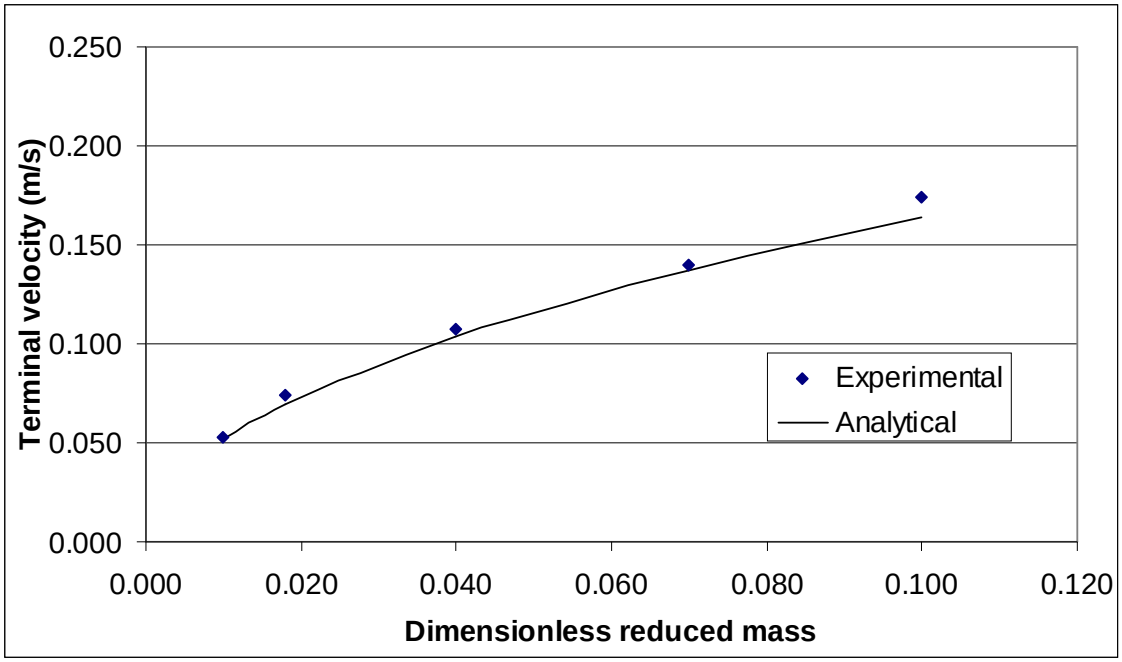

Figure 4: Terminal velocity versus Δ for experiments and analytical theory

Table 1 and Figure 4 show a very good agreement between experimental and analytical results, even if the terminal velocity has been calculated by only considering Phase 2. This shows that Phase 1 is very short and can consequently be neglected in the determination of the terminal velocity.

3.2. Experiments of Weng et al [8] (confined)

In these experiments, one series is performed with a full opening. All the v* results (terminal velocity in [8]) are v* = 0.49-0.50. This terminal velocity is calculated the same way as C_Δ (Equation (27)) except that Weng et al use the lighter fluid as reference density. Consequently, the v* results are 2 – 5 % higher than our C_Δ for the values reported in Table 1 in [8]. They would be C_Δ = 0.46 – 0.48, or about 5 % higher than the v* values. However the agreement is very good.

3.3. Experiments of Moghtaderi [15] (unconfined)

Moghtaderi carried out experimental studies of the structure of gravity currents using a Laser Doppler velocity meter. Experiments were done in both adiabatic and isothermal conditions. The isothermal boundary conditions showed a three-dimensional turbulence, whereas adiabatic showed a more two-dimensional behavior. The turbulence was found to be highly heterogeneous and its distribution was governed by the location of large eddies, so one uses the adiabatic condition where this extra turbulence is not present. In these experiments, one has an unconfined (open channel) wave. The measured head velocity is V_2 = 0.1 m/s, Δ = 0.048 giving C_Δ = 0.42 and the reported L/h ≅ 0.8/0.12 = 6.7. From Table 1 in [15], the Reynolds number of the wave can be estimated as $R_{e,L} = Vh/\nu \approx 8880$. As the L/h value is rather low [13], one uses Equation (24) for C_f.

$$C_f = \frac{1.3}{\sqrt{R_{e,L}}} = \frac{1.3}{\sqrt{R_e \frac{L}{h}}} = \frac{1.3}{\sqrt{8880 * 6.7}} = 0{,}005$$

Giving B = 0.034, Figure 3 shows ψ = 0.66. This results in $y_{2,0}$ = 0.08 and compares well to Figure 9 in [15]. Then A = 0.3 is found by giving f_i = 0.04, considerably lower than the value of 0.1. Here one has a higher A and a lower f_i than in Fleischmann and McGrattan's experiments [1], just as one should have according to the appendix.

4. Applications

Both physical and numerical experiments need to be carefully designed. A study of Figure 3 shows that C_Δ varies between 0.3 and 0.45 depending on A and B. Experiments with L/h ratios from 5 to 10 as is common in large buildings may be difficult to perform in a laboratory. This may be helped by making the floor rough to increase C_f in order to bring laboratory A and B up to prototype values.

4.1. Example 1

A reception hall is 25 m deep and 3 m high. At one end is a fireplace, and one wants to know the eventual travel time of the gravity wave to the fire place and measure it in a salt water experiment in a compartment in the scale λ_h = 10 in height and λ_L = 15 in length. Prototype C_f is estimated at 0.05 including furniture and decorations. What C_f for the model is needed?

$C_{f,m}/C_{f,p} = (R_{eL,p}/R_{eL,m})^{1/2} = (V_p/V_m)^{1/2} (L_{c,p}/L_{c,m})^{1/2} (\nu_m/\nu_p)^{1/2} = (\square\square\lambda_h\square\Delta_p/\Delta_m)^{1/4} \lambda_h^{1/2} (\nu_m/\nu_p)^{1/2} = (\Delta_p/\Delta_m)^{1/4}$ 1.8 3.9 0.26 = approximately 3 – 4. (here the subscripts m and p stand for the model and the prototype respectively).

This applies if one builds a scaled model of the hall with all furniture and decorations. This will increase model A and B and bring up too low C_Δ results, and time travel results may be 20 % too low. One must find a way to reduce model $C_{f,m}$ to approximately 25% of prototype $C_{f,p}$.

4.2. Example 2

A 40 m long corridor, 2.8 m high, is filled with hot gas with density 75 % of air. It becomes extremely flammable when mixed with air. A glow has been detected at the far end. A deflagration travel time of 4 seconds can be added to the gravity wave travel time. Firemen can open the door and run for cover in 40 seconds. Is it enough to escape the fireball? C_f is estimated 0.003.

L/h = 17.9, B = 0.1, A = 0.22 => C_Δ = 0.43. t = 50/(0.43 (0.25 9,82 2.8)$^{1/2}$) = 44 s.

That should be OK! Even when not counting the deflagration travel time, which is reassuring. Nevertheless, a CFD analysis should be recommended.

5. Discussion of the physics of the experiments

5.1. Experimental results

The analytical values from Figure 4 are generally in good agreement with the experimental data. Taking Phase 1 into account improves the agreement a little, showing that friction terms must be interpreted carefully when the Length/Height (L/h) ratio is low. This is because of the Phase 1 time necessary for the accelerating wave to reach the terminal velocity value and the fact that Phase 1 is dominated by inertial forces rather than friction. The friction developed at the end of Phase 1 is quite high, but has little effect because of how small the L/h ratio is, it increases with the increasing L/h ratio of the wave, and can be estimated to be the dominating force when L/h reaches about 40. This is very close to the entrance length in pipes, or the length it takes for the boundary layer to reach the middle in a smooth pipe.

In Moghtaderi's experiments [15], one has a Phase 2 wave with L/h ratio significantly larger than in the unconfined experiments, but still too small to dominate the flow or bring it close to Phase 3. The consequences are that friction factors are high in the low L/h ratio experiments but diminish quickly. They are already up to 0.3 in Moghtaderi's experiment (L/h = 6.7) from about 0.1 in the other experiments.

In Phase 2 gravity flow, no appreciable mixing is produced. Entrainment is high at the beginning, but it decreases quickly, so when the compartment is fully open, a short gravity wave transports more or less clean air to the ignition point. When the air wave comes flowing through a narrow door or a window, one has a situation where the size of the opening determines the flow into the room through the formation of critical velocities in the opening. In this situation one will have a gravity wave with a constant flow, but such waves are a little different from the purely translatory wave treated here. Another difference is that the plume into the compartment can easily cause appreciable forced mixing if it hits the floor from a considerable height. Then the initial mixture in the wave can have a Froude number different from the inflow.

5.2. CFD calculations of gravity waves

Fleischmann and McGrattan's [1] CFD flow pictures are very interesting as they show a beginning vortex entrainment, which is generated inside the grid. Vortex entrainment and

cusp entrainment exist in practice, and are discussed by Pedersen [13] (figure 6.2). The vortexes in [1] are however far too great and they cannot be seen in the actual experimental figures. The explanation of this discrepancy is twofold, firstly vorticity stretching is prohibited in 2D simulations, and secondly stable stratification slows down the mixing process. Mixing across a density stratification interface by action of turbulence creates potential energy that is taken out of the turbulent energy that otherwise would be dissipated. Turbulent dissipation is present in the sub-grid model only. The model may have to be modified to include this recycling of turbulent energy back into potential energy by action of turbulence, in order to represent the interface processes correctly. Figure 4.2.6 in Pedersen [13] explains this modification in a quantitative manner. Bournet et al [16] calculate a plunging density current by using a k–ε model where buoyancy is included in the macroscale model as well as in the sub-grid model, by including a term function dependent on the Prandtl number. They produce a convincing relation between entrainment and Richardson's number showing the characteristic sharp decline of entrainment with increasing stability (higher R_i). But they use a very special grid and special calculation procedures in order to preserve numerical stability. Kassem et al [17] go a similar way with the same problem, and include the strain rate in the sub-grid model. They also produce convincing results, even for negative buoyancy. Comparing Fleischmann and McGrattan's simulation to Bournet and Kassem's leave an unsolved question: should the potential energy gain be included in the sub-grid model in order to simulate gravity waves in backdraft simulations?

6. Conclusion

The gravity wave that feeds fresh air to closed compartments can be calculated using the equations of stratified flow given in the review papers by Pedersen [13]. Three flow phases can be identified, accelerating flow (Phase 1), translatory wave (Phase 2) and retarding flow (Phase 3).

The basic physical model for the unsteady motion of the gravity wave in Phase 2 is the translatory wave model. The wave progresses with constant velocity driven by the pressure gradient of the sloping interface. Such gravity waves on a horizontal bottom in a zero pressure environment do have the form of a parabola. In the mild adverse pressure gradient that drives the outflow, the parabolic form is assumed to be preserved without any loss of generality. The unknowns are basically the wave velocity, the wave's depth and the pressure gradient driving the outflow. To calculate these quantities, there are 3 equations:

a) The depth integrated energy equation for the upper layer.

b) The momentum equation for both layers.

c) The momentum equation for the lower layer.

The velocity of this wave is governed by the densimetric Froude number of the wave, based on total fluid depth. With small friction, this Froude number turns out to be close to 0.44 in three different experiments, giving the entrance depth of the gravity wave up to 70 % of the total depth.

The velocity of the wave and the thickness of the gravity wave in the entrance of the box can be found using Figure 3, provided that the interfacial and bottom friction is known. For short gravity waves, when interfacial and bottom friction are still small and the flow is in

transition from Phase 1 to Phase 2, a dimensionless velocity C_Δ around 0.45 and a wave height ration ψ (Equations (26) and (27)) around 0.72 are found.

A review of recent CFD calculations of stratified flows show a tendency to improve the sub-grid turbulence models by including terms that recycle a part of the turbulent energy production back into potential energy. This helps to reproduce the effect of the increasing stability of the stratification observed in nature on the entrainment. So far, it is unclear whether these improvements are necessary or not to cope with the gravity wave in numerical backdraft simulations as frictional effects are not very important in low L/h waves. At least Fleischmann and McGrattan produce simulation results for a gravity wave on the borderline between Phase 1 and Phase 2 that, apart from large interface vortices, look convincing. Their results that fall within the formulas for both Phase 1 and Phase 2 are presented here.

Finally, it may be concluded that the method presented here gives reliable results for Phase 2 flows, and can be valuable in estimating gravity wave velocities and air carrying capacity. Scientists planning model tests and CFD simulations get a valuable advance knowledge of their problem when using this method. It also shows that fire safety experts can utilize research done inside the fluid mechanic community for the benefit of their own science.

Nomenclature

A	Dimensionless coefficient. $A=(L/h)f_i$
B	Dimensionless coefficients. $B=2(L/h)C_f$
C_f	Bottom friction factor
C_Δ	Non dimensional wave velocity
D	Depth
f	Friction factor
f_i	Interfacial friction factor
F_Δ	Densimetric Froude number
g	Acceleration of gravity
g'	Reduced acceleration of gravity
h	Height of the compartment (confined case) or total depth (unconfined case)
I	Energy gradient
ℓ	Length of the closed pathline
L_c	Length of the compartment
L	Longitudinal length of the wave
P	Pressure
q	Discharge per unit width
q_1	Flow rate of hot fluid
q_2	Flow rate of cold fluid

R_e	Reynolds number
R_{eL}	Reynolds number based on boundary layer length
R_i	Richardson number
S	Coordinates in flow direction
t	Elapsed time after compartment opening
t_a	Acceleration time
t*	Characteristic time
U	Velocity of the entrained fluid
U_i	Minimum velocity of the flow
U_m	Maximum velocity of the flow
V	velocity of the gravity wave
V_{av}	Average velocity during the acceleration phase
V_E	Entrainment velocity
V_{ex}	Velocity values from experiments
V_{max}	Maximum velocity, at the end of the acceleration phase
V_n	Flow velocity at point n
V_x	Horizontal component of velocity
V_y	Vertical component of velocity
V_1	Velocity of the hot fluid layer
V_2	Velocity of the cold layer
v*	Terminal velocity
x	Horizontal coordinates
y	Vertical coordinates
y_c	Critical depth
y_L	Total depth in front of the gravity wave
y_n	Vertical coordinates of point n
y_1	Thickness of the hot fluid layer
y_2	Thickness of the cold layer
$y_{1,n}$	Thickness of the hot layer at point n
$y_{2,n}$	Thickness of the cold layer at point n
z	Elevation
δ	Boundary layer thickness
Δ	Dimensionless reduced mass. $\Delta=(\rho-\rho_R)/\ \rho_R$
λ	Compartment scale factor for prototype

λ_h	Compartment scale factor (height)
λ_L	Compartment scale factor (length)
ν	Kinematic viscosity of the flow
ξ	Horizontal position inside the gravity wave
ρ	Fluid density
ρ_R	Density of reference fluid
ρ_1	Density of the hot fluid
ρ_2	Density of cold fluid
τ	Combined interfacial and bottom shear stress
τ_i	Interfacial shear stress
τ_b	Bottom shear stress
ϕ	Velocity potential function
ψ	Dimensionless gravity current thickness on depth ratio. $\psi = y_{2,n}/h$

List of references

[1] Fleischmann, C.M. and McGrattan, K.B. (1999). Numerical and Experimental Gravity Currents Related to Backdrafts, Fire Safety Journal, 33(1): 21–34.

[2] Gojkovic D., "Initial Backdraft Experiments", Report 3121, Department of Fire Safety Engineering, Lund University, Sweden, 2001.

[3] Weng, W.G. and Fan, W.C. (2002). Experimental Study on the Mitigation of Backdraft in Compartment Fires with Water Mist. Journal of Fire Sciences, Vol. 20, No. 4, 259-278 (2002), DOI: 10.1177/073490402762574721.

[4] Zhou, F. and Wang, D. (2005). Backdraft in Descensionally Ventilated Mine Fire. Journal of Fire Sciences, Vol. 23, No. 3, 261-271 (2005) DOI: 10.1177/0734904105047915.

[5] Fahy, R.F. and LeBlanc P.R. (2006). Fire-fighters Fatalities in the United States – 2005. Fire Analysis and Research Division, National Fire Protection Association.

[6] Weng, W.G. and Fan, W.C. (2003). Critical Condition of Backdraft in Compartment Fires: A Reduced Scale Experimental Study, Journal of Loss Prevention in the Process Industries, 16(1):19–26.

[7] Fleischman, C.M., Pagni, P. J. and Williamson, R. B. (1994). Salt Water Modeling of Fire Compartment Gravity Currents. Fire Safety Science. Proceedings of the forth international Symposium, pp. 253- 264; June 13 – 17, Ottawa, Ontario, Canada 1994.

[8] Weng, W.G., Fan, W.C., Qin, J. and Yang, L.Z. (2002). Study on Salt Water Modeling of Gravity Currents Prior to Backdrafts using Flow Visualization and Digital Particle Image Velocimetry, Experiments in Fluids, 33(3): 398–404. DOI 10.1007/s00348-002-0448-1.

[9] Weng, W.G. and Fan, W.C. (2004). Nonlinear Analysis of the Backdraft Phenomenon in Room Fires, Fire Safety Journal, 39(6): 447–464.

[10] Yanga, R., Weng, W.G., Fan, W.C. and Wang, Y.S. (2005). Subgrid Scale Laminar Flamelet Model for Partially Premixed Combustion and its Application to Backdraft Simulation, Fire Safety Journal, 40(2): 81–98.

[11] Eliasson, J., Kjaran, S.P., Holm, S.L., Gudmunsson, M.T. and Larsen, G. (2007). Large Hazardous Floods as Translatory Waves, Environmental Modeling and Software, 22(10): 1392–1399.

[12] Stoker, J.J. (1957). Water Waves. The Mathematical Theory with Applications. Interscience Publishers, London.

[13] Pedersen F.B. (1986). Environmental Hydraulics: Stratified Flows. Springer-Verlag Editions, Berlin Heidelberg.

[14] Olson R. M. and Wright S. J. (1990). Essentials of Engineering Fluid Mechanics, Fifth Edition. Harper and Row Publishers, New York.

[15] Moghtaderi B. (2004). Application of Laser Doppler Velocimetry (LVD) to Study the Structure of Gravity Currents under Fire Conditions. Experimental Thermal & Fluid Science, 28 (2004) 843-852.

[16] Bournet, P.E., Bartus, D., Tassin, B., and. Vinçon-Leite, B. (1999). Numerical Investigation of Plunging Density Current. Journal of Hydraulic Engineering, Volume 125, Issue 6, pp. 584-594 (June 1999).

[17] Kassem A., Imran J. and Khan, J.A. (2003). Three Dimensional Modeling of Negatively Buoyant Flow in Diverging Channels. Journal of Hydraulic Engineering, Volume 129, Issue 12, pp. 936-947 (December 2003).

Appendix 1: Hydrodynamics of stratified flows

Here the general theory of stratified flows developed by Pedersen [13] is followed. We start by showing a simple case of non-miscible flow, then develop the theory leading to the flow chart on Figure 2, and introduce the effect of mixing later on stationary dense bottom currents.

A one-dimensional flow of heavy fluid along the bottom of a basin of light fluid of density ρ_R is considered. One can study the effect of a local hump by applying Bernoulli's equation along a streamline from A to B (see Figure A1):

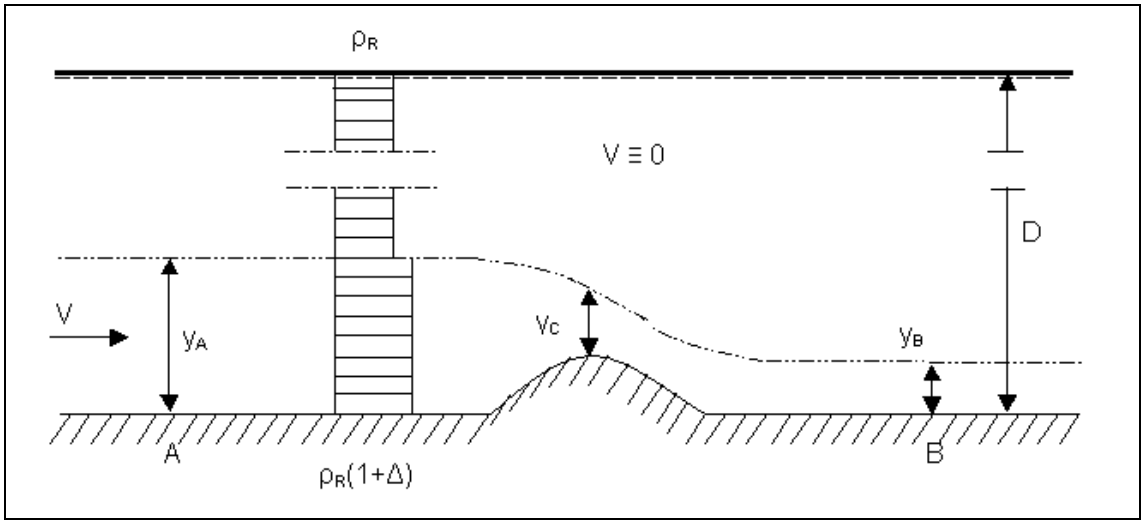

Figure A1: Schematic control volumes in a two layer zone model

$$\rho_R g D + \Delta\rho_R g y_A + \frac{1}{2}\rho_R (1+\Delta) V_A^2 = \rho_R g D + \Delta\rho_R g y_B + \frac{1}{2}\rho_R (1+\Delta) V_B^2 \qquad \text{(A1)}$$

By using Boussinesq's approximation, one can neglect the difference between ρ_R and $\rho_R(1+\Delta)$ except in the buoyancy term. One obtains, after simplification:

$$y_A + \frac{V_A^2}{2\Delta g} = y_B + \frac{V_B^2}{2\Delta g} \qquad \text{(A2)}$$

$$y_A + \frac{V_A^2}{2g'} = y_B + \frac{V_B^2}{2g'} \qquad \text{(A3)}$$

This shows that by using g'=Δg, all the well-known open channel flow equations can be reproduced. The dimensionless number:

$$F_\Delta = \frac{V}{\sqrt{g' y}} = \frac{V}{\sqrt{\Delta g y}} \qquad \text{(A4)}$$

is called the densimetric Froude number and it characterizes the flow. All the well-known phenomena and relations applicable in open channel flow can be directly transferred to the dense bottom currents of the immiscible fluids using it. We just have to treat the current as if the acceleration of gravity were reduced to Δg. Then, specific energy and critical velocity arise when the Froude number is equal to one.

The stationary salt water wedge

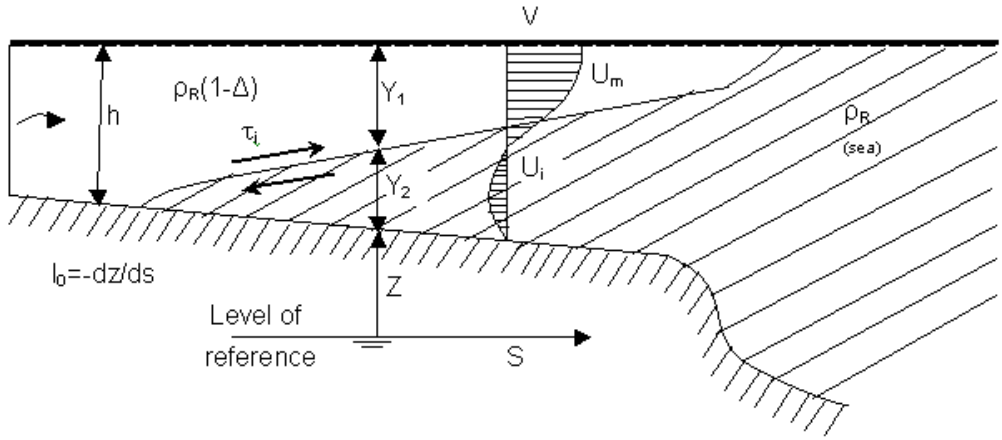

Figure A2: Stationary salt water wedge (highly distorted scale)

This is an estuarine process, which has been much studied in laboratory testing and field observations. References to works by hundreds of researchers are in [13]. The light fresh water from a river floats on the more dense salt water of the sea (see Figure A2). The density difference maintains a discharge in the upper fresh layer, and a circulation in the lower salt layer. This is very similar to the unsteady translatory wave used in many salt water tests in backdraft studies. In the interface, there is a shear stress:

$$\tau_i = \frac{f_i}{2}\rho(U_m - U_i)^2 = \frac{f_i}{2}\rho V^2 \qquad \text{(A5)}$$

where f_i is the friction factor at the interface. The shear stress at the interface is balanced by the longitudinal pressure gradient in the lower fluid. One then has the differential equation for open channel flow. The depth integrated energy equation for the upper layer is:

$$I = -\frac{d}{dS}\left[y_2 + y_1 + \frac{V^2}{2g} \right] \qquad \text{(A6)}$$

The depth integrated momentum equation allows one to write:

$$\tau_i = \rho_R (1-\Delta) g y_1 I \approx \rho_R g y_1 I \qquad \text{(A7)}$$

Appendix 2: Unsteady translatory gravity wave on a flat bottom

a) No mixing

The wave starts when the compartment door is opened. In practice this will cause some initial pressure disturbance and a vortex formation in the compartment, which do not seem to be included in CFD simulations. The wave progresses with more or less constant velocity V (Figure 2), so the velocity of the fluid will also be V. Then the continuity Equation (12) allows the solution:

$q = y\,V \qquad y = y(\xi) \qquad \xi = x - Vt$

when V is constant energy loss is equal to surface slope. With friction proportional to the velocity squared and f_i representing the friction factor, the momentum equation gives:

$$\text{Momentum:}\quad \frac{\partial y}{\partial \xi} = -I = -f_i \frac{V^2}{2gy} \tag{A8}$$

This equation integrates to:

$$\text{Wave form:}\quad y^2 = f_i \frac{V^2}{\Delta g}(L - x); \tag{A9}$$

The friction factor f is in two parts as before, bottom friction C_f and interfacial friction f_i that for small F_Δ can be estimated using Equation (23). L = V.t is the length of the wave from the opening. If y_0 corresponds to y in x = 0, the following wave form can be used instead of Equation (A9):

$$y^2 = y_o^2(1 - x/L)$$

This is the most elementary form of a translatory wave. More complete forms can be for example found in Stoker [12].

b) With mixing

No literature about mixing in translatory wave can be found, therefore the only possible way to estimate mixing effect is to use data for steady state (constant q) results. Phase 2 translatory waves are quasi-steady (V is constant) and in equilibrium with flow resistance, so effects of mixing should be similar. In CFD calculation this is the only data that the sub grid model, controlling local mixing, can be built on.

We have ([13] Equation (4.2.3))

$$\frac{\partial}{\partial x}\left(\frac{1}{2}\Delta\rho g y^2 + \rho V^2 y\right) + \rho V_E U + \tau_b + \tau_i = 0 \tag{A10}$$

V_E is the entrainment velocity and U the velocity of the entrained fluid, that would essentially be proportional to the velocity of the upper fluid, that again is close to V. According to [13], V_E/V for high densimetric Froude numbers is of the order of magnitude 0.1 for buoyant plumes ([13] Equation (4.2.9)) and in dense bottom currents ([13] Figure 6.6 and Equation (6.14)). These estimates by Pedersen are based on an immense number of laboratory data (see [13] figures 7.1 and 7.2).

Judging from this, we would have three flow resistance terms, bottom friction, interfacial friction and entrainment resistance, all proportional to ρV_2: Adding all up, the flow resistance in the mixing case should be:

$$f_i \frac{1}{2}\rho V^2 = (\frac{V_E}{V} + C_f + f_i)\frac{1}{2}\rho V^2) \qquad \text{(A11)}$$

C_f and f_i are estimated using Equations (23) and (24), the friction factors are both an order of magnitude less than 0.1. In the mixing case, we therefore have $f_i \approx 0.1$.

The Phase 2 flow will start out with great mixing and a densimetric Froude number of 0.7 – 1.0 (Equation (4)). Judging from [13] Figure 6.6 when the velocity diminishes and Phase 2 turns into Phase 3, V_E/V quickly reduces and approaches the f_i and C_f values, but at the same time, L/h increases so A and B will most likely not diminish.

It should also be noted that mixing will increase the volume of the wave. The continuity equation only counts the dense liquid flow, ([13] chapter 4.1), so the neutral plane (V = 0) will be higher. The total flow in the gravity wave will be the dense fluid plus entrained fluid.

$q_t = q(x) + V_E x$

Great care must therefore be taken when extending the Figure 3 results to Phase 3 flows. This can produce reliable results but cannot be generally recommended.

Paper [D]

Analytic Calculation and Computer Simulation of Gravity Flows in Backdraft Studies

Journal of Fire Sciences

Submitted in May 2008

Georges Guigay[a], Jónas Elíasson[a], Andrej Horvat[b], Yehuda Sinai[b], Björn Karlsson[c]

AFFILIATIONS:

[a]Department of Civil and Environmental Engineering, University of Iceland, Hjarðarhagi 6, 107 Reykjavík, Iceland

[b]ANSYS Europe Ltd., West Central 127, Milton park, Abingdon, Oxfordshire, OX14 4SA, United Kingdom

[c]Iceland Fire Authority, 101 Reykjavik, Iceland

CORRESPONDING AUTHOR: Georges Guigay

Tel: 00 354 525 5882

Fax: 00 354 525 4632

E-mail: gjg3@hi.is

Abstract

In enclosure fires, density driven vent flow through an opening to the fire compartment is directly dependant to the state of the fire and the evacuation of smoke and hot gases. If a fire is strongly under-ventilated, there may be sources of heavy production of flammable gases. If a sudden opening occurs, e.g. a window breaks or a fireman opens a door to the fire compartment, fresh air enters the compartment and mixes with hot gases, thus creating a flammable mixture that might ignite and create a backdraft. In this article, we consider the critical flow approach to solve the classical hydraulic equations of density driven flows in order to determine the gravity controlled inflow in a shipping container full of hot unburnt gases. 1/3 of the container's height is covered by the horizontal opening. For the initial condition, i.e. just before opening the hatch, zero velocity is prescribed everywhere. When the hatch is opened, the incoming air flows down to the container floor and crosses it without meeting any resistance other than normal frictional resistance. The classical way of estimating vent flows in fire safety engineering is to assume that the gases in the fire compartment are either well-mixed or stratified. In this paper, we take a different approach to estimating vent flows, using the critical flow condition and an alternative velocity profile based on experiments. Two flow correction coefficients are considered at the opening, taking into account the uneven distribution of velocity (α) and the effect of mixing and entrainment (C). These semi-analytical results are then compared with CFD simulations performed for the same geometry. Good agreement is found between semi-analytically calculated and numerically obtained flow characteristics, confirming that the quantitative determination of the α and C correction coefficients was reasonably accurate. This also shows that the proposed semi-analytical method can give a good approximation of average velocities and flow rates in gravity currents, for this geometry.

KEY WORDS: critical flow, vent flow, backdraft, gravity currents, CFD.

1. Introduction

This study is a part of a research project which aims at understanding the gravity currents that are important in fire safety engineering, because of their role in transport and mixing of gases and smoke, which can lead to backdraft. When an under-ventilated fire dies from a lack of oxygen, the enclosed room can remain full of hot unburnt gases. If an opening occurs, for example a window breaks or firefighters open a door to the room, fresh oxygen is carried by gravity currents, and mixes with gases. The dilution of gas with oxygen may create a flammable mixture resulting in ignition and a backdraft gas explosion. This phenomenon is very hazardous and dangerous, and has killed many firefighters in the past years.

Many of the studies and observations concern the plunging density current produced as a cold river enters a warmer lake. The density difference makes the cold water sink under the ambient water, and creates an underflow. Pedersen [1] has achieved very complete and detailed works on gravity currents, studying and describing in detail the theory of non-miscible and miscible density driven flows, as well as wind driven and buoyant flow. This theory of density driven flows has been discussed and applied to a gravity wave entering a flat bottom compartment with full opening (Elíasson et al. [2]).

Essential problems such as the state and evolution of the fire or smoke filling and evacuation depend on the flow through the opening to the fire compartment. Kawagoe [3] suggested the first semi-empirical model for vent flow calculation, assuming a ventilation-controlled fire and a “well mixed” condition inside the compartment. Based on the same assumption, Rockett [4] showed that the inflow was mainly dependant on the shape of the opening rather than on the temperatures. However, several studies have found that his model tends to overestimate the actual vent flow, particularly for large openings. Precise descriptions can be found for various shapes of openings, resulting from experiments (Steckler et al. [5], Thomas et al. [6], Babrauskas and Williamson [7]) or from numerical simulations (Chow and Zou [8]).

There are various publications containing formulas for a density driven flow through an opening. The best known is perhaps from Emmons [9], also presented in textbooks such as Karlsson et al. [10] and Drysdale [11]. Traditionally, two different flow situations are considered in vent flow calculations: the well-mixed-case where the enclosure is considered to have a uniform gas temperature over its entire volume, and the stratified case where the enclosure is only partially filled with hot gases, creating a two-zone model with a upper volume with uniformly distributed gases, and a lower layer of ambient temperature. In both cases, the relationship between the velocity profile and the pressure profile through the vent, obtained with the Bernoulli equation, is used to express the velocity as a function of the height, for both inflow and outflow. In the well-mixed case, the mass flow through the vent depends only on the interface height at the opening, which is determined by equating the mass in and out, using the principle of mass conservation. On the other hand, in the stratified case, the mass flow rate depends not only on the interface height but also on the hot layer height in the compartment, leading to a system composed of two unknowns for one equation. The classical approach does consequently not allow an explicit solution in the stratified case, but demands a numerical solution. In this article, we will use a different approach based on the critical flow theory. This theory assumes that the hot fluid flows freely out of the compartment, and consequently passing the obstacle at the top of the vent requires minimum specific energy. This leads to a Froude number equal to one, adding an extra equation to the traditional approach. In the particular case developed in this paper, the results obtained using the critical flow theory are similar to the ones obtained with the traditional approach in the well-mixed case. One of the interesting aspect of using the critical flow theory is that it adds an equation to the traditional approach and therefore allows an explicit solution to the vent flow problem. A short description of the theory of critical flow and its application to vent flow is presented in Appendix at the end of this article.

The inflow also depends on flow coefficients that are due to boundary layer mixing and friction at the interface between the two fluids. Such coefficients have to be extracted from experiments or numerical studies and are often admitted from literature without further research. Fleischmann and McGrattan [12] obtained experimentally a very different velocity profiles (see Fig. 3) than the ones described by the traditional approach, which was confirmed by numerical calculations. This particular velocity profile justifies the particular effort made in this paper to determine the flow coefficients that suit our geometry and boundary conditions. The primary results were adjusted by comparing them with the data from Fleischmann and McGrattan [12], who conducted experimental and numerical analysis of gravity current prior to backdraft..

The semi-analytical description of the flow through the opening is then applied to the experiments carried by Gojkovic [13], who conducted a series of 13 experiments using a

bigger experimental compartment. The results are then compared to a transient numerical simulation using the ANSYS CFX computational fluid dynamics code [14]. In the reported simulations, the Detached Eddy Simulation (DES) approach [15] was used to model flow's turbulent behavior.

The geometry and boundary conditions in this paper follow the experiments carried by Gojkovic [13], who conducted a series of 13 experiments using methane as fuel, giving a detailed picture of the temperature field during the backdraft.

2. Geometry of the backdraft experimental apparatus

The geometry container used for our calculation is a standard shipping container, measuring 5.5x2.2x2.2 m (length x width x height). The container has been modified in several ways to fulfill its purpose as an experimental apparatus. This geometry is shown in Fig. 1. Complete description of the apparatus's geometry and the experiments are reported by Gojkovic [13].

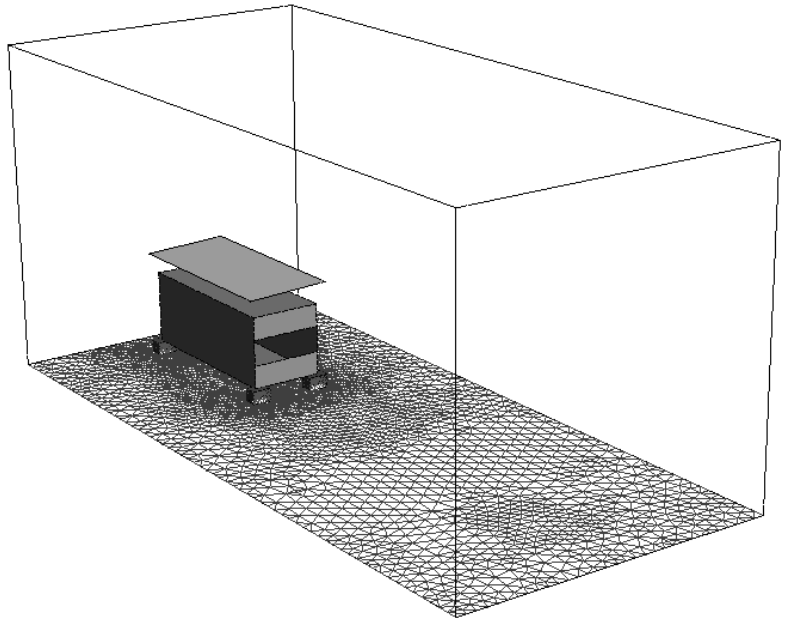

Fig. 1: CFD geometry of the backdraft experimental apparatus (Gojkovic [13])

In this article, we are particularly interested in the shape of the opening. It is vertically centered, 0.8 meters high and 1.90 meters wide.

3. Semi-analytical technique

3.1. Determination of the equations of the inflow and outflow

In order to determine the velocity field at the inflow, we follow the general theory of density driven flows developed by Pedersen [1]. A sketch of the opening is shown in Fig. 2.

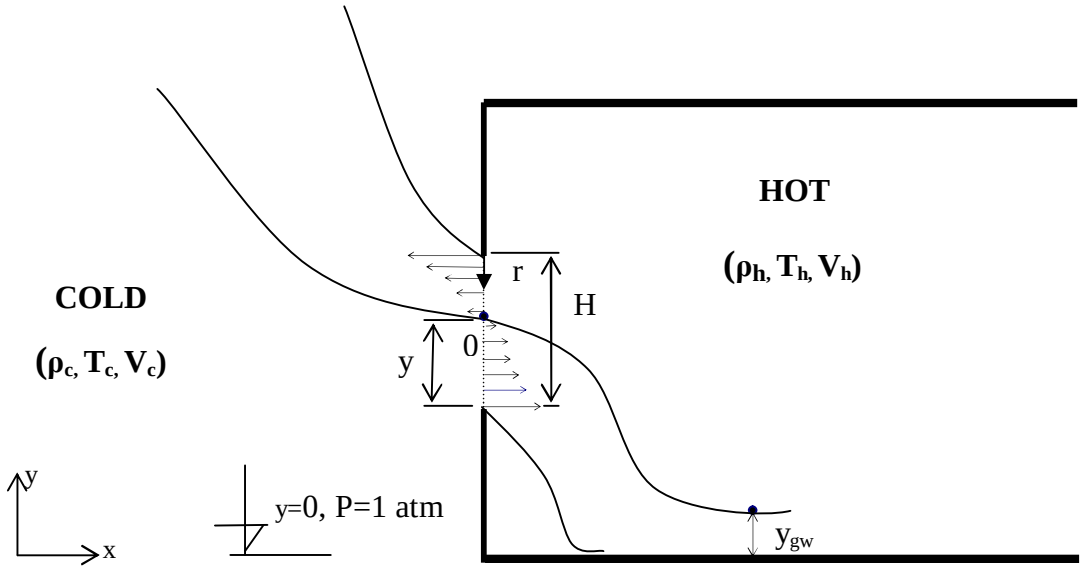

Fig. 2: Sketch of the inflow at the opening of the container

The depth-integrated energy equation for the hot layer in the opening is:

$$E_S = P_0 + \rho_h g y + \frac{1}{2}\alpha_h \rho_h V_h^2 = P_0 + \rho_h g y + \frac{1}{2}\alpha_h \rho_h \frac{q_h^2}{(H-y)^2} \qquad (1)$$

where α is the velocity head factor of classical hydraulics [16] accounting for uneven distribution of velocity in the flow section. This factor equals one when the velocity distribution is even, and it will be discussed in section 3.2.2.

We seek a steady state solution for the velocities V_h and V_c that only depends on the density difference, but not on the initial pressure P_0. In the beginning, just after the opening of the hatch, the flow is indeed influenced by the initial pressure conditions as the velocity fluctuations in Fig. 6 in [12] clearly show. When steady state is obtained, a difference in static pressures between the inside and the outside develops so the inflow and outflow will be equal. This requires critical flow (Eq. 3.1.6 in [1]) in both layers. In a critical section the specific energy has a minimum:

$$\frac{dE_s}{dy} = \frac{dP_0}{dy} + \rho_h g + \alpha_h \rho_h \frac{q_h^2}{(H-y)^3} = 0 \qquad (2)$$

Assuming a constant density ρ_c and hydrostatic pressure distribution in the section of opening where the streamlines are almost horizontal, we will have:

$$\frac{dP_0}{dy} = \frac{d}{dy}(-\rho_c g y) = -\rho_c g \qquad (3)$$

Inserting this in Eq. (2), we have:

$$\alpha_h \rho_h \frac{q_h^2}{(H-y)^3} = (\rho_c - \rho_h) g \qquad (4)$$

This is similar to a critical flow condition in conventional open channel hydraulics [16]. Here, it is necessary to introduce a velocity correction factor C_h. This correction factor would be equal to one for immiscible frictionless flow, but will in reality be somewhat less

than one as mixing slows up the flow. Eq. (5) ensures a densimetric Froude number F_Δ=1, as required for critical flows when C_h=1, which finally leads to:

$$V_h^2 = C_h^2 \frac{\Delta_h g(H-y)}{\alpha_h} \text{ with } \Delta_h = \frac{\rho_c - \rho_h}{\rho_h} \text{ and } q_h = V_h(H-y) \tag{5}$$

Similar considerations for the cold layer result in:

$$V_c^2 = C_C^2 \frac{\Delta_c g y}{\alpha_c} \text{ with } \Delta_c = \frac{\rho_C - \rho_h}{\rho_C} \tag{6}$$

With C_c = 1, when friction and mixing are not taken into account, the densimetric Froude number of the outflow will also be F_Δ = 1.

The C_h and C_c are empirical correction factors, which are functions of the Reynolds number as discussed in [12].

Pedersen [1] explains that the same formulae apply in density driven flows as in conventional open channel flows just by exchanging the acceleration of gravity g with a reduced acceleration of gravity Δg. This is what we will do here, only in our case, we consider two different Δ, Δ_h for the hot layer and Δ_c for the cold layer.

Assuming incompressibility of both flows, the continuity equation leads to $q_h = q_c$, which is equivalent to:

$$\sqrt{\alpha_c}\, y V_c = \sqrt{\alpha_h}\,(H-y)V_h \tag{7}$$

Eq. (7) can be expressed as:

$$\left(\frac{V_h}{V_c}\right)^2 = \left(\frac{y}{H-y}\right)^2 \frac{\alpha_c}{\alpha_h} \tag{8}$$

We can as well combine Eqs (5) and (6):

$$\left(\frac{V_h}{V_c}\right)^2 = \frac{H-y}{y}\frac{\alpha_c \rho_c}{\alpha_h \rho_h} \tag{9}$$

Equalizing the Eqs (8) and (9), we get:

$$\left(\frac{y}{H-y}\right)^3 = \frac{\rho_c}{\rho_h} \tag{10}$$

We finally obtain the depth of the cold layer:

$$y = \frac{H}{1+(\rho_h/\rho_c)^{1/3}} \tag{11}$$

Using Eqs. (5), (6) and (11), the average velocities V_h and V_c can then be expressed as:

$$V_h = C_h \sqrt{\frac{1}{\alpha_h}\Delta_h g\left(1 - \frac{1}{1+(\rho_h/\rho_c)^{1/3}}\right)H} \tag{12}$$

$$V_c = C_c \sqrt{\frac{1}{\alpha_c} \Delta_c g \left(\frac{1}{1+(\rho_h/\rho_c)^{1/3}} \right) H} \qquad (13)$$

The equations (11), (12) and (13), obtained by the critical flow theory, are similar to the ones obtained by Emmons [9] with the traditional approach in the well-mixed case, except for the correction coefficients. These coefficients allow considering the particular shape of the inflow velocity profile, which is very different from the one considered in the traditional approach.

Note that the flow regime described above with critical flow condition for both layers is only valid before the filling of the container has reached a certain level. When the depth of the gravity current y_{gw} approaches the level of the neutral plane, we will reach a different flow regime, with the neutral plane moving up. In this second flow regime, only the upper layer will remain critical, and the lower layer will be sub-critical, with velocity $V_c < V_h$. In this article, we assume that backdraft will occur during the primary flow regime. We will not, therefore, describe the second flow regime in detail.

3. Discussion of the flow situation and the correction factors α and C

The flow correction factors are often included in one general flow coefficient, whose value can be between 0.6 and 0.7 for vents and openings [10]. In this section, we will discuss their physical meaning, the flow situation and try to define realistic value for our geometry.

3.2.1. The flow situation

When inside the container, the inflow falls down to the floor (Fig. 2) and the neutral plane between the hot and the cold air will rise. This will not change the inflow, as changes in back pressure do not change critical flows, until the neutral plane has reached a level sufficiently high to affect the pressure in the critical section in the opening. The inflow will then change to subcritical, slow down and the neutral plane in the opening will rise. The rise can be calculated as the outflow in the hot layer will stay critical.

These calculations will however be difficult. The free fall of the cold air will create quite a splash on the container floor and forced mixing. The mixed air flows across the container through a hydraulic jump [17] with more mixing, splashes on the back wall and is reflected back. All this happens in a matter of seconds and the density of the resulting mixture in the bottom of the container is difficult to determine.

Nevertheless, the volume of cold air inside the container will be known at any time so the position of the effective neutral plane, i.e. the neutral plane position if there was no mixing, can be determined. Using it in the calculations will give the time for the rise of the neutral plane up to the opening. This could be a measure of the maximum time from the opening of the hatch until backdraft sets in.

When subcritical inflow has set in and there is no longer a significant pressure difference between the cold air on the outside and the hot air on the inside, Eq. 1 can be used to find the height of the neutral plane inside the container. If the velocity approaching the opening in the hot layer is small, the distance from the upper edge of the opening to this neutral plane will be equal to 2/3 the depth of the hot layer at the opening (see Appendix). As soon as the neutral plane is in this position, the interface at the opening will rise and the flow discharge will start to diminish.

3.2.2. Significance of the coefficient α

The coefficient α is defined in [16] as the kinetic energy correction factor of conventional hydraulics, due to uneven distribution of velocity in the opening section. With our notations, Eq. (14) in [16] gives:

$$\alpha = \frac{1}{r}\int_{\delta_b}^{y}\left(\frac{V}{V_{av}}\right)^3 dr \qquad (14)$$

In [11], the shape of the velocity profile is similar to potential flow in a 180 degree bend around a wall end. In that situation the velocity obeys V ~ 1/r. (see Section 6 in [18]). We have to relate our velocity profile to the boundary layers that exist in real flows but not in potential flow. We also introduce an empirical constant A. Now, the velocity profile can be modified to $V=A/r+V_{min}$ and this is used as an approximation to the true velocity profile in the opening. A sketch of this profile is shown in Fig. 3. A more precise plot of the velocity profile is shown in [12].

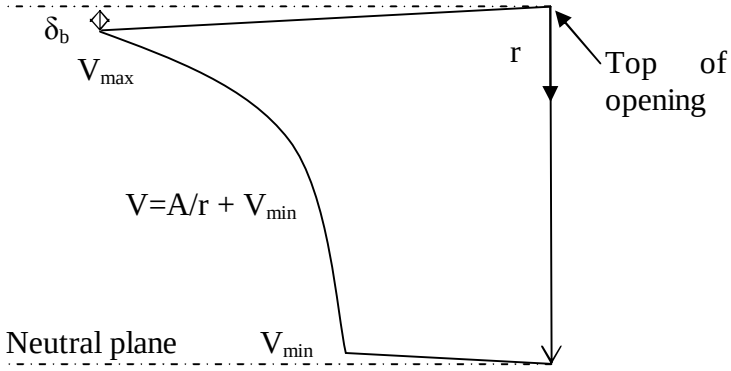

Fig. 3: Details of the shape of the outflow

With the modified potential flow condition, Eq. (14) is:

$$\alpha = \frac{1}{r}\int_{\delta_b}^{y}\left(\frac{V}{V_{av}}\right)^3 dr = \frac{\dfrac{1}{y-\delta_b}\displaystyle\int_{\delta_b}^{y}\frac{A^3}{r^3}dr}{\dfrac{1}{(y-\delta_b)^3}\left(\displaystyle\int_{\delta_b}^{y}\frac{A}{r}dr\right)^3} = \frac{\dfrac{(y-\delta_b)^2}{2}\left(\dfrac{1}{\delta_b^{\,2}}-\dfrac{1}{y^2}\right)}{\left(\ln\left(\dfrac{y}{\delta_b}\right)\right)^3} \qquad (15)$$

Observations of values for y and δ from [12], using Eq. (14), give us as reasonable estimate for the value of α: $\alpha_h = \alpha_c = 1.2$

3.2.3. Significance of the coefficient C

A detailed qualitative description of the mixing in gravity currents was given by Fleishmann and McGrattan [12], for the experiment as well as for the numerical simulation. Their figures show the importance of the mixed region at the interfacial boundary layer, especially near the opening. We see from the figures the influence of the shape of the opening. Namely, the opening that covers 1/3 of the container's height produces gravity currents with much more mixing than the full opening.

We consider the interface between the two layers, where we have the entrainment velocity V_E [1] and the mixed density ρ_{mix}. Details at the interface are shown in Fig. 4.

The continuity equation for the control volume in Fig. 4 gives:

$$\rho_h(V_h(H-y)-V_E l_{i,cv})+\rho_c V_E l_{i,cv}=\rho_{mix} V_h l_{o,cv} \quad (16)$$

$$1+\frac{V_E l_{i,cv}}{V_h(H-y)}\Delta_h=\frac{\rho_{mix}}{\rho_h} \quad (17)$$

$$B\frac{V_E}{V_h}\Delta_h=\Delta_{mix} \text{ with } \Delta_{mix}=\frac{\rho_{mix}-\rho_h}{\rho_h} \quad (18)$$

We can define the "true Δ", denoted by Δ_{true}, which takes into account the mixing. $\Delta_{true}=\Delta_h-\Delta_{mix}$.

The critical densimetric Froude number can be written as:

$$F_\Delta=\frac{V_h}{\sqrt{\Delta_{true} g l_{o,cv}}}=1 \quad (19)$$

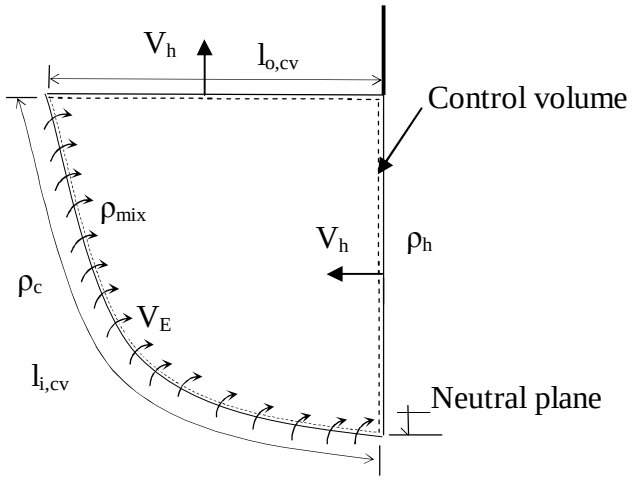

Fig.4: Details of the mixing area at the interface

$$F_\Delta=\frac{V_h}{\sqrt{\Delta_h g(H-y)}}=\sqrt{\frac{l_{o,cv}}{H-y}}\sqrt{(1-\frac{\Delta_{mix}}{\Delta_h})}=C\sqrt{\frac{l_{o,cv}}{H-y}} \quad (20)$$

$$\frac{\Delta_{mix}}{\Delta_h}=B\frac{V_E}{V_h}=1-C^2=Pol(\Delta) \quad (21)$$

Eq. (21) assumes that the relation between the coefficient C and Δ is a polynomial of Δ that approximates the true unknown function [1]. The coefficient is therefore considered to be a polynomial in Δ. We choose to determinate the C coefficient using the results of Fleischmann and McGrattan [12], as their results for physical experiments and numerical simulations are in good agreement. We will use their simulated values for comparison.

However, their results do not show the real average velocities for inflow and outflow, respectively. This is because the position of the velocity probes is fixed and not regulated according to the variations in the depth of the cold layer y as shown by Eq. (11). Therefore, a minor adjustment of the measured average probe velocity values in [12] is needed in order to find the adjusted average velocities in the two layers.

The continuity equation at the opening, considering the simulated average probe velocities and the position of the neutral plane y, must be fulfilled. But with the average probe velocities reported in [12], the following inequality is obtained:

$$V_{Sc}\,y > V_{Sh}\,(H - y) \tag{22}$$

This does not respect the continuity equation. But if a small correction dV is applied to the simulated average probe velocities, the following relations are obtained:

$$(V_{Sc} - dV)\,y = (V_{Sh} + dV)(H - y) \tag{23}$$

$$dV = V_{Sc}\,y - V_{Sh}\,(H - y) \tag{24}$$

We finally have our adjusted average velocities of outflow and inflow, noted $V_{h,adj}$ and $V_{c,adj}$:

$$V_{h,true} = V_{Sh} + dV \tag{25}$$

$$V_{c,true} = V_{Sc} - dV \tag{26}$$

We calculate V_h and V_c using Eqs. (12) and (13) for different values of Δ_h taking into account $\alpha_h = \alpha_c = 1.2$ and H = 0.4 m as in [13]. Fig. 5 shows these calculated values, the simulated values extracted from Fig. 8.b in [12], and the adjusted velocities calculated with Eqs (25) and (26).

The simulated velocities give us the C coefficient, defined as the ratio between the simulated values and the calculated velocity values for the geometry of the experiments described in Fig. 8.b in [12]. The adjusted velocities allow us to calculate the adjusted coefficient $C_{i,adj} = V_{is,adj} / V_i$. These coefficients are shown in Fig. 6. We can note that $C_h \neq C_c$, but $C_{h,adj} = C_{c,adj}$ (the two curves match perfectly). This confirms the necessity to adjust the average probe velocity, so the position of the neutral plane is respected in estimating the real average velocities of inflow and outflow, respectively. The function $1 - C_{i,adj}^2$ is also plotted. The trendline gives us a polynomial function, which confirms the observation from Eq. (21).

Finally, if we apply a power curve fit to $C_{h,adj}$ and $C_{c,adj}$, we obtain the following relation (with max. error = 3.2 %):

$$C_{c,adj} = C_{h,adj} = 0.6641\Delta_h^{-0.1964} \tag{27}$$

This relation will be used in section 5 of this paper, where comparison between Gojkovics's [13] experiments and calculations are made.

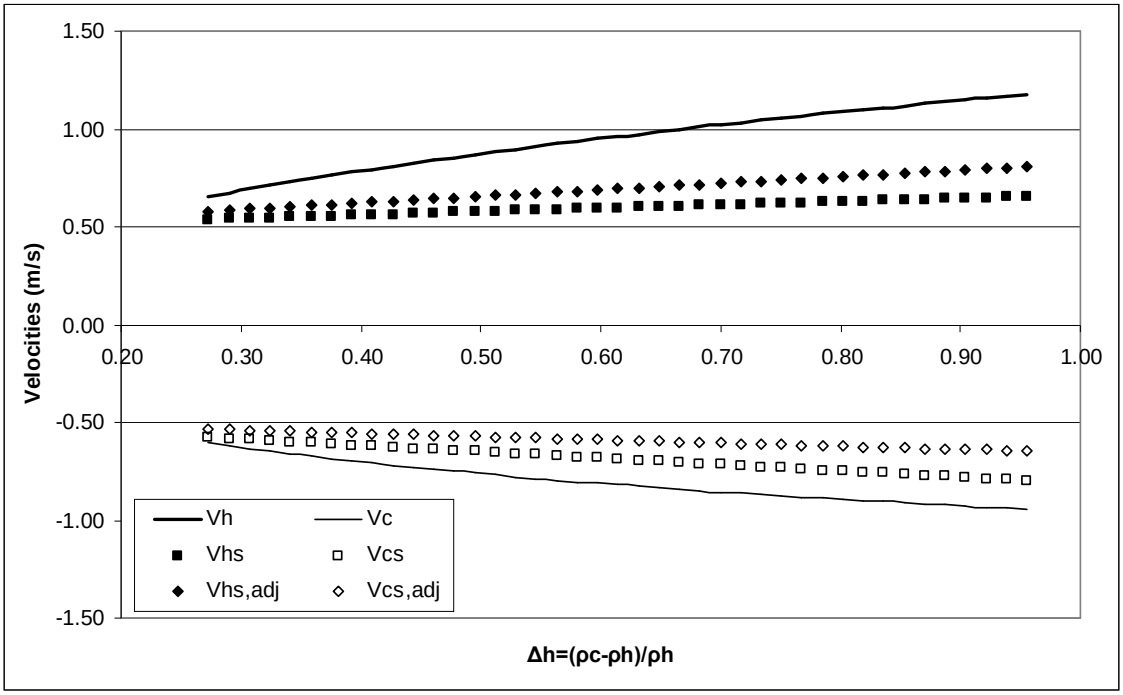

Fig. 5: Average Velocities at the opening for the Fleischmann-McGrattan geometry (height of the opening = 0.4 m); calculated velocities, simulated (V_{hs} and V_{cs}) and adjusted simulated values ($V_{hs,adj}$ and $V_{cs,adj}$)

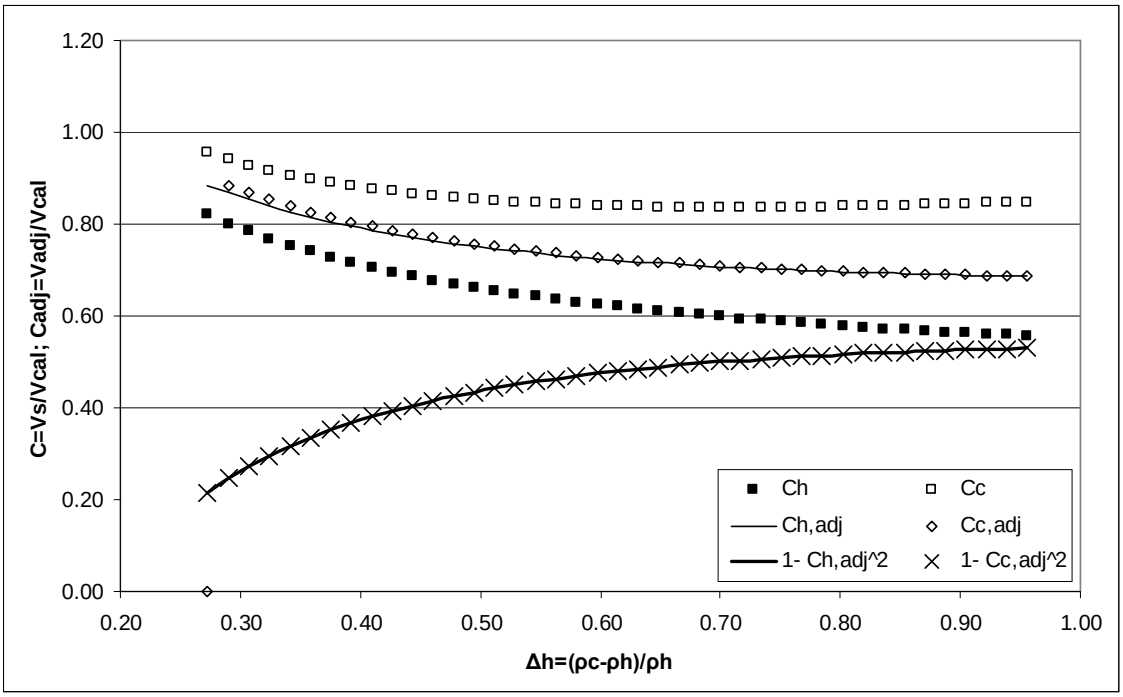

Fig. 6: C correction coefficients, calculated coefficients (C_h and C_c), adjusted coefficients ($C_{h,adj}$ and $C_{c,adj}$), ($1-C^2_{h,adj}$ and $1-C^2_{c,adj}$) functions and their trendlines.

It should be noted that changes in geometry and all external disturbances of the flow will influence the value of correction coefficient C presented in Fig. 6. The coefficient takes into account the gravitational effect of mixing and the retarding effect of the internal fluid friction at the interface. These two effects are also related, because both result from the

fluid entrainment across the neutral plane rather than free boundary shear. The use of one coefficient is therefore not as unrealistic as it might seem. The possibility exists to find this coefficient with CFD simulations and this will be discussed further in the paper.

4. CFD approach

The approach is based on solving a complete set of transport equations in their discretized form. Due to turbulence and changes in material composition, the Favre-averaged form [14] of transport equations has to be used. Beside the mass and the momentum transport equation for the mixture:

$$\partial_t \rho + \partial_j(\rho \bar{v}_j) = 0 \tag{28}$$

$$\partial_t(\rho\bar{v}_i) + \partial_j(\rho\bar{v}_j\bar{v}_i) = -\partial_i\bar{p} + \partial_j\left(\mu(\partial_i\bar{v}_j + \partial_i\bar{v}_i) - \frac{2}{3}\mu(\partial_l\bar{v}_l)\delta_{ji}\right) + g(\rho - \rho_{ref}) - \partial_j(\rho\overline{v_j'v_i'}) \tag{29}$$

the transport equations for the components CH_4, O_2, H_2O and CO_2 are needed:

$$\partial_t\left(\rho\bar{\xi}_c\right) + \partial_j\left(\rho\bar{v}_j\bar{\xi}_c\right) = \partial_j\left(\rho D_c\partial_j\bar{\xi}_c\right) - \partial_j\left(\rho\overline{v_j'\xi_c'}\right) \tag{30}$$

Furthermore, the energy equation was written for the total specific enthalpy:

$$\partial_t\left(\rho\bar{h}_{tot}\right) - \partial_t p + \partial_j\left(\rho\bar{v}_j\bar{h}_{tot}\right) = \partial_j\left(\lambda\partial_j\bar{T}\right) - \partial_j\left(\rho\overline{v_j'h_{tot}'}\right) \tag{31}$$

In the present work, the CFX version of the Detached Eddy Simulation (DES) model [14] was used to model turbulence. Using the Large Eddy Simulation (LES) turbulence model to resolve flow structures in wall boundary layer flows at high Re numbers requires fine grid resolution, which is computationally extremely expensive, and therefore not useful for most industrial flow simulations. The DES model is an attempt to combine elements of RANS and LES formulations into a hybrid formulation, where Menter's Shear Stress Transport (SST) model is used inside attached and mildly separated boundary layers, and the LES model is applied in massively separated regions. To distinguish these two regions, a turbulence length scale, calculated as [19], [20]:

$$l_{RANS} = \frac{\sqrt{k}}{C_\mu\omega} \tag{32}$$

is compared with a length scale associated with the local grid spacing δ and the LES model:

$$l_{LES} = C_{DES}\,\delta \tag{33}$$

The DES model switches from the SST model to the LES model in the regions where the turbulence length scale l_{RANS} is larger than the local LES model scale l_{LES} .

Turbulent viscosity is defined as in the SST model as a ratio between turbulence kinetic energy k and eddy frequency ω:

$$\mu_t = \frac{a_1 k}{\max(a_1\omega, F_2 S)} \tag{34}$$

Turbulence heat and mass fluxes are then calculated as

$$\rho\overline{v_j' h_{tot}'} = -\frac{\mu_t}{Pr_t}\partial_j \bar{h} \quad \text{and} \quad \rho\overline{v_j' \xi'} = -\frac{\mu_t}{Sc_t}\partial_j \bar{\xi} \tag{35}$$

Usually, the molecular mass diffusivity ρD_c is small compare to the turbulence mass diffusivity μ_t/Sc_t and is often unknown.

Initially, the container is filled with a mixture that contains methane, air and combustion products. Gojkovic [13] reported the total amount of methane that was released into the compartment. The fuel inventory was partially reduced due to initial burning, and the resulting composition of the mixture was rich in unburned methane and combustion products with a relatively small amount of oxygen that is unable to support burning. In view of the uncertainties, the following initial content was assumed in the model for all simulated cases:

$$\overline{\Psi}_{CH_4} = 0.22,\ \overline{\Psi}_{CO_2} = 0.02 \tag{36}$$

$$\overline{\Psi}_{H_2O} = 0.04,\ \overline{\Psi}_{O_2} = 0.1196,\ \overline{\Psi}_{N_2} = 0.6004$$

The initial velocity was set to 0.0. Temperature inside the container was varied to obtain a desirable value of Δ_h. Therefore, T_h was 37.5°C for Δ_h = 0.2, 75.0 °C for Δ_h = 0.4, 125.0 °C for Δ_h = 0.6, and 175°C for Δ_h = 0.8.

For the external initial composition, we assumed fresh air:

$$\overline{\Psi}_{CH_4} = 0.0,\ \overline{\Psi}_{O_2} = 0.21,\ \overline{\Psi}_{N_2} = 0.79,\ \overline{\Psi}_{CO_2} = 0.0,\ \overline{\Psi}_{H_2O} = 0.0 \tag{37}$$

and an initial temperature of 5 °C in all cases.

For the simulations' boundary conditions, the no-slip, smooth, adiabatic boundary conditions were set for all walls. At the outermost boundaries of the domain, wall conditions were set at the floor and pressure conditions ('openings') at the remaining boundaries, with an ambient temperature of 5 °C. At openings, flow may enter or leave, depending on the local pressure just inside the boundary.

The ANSYS CFD software [14] was used to set up the gravity current model and to solve the transport equations for mass (28), momentum (29), species (30), total enthalpy (31), turbulence kinetic energy and eddy frequency, with the described initial and boundary conditions.

5. Application to Gojkovic's experimental compartment - comparison between semi-analytical and numerical results

We have, in the previous part, defined the equations of the outflow (5) and inflow (6) at the opening of the container as well as the position of the neutral plane. The equations and flow correction coefficient can be now adapted to the experimental container. Fig. 7 shows the velocities computed semi-analytically, as well as the results of the numerical simulations performed with the ANSYS CFX code. A three-dimensional numerical mesh with 162552 nodes and 862811 elements was generated to perform the numerical analysis. The average mesh spacing inside the enclosure was 5 cm. The initial time step was set to dt=0.005 of the

gravity wave timescale $L/\sqrt{\Delta_h gH}$. Four different cases were simulated with Δ_h = 0.2, 0.4, 0.6 and 0.8, respectively.

Fig. 8 shows the height of the neutral plane for both the semi-analytical and the numerical calculations.

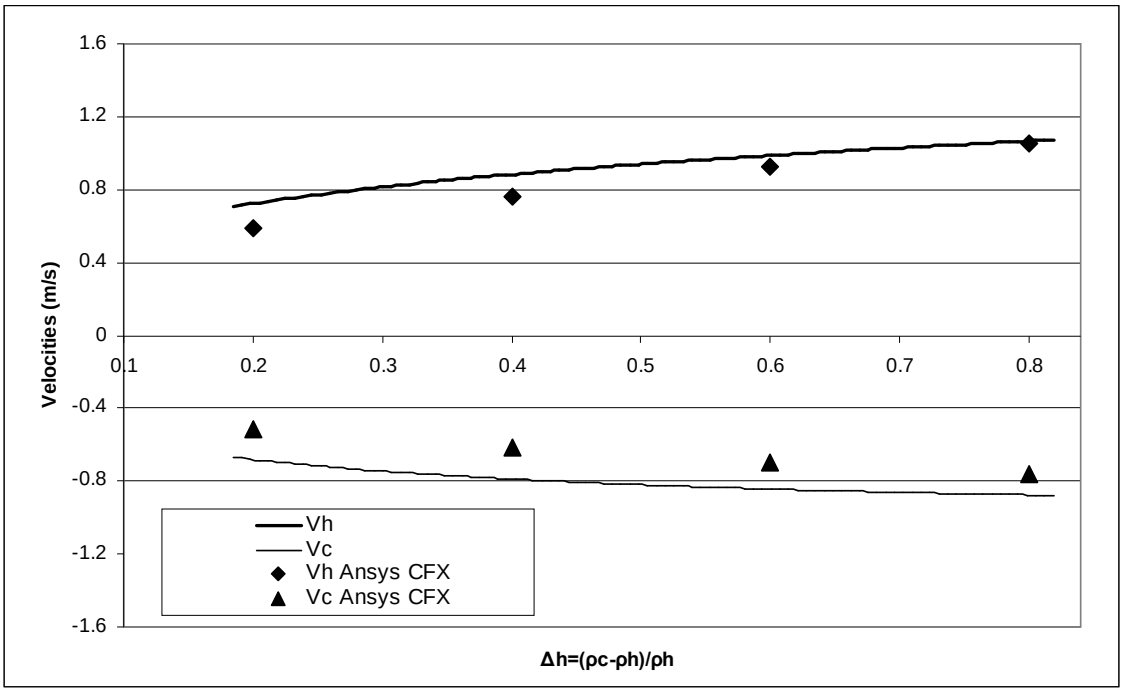

Fig. 7: Average Velocities at the opening for the Gojkovic experimental apparatus (height of the opening =0.8 m)

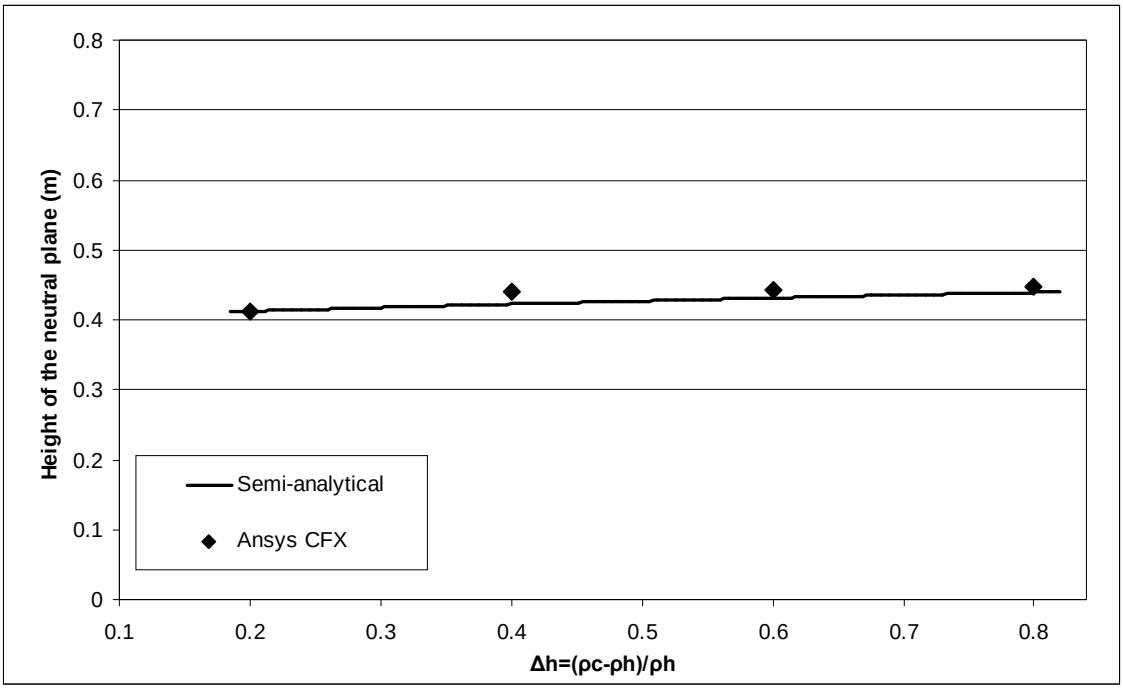

Fig. 8: Height of the neutral plane at the opening for the Gojkovic experimental apparatus (height of the opening = 0.8 m)

Table 1: Flow characteristics at the opening for the Gojkovic experimental apparatus (height of the opening = 0.8); comparison between semi-analytical and numerical results

	Correction Fact		V_h (m/s)		V_c (m/s)		Q (m^3/s)	Q_h (m^3/s)	Q_c (m^3/s)	Y (m)	
Δ_h	α	C	analyt	simul	analyt	simul	analyt	simul	simul	analyt	simul
0.2	1.2	0.905	0.729	0.588	-0.685	-0.518	0.537	0.501	0.469	0.412	0.413
0.4	1.2	0.793	0.884	0.760	-0.790	-0.611	0.634	0.601	-0.591	0.423	0.441
0.6	1.2	0.734	0.987	0.929	-0.844	-0.697	0.691	0.731	-0.677	0.431	0.442
0.8	1.2	0.694	1.065	1.057	-0.876	-0.761	0.731	0.821	-0.747	0.439	0.447

Note that the CFD results are averaged over a time period between 1.2 and 6.8 s after door opening, when the flow is stabilized after the initial phenomena.

Analysis of the results

The comparison given in Fig. 7 and 8, as well as in Table 1, show a good agreement between the semi-analytical and the simulated values when Eq. (27) is used for the correction coefficient. A small change in C causes the semi-analytical results to be within 5 % of the CFD simulation. The correction coefficient for the Gojkovic experiment in the semi-analytic method is therefore:

$$C_{c,adj} = C_{h,adj} = 0.6229\Delta_h^{-0.0741} \tag{38}$$

The semi-analytical results show an increasing height of the neutral plane as a function of the density temperature, whereas in the CFD results the height stays approximately constant. The semi-analytical calculations take into consideration only the conservation of volume and mass. On the other hand, the numerical simulations also capture mixing phenomena in the developing shear layer, and related heat and mass transfer effects.

We can define a difference ratio R for a value X as:

$$R(X) = \left| \frac{X_{analyt} - X_{simul}}{X_{analyt}} \right| \% \tag{39}$$

By considering the values in Table 1, we can calculate the difference for each flow characteristics. The calculated values of difference ratio R are summarized in Table 2.

Table 2: Difference ratio between analytical and simulated flow characteristics at the opening for the Gojkovic experimental apparatus. (height of the opening =0.8)

Δ_h	$R(V_h)$ %	$R(V_c)$ %	$R(Q_h)$ %	$R(Q_c)$ %	R(Y) %
0.2	19.35	24.46	6.77	12.68	0.03
0.4	14.10	22.64	5.26	6.74	4.31
0.6	5.92	17.35	5.75	2.04	2.54

0.8	0.77	13.10	12.43	2.25	1.78

Most of the cases show 5% to 20% difference between the results of the semi-analytical procedure and the CFD simulations when Eq. (27) is used. Moreover, this difference drops to under 5 % when Eq. (38) is used. Eq. (18) shows that the mixing area and entrainment at the interface is inversely proportional to the velocity. It shows that the influence of mixing at the opening increases with smaller velocities. Consequently, the imprecision of the presented semi-analytical approach due to mixing and entrainment is larger at small Δ. This explains why a better match between the semi-analytical and the CFD results is obtained for higher velocities.

The correction factor Eq. (27) is calculated from the results of Fleischmann and McGrattan [12]. A source of inaccuracy in their data comes from positioning of the probes relative to the neutral plane. Specifically, the probes were fixed but the neutral plane varies with Δ. Moreover, once we have determined the correction factors, we use them for a different geometry, which is potentially a source of additional error. The comparison of Eq. (27) and Eq. (38) shows the size of this error.

6. Conclusion

In this article, we discuss a semi-analytical approach, which calculates the characteristics of the steady-state flow created by density difference at the opening of a container full of hot gases. In a stratified case, solving vent flow equations by application of the Bernoulli principle leads to two unknowns, the height of the neutral plane and height of the hot layer, which does not allow an analytical solution of the problem but demands a numerical solution. This new approach, based on the critical flow condition, overcomes this and allows direct calculation of the flow through the vent.

Our goal was to determinate the characteristics of the flow in a container used by Gojkovic [13] to perform backdraft experiments. Therefore, we used the results of two transient analyses, one based on experimental and simulated results for a small container [12], and the other simulating the Gojkovic's backdraft experiments using the ANSYS CFX software.

An essential element in this study is the mixing and entrainment at the interface between the hot and cold layer. This mixing, in a geometry similar to but smaller than the one used by Gojkovic, was particularly well described by Fleischmann and McGrattan [12]. These observations show the necessity to add correction factors to the results obtained by the classical hydraulic equations, taking into account the shape of the opening and the mixing at the interface. Therefore, we used their results to determine the correction factors C and α, and then adapt them to the Gojkovic experiments.

The semi-analytical results are then compared to the CFD results. These comparisons show good agreement between the semi-analytically calculated and the numerically obtained flow characteristics, even if the semi-analytical approach is based on volumetric flow rate (incompressible), whereas the numerical approach considers compressible flows. This confirms the necessity to use the correction factors, although small differences show that improvement could be achieved, especially at smaller velocities where the effect of mixing on the flow is the more important. It also confirms that correction factors calculated for one geometry cannot readily be applied to an other geometry.

The behavior of the gravity wave inside the container under the influence of forced mixing and hydraulic jumps is currently being studied by a number of workers in the field. The results presented in this article, with the description of the opening flow characteristics, are therefore essential for this research project on under-ventilated fires.

Nomenclature

Latin letters

a_1	SST model coefficient, equal to 0.31
A	Empirical constant
B	Empirical constant
C	Velocity correction factor
C_c	Velocity correction factor for the cold layer
C_h	Velocity correction factor for the hot layer
C_{DES}	Turbulence model coefficient, equal to 0.61
C_μ	Turbulence model coefficient, equal to 0.09
$C_{c,adj}$	Adjusted velocity correction factor for the cold layer
$C_{h,adj}$	Adjusted velocity correction factor for the hot layer
$C_{i,adj}$	Adjusted velocity correction factor for the layer i
D_C	Kinematic mass diffusivity
dt	Initial time step
dV	Velocity correction
E_S	Depth integrated energy
F_2	SST model function
F_Δ	Densimetric Froude number
g	Acceleration of gravity
H	Height of the opening
h_{tot}	Total enthalpy
k	Turbulent kinetic energy
L	Length of the container
l	Turbulence length scale
l_{LES}	Turbulence length scale for the Large-Eddy Simulation model
l_{RANS}	Turbulence length scale for the Reynolds Averaged Navier-Stokes model
$l_{i,cv}$	Length of the interface at the control volume
$l_{o,cv}$	Length of the flow out of the control volume
P_0	Pressure at the neutral plane

Pr_t	Turbulent Prandtl number, equal to 0.9
p	Pressure
Q_c	Volumetric flow rate of the cold layer
Q_h	Volumetric flow rate of the hot layer
q_c	Flow rate of the cold layer per unit width
q_h	Flow rate of the hot layer per unit width
R	Difference ratio between analytical and simulated results
Re	Reynolds number
r	Distance to the top of the opening for potential theory
S	Invariant measure of the strain rate
Sc_t	Turbulent Schmidt number, equal to 0.9
T	Temperature
T_c	Temperature of the cold layer
T_h	Temperature of the hot layer
t	Time, time scale
V	Velocity for potential flow profile
V_{av}	Average velocity at the opening
V_c	Average velocity of the cold layer at the opening
V_E	Velocity entrainment at the interface
V_h	Average velocity of the hot layer at the opening
V_i	Average velocity of the layer i at the opening
V_{max}	Maximum velocity for potential flow profile
V_{min}	Minimum velocity for potential flow profile
V_{cs}	Simulated average velocity of the cold layer at the opening
V_{hs}	Simulated average velocity of the hot layer at the opening
V_{is}	Simulated average velocity of the layer i at the opening
$V_{cs,adj}$	Adjusted simulated average velocity of the cold layer at the opening
$V_{hs,adj}$	Adjusted simulated average velocity of the hot layer at the opening
$V_{is,adj}$	Adjusted simulated average velocity of the hot layer i at the opening
$V_{c,true}$	True average velocity of the cold layer at the opening
$V_{h,true}$	True average velocity of the hot layer at the opening
W	Width of the container
W_{op}	Width of the opening
X_{analyt}	Analytical value of a function X
X_{simul}	Simulated value of a function X

x	Spatial coordinate
y	Height of the cold layer at the opening
y_{gw}	Height of the gravity wave

Greek letters

α	Velocity head factor
α_c	Velocity head factor of the cold layer
α_h	Velocity head factor of the hot layer
δ	Grid spacing
δ_b	Thickness of the boundary layer
δ_{ij}	Kronecker delta function
Δ	Dimensionless reduced mass function
Δ_c	Dimensionless reduced mass. $\Delta_c = (\rho_c - \rho_h)/\rho_c$
Δ_h	Dimensionless reduced mass. $\Delta_h = (\rho_c - \rho_h)/\rho_h$
Δ_{mix}	Dimensionless reduced mass. $\Delta_{mix} = (\rho_{mix} - \rho_h)/\rho_h$
Δ_{true}	True dimensionless reduced mass
λ	Wave length, eigenvalues
μ	Dynamic viscosity
μ_t	Eddy viscosity
ν_j	Velocity (component j)
ξ_C	Mass fraction of component c
ρ	Density
ρ_h	Density of the hot layer
ρ_c	Density of the cold layer
ρ_{mix}	Mixed density at the interface
ρ_{ref}	Density at reference state (for CFD model)
Ψ	Volume fraction
ω	Eddy frequency

Symbols

$\bar{}$	Turbulence model time averaged value
$'$	Turbulence model fluctuating component
∂_j	Partial derivative in j-direction

List of references

[1] F.B. Pedersen (1986). “Environmental hydraulics: Stratified flows”. Springer Verlag Editions, Berlin Heidelberg.

[2] J. Elíasson, G. Guigay, B. Karlsson (2008). “Enclosure Fires, Gravity Currents and the Backdraft Problem”. Journal of Fire Sciences, JFS 092116, DOI: 10.1177/0734904108092116. In press.

[3] K. Kawagoe (1958). ‘‘Fire Behaviour in Rooms,’’ Report No. 27, Building Research Institute, Japan, pp. 1–72.

[4] J. Rockett (1976). “Fire Induced Gas Flow in an Enclosure” Comb. Sci. Tech., Vol. 12, pp. 165–175 .

[5] K.D. Steckler, J.G. Quintiere, W.J. Rinkinen (1982). “Flow induced by fire in a compartment”. US Department of Commerce, NBSIR 82-2520.

[6] P.H. Thomas, A.J.M. Heselden, M. Law (1967). ‘‘Fully-developed Compartment Fires –Two Kinds of Behaviour’’, Fire Research Technical Paper No. 18, Ministry of Technology and Fire Offices’ Committee, Joint Fire Research Organisation, HMSO, UK, pp. 2–5.

[7] V. Babrauskas, R.B.Williamson (1978). “Post-Flashover Compartment Fires: Basis of a Theoretical Model”. Fire and Materials, Vol. 2, No. 2, pp. 39–53.

[8] W.K Chow, G.W. Zou (2004). “Correlation equations on fire-induced air flow rate through doorway derived by large eddy simulation”. Building and Environment, 40 (2005)897-906.

[9] H. W. Emmons (1995). “Vent Flows”. The SFPE Handbook of Fire Protection Engineering, Section 2 Chapter 5, 2nd Edition.

[10] B. Karlsson, J. G. Quintiere (1986). “Enclosure Fire Dynamics”. CRC press.

[11] D. Drysdale (1998). “An Introduction to Fire Dynamics”, 2nd Edition, John Wiley and Sons, Chichester.

[12] C.M. Fleischmann, K.B. McGrattan (1999). “Numerical and experimental gravity currents related to backdrafts”. Fire Safety Journal, vol. 33, pp. 21-34.

[13] D. Gojkovic (2000). “Initial backdraft experiments”. Department of Fire Safety Engineering, Lund University, Sweden.

[14] ANSYS CFX, http://www.ansys.com/products/cfx.asp and online documentation, http://www-waterloo.ansys.com/community/

[15] F. R. Menter, M. Kuntz. “Development and application of a zonal DES turbulence model for CFX-5”, CFX-Validation report, CFX-VAL17/0503.

[16] J.J. Titus (1995). “Hydraulics”, The SFPE Handbook of Fire Protection Engineering, Section 4, Chapter 2, 2nd Edition.

[17] White (1999). “Fluid Mechanics”, 4th Ed., WCB McGraw-Hill.

[18] R.M Olson, S.J Wright (1990). “Essential of engineering fluid mechanics”, 5th Ed., Harper and Row Publishers Inc., New York.

[19] F.R. Menter (1994). "Two-equation eddy-viscosity turbulence models for engineering applications", AIAA Journal, Vol. 32, No. 8.

[20] F.R. Menter, M.Kunz & R.Langtry (2003). "Ten Years of Industrial Experience with the SST Turbulence Model", in "Turbulence, Heat and Mass Transfer 4", Ed. K. Hanjalic, Y. Nagano & M. Tummers, Begell House.

Appendix 1: Application of critical flow conditions to vent flow

Generality on specific energy and critical flow

The concept of specific energy and critical flow has been developed to study open channel flow [16]. The specific energy of a channel flow of depth y is:

$$E = y + \frac{V^2}{2g} \tag{A1}$$

In the case of a rectangular channel, considering the discharge per unit width q = Q/b = V.y, the specific energy is:

$$E = y + \frac{q^2}{2gy^2} \tag{A2}$$

This energy is minimum for dE/dy = 0, referred as the critical flow condition, and the corresponding depth called the critical depth y_{cr}.

$$\frac{dE}{dy} = 0 = 1 - \frac{q^2}{gy_{cr}^3} \tag{A3}$$

$$y_{cr} = \left(\frac{q^2}{g}\right)^{\frac{1}{3}} \tag{A4}$$

$$q^2 = gy_{cr}^3 = (gy_{cr})y_{cr}^2 = V_{cr}^2 y_{cr}^2 \tag{A5}$$

The former equation can finally be expressed as the Froude number:

$$Fr = \frac{V_c}{\sqrt{gy_{cr}}} = 1 \tag{A6}$$

The evolution of the specific energy is shown on Fig. A1.

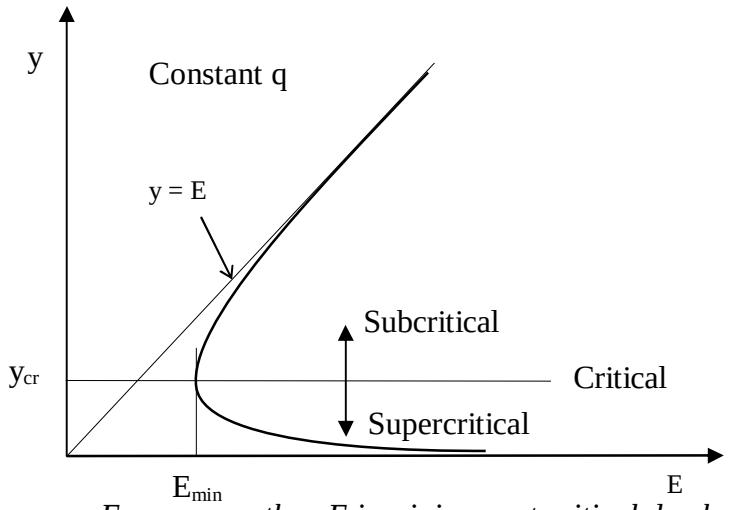

Fig. A1: Specific energy E versus aepth y. E is minimum at critical depth y_c

For $E < E_{min}$, there are no solutions, and thus such a flow is physically impossible.

For $E < E_{min}$, there are 2 possible solutions:

- Subcritical flow at large depth with $V < V_c$. In this case, $Fr < 1$.
- Supercritical flow at small depth with $V > V_c$. In this case, $Fr > 1$.

For $E = E_{min}$, the flow is critical and $Fr = 1$. This corresponds to an equilibrium state where the flow requires minimum specific energy to pass over an obstacle.

Application to density driven flows in Fire Safety Engineering

A vent flow though an opening into a fire compartment or gravity waves are density driven flows. This problem has been studied extensively by Pedersen [1], where he demonstrates that the conventional equations of open channel flow can be applied to density driven flow, by exchanging the acceleration of gravity g with a reduced acceleration of gravity Δg. Δ is called the dimensionless reduced mass defined as: $\Delta_c = (\rho_c - \rho_h)/\rho_c$.

The densimetric Froude number characterizing a density driven flow is therefore:

$$Fr_\Delta = \frac{V}{\sqrt{\Delta g y}} \qquad \text{(A7)}$$

This obeys the same rules for critical flow in open channel described above.The concept of reduced acceleration of gravity and its application to gravity wave in potential backdraft condition is described and discussed in [2].

The densimetric Froude approach is particularly interesting to describe the flow through a vent opening. In Fire Safety Engineering, the most widely used calculation methods are based on the Bernoulli equation of the flow ([9], [10]). In these textbooks, there are a few references to literature in hydraulic science, but since they have appeared there has been import progress in hydrodynamics and hydraulics, especially in stratified flows that has not found its way into vent flow formulas available to Fire Safety Engineers. In well-mixed case,

the inflows and outflows can be calculated using only the Bernoulli approach. In stratified flows, this approach leads to two unknowns, the height at the interface and the depth of the hot layer inside the compartment, which does not allow an analytical solution. This problem is solved by applying the critical flow condition.

Well mixed case

The following Eq. ((A8) and (A9) are presented widely in the literature, and correspond for example to Eq. (5.18) and (5.19) in [10]. The mass flow of the hot and cold fluid are integrated over y_h and (H- y_h) respectively.

$$q_h = \frac{2}{3} C_d \sqrt{\frac{2g\Delta_h}{\alpha}} y_h^{\frac{3}{2}} \qquad \text{(A8)}$$

$$q_c = \frac{2}{3} C_d \sqrt{\frac{2g\Delta_h}{\alpha}} y_c^{\frac{3}{2}} = \frac{2}{3} C_d \sqrt{\frac{2g\Delta_h}{\alpha}} (H - y_h)^{\frac{3}{2}} \qquad \text{(A9)}$$

Where C_d is a flow correction factor between 0.6 and 0.7. α is added to consider the uneven distribution of velocities.

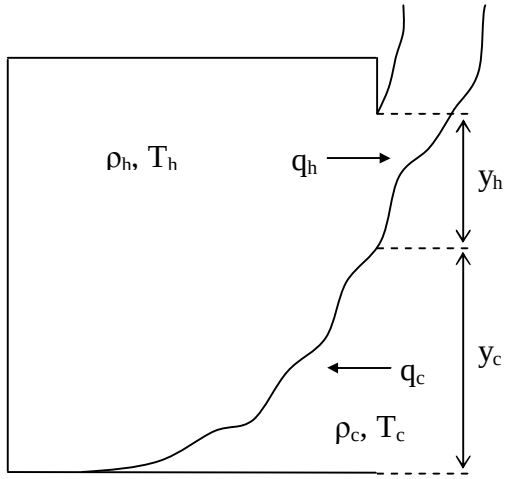

Fig. A2: Sketch of the flow through a compartment vent in the well-mixed case

The height of the interface is determined by considering the conservation of mass and thus equalizing the mass flow rates in and out. The flow rates can then be calculated.

Stratified flows

In stratified flows, there is formation of a hot layer under the ceiling. The problem arises because the height of the neutral plane is different from the height of this hot layer, with a mixed zone between the layers, thus adding and extra unknown to the set of Eq. (A8) and (A9).

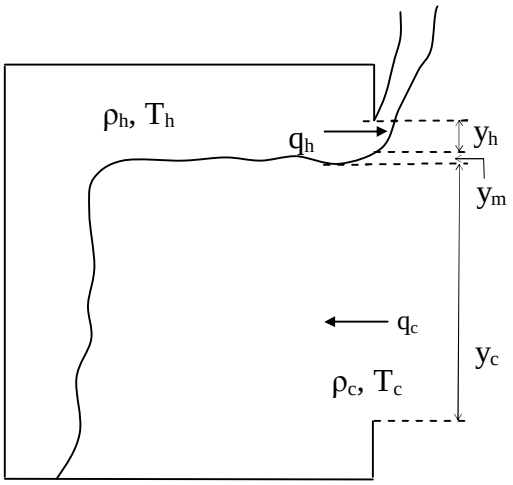

Fig. A3: Sketch of the flow through a compartment vent in the stratified case

Applying the theory of critical can overcome this problem. The hot fluid flows freely out of the compartment, pushed by the gravity difference. Passing the obstacle at the top of the vent requires minimum specific energy. The depth of the hot layer is consequently critical at the opening and the critical Froude number is:

$$Fr_{\Delta} = \frac{V_{cr}}{\sqrt{\frac{\Delta g y_{cr}}{\alpha}}} = \frac{V_h}{\sqrt{\frac{\Delta g y_h}{\alpha}}} = 1 \qquad \text{(A10)}$$

When the y_{mix} is relatively small compared to the total height of the hot zone $h = y_h + y_{mix}$ we have $h - y_h = y_h/2$ and we can calculate the flow in terms of h.

This gives the following flow rate:

$$q_h = C_Q y_h \sqrt{\frac{\Delta_h g y_h}{\alpha}} = C_Q \frac{2}{3} h \sqrt{\frac{2}{3}} \sqrt{\frac{\Delta_h g h}{\alpha}} = C_Q h \sqrt{\frac{8}{27}} \sqrt{\frac{\Delta_h g h}{\alpha}} \qquad \text{(A11)}$$

The coefficient C_q is generally between 0.9 to 0.94. A complete discussion about loss coefficients for different flows is in [15].

Paper [E]

Numerical and Simple Engineering Approach to the Determination of Combustion Products in Strongly Under-ventilated Fires Prior to Backdraft

Presented at the First Workshop on Fires in Enclosures, Jordanstown, Ulster, May 2006.

Georges Guigay[a], Björn Karlsson[b], Jónas Elíasson[a]

AFFILIATIONS:

a- Civil and Environmental Department, Faculty of Engineering, University of Iceland, Reykjavik, Iceland

b- Iceland Fire Authority, Reykjavik, Iceland

CORRESPONDING AUTHOR: Georges Guigay

Tel: 00 354 525 5882

Fax: 00 354 525 4632

E-mail: gjg3@hi.is

Abstract

The work described in the paper aims at determining the gas composition in the case of a strongly underventilated fire, when the flame is dying from lack of oxygen. This is important as the amount of dangerous gases produced by a fire is directly related to the incompleteness of the combustion.

This study is based on experimental results from backdraft studies in reduced scale and real-scale poorly ventilated compartment conditions. Results from computer simulations and analytical calculations are compared to the experimental results and observations. The reliability of gas measurements in the experiments causes some problems, so does the inaccuracy in the flame extinction routine in the numerical model and the simplifications made in the analytical calculation, especially concerning carbon monoxide. The results of the comparisons are found useful to evaluate the performance of the different methods to describe the combustion products due to strongly underventilated fires, as well as the flame behavior in its transition from full burning conditions to partial or total quenching.

1. Introduction

The University of Iceland and the Iceland Fire Authority have been participating in the European network project Firenet [1], dedicated to the study of underventilated fires, and focusing especially on backdrafts. When an underventilated fire is extinguished due to lack of oxygen, the enclosed room can remain full of hot unburnt gases. If an opening occurs, for example when a window breaks or firefighters enter the room, fresh oxygen is carried into the room by gravity currents, and mixes with gases. This creates the flammable mixture, as, by dilution with oxygen, the gas may reach its flammability limit, often resulting in ignition and backdraft. This phenomenon is very hazardous, and has caused the deaths of many firefighters in past years [2].

In order to mitigate the danger of backdraft, it is essential to determinate the key mechanisms leading to its occurrence, and therefore study in detail the conditions prior to the explosion itself. To this purpose, special efforts have been dedicated to the study of the hydrodynamics of the phenomenon, i.e describing the gravity currents analytically and by mean of computer simulations, especially the behavior and velocity of the gravity wave ([3], [4], [5], [6]). We are now focusing on the gas composition in the compartment before the opening occurs, as experiments have shown that the mass fraction of unburnt fuel may be one of the key parameters in the occurrence of backdraft.

The determination of the gas composition in compartments raged by an underventilated fire is essential in Fire Safety Engineering, as most of the casualties in fire are due to CO inhalation. The incompleteness of the combustion, and by consequence the amount of CO produced, is directly related to the amount of oxygen available. Well ventilated fires have been widely studied in enclosures where enough oxygen is available for combustion ([7], [8]). In most cases, fires leading to backdraft occur in very tight compartments, and become by consequence heavily underventilated very quickly. Little data is available for such fires, and describing the extinction due to exhaustion of oxygen is still a challenge for computer models, for various reasons.

In this article, observations from experiments studying the effect of ventilation on the behavior of the fire and production of combustion gases in various stages of ventilation, from well [9] to poorly ([10], [11], [12]) ventilated compartments are used. In the same way backdraft experiments ([13], [14], [15], [16], [17]) we will also be studied. These observations will be analyzed in order to achieve the following goals:

- Find the key parameters in the occurrence of backdraft.
- Find some solutions to improve the CFD models, especially their performance during transition from well to under-ventilated fires and flame extinction by oxygen exhaustion. Modifications are applied to a basic model, to obtain a new model where fire behavior is physically more correct and fits with the experimental results.
- Create an analytical model that calculates the gas composition in a compartment. This typical engineering approach is very useful when a simple and fast estimation is needed, and can be an excellent complement to complex CFD models.

In order to achieve these goals, the study can be divided in the following different steps:

The first step of the study is to identify in the literature the problems due to lack of oxygen in compartment fires and find experimental observation describing the behavior of the fire. This will be used to improve the different models at the third step.

The second step is to create 2 basic tools. The first tool is a CFD model using Fire Dynamic Simulator (FDS) [18]. The second tool one is an analytical model using an engineering approach based on combustion equations.

The third step is the improvement of the models. For the CFD model, comparisons with experimental observations show that two improvements are necessary to solve problems due to unrealistically low oxygen concentration. For the analytical model, assumptions are made to split the fire behavior in 3 different phases, well ventilated, under ventilated and concentration built-up phase.

Results from these improved models are then compared to experimental results, and their combination allows a rough estimation method of probability of backdraft.

2. Problem description

2.1. Observation from former studies

From the literature, observations are extracted that will be used during this study to point out the weaknesses of the primary tools, find some improvement possibilities and finally check that the improved tools give physically reasonable results.

2.1.1. From poorly ventilated fires:

- Obs 1: Heat Release Rate is irregular ([9], [10]):

There is a first short phase were the Heat Release Rate (HRR) is similar to the rate in free atmosphere. Then starts a peak where the HRR increases significantly (About 50 % in [9]), corresponding to the moment of appearance of vitiated air (yield of O2 decreases and CO2 increases). After a few seconds, the HRR drops suddenly, due to lack of oxygen.

- Obs 2: The flame is “crawling” for oxygen ([11], [12], [13]):

Depending on the ventilation and combustion regime, the fame might be ghosting (lifting off the liquid fuel and floating aimlessly away from the surface) or oscillating (flame shrinking to extinction, but cycling back to its original size). When oxygen is really

lacking, the flame might burn at the vent, where the fire seems to be “crawling for oxygen” before extinction.

2.1.2. Strongly underventilated fires (backdraft):

- Obs 3: The hot layer interface, calculated using the idealized 2-zones approximations [19], is situated slightly above the burner surface ([14], [15]).
- Obs 4: The flame is completely extinguished after a certain time, depending on the available amount of oxygen. This is observed for every backdraft study ([14], [15], [16]). Moreover, there is a Limiting Oxygen Index, noted LOI, concentration level under which methane can not burn (about 15 mol %).
- Obs 5: The mass fraction of unburnt fuel is a key parameter [14] (8.5% for slot opening half way up the wall).

2.2. Description of the experiments

The experiments that are chosen for simulation and comparison are from Fleischmann and McGrattan [15]. This is a series of 17 experiments using methane (2 different burner flow rates, 70 and 200 kW). The reason of this choice is that the document presents the complete temperature and combustion products concentration history for all the duration of the experiments.

2.2.1. Experimental set-up:

- Compartment size: (LxWxH): 2.4x1.2x1.2 m.
- Burner size: 0.3 m square and 0.3 m high, placed against the back wall.
- Species concentration: Oxygen (O2), carbon dioxide (CO2), carbon monoxide CO and hydrocarbons (HC) are recorded continuously with stainless probes, located at 0.6 m from opening wall, 0.2 m from ceiling, and 0.6 m from the side wall.
- Temperatures: A thermocouple tree was placed 0.6 m form the opening wall and 0.2 meters from the side wall (relief panel), 10 thermocouples are located at 0.10 m intervals, with the highest at 0.15 m form the ceiling.

In these experiments, the methane flow was still left on after the flame is extinguished form lack of oxygen, and shut down 5 seconds before the hatch opening. Complete details on the geometry and the procedure are given in [14].

3. The CFD model

The size of the compartment is the same as the experimental set-up, except that symmetry of flow is assumed because of the symmetry of the geometry (with the assumption that there is no effect form the gas panel). Several meshes have been tested. In this case, the mesh resolution is 4 cm (60x30x30).

The dimensions, considering the symmetry, are:

- Compartment: (LxWxH): 2.4x0.61.2 m
- Burner: (LxWxH): 0.16x0.14x0.3 m.
- Temperature: Thermocouple tree placed as in the experiments, but with 15 thermocouples placed every 0.08 meters. The reason for having more thermocouples than in the experiments is to have them regularly placed and fitting the mesh size. These temperature values will be averaged into 2 zones, so having more thermocouples improves the precision.
- Gas measurements: The sensor is placed as in the experiments, except that measurements are made at several heights close to the experimental sensors and then values are then averaged. There is an exception concerning the oxygen measurements, where it is measured and averaged on the entire height. This is to correct the uneven distribution of fresh oxygen entering through leakages.

The experimental set-up and the corresponding CFD geometry are shown in Fig. 1.

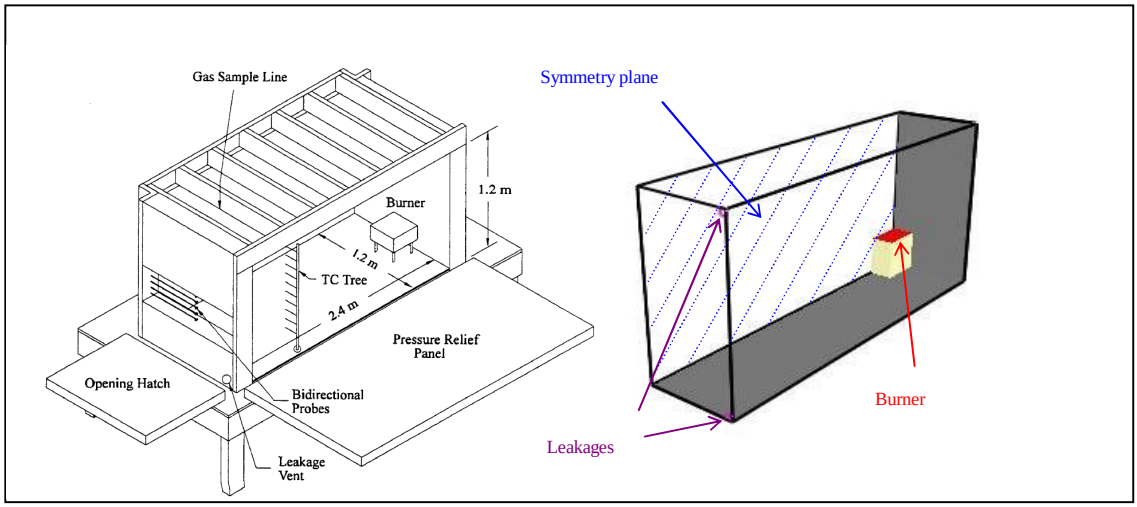

Fig. 1: Experimental set-up (Fleischmann et al [15]) and corresponding model

3.1. Runs in the FDS models, M0 – M2

In this section of the paper, we shall give a step by step description of the modification of the model, from the basic to the improved model. Results are compared with experimental observations described previously, which gives clues for improvements. A new model is built, and so on. Several trial runs were made with variations of grid size, radiation model etc. before the final setup was selected, resulting from 2 major improvements.

3.1.1. Basic model M0

The results from this model 1 are shown with thin green lines with symbols on Fig. 2 (O2 concentration) and Fig. 3 (HRR). Two problems are identified:

- The oxygen concentration reaches very small values, meaning that combustion continues well below the Limiting Oxygen Index LOI, which doesn't compare with Obs 4.

- The Heat Release Rate is regular during the fully developed phase, which doesn't compare with observation Obs 1.

The improvement needed is to keep a minimum of oxygen supply, by introducing leakages. In reality, even a very tight compartment will not be 100% sealed, which justifies this improvement [20].

3.1.2. Improvement step 1: Model M1

This improvement is the FDS model with 4x4 cm holes at the corners of the front wall (as indicated in Fig. 1). Leakages are placed at the corner to simulate as well as possible leakages all along the wall connections, and keeping them as small as the mesh allows it to. The results are the red dotted lines on Fig. 2 and 3.

- The oxygen concentration is improved, but still reaches very low values.
- The HRR is irregular with a peak at roughly 50% from the value after ignition, which agrees well with Obs 1. Nevertheless, the flame keeps quenching, and the fire is then never completely extinguished, which disagrees with Obs 4

Studying the results show that introducing leakages definitely brings some improvements, but shows the necessity to force the combustion extinction.

3.1.3. Improvement step 2: Model M2

The model M2 is the FDS model with leakages and forced extinction. The extinction criterion is described later in this section. The results are the blue bold line on Fig.2 and 3.

The oxygen concentration level is definitively improved, as there is always a minimum of oxygen slowly increasing after extinction. Note that the minimum O_2 value (approx. 0.03) is well above the LOI, but these values are averaged on every cell of the compartment, and the concentration of oxygen will definitely be higher near the burner, as will be shown later in this article.

The HHR compares well with Obs 1 and with the peak discussed in model M1, and the flame is completely extinguished after a while (no endless flame quenching seen with model M1), which agrees with Obs 4.

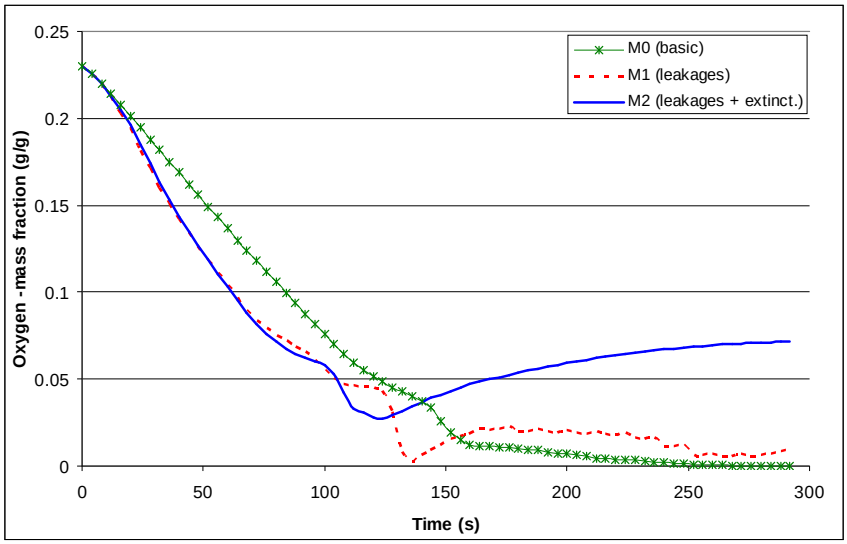

Fig. 2: Oxygen mass fraction for the 3 different FDS models M0, M1 and M2

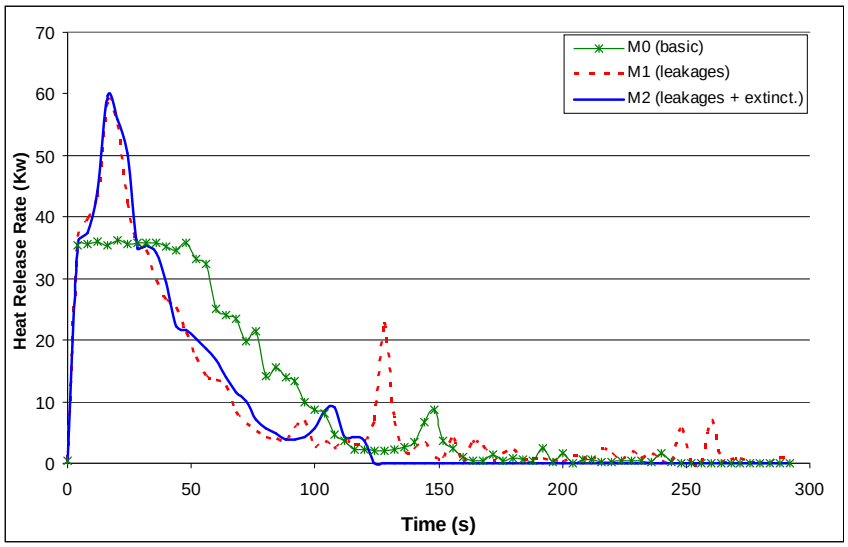

Fig. 3: Heat Release Rate for the 3 different FDS models M0, M1 and M2

3.1.4. The extinction criterion

This extinction criterion has been developed in order to force the fire to extinguish completely, as observed in most backdraft experiments. The O2 concentration is measured at various points very close to the burner surface with the FDS model M1. The assumption is made that fire extinguishes when the oxygen concentration at these measurement points reaches the LOI. This is shown in Fig. 4, for Run 1 (HRR=70 Kw) and 13 (HRR=200 Kw). The intersection of O2 concentration and the LOI gives the extinction time (see Fig. 4):

t_{ext} = 127 sec. for HRR = 70 Kw.

t_{ext} = 36 sec. for HRR = 200 Kw.

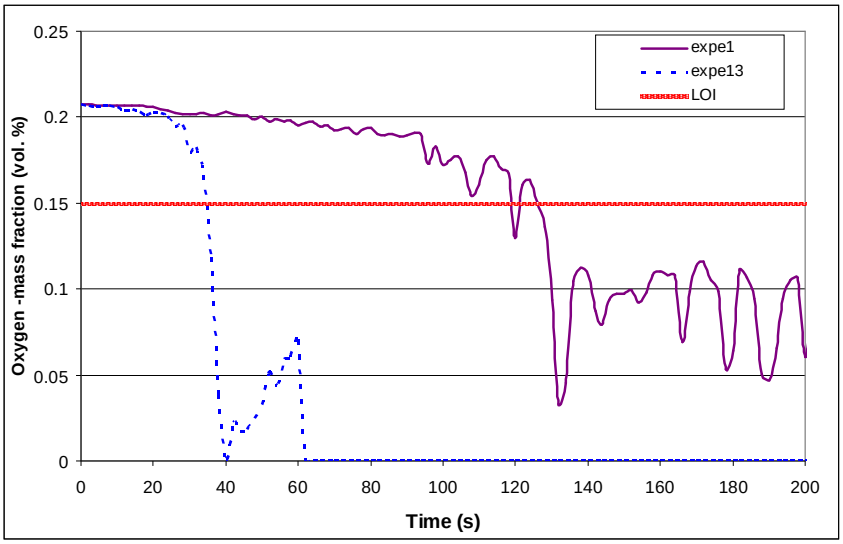

Fig. 4: Extinction criterion for experiment 1 (HRR = 70Kw) and experiment 13 (HRR = 200 Kw). The intersection with the O2 Limiting Index (LOI) line gives the extinction time

In CFD model M2, the combustion is shut down manually (by stopping the calculation and restarting after setting the LOI to a value higher than 0.21, oxygen concentration in air, which forbids combustion) at the extinction time. This extinction time depends on the HHR. This extinction criterion is a fairly crude assumption, but still fulfills the extinction requirement, and gives some indications for future improvements.

3.2. Qualitative results

In this section, we carry out a quantitative study of results from the improved model M1, described previously. We check that the modified model compares with experimental observations and physical behavior. Here, we show the oxygen concentration, as well as the velocity, the temperature and the HHR fields.

3.2.1. Oxygen concentration

The following Fig. 5-a to-5.d show slides of the oxygen concentration for Run1 (HRR=70kW, tend=295 s), at different time steps of interest. We observe a typical 2 zone behavior (5-a), with the oxygen concentrated in the lower zone, flowing towards to the burner. This 2 zone behavior is suddenly broken (5-b and 5-c), with a mixing between the 2 layers that last only a few seconds, then the 2 zones are recreated (5-d).

This sudden mixing happens approximately 10 seconds after complete extinction. Before extinction, the upper layer is much warmer, creating, by density difference, the 2 separate zones. When the fire extinguishes, cold methane is still flowing in through the gas burner surface, cooling the upper zone until almost equilibrium on densities is reached, so that the upper layer drops suddenly, and mixes with the lower layer (5-b and 5-c). The 2 zone behavior is then recreated by oxygen build-up through the leakages.

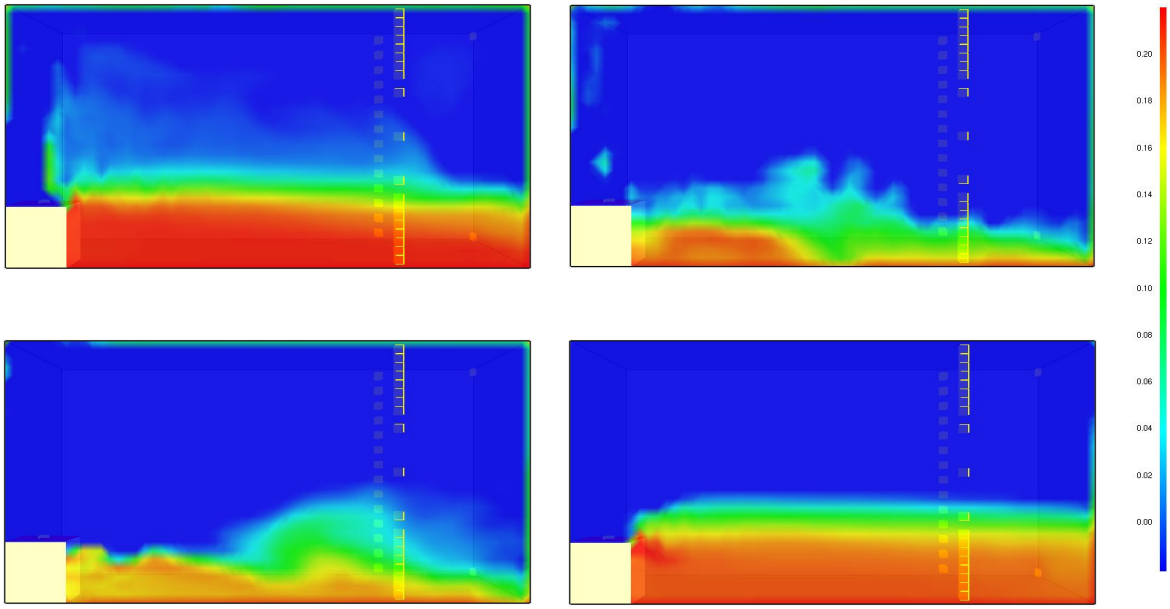

Fig. 5-a to 5-d: Oxygen concentration for run 1(HRR = 70Kw, t=295 s) after 80 s (5-a, up left), 126 s (5-b, up right), 136 s (5-c, down left) and 260 s (5-d, down right left)

3.2.2. Velocity vectors and temperatures

Fig. 6-a and b show that the upper layer is composed of an upper flow field near the ceiling, a recirculation closed to the front wall, and then a middle flow in the direction of the burner.

The lower layer is composed of a cold flow in the direction of the burner. When the fire starts decaying, the upper layer begins to cool, and start to lower, as the density difference decreases with the temperature.

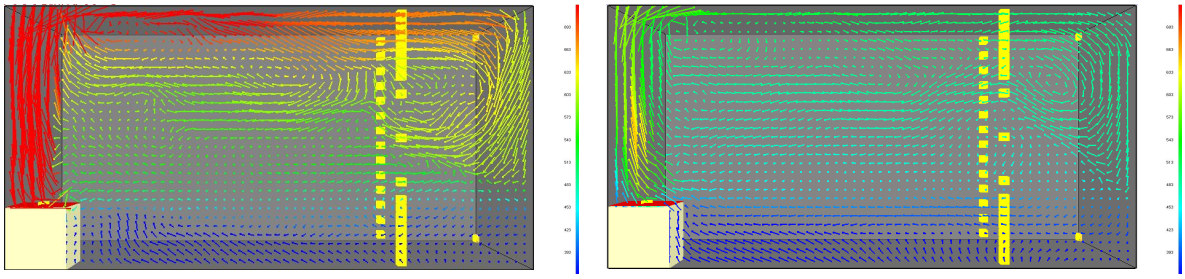

Fig. 6-a and 6-b: vectors colored by temperatures after 50 s (6-a, left) and 80 s (6-b, right)

3.2.3. HRR and temperatures

Fig. 7-a and 7-b show the temperature and the Heat Release Rate respectively a few seconds before extinction. At this moment, the fire becomes strongly underventilated, and there is clearly some spreading over the lower layer, in the direction of the leakages, where there is more oxygen. The fire seems to be “crawling for oxygen”, which fits with experimental observation.

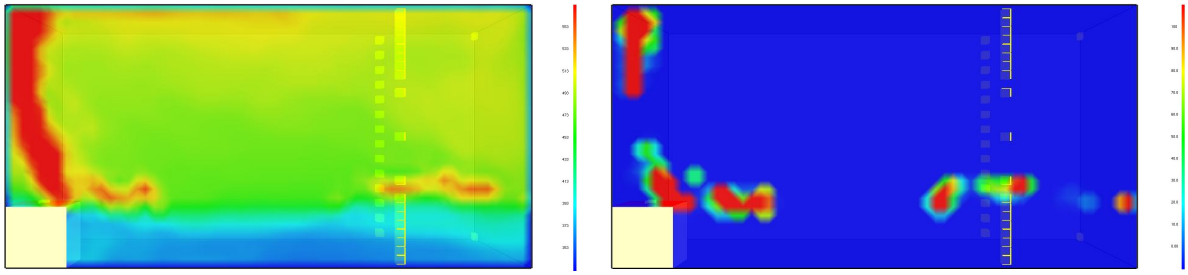

Fig. 7-a and 7-b: Temperature (6-a, left) and HRR (6-b, right) after 98 s

3.3. Quantitative results

In the previous qualitative study, it was shown that the improved FDS model (model M2), with introduction of leakages and forced extinction improved the physical behavior of the fire. In this section, we will compare results of the improved models against experimental data, by studying temperature fields and combustion products.

3.3.1. Temperature fields

The following temperature histories are calculated from the time dependent temperature profiles recorded from the thermocouple tree. The profiles were converted into the average upper and lower layer temperatures using Quintiere´s method [19] applied to steady state temperature profiles.

$$\int_0^{h_L} \left(\frac{1}{T}\right) dx = \frac{h_{comp} - h_L}{T_{UL}} + \frac{h_L}{T_{LL}} \qquad (1)$$

$$\int_0^{h_L} T\,dx = (h_{comp} - h_L)T_{UL} + h_L T_{LL} \qquad (2)$$

Here T_{UL} and T_{LL} are the upper and lower layer temperatures, and h_{comp} and h_L are the heights of the compartment and the layer interface, respectively.

The experimental data are treated using the assumptions of Fleischmann [15] considering that the lower layer temperature as the arithmetic average of the two lowest thermocouples. As the distance between the probes is smaller in the simulation, we will consider the average of the three lowest probes for the upper layer temperature.

The upper temperature T_{UL} and thermal interface height h_L can than be calculated using Eq. (1) and (2).

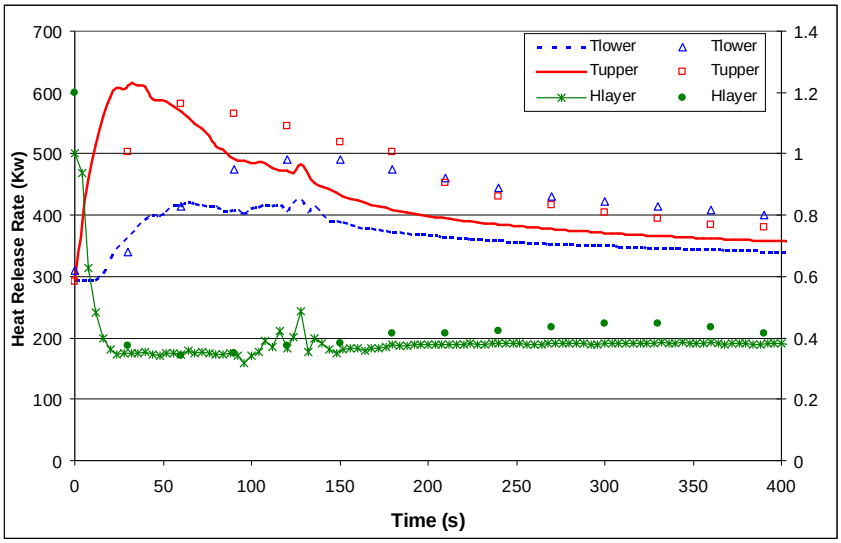

Fig. 8: Temperature history (upper and lower layer) for Run 3 (HRR = 70 Kw, t= 415 s) and layer height for simulation (lines) and experiments (symbols)

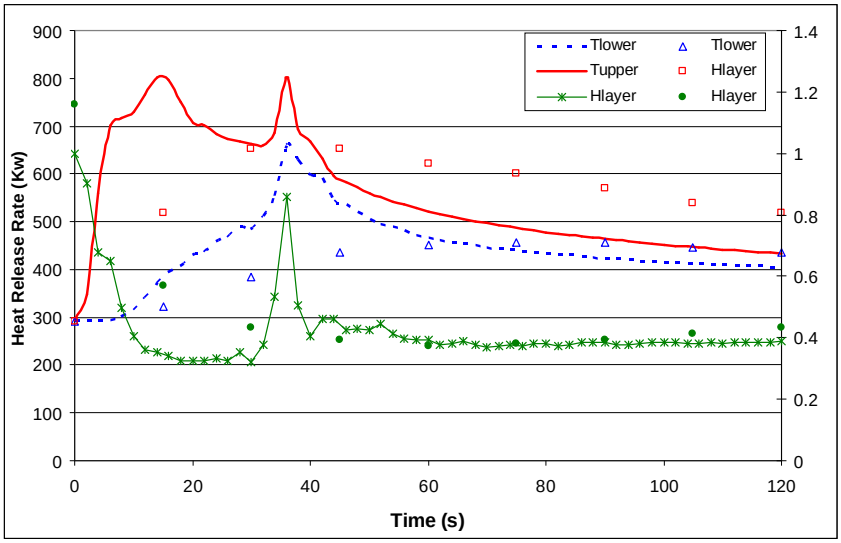

Fig. 9: Temperature history (upper and lower layer) for Run 13 (HRR = 200 Kw, t= 115 s) and layer height for simulation (lines) and experiments (symbols)

The temperature histories show that the maximum temperature is reached sooner in the simulation (50 sec. instead of 80 sec.) and drops more abruptly. The layer height stabilizes also sooner, showing that the fire growth to fully developed fire is much faster in the simulation. The model underestimates the temperatures in the upper layer, as the fire is decaying earlier. Anyway, there is a good correlation for the lower layer temperature (especially for HRR= 70 Kw), and an excellent correlation concerning the layer height. Considering that the 2-layers approximation induces imprecision, the correlation with experimental data for temperatures and layer height histories is considered good.

Instabilities can be seen close to extinction time (approximately between 110 and 140 sec. in Fig. 8 and between 35 to 40 sec. in Fig. 9). This corresponds to the rupture of the 2-zones

behavior observed in Fig. 5-b and 5-c. This rupture happens when the temperature in the 2 layers becomes quite close, involving mixing between the layers.

Studying the temperature history for each probe individually (without using the 2 layers approximations) shows that there is more stratification in the simulation, meaning that the mixing is more efficient in the experiments. It also shows that the maximum temperature is reached sooner in the simulation (50 sec. instead of 80 sec.).

Table 1 shows the temperatures in both layers and the layer height just before the hatch opening, for the 17 experimental tests from [15], and corresponding results from improved FDS model.

Table 1: Temperatures and layer height from experiments and numerical model

			Experimental data			Improved FDS model			
Run	HRR	t(total)	T_{uL}	T_{LL}	H_L	Y_{O2}	T_{ul}	T_{ll}	H_l
	(Kw)	(s)	(K)	(K)	(m)	(%)	(K)	(K)	(m)
1	72	295	417	378	0.43	9.64	372	350	0.38
2	72	355	390	361	0.43	10.07	363	344	0.38
3	72	415	379	353	0.42	10.28	356	338	0.37
4	72	475	362	339	0.42	10.37	350	334	0.37
5	69	535	377	356	0.43	10.23	345	330	0.37
6	77	535	363	344	0.41	9.92	345	331	0.36
7	69	555	359	340	0.42	10.10	344	329	0.36
8	69	595	363	346	0.41	9.85	342	328	0.37
9	73	655	350	331	0.43	9.51	338	326	0.4
10	71	715	348	332	0.44	9.34	335	324	0.36
11	68	715	347	332	0.42	9.39	339	327	0.37
12	70	775	344	330	0.41	9.06	333	322	0.36
13	200	115	517	445	0.44	5.49	438	407	0.39
14	200	145	570	475	0.34	6.47	418	392	0.39
15	200	175	474	427	0.41	7.58	402	381	0.39
16	200	205	447	408	0.43	8.00	392	373	0.38
17	200	235	433	400	0.43	8.10	383	366	0.38

The temperature fields and interface layer height show excellent agreement between experiments and simulation. The difference is more important for higher HRR and short time, probably explained by the fact that the mixing is more efficient in the experiments, and that the fire is idealized in the simulation

3.3.2. Gas concentration

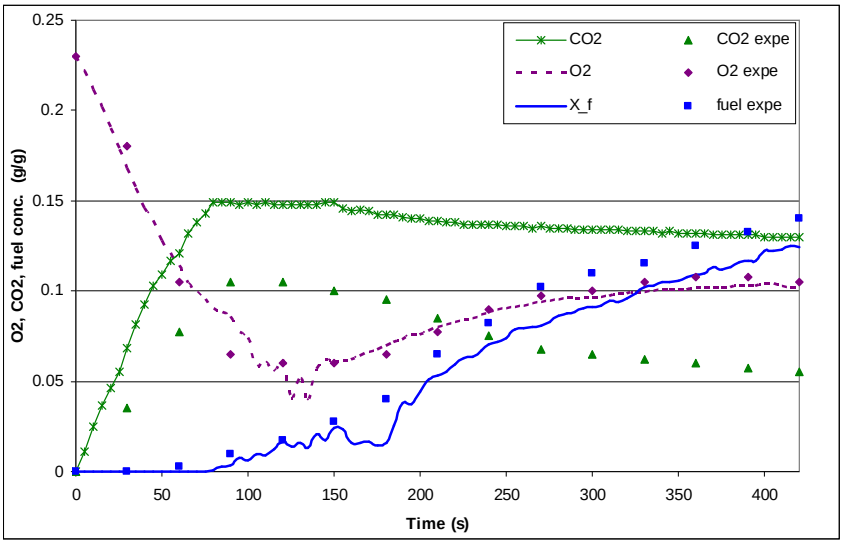

Fig. 10: Gas concentration history (CO2, fuel and O2) for Run 3 (HRR = 70 KW, t= 415 s) for simulation (lines) and experiments (symbols)

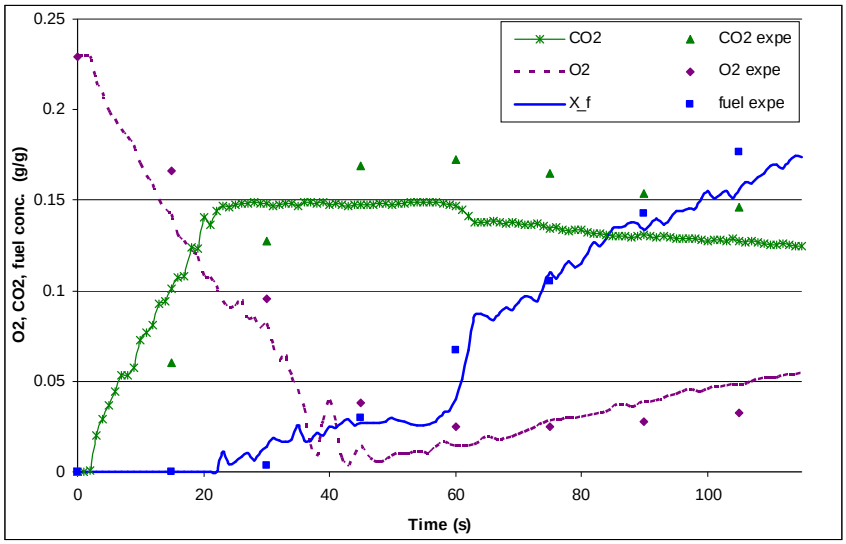

Fig.11: Gas concentration history (CO2, fuel and O2) for Run 13 (HRR = 200 KW, t= 115 s) for simulation (lines) and experiments (symbols)

We can note that the model overestimates the CO2 production. The combustion is "idealized". From run 3, the CO2 production starts to decrease roughly in the same time in the experiments and the simulation. This decrease is due to dilution by fuel and oxygen build-up. It also tends to show that the fire completely extinguishes roughly around t=120 to 140 seconds, consequently stopping the production of CO2. Moreover, the concentration of CH4 increases very linearly after roughly 130 seconds, showing that almost no fuel is burnt after this time. This tends to justify the insertion of an extinction criterion.

There is a good correlation concerning O2 and CH4 concentration between experiments and simulations. This is even more relevant for the concentration build-up of oxygen, showing that the flow rate through leakages is well calibrated; even though the leakage flow

is localized and not uniform. No relevant experimental history of CO concentration is shown here, since this is extremely small and insignificant in the mass balance.

4. Simple analytical model

This analytical model is an Excel calculation sheet, based on engineering correlations ([21], [22]) and a simple mass balance, without leakages. The behavior of the fire can be divided in three distinct phases, well ventilated, underventilated, and the fuel concentration built-up, after extinction.

If we neglect the production of CO and soot, the simplified reaction for the combustion of methane can be written as follow, considering a combustion efficiency χ:

$$CH_4 + 2\chi O_2 \rightarrow \chi CO_2 + 2\chi H_2O + (1-\chi)CH_4$$

The equivalence ratio, for a phase φ is defined as:

$$\Phi_\varphi = \frac{m_{CH4}/m_{O2}}{r} \qquad (3)$$

With the molecular weight of the different components and the coefficients of the reaction, Eq. 3 gives:

$$\Phi_\varphi = \frac{M_{CH4}/2\chi M_{O2}}{r} = \frac{1}{\chi_\varphi} \qquad (4)$$

For each phase, the following assumptions are made:

Well ventilated phase: the reaction is complete and all the fuel is burnt, consequently $\chi_{wv}=1$. Substituting this value in the above reaction gives the stoichiometric reaction of methane.

Underventilated phase: the fire is decaying, form all the methane burning (χ = 1) to extinction (χ = 0). During this phase, the relation between reaction efficiency and oxygen mass fraction is considered linear. This is a coarse approximation, but observation from experiments show that the fire is decaying quite linearly, and that this decay is directly related to the oxygen mass fraction. According to [22], the fire becomes non-flaming for $\Phi>4$ ($\chi < 0.25$), but there is still smoldering combustion at this stage.

Fuel concentration build-up: the fire is dead, the methane flows freely inside the compartment (χ_{cb} = 0).

These assumptions are illustrated in Fig. 12, showing the evolution of the efficiency as a function of the oxygen mass fraction.

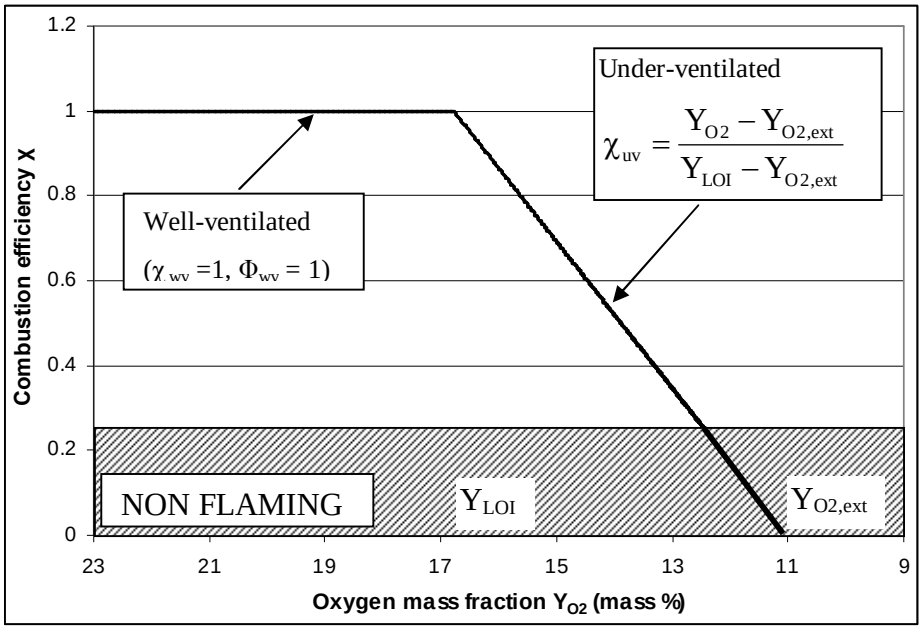

Fig. 12: Assumption of 3 different phases: well-ventilated, under-ventilated and concentration built-up (non flaming) phases

An example of the calculation sheet is shown in Table 2. Each calculation is divided in different steps, as follows:

Step 1: Geometry and problem inputs

Enter the geometry, the burner characteristic (flow rate), and the fuel flow time.

Considering the principle of mass conservation, the total mass of gas in the compartment (fuel released and initial mass of air) is obtained.

Initial volume of gas:

$$V_{air,init} = V_{comp} - V_{burn} - V_{obst} \quad (5)$$

$$m_{air,init} = \rho_{air} V_{air,init} \quad (6)$$

$$m_{fuel,total} = \dot{m}_{fuel} t_{total} \quad (7)$$

$$m_{gas,total} = m_{air,init} + m_{fuel,total} \quad (8)$$

Step 2: Gas property and combustion data

Enter the physical properties of the fuel and products (stoichiometric ratio and max theoretical yields) or use default values if fuel is CH4. Tables and correlations developed in [21] give equivalence ratios and corresponding normalized yields of species.

During the underventilated phase, the equivalence ratio and the normalized yields of species depend on the available amount of oxygen. An iterative method is therefore necessary to determine Φ_{uv} at each time step. This method is described in step 3.2 below

Step 3: Calculation of products phase by phase

During the well-ventilated phase, the fire is considered fully developed with ideal combustion (stoichiometric conditions), until the mass fraction of oxygen Y_{O2} reaches the Oxygen Limiting Index Y_{LOI}, where the underventilated phase starts. There is no clear oxygen concentration limit where complete extinction occurs defined in literature, but it is often considered to be between 8 to 11 (mol %), depending on temperature ([7], [11]). In this calculation, complete extinction will be considered for $Y_{O2,ext}$ = 10 (mol %) = 11.2 (mass %)

Finally, during the concentration built-up phase, fuel flows freely into the compartment and no combustion product is created.

The different products are calculated as follow:

$$m_{O2,init} = 0.23 m_{air,init} = 0.23 m_{gas,init} \tag{9}$$

The variation of oxygen concentration can be expressed using Eq. (4):

$$\frac{\partial m_{O2}}{\partial t} = \frac{\dot{m}_{fuel}}{r\Phi_{\varphi}} \tag{10}$$

At each step δt, a mass of fuel $m_{fuel,\delta t}$ is released, corresponding to the following consumption:

$$m_{O2,cons,\delta t} = \int_{t}^{t+\delta t} \frac{\dot{m}_{fuel}}{r\Phi_{\varphi}} dt = \frac{\dot{m}_{fuel}}{r\Phi_{\varphi}} \delta t \tag{11}$$

The total mass of oxygen at $(t+\delta t)$ is:

$$m_{O2,t+\delta t} = m_{O2,t} - m_{O2,cons,\delta t} = m_{O2,t} - \frac{\dot{m}_{fuel}}{r\Phi_{\varphi,t+\delta t}} \delta t \tag{12}$$

The total mass of gas is:

$$m_{gas,t} = m_{gas,init} + \dot{m}_{fuel} t_{\varphi} \tag{13}$$

The O2 concentration $Y_{O2,}$ can then be written:

$$Y_{O2,t+\delta t} = \frac{m_{O2,t} - \frac{\dot{m}_{fuel}}{r\Phi_{\varphi,t+\delta t}} \delta t}{m_{gas,init} + \dot{m}_{fuel}(t_{\varphi} + \delta t)} \tag{14}$$

From Eq. (14), the oxygen concentration is calculated by iteration at each time step $t+\delta t$, knowing the concentration of species at t, plus the amount of fuel added during δt.

The number of iteration and the time step gives the length of each phase. The yields and mass for each species i are:

$$y_{i,\varphi} = y_{i,max} y_{i,norm,\varphi} \tag{15}$$

$$m_{i,\varphi} = y_{i,\varphi} m_{fuel,\varphi} \tag{16}$$

This operation is done for each of the 3 phases, with different combustion data:

Step 3.1: Well-ventilated phase (until Y_{O2} = 16.8 mass %):

This phase ends when $Y_{O2} = Y_{LOI} = 16.8$. With this value, the length of the well ventilated phase t_{wv} is determined by iteration on δt. Eq. (12) and (13).give the mass of oxygen $m_{O2,wv}$ and gas $m_{gas,wv}$ at the end of the phase, and Eq. (16) gives the mass of each combustion species .

Step 3.2: Under-ventilated phase (until Y_{O2} = 11.2 mass %):

This phase ends when $Y_{O2} = Y_{O2,ext} = 11.2$. In this phase, the combustion efficiency, and consequently the equivalence ratio vary linearly with $Y_{O2.}$ Therefore, they are also calculated at each time step by iteration using:

$$\chi_{uv,t+\delta t} = \frac{Y_{O2,t} - Y_{O2,ext}}{Y_{LOI} - Y_{O2,ext}} \tag{17}$$

This is the slope shown in Fig. 12. The equivalence ratio $\Phi_{t+\delta t}$ is then calculated and placed in Eq. (11). Note that initial masses to be considered are the one at the beginning of the phase, e.g. $m_{gas,wv}$ and $m_{O2,wv}$ calculated at the previous step.

In this phase, only a fraction of the released fuel is used in the combustion, this excess of fuel is calculated as follows:

$$m_{fuel,uv,exc,t} = \chi_{uv,t}\dot{m}_{fuel}\delta t \tag{18}$$

And the total fuel in excess at the end of the phase is obtained by summing on each step.

Step 3.3: Concentration built-up phase.

There is no combustion ($\Phi_{cb} = \infty$), so there is only fuel flowing in, with:

$$m_{fuel,cb} = \dot{m}_{fuel}(t - t_{uv} - t_{wv}) \tag{19}$$

Final step: For each species i, the mass is summed up individually. For the fuel, it is the excess fuel that is summed up, and the mass of oxygen is the initial mass minus the oxygen consumed during each phase. Note that leakages are not considered in this calculation; consequently there is no oxygen concentration build-up. Anyway, The amount of oxygen added form leakages should be small compared to the fuel flow rate, and should not have a big influence on the concentration of excess fuel that is the critical factor for the estimation of probability of backdraft.

4.1. Example of result table

Table 1 gives an example of calculation, for experimental run 1 in [15]. Values in bold are calculated by the above equations, and values in colored cells (STEP 3) have to be added specie by specie to obtain the final mass in the compartment (FINAL STEP). The other values are either set-up data, physical properties of fuel and products (stoichiometric ratio and max theoretical yields) taken from tables and simple engineering correlations described in [21].

Table 2: Example of simple analytical model for run 1 (HRR = 70 Kw, t = 295 sec.)

STEP 1							
$V_{air,init}$ (m^3)	ρ_{air} (Kg/m^3)	$m_{air,init}$ (Kg)	$m_{O2,init}$ (Kg)	$\dot{m}_{fuel}$ (Kg/s)	t_{tot} (s)	$m_{fuel,tot}$ (Kg)	$m_{gas,tot}$ (Kg)
3.43	1.17	**3.83**	$8.81.10^{-1}$	$2.06.10^{-3}$	295	**0.61**	**4.44**

STEP 2					
FUEL DATA		COMBUSTION DATA			
r	0.25	*Phase*	*WV*	*UV*	*CB*
$y_{CO,max}$	1.75	Φ_φ	1	variable	∞
$y_{CO2,max}$	2.75	$y_{CO,norm,\varphi}$	0.01	0.2	0
$y_{H2O,max}$	2.25	$y_{CO2,norm,\varphi}$	1	$0.69/\Phi$	0
		$Y_{H2O,norm,\varphi}$	1	$0.86/\Phi$	0

STEP 3			
Phase	*WV*	*UV*	*CB*
t_φ (s) (iteration)	**27.60**	**100**	**167.40**
$m_{fuel,\varphi}$ (Kg)	**$5.69 .10^{-2}$**	**$2.06 .10^{-1}$**	**$3.45 .10^{-1}$**
$m_{O2,cons,\varphi}$ (Kg). (Eq. 11)	**$2.27 .10^{-1}$**	**$2.02 .10^{-1}$**	**0**
$m_{fuel,exc,\varphi}$ (Kg) (Eq.18 and 19)	**0**	**$1.56 .10^{-1}$**	**$3.45 .10^{-1}$**
$y_{CO,\varphi}$ (Eq.15)	**$1.175 .10^{-2}$**	**0.35**	**0**
$y_{CO2,\varphi}$ (Eq.15)	**2.75**	**0.46**	**0**
$y_{H2O,\varphi}$ (Eq.15)	**2.25**	**0.47**	**0**
$m_{CO,\varphi}$ (Eq.16)	**$9.95.10^{-4}$**	**$7.21.10^{-2}$**	**0**
$m_{CO2,\varphi}$ (Eq.16)	**$1.56 .10^{-1}$**	**$9.59.10^{-2}$**	**0**
$m_{H2O,\varphi}$ (Eq.16)	**$1.28 .10^{-1}$**	$9.78.10^{-1}$	**0**

FINAL STEP		
Specie	Final mass (Kg)	Mass fraction (mass %)
O2	**$4.51.10^{-1}$**	**10.16**
CO	**$7.31.10^{-2}$**	**1.65**
CO2	**$2.52.10^{-1}$**	**5.68**
Fuel	**$5.0.10^{-1}$**	**11.28**

This analytical model has the advantage to be very simple and practical. If the physical properties of the fuel are already entered in the calculation sheet, the user just need to enter the geometry, the flow rate and the total calculation time to obtain the mass fraction of fuel, which allows concluding on the estimation of the probability of backdraft [14].

4.2. Comparison with experiments

4.2.1. Comparison with experimental results from [15]

Table 3 presents the experimental results from [15], as well as the two tools developed in this study, the improved FDS model and the simple analytical model, with combustion products and temperature field just before the opening.

Table 3: Results from experiments, simulation and analytical model

			Experimental data				Improved FDS model				Analytical model			
Run	HRR	t_{total}	Y_{O2}	Y_{CO}	Y_{CO2}	Y_{CH4}	Y_{O2}	Y_{CO}	Y_{CO2}	Y_{CH4}	Y_{O2}	Y_{CO}	Y_{CO2}	Y_{CH4}
	(Kw)	(s)	(%)	(%)	(%)	(%)	(%)	(%)	(%)	(%)	(%)	(%)	(%)	(%)
1	72	295	9	1	7	10	9.64	0.02	13.43	9.86	10.16	1.65	5.68	11.28
2	72	355	11	0	6	12	10.07	0.02	13.20	11.49	9.89	1.60	5.53	13.68
3	72	415	11	0	6	14	10.28	0.02	13.04	12.37	9.63	1.56	5.38	15.96
4	72	475	11	0	5	16	10.37	0.02	12.96	13.58	9.38	1.52	5.25	18.12
5	69	535	11	0	5	16	10.23	0.02	12.95	13.80	9.22	1.50	5.18	19.39
6	77	535	11	0	5	20	9.92	0.02	12.73	15.55	8.99	1.46	5.05	21.36
7	69	555	11	0	5	19	10.10	0.02	12.90	14.18	9.14	1.48	5.14	20.04
8	69	595	12	0	4	19	9.85	0.02	12.84	14.73	9.00	1.46	5.06	21.30
9	73	655	12	0	4	21	9.51	0.02	12.62	16.40	8.66	1.41	4.87	24.22
10	71	715	11	0	4	20	9.34	0.02	12.66	16.42	8.53	1.38	4.79	25.43
11	68	715	12	0	4	22	9.39	0.02	12.78	15.47	8.63	1.40	4.85	24.56
12	70	775	12	0	4	22	9.06	0.02	12.61	16.83	8.37	1.36	4.70	26.81
13	200	115	4	1	9	13	5.49	0.02	12.42	17.60	10.03	1.61	5.63	12.26
14	200	145	4	1	10	10	6.47	0.02	11.82	21.61	9.66	1.55	5.43	15.49
15	200	175	5	1	7	24	7.58	0.02	11.56	23.94	9.32	1.49	5.23	18.48
16	200	205	6	1	6	29	8.00	0.02	11.29	26.30	9.00	1.44	5.06	21.28
17	200	235	6	1	6	29	8.10	0.02	11.02	28.68	8.70	1.40	4.89	23.89

Fig. 13 and 14 show that there is a good agreement concerning the fuel (Fig. 13) and oxygen (Fig. 13) for both tools and experiments. It is especially important to notice the excellent agreement for fuel concentration between experimental and analytical results.

As mentioned earlier, the combustion is idealized during the fully developed phase for both simulation and analytical calculation, consequently overestimating the CO2 production. CO concentration measurements are shown in Table 2, but as they are extremely small and insignificant in the mass balance, the results from simulation and analytical calculation are considered not relevant. Experimental concentration measurements are very difficult, due mainly to the fact that they are measured at one point. This can explain some differences between the results, especially for high flow rate (experimental runs 13 to 17).

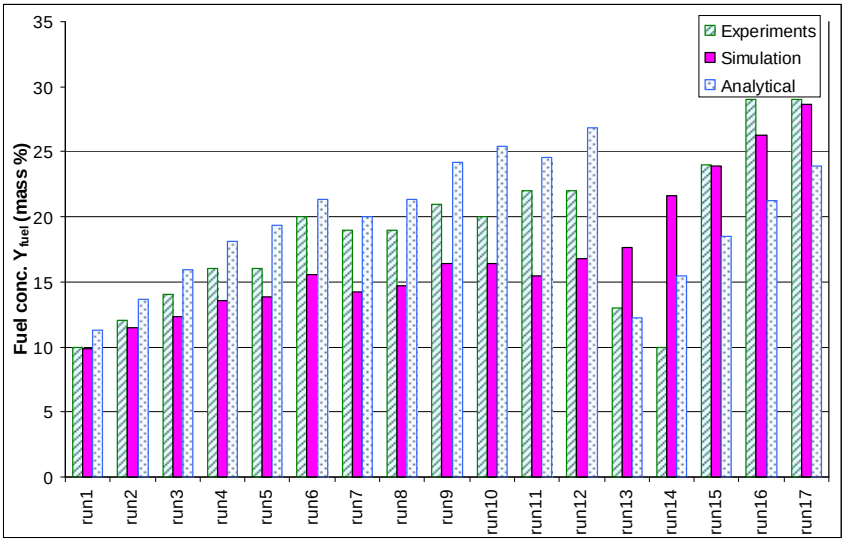

Fig. 13: Fuel concentration for experiments, simulation and analytical model

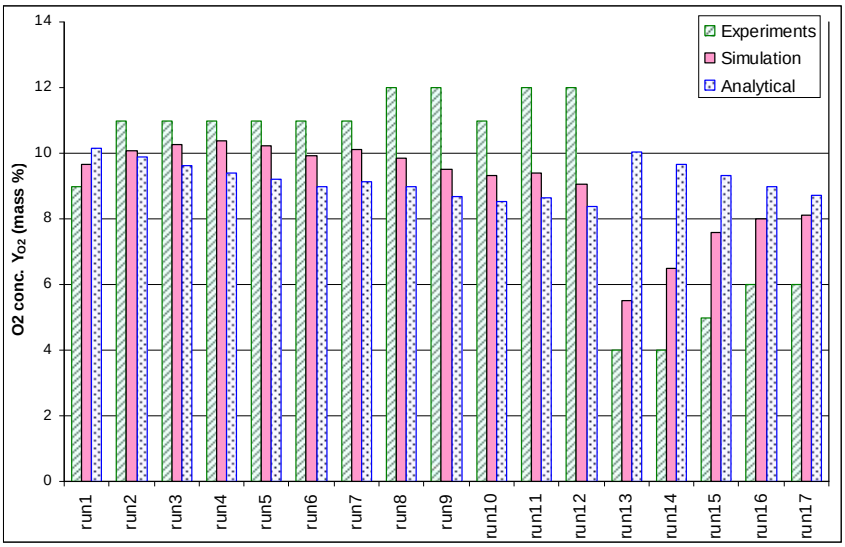

Fig. 14: Oxygen concentration for experiments, simulation and analytical model

4.2.2. Comparison with experimental results from [14]

Some comparisons are also carried from experiments from Weng [14]. These experiments are very similar to the ones carried out in [15]. In addition, a certain critical fuel fraction above which backdraft should occur for different opening. These critical mass fractions are

7.1 % for high-slot, 8.5 for middle slot and 9 for low slot opening. The geometry and experimental inputs are applied to the analytical model and results are showed on Fig. 15.

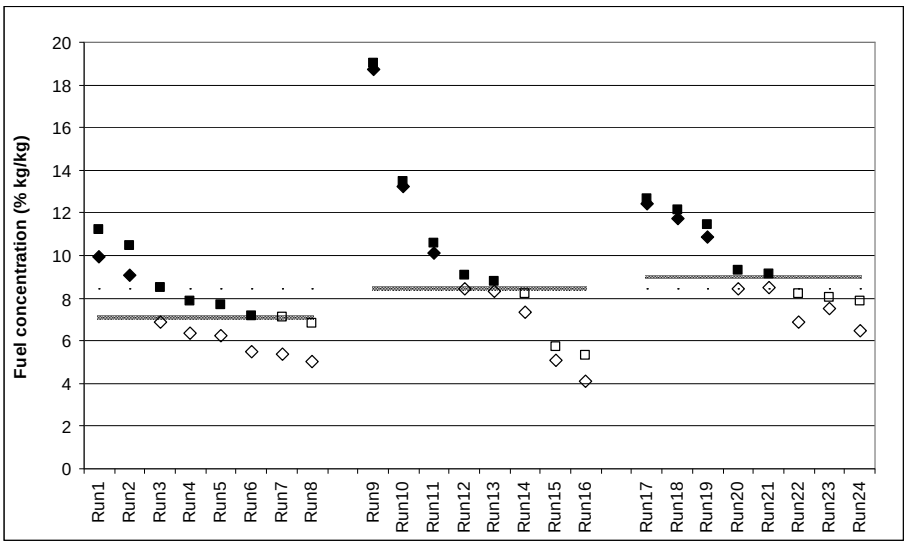

Fig. 15: Mass fraction of unburnt fuel determining the occurrence (solid) and non-occurrence (hollow) of backdraft

Results show that an agreement on occurrence of backdraft is reached for 16 runs out of 24. On the 8 remaining runs, 4 of them (runs 11, 12, 20 and 21) give very close results, especially for high flow rate or longer concentration build-up, due to higher dilution rate. Considering the uncertainties due to measurements and consequently on the critical fuel volume fraction, the results are considered fair.

5. Conclusion

Underventilated fires are in many ways more complex than well ventilated fires since the lack of oxygen creates complicated phenomena such as ghosting flames, flame quenching and extinction. Moreover, it produces dangerous gases due to the incompleteness of combustion. Former studies have shown that a reasonable modeling of the extinction by CFD has not been achieved yet, an such modeling resulted in an unnatural behavior of the fire. In this study, possibilities of improvement for CFD models are investigated, and it is shown that an improved CFD model (tool1, Model M2), that takes into account leakages and an extinction criterion, depending on the Oxygen Limiting Index, resulted in a fire behavior in much better agreement with experimental observation than the standard CFD model.

A second tool, a simple analytical model based on engineering calculation, on mass conservation and on the assumption of 3 separate phases is developed. The goal of this model is to give a rough estimate of the probability of a backdraft, based on the fuel critical mass fraction, giving a value of fuel concentration above which backdraft can occur. The analytical sheet gives the fuel mass fraction for simple geometry by entering just a few data, allowing the estimation. Comparison with experiments shows an excellent agreement concerning the oxygen concentration and the fuel mass fraction. Anyway, this could be improved by description with a non-linear function, but this would require many

experimental data describing precisely the decaying phase. Including leakages could also bring a significant improvement.

One of the goals of this study was to provide a methodology for the estimation of the amount of carbon monoxide, as its inhalation is the main source of casualties in fire. Due to its very small contribution in the mass balance and the uncertainties in experimental measurements, the developed tools fail to give a reliable estimation.

These two tools are developed using simple assumptions like the extinction criterion or considering an average equivalence ratio for the decaying phases. These assumptions need to be refined and completed, but give interesting indications clue for future useful tools for the study of strongly underventilated fires.

Nomenclature

H	Height
HRR	Heat Release Rate
L	Length
LOI	Limiting Oxygen Index
m_i	Mass of a specie i
$m_{i,\varphi}$	Mass of specie i produced during phase φ
$\dot{m}_i$	Mass flow rate of specie i
M_i	Molecular weight of specie i
r	Stoichiometric fuel to oxygen ratio for complete combustion
t	Time
t_φ	Time length of phase φ.
T	Temperatures
V	Volume
W	Weight
$y_{i,\varphi}$	Yield of specie i during phase φ.
$y_{i,max}$	Maximum yield of specie i.
$y_{i,norm,\varphi}$	Normalized yield of specie i during phase φ.
Y_i	Mass fraction of specie i
Φ	Equivalence ratio
φ	Phase φ of the fire
ρ	Density
χ	Combustion efficiency

Subscript

Air	Air

aver:	Average value
burn	Burner
cb	Concentration built-up phase
CH4	Methane fuel
CO	Carbon monoxide
CO2	Carbon dioxide
comp	Compartment
cons	Consumed
exc	Excess fuel
ext	Extinction
fuel	Fuel
gas	Gaseous mixture
H2O	Water
init	Initial
L	Layer interface
LL	Lower layer
LOI	Limiting Oxygen Index
obst	Obstacle
O2	Oxygen
t	Time
total	total
ul	Upper layer
uv	Under-ventilated phase
wv	Well-ventilated phase
δt	Time step
φ	Phase φ of the fire

References

[1] Firenet project web site: http://www.kingston.ac.uk/thermofluids/

[2] Fahy R.F. and LeBlanc P. R. "*Fire-fighters fatalities in the United States – 2005*". Fire Analysis and Research Division, National Fire Protection Association. June 2006.

[3] Eliasson J., Guigay G., Karlsson B., "Enclosure fires, gravity currents and the backdraft problem". Intended for publication in Journal of Fire Sciences. (June 2005).

[4] Guigay G., Eliasson J., Horvat A., Sinai Y., “Semi-analytic and CFD calculation of gravity flows in backdraft studies. Intended for publication in Fire Safety Journal (February 2006).

[5] Gojkovic D., Karlsson B. ,.”Describing the Importance of the Mixing Process in a Backdraft Situation Using Experimental Work and CFD”, Proceedings of the 3rd international seminar on Fire and Explosion Hazards, 2000.

[6] Guigay G., Gojkovic D., Bengtsson L., Karlsson B. , “Evaluation of fire-fighting tactics in a possible backdraft situation using CFD calculation”, Intended for publication in Fire Safety Journal.

[7] Drysdale D., “An Introduction to Fire Dynamics”, Second edition, Wiley, 1998.

[8] Karlsson B., Quintiere J. G.. “*Enclosure Fire Dynamics*”. CRC press, 1986.

[9] Pretrel H., Querre P., Forestier M., “Experimental Study of Burning Rate Behavior in confined and Ventilated Fire Compartments”, Proceedings of IAFSS Symposium, Baltimore, 2005.

[10] Hu, Z., Utiskul, Y., Quintiere, J., Trouve, A., “A Comparison between Observed and Simulated Flame Structures in Poorly Ventilated Compartment Fires”, Fire Safety Science – Proceedings of IAFSS Symposium, Baltimore, 2005.

[11] Utiskul Y., Quintiere J., Rangwala A., Ringwelski B., Wakatsuki K., Naruse T., “Compartment fire phenomena under limited ventilation”, Fire Safety Journal 40 (2005) 367-390.

[12] Utiskul Y., Quintiere, J., Naruse T., “Wall-vent compartment fire behavior under limited ventilation”, proceedings of 10th Interflam conference, Edinburgh 2004.

[13] Most J.M., Pearson A., Guigay G., Karlsson B., “*Transition to an underventilated compartment fire to the backdraft phenomenon*”. Congres Francophone de Techniques Laser, CFTL 2006, September 2006.

[14] Weng, W.G., Fan, W.C., “Experimental Study of Backdraft in a Compartment with Different Opening Geometries and its Mitigation with Water Mist”, Journal of Fire Sciences, Vol. 20 – July 2002.

[15] Fleischmann. C.M., Pagni P.J., Williamsson R.B. “Quantitative Backdraft Experiments”, Fire Safety Science- Proceedings of the 4th international symposium, Ottawa 1994.

[16] Gojkovic D., ”Initial Backdraft Experiments”, Report 3121, Department of Fire

Safety Engineering, Lund University, Sweden, 2001.

[17] Gottuk D.,T., Peatross M.J., Farley J.P., Williams F.W., ”The development and mitigation of backdraft: a real-scale shipboard study”, Fire Safety Journal 33 (1999) 261-282.

[18] FDS Fire Dynamic Simulator, NIST. http://fire.nist.gov/fds/

[19] Quintiere J., Steckler K, Corley D., ”An assessment of fire induced flows in compartments”, Fire Sciences and Technology, Vol. 4, No 1, 1984, pp. 1-14.

[20] Sinai Y.L., “Comments on the role of leakages in field modeling of underventilated compartment fires”, Fire Safety Journal 33(1999) 11-20.

[21] Gottuk D.T., Roby R.: “Effect of combustion on species production”, chapter 2-7, NFPA Handbook of Fire Protection Engineering.

[22] Tewardson A. ,”Generation of heat and Chemical Compounds in Fires”, section3-4, NFPA Handbook of Fire Protection Engineering.